The Role of NF-κB2 in Secondary and Tertiary Lymphoid Tissue Development

By Emma Mader

A thesis submitted to
The University of Birmingham
for the degree of
DOCTOR OF PHILOSOPHY

School of Immunity and Infection
College of Dental and Medical Sciences
University of Birmingham
October 2010

Abstract

The role of the alternative NF-κB pathway in the development of secondary lymphoid organs (SLOs) has been well described. Tertiary lymphoid organs (TLOs) include intestinal cryptopatches (CPs) and isolated lymphoid follicles (ILFs). This thesis investigates the role of the alternative NF-κB pathway in the development of colonic ILFs, using the p100Δ mouse model, where the alternative pathway is constitutively active. We present compelling data that p100Δ mice develop significantly more lymphoid aggregates in the colon, compared with WT littermates, and provide several lines of evidence showing that these aggregates are analogous to ILFs. Additionally, we demonstrate that in the p100Δ a significant increase in the numbers of B and T cells, and DCs in the colon and show alterations in the subsets of colonic T cells and DCs. We also present evidence that constitutively active NF-κB2 p100 in LTα deficient mice induces recovery of B and T cell segregation in the spleen. Most strikingly, we show recovery of iLNs and mLN development in one of five *p100ΔLTα*$^{-/-}$ mice generated.

These findings demonstrate that the alternative NF-κB pathway plays an important role in not only SLO development and splenic organisation, but also in the development of TLOs, specifically colonic ILFs.

Acknowledgements

Firstly, I'd like to thank my supervisor Dr. Jorge Caamaño for the opportunity to work on this project and for his scientific guidance. Dr. Cécile Bénézech has been an invaluable source of emotional and scientific support, and her encouragement and patience throughout my studies has been, and still is, greatly appreciated. Professor Graham Anderson has been an incredibly supportive mentor, who's advice throughout my PhD has been hugely helpful.

I would also like to acknowledge the students and staff members in the IBR who made my time at the University of Birmingham a very enjoyable and unforgettable experience.

Finally, I wish to extend my sincere thanks to my family, friends and partner for all their help, support, encouragement and patience over the past three years.

Table of Contents

List of Figures

List of Tables

Abbreviations

-/-	Deficient (knock-out)
+/-	Heterozygous
AID	Activation-induced cytidine deaminase
APC	Antigen presenting cell
APRIL	A PRoliferation Inducing Ligand
ARTN	Artemin
BAFF/-R	B cell activating factor/-receptor
BCMA	B cell maturation antigen
BM	Bone marrow
BMDC	Bone marrow-derived dendritic cell
BSA	Bovine serum albumin
CCL	CC-chemokine ligand
CCR	CC-chemokine receptor
cDC	Conventional dendritic cell
cDNA	Complementary DNA
CDP	Common DC precursor
CP	Cryptopatch
CTL	Cytotoxic T lymphocyte
CXCL	CXC-chemokine ligand
CXCR	CXC-chemokine receptor
DC	Dendritic cell
dsRNA	Double stranded RNA
DSS	Dextran sodium sulphate
E15	Embryonic day 15
FACS	Fluorescence activated cell sorting
FAE	Follicle-associated epithelium
FCS	Foetal calf serum
FDC	Follicular dendritic cell
FLC	Foetal liver cell
Flt3	FMS-like tyrosine kinase 3
Foxp3	Forkhead box P3
FRC	Fibroblastic reticular cell
GALT	Gut-associated lymphoid tissue
GC	Germinal centre
Gp	Glycoprotein
Gr-1	Granulocyte differentiation antigen 1
HEV	High endothelial venule
HTLV-1	Human T-cell leukaemia virus type 1
IBD	Inflammatory bowel disease
ICAM-1	Intercellular adhesion molecule -1
IEL	Intraepithelial lymphocyte
IFN	Interferon
Ig	Immunoglobulin
IκB	Inhibitor of NF-κB
IKK	IκB kinase
IL	Interleukin

IL-7Rα	Interleukin seven receptor alpha
ILF	Isolated lymphoid follicle
iLN	Inguinal lymph node
ki	Knock-in
LMP-1	Latent membrane protein 1
LN	Lymph node
LP	Lamina propria
LP-DC	Lamina propria dendritic cell
LPS	Lipopolysaccharide
LT	Lymphotoxin
LTi	Lymphoid tissue inducer cell
LTint	Lymphoid tissue initiator cell
LTo	Lymphoid tissue organiser cell
LTα	Lymphotoxin alpha
LTβ	Lymphotoxin beta
LTβR	Lymphotoxin beta receptor
Lyve-1	Lymphatic vessel endothelial receptor -1
M cells	Microfold cells
MAdCAM-1	Mucosal addressin cell adhesion molecule -1
MARCO	Macrophage receptor with collagenous structure
MDP	monocyte, macrophage and dendritic cell precursor
MFI	Mean fluorescence intensity
MHC	Major histocompatibility complex
mLN	Mesenteric lymph node
MMM	Marginal zone metallophilic macrophage
mRNA	Messenger RNA
MyD88	Myeloid differentiation primary response gene (88)
MZ	Marginal zone
NF-κB	Nuclear factor kappa B
NIK	NF-κB inducing kinase
NK cell	Natural killer cell
NLR	NOD-like receptor
NLR	Nucleotide-binding domain and leucine-rich repeat-containing receptor
NLS	Nuclear localisation signal
NOD-1	Nucleotide-binding oligomerization domain containing 1
P21	Postnatal day 21
PAMP	Pathogen-associated molecular pattern
PBS	Phosphate buffered saline
PDC	Plasmacytoid dendritic cell
PDGFR	Platelet-derived growth factor receptor
PNAd	Peripheral node addressin
PP	Peyer's Patch
Pre-cDC	Conventional DC precursor
Prox-1	Prospero homeobox -1
PRR	Pattern recognition receptor
Rag	Recombinase activating gene
RANK	Receptor activator of nuclear factor-κB
RANKL	Receptor activator of nuclear factor-κB ligand

RET	Receptor tyrosine kinase
RHD	Rel-homology domain
RLR	RIG-1-like receptor
ROI	Region of interest
ROR	Retinoic acid related orphan receptor
RT-PCR	Reverse transcriptase polymerase chain reaction
SCID	Severe combined immunodeficiency
SD	Standard deviation
SILT	Solitary isolated lymphoid tissue
SLO	Secondary lymphoid organ
SPF	Specific Pathogen Free
ssRNA	Single stranded RNA
TACI	Transmembrane activator and CAML interactor
TCR	T cell receptor
TD antigen	Thymus dependent antigen
T_H cell	T helper cell
TI antigen	Thymus independent antigen
TLO	Tertiary lymphoid organ
TLR	Toll-like receptor
TNF	Tumour necrosis factor
TRAF	Tumour necrosis factor associated factor
Treg	Regulatory T cell
UC	Ulcerative colitis
VCAM-1	Vascular cell adhesion molecule -1
VEGF	Vascular endothelial growth factor
VEGFR	Vascular endothelial growth factor receptor
WT	Wild type

1. General Introduction

1.1. The Immune System

The immune system consists of specialised cells and tissues, which collectively, orchestrate defence mechanisms to fight against invading pathogens. The two main effector arms of the immune system are the innate and adaptive immune responses.

The innate immune system initiates a non-specific, rapid response to invading pathogens. The cellular compartment of the innate immune system includes cells capable of endocytosing foreign macromolecules, as well as those able to phagocytose whole micro-organisms, these cells include blood monocytes, neutrophils, macrophages and dendritic cells (DCs). The innate immune system is described in more detail in Section 1.7.

1.2. The Adaptive Immune System

The adaptive immune system involves mounting a specific response to targeted antigens. The main characteristics of adaptive immunity are the ability to recognise self and non-self, the development of antigenic specificity, the identification of a diverse range of foreign antigens and the ability to generate immunological memory. These responses occur within various lymphoid tissues, which are highly organised and tightly regulated. There are three main types of lymphoid tissue: primary, including the bone marrow and thymus, secondary, including the spleen, lymph nodes and Peyer's patches (PPs) (Figure 1.1) and tertiary, including cryptopatches (CPs) and isolated lymphoid follicles (ILFs).

The effector cells of the adaptive immune system include B and T lymphocytes, both requiring activation in order to initiate an immune response. Activation of naïve B cells occurs following antigen interaction in response to two main types of antigens: thymus-independent (TI) antigens, and thymus-dependent (TD) antigens. TI antigens include LPS and flagellin, and most TI antigens act as polyclonal B cells activators; activating B cells regardless of antigen specificity and requiring no direct help from T cells. Conversely, B cell responses to TD antigens require direct contact with T helper cells and in this situation activated B cells are able to differentiate into plasma cells, capable of producing immunoglobulins, or into memory B cells. The humoral response of B cells differs depending on the type of antigen encountered and memory B cells are only generated following interaction with TD antigens.

T cells are activated occurs following T cell receptor (TCR) engagement by major histocompatibility complex (MHC) molecules presenting antigenic peptide. Antigen presenting cells (APCs), such as DCs, macrophages and B cells, are able to process antigen and present the associated peptides on surface MHC. Activation of T cells induces clonal proliferation and differentiation into either effector or memory T cells. Effector T cell subsets include: $CD4^+$ T helper (T_H) cells and $CD8^+$ cytotoxic T cells (CTL). $CD4^+$ T_H cells can be subdivided into several populations: T_H1, T_H2, T_H17 (Dong, 2008), inducible T regulatory (Treg) cells (Wing et al., 2006) and T follicular helper (Tfh) cells (Vinuesa et al., 2005; Linterman and Vinuesa, 2010). The effector cell subpopulations T_H1, T_H2 and T_H17 can be characterised based on their differing cytokine production profile and subsequent function (Table 1.1). Memory T cells are generated during the initial response to a newly encountered antigen and

reside in the body in a quiescent state, ready to induce effector functions if the same antigen is encountered a second time.

Effector Immune Response		
T_H1	T_H2	T_H17
Activation of macrophages. Production of IgG2a. Inflammatory response.	Activation of eosinophils. Production of IgM and IgE Allergic response.	Induction of neutrophil and macrophage recruitment. Involved in autoimmune and inflammatory diseases.
IFNγ	IL-4	IL-17A/ IL-17E
TNFβ	IL-5	IL-21
IL-2	IL-10	IL-22
	IL-13	

Table 1.1 Overview of T_H1 and T_H2 immune responses.

1.3. Primary Lymphoid Organs

Haematopoiesis of immature lymphocytes occurs in the primary lymphoid organs, which includes the bone marrow (BM) and thymus. The BM is the major site for B cell development, where an intricate network of stromal cells release cytokines required for their development. T cell development occurs in the thymus, where a tightly organised microarchitecture allows for migration of thymocytes to specific areas where they undergo positive selection; a protective survival signal is received by the thymocyte if it is able to bind MHC molecules expressed on cortical epithelial cells, and negative selection; thymocytes with high affinity receptors for MHC molecules bearing self antigen undergo apoptosis. The generation of TCRs is a random process and selection in the thymus allows development of T cells recognising self and deletion of potentially autoreactive T cells.

1.4. Secondary Lymphoid Organs

The initiation and maintenance of adaptive immune responses occurs in the highly specialised and strictly organised SLOs: spleen, LNs and PPs. The spleen and LNs are key sites for initiation of adaptive immune responses, providing a micro-environment where lymphocyte contact with trapped antigens and APCs is optimised. To complement this, LNs are located at specific positions along the lymphatic vasculature, at sites where their exposure to draining lymph fluid from associated tissues is maximised (Figure 1.1).

1.4.1. Structure and Function

1.4.1.1. Structure of the Lymph Node

The lymph node can be divided into three main structural regions, i) the cortex, ii) the paracortex and iii) the medulla (Figure 1.2. A). The cortex is the outer most region of the LN and consists of mainly B lymphocytes, macrophages and follicular dendritic cells (FDCs), arranged into primary follicles. The paracortex is located beneath the cortex and is the site for T lymphocyte interaction with interdigitating DCs. Circulating lymphocytes enter the LN in this region via high endothelial venules (HEVs). The innermost layer, the medulla, is more sparsely populated with lymphoid cells, including antibody producing plasma cells.

The main stromal cells generating the three-dimensional structure the LN are fibroblastic reticular cells (FRCs), within the paracortex, and FDCs, within the B cell follicles. These stromal cells are involved in cellular organisation by the production of lymphocyte homing chemokines, and provide the conduit system along which lymphocytes are able to traffic (Bajénoff et al., 2006).

Figure 1.1 Position of lymph nodes in the body

The lymph nodes (LNs) are located at strategic sites in the body, along the lymphatic vasculature. This enables them to perform their function of filtration of lymph fluid, sequestration of antigen and antigen-presenting cells (APCs), and provision of a specialised micro-environment maximising APC-lymphocyte interaction and initiation of an effective immune response.

Position of Lymph Nodes in the Body

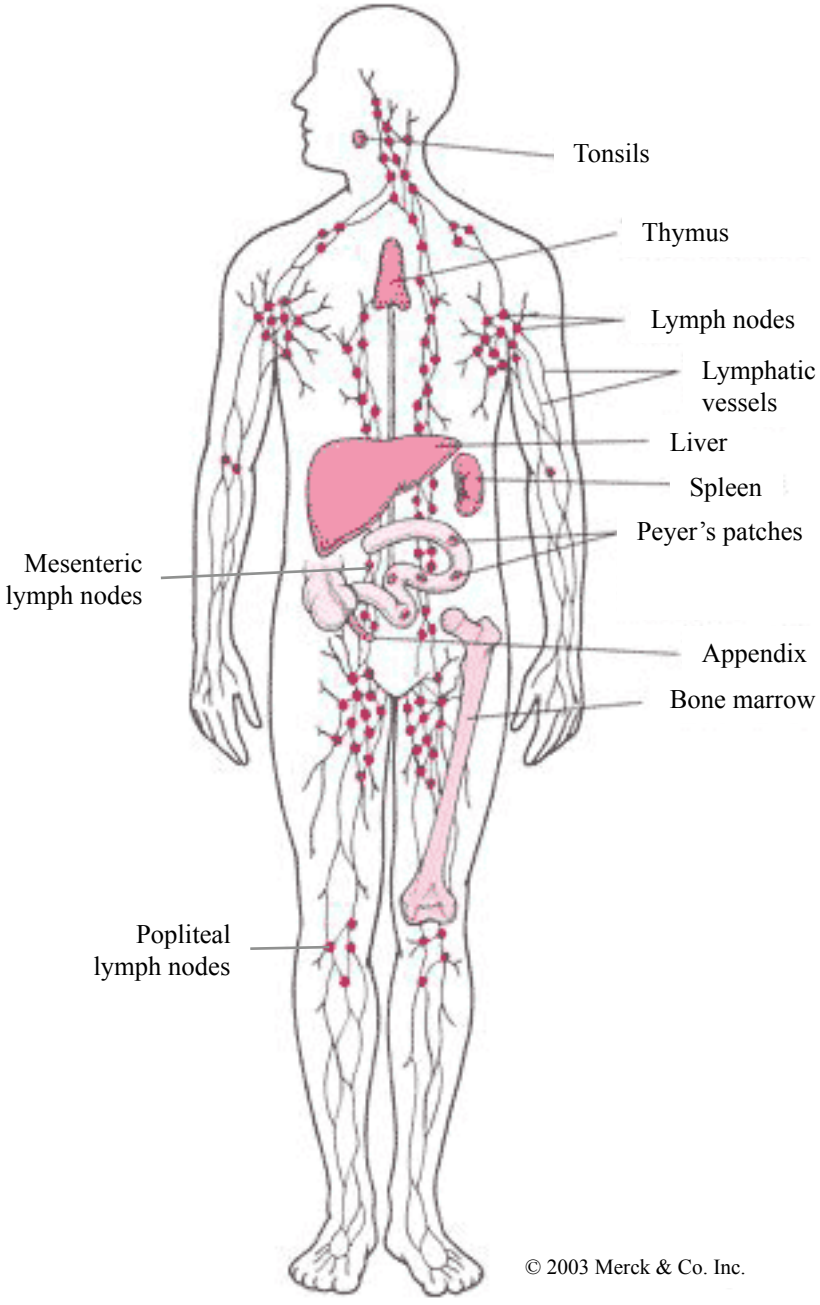

Primary Lymphoid Organs	Secondary Lymphoid Organs
Bone marrow	Spleen
Thymus	Lymph nodes
	Peyer's Ptaches

Figure 1.1

1.4.1.2. Structure of the Spleen

The spleen consists of two functionally distinct regions, the red and white pulp areas. The red pulp area is the location of blood filtration, sequestration of dead and damaged red blood cells and subsequent iron recycling. In addition, long-lived plasma cells and macrophages are located in the red pulp (MacLennan et al., 2003). The white pulp is the lymphoid area of the spleen and is the site for mounting innate and adaptive immune responses. The white pulp has a highly organised structure specialised to optimise antigen and APC retrieval from the blood and to promote cell-cell interactions critical for immune responses. The organisation and maintenance of splenic structure is dependent on the expression of specific chemokines from specialised stromal cells.

Chemokines are a superfamily of molecules involved in recruitment and trafficking of leukocytes. There are several groups, distinguished by the position of conserved cysteine residues. The two groups of interest for this thesis are those designated CXC, where one amino acid residue sits between the two cysteine residues, e.g. CXCL13, and the group designated the CC chemokines, with no amino acid located between the two cysteine residues, e.g. CCL19. All chemokines elicit their effects through seven transmembrane G-protein coupled receptors. These receptors can be promiscuous in their chemokine ligands (Table 1.2).

	Chemokine	*Expression*	*Receptor*	*Expression*
CCL Chemokines	CCL19	T-zone reticular cells (spleen)	CCR7	T cells, mature DCs
	CCL21			
	CCL20	Intestinal epithelium	CCR6	B cells, T cells, mature DCs
	CCL25	S.I epithelium	CCR9	T cells
	CCL28	Colonic epithelium	CCR3/ CCR10	T cells
CXCL Chemokines	CXCL13	FDCs	CXCR5	Naïve B cells, follicular T_H cells

Table 1.2 Overview of chemokines of interest and their respective receptors.

Several chemokines have been shown to be crucial in secondary lymphoid tissue microarchitecture. Within the spleen, specialised cells in the T-zone express CCL19/21 (T-zone stromal cells and DCs (Luther et al., 2000)), allowing localisation of T cells and DCs, and Gp38/Podoplanin, a transmembrane mucin-type protein. Expression of CXCL13 in the B cell area by stromal cells and FDCs (Ansel et al., 2000), allows for the migration of B cells to the follicles (Förster et al., 1999; Cyster et al., 1999). The expression of these chemokines, and others, creates the unique organisation of the white pulp into discrete B and T cell areas (Figure 1.2. B). Mice deficient in CXCL13, or its receptor CXCR5, maintain B/T cell segregation but lack primary B cell follicles, and GCs form in aberrant locations (Ansel et al., 2000; Förster et al., 1996). A spontaneous mutation in *plt/plt* mice results in non-functional CCL19 and CCL21, in these mice T cells fail to migrate into the spleen due to lack of expression of these chemokines, resulting in a disrupted splenic microarchitecture (Nakano et al., 1998). Furthermore, *Ccr7*$^{-/-}$ mice present with disorganised splenic

architecture, with random distribution of T cells and little evidence of discernable T cell areas, however, GCs were able to form in these mice (Förster et al., 1999) (Table 1.3).

Therefore, the white pulp is organised into specific compartments: the T zone, arranged around the central arteriole; the B cell area, surrounding the T zone and arranged into primary follicles, and finally, the marginal zone (MZ) that encapsulates the whole structure. The MZ is made up of specialised macrophages and B cells. The MZ macrophages express MARCO and are necessary for the recruitment and retention of MZ B cells (Karlsson et al., 2003). MZ B cells express alphaLbeta7 ($\alpha_L\beta_7$) and alpha4beta1 ($\alpha_4\beta_1$), allowing them to localise to the MZ by interaction with the ligands ICAM-1 and VCAM-1, respectively (Lu and Cyster, 2002). Positioned beneath the MZ is the marginal sinus, which is lined by a single layer of MAdCAM-1^+ sinus-lining cells and located underneath is a layer of MZ metallophilic macrophages (MMMs) expressing CD169 (Mebius and Kraal, 2005).

Splenic microarchitecture is tightly regulated and highly organised and this signifies the importance of this architecture in the development of adaptive immune responses. Orchestration of cells of the immune system in order to maximise cellular contact and proximity is crucial for enhancing cellular interaction and subsequent immune responses.

Expression of CXCL13, CCL19 and CCL21 is under the control of Lymphotoxin (LT) and tumour necrosis factor alpha (TNFα)ADDIN BEC{Ngo, 1999, π07635}(, 1999, π07635Νγο ετ αλ., 1999 and expression of Gp38/Podoplanin is dependent on LTβR signalling (Ngo et al., 2001) via expression of LT on LTi cells and provision of additional alternative signals from lymphocytes (Withers et al., 2007). LT and TNFα are structurally related members of the TNF

superfamily. Lymphotoxin alpha (LTα) forms a membrane bound heterotrimeric complex with Lymphotoxin beta (LTβ), $LT\alpha_1\beta_2$ and the corresponding receptor is the Lymphotoxin beta receptor (LTβR). In mice lacking either LTα or LTβ, chemokine levels are significantly reduced, leading to disrupted organisation of splenic white pulp, with little segregation of B and T zones (Ngo et al., 1999; Alimzhanov et al., 1997; Alexopoulou et al., 1998; Kuprash et al., 2002). Interestingly, *Tnfα*$^{-/-}$ mice demonstrate normal B/T cell segregation in the spleen, but with reduced expression of CXCL13, CCL19/21, albeit at less severely reduced levels than that seen in *Ltα*$^{-/-}$ or *Ltβ*$^{-/-}$ mice (Kuprash et al., 2002; Neumann et al., 1996; Ngo et al., 1999) (Table 1.3).

The maintenance of lymphoid tissue architecture is dependent on continued expression of LT and TNF. Indeed, the expression of CXCL13 by splenic stromal cells and the maintenance of FDCs in the B cell follicle, are dependent on LT and TNF expression by mature B cells (Endres et al., 1999; Fu et al., 1997). Additionally, the expression of peripheral node addressin (PNAd) and mucosal addressin cell adhesion molecule -1 (MAdCAM-1) by HEVs of the LN, and the marginal sinus of the spleen, are dependent on LT signalling (Rennert et al., 1998; Browning et al., 2005). Interestingly, in mice with a specific lack of LTβ expression on B cells, normal chemokine production, FDC differentiation and B cell follicle formation occurs (Tumanov et al., 2002; Tumanov et al., 2004), suggesting that LT expression by T cells is sufficient to induce/maintain these events. In addition to the maintenance of lymphoid tissue architecture, LT also plays a key role in homeostasis of DC populations (See Section 1.8.3).

1.4.1.3. Spleen and Lymph Node Function

There are many similarities in function and orchestration of immune responses in the spleen and LN. Both organs are responsible for sequestration of antigens and APCs and the structure, as already described, is arranged in such a way as to maximise presentation of these molecules and cells to B and T lymphocytes, thereby eliciting an immune response.

The LNs are responsible for filtering lymph fluid that has drained from peripheral tissue and free antigen and antigen-bearing DCs are trapped ready for recognition by naïve T cells. Circulating naïve T cells travel through the blood to lymphoid tissues in search of their cognate antigen. They express receptors for cell adhesion molecules and chemokine receptors, such as Integrin $\alpha_4\beta_7$ and CCR7, which allow them to enter the paracortex of the LN via HEVs, expressing MAdCAM-1 (ligand for Integrin $\alpha_4\beta_7$) (Berlin et al., 1993), and to home to T cell areas within the LN, which express CCL19/21 (ligands for CCR7) (Cuff et al., 1999). It is within the paracortex that naïve T cells encounter resident DCs presenting soluble antigen collected from the lymph fluid. Activation of naïve T cells results in the maturation of T_H cells and these effector cells exit the LN via the efferent lymph (Masopust et al., 2001; Iezzi et al., 2001). A unique subset of T cells remain and express CXCR5, the receptor for the B cell homing chemokine CXCL13, that is expressed in the cortical B cell areas of the LN, thus allowing migration to the primary B cell follicles in the cortex (Schaerli et al., 2001; Moser et al., 2002). These cells are termed T follicular helper cells (Tfh cells) and are able to promote terminal B cell differentiation and are critical for humoral immunity (Linterman and Vinuesa, 2010).

One of the key differences between spleen and LN function is the manner in which cells enter the organs. In the spleen, cells and antigens enter via the blood and

infiltrate through the marginal zone before leaving via the afferent splenic artery. Whereas, in the LN cells enter carried by lymph fluid, which enters the LN via multiple afferent lymphatics and permeates through the LN before leaving via the efferent lymphatic vessel. Naïve B and T cells are able to enter the LN through numerous HEVs, located in the paracortex, in a chemokine dependent manner (Mebius and Kraal, 2005; Crivellato et al., 2004).

1.4.2. Structure and Function of Peyer's Patches

1.4.2.1. Structure

Peyer's Patches (PPs) are organised lymphoid structures located along the anti-mesenteric border of the small intestine. PPs contain multiple, distinct large B cell follicles, with germinal centres and intervening T cell areas arranged within a reticular connective tissue network (Azzali, 2003) (Figure 1.2. C). This structure is separated from the intestinal lumen by follicle-associated epithelial cells (FAE), within the FAE, specialised microfold (M) cells can be found (Mowat, 2003). M cells are specialised enterocytes, lacking microvilli, capable of sampling antigens and invasive bacteria from the intestinal lumen (Kraehenbuhl and Neutra, 2000; Pabst et al., 2007). Beneath the FAE is the subepithelial dome, stromal cells in this area express VCAM-1 and selectively express receptor activator of nuclear factor-κB ligand (RANKL) (Taylor et al., 2007). VCAM-1 is expressed by activated endothelial cells and is involved in lymphocyte adhesion via it's ligand $\alpha_4\beta_1$ (also known as very late antigen-4, VLA-4) (Osborn et al., 1989; Chen et al., 1999). RANKL is a member of the TNF family that plays a major role in osteoclast differentiation and LN

development, and is also expressed by activated T cells promoting the survival and cytokine production of DCs (Wong et al., 1999; Josien et al., 1999; Blair et al., 2007).

1.4.3. Function

PPs are an important site for the production of specific IgA antibodies. The M cells provide a window for antigen sampling and uptake, allowing for presentation by APCs. M cells lack MHCII expression and are therefore unlikely to act as APCs (Mowat, 2003). The functional significance of M cells has been demonstrated by Knoop, *et al*, where they revealed a severe reduction or total lack of M cells in the PPs of *Rankl*$^{-/-}$ mice and showed that uptake of immunofluorescent beads from the intestinal lumen was reduced. Treatment of *Rankl*$^{-/-}$mice with exogenous RANKL restored M cells, and immunofluorescent bead uptake. Additionally, PP germinal centre formation and faecal IgA production in *Rankl*$^{-/-}$ mice was reduced compared with WT controls (Knoop et al., 2009). This indicates that M cells play a crucial role in the uptake of antigens and bacteria from the intestinal lumen and differentiation of M cells is dependent on RANKL.

Figure 1.2 Secondary and tertiary lymphoid tissue structures

A. Structure of the lymph node (LN). *Lymph fluid enters the LN via afferent lymphatics and leaves via the efferent lymphatics. The innermost region of the LN is the medulla, moving outwards to the paracortex, the location of T cells, recruited by CCL21 expression by resident stromal cells, and high endothelial venules (HEVs). The outermost region is the cortex, consisting of B cell follicles and CXCL13 expressing follicular DCs (FDCs). Surrounding these areas is the subcapsular sinus.*

B. Structure of the spleen*. Blood enters the white pulp of the spleen via the MAdCAM-1^{+} marginal zone, which is inhabited by specialised marginal zone B cells. Below this structure is the marginal sinus. The central area of the spleen is the T zone, containing stromal cells expressing CCL19/21, required for recruitment and retention of T cells. Central arterioles are located in the T zone. B-cell follicles are located around the T zone and FDCs in this area express CXCL13, as in the LN.*

C. Structure of cryptopatches (CPs), isolated lymphoid follicles (ILFs) and Peyer's patches (PPs). *CPs and ILFs are located in the small intestine and colon, PPs are located in the small intestine only. CPs consist of a cluster of LTi-like cells and DCs. CPs develop into ILFs following the recruitment of B cells. ILFs are made up of a central cluster of B cells, surrounded by DCs and interspersed with T cells. PPs have a structure similar to that of LNs, with a T zone, containing HEVs, surrounded by B cell follicles. The follicle-associated epithelium (FAE) is situated above the PP and contains specialised epithelial cells termed M-cells.*

A Lymph Node

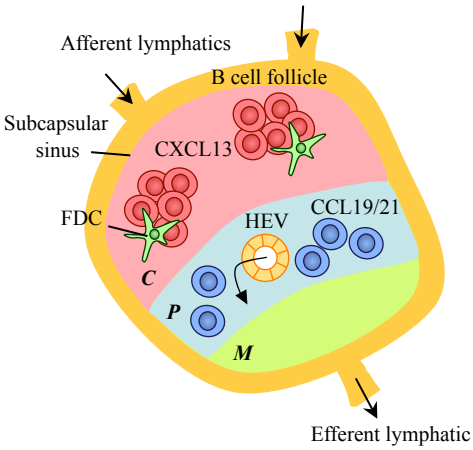

C: Cortex
P: Paracortex
M: Medulla

B Spleen- white pulp

FDC: Follicular DC
CA: Central arteriole
MZ: Marginal zone
MS: Marginal sinus
MMM: MZ metallophilic macrophages

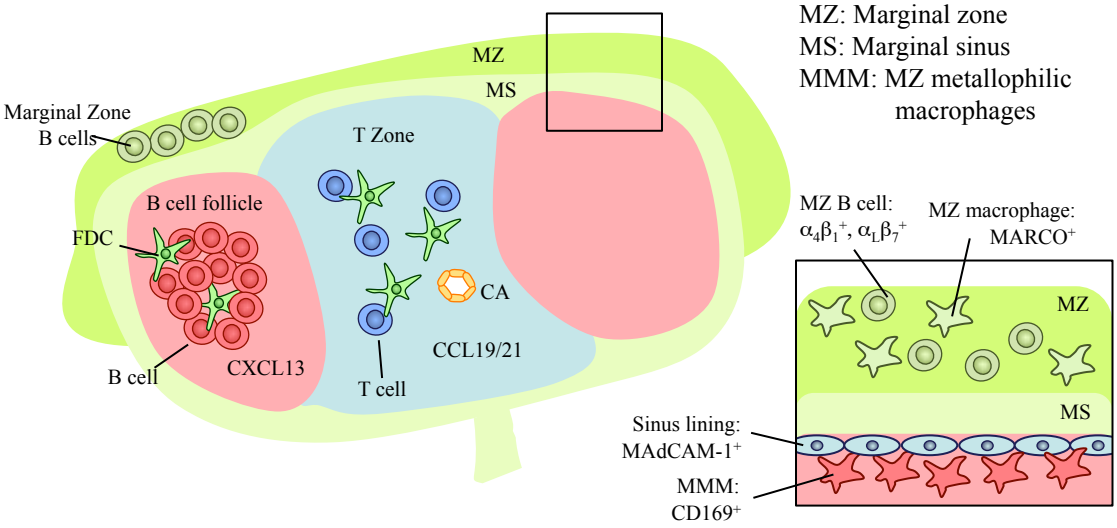

C Peyer's Patch, ILF and CP

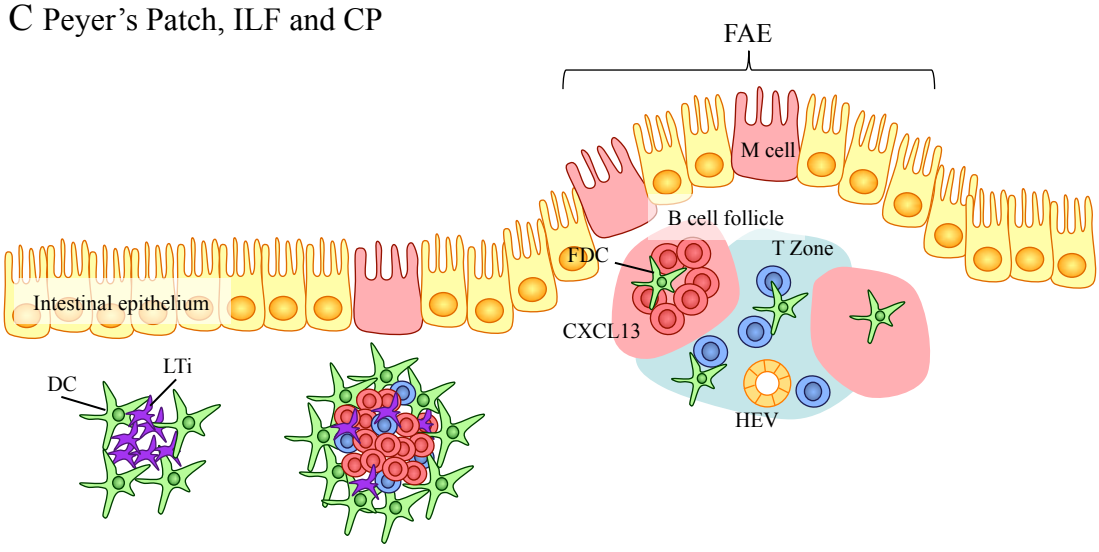

Cryptopatch

Isolated Lymphoid Follicle

Peyer's Patch

Figure 1.2

	Splenic architecture				
	Mouse model	*B/T cell segregation*	*B cell follicles/ GCs*	*Chemokine expression*	*Refs*
TNF & TNFR superfamily	*Lt$\alpha^{-/-}$*	×	×	× CXCL13 × CCL19/21	(Kuprash et al., 2002; Banks et al., 1995; Alexopoulou et al., 1998; Matsumoto et al., 1997)
	Lt$\beta^{-/-}$	✓*	×	× CXCL13 × CCL21 🡻 CCL19*	(Alimzhanov et al., 1997; Alexopoulou et al., 1998; Kuprash et al., 2002; Ngo et al., 1999)
	LtβR$^{-/-}$	×	×	-	(Fütterer et al., 1998)
	Tnf$^{-/-}$	✓	× B follicles	🡻 CXCL13 🡻 CCL19/21$^{\$}$	(Kuprash et al., 2002; Ngo et al., 1999)
	Tnfr$^{-/-}$	✓	× B follicles ✓ GC**	🡻 CXCL13 🡻 CCL19/21$^{\$}$	(Neumann et al., 1996; Ngo et al., 1999)
	Rankl$^{-/-}$	✓	+/- B follicles ✓ GC	-	(Kim et al., 2000)
	Rank$^{-/-}$	✓	✓	-	(Dougall et al., 1999)
NF-κB components	*Nfkb2$^{-/-}$*	✓	×	× CXCL13 🡻 CCL21 🡻 CCL19	(Franzoso et al., 1998; Caamaño et al., 1998)
	p100Δ	✓	✓	🡹 CXCL13 🡹 CCL21 🡻 CCL19	(Guo et al., 2007; Ishikawa et al., 1997)
	Rela$^{-/-}$ TnfrI$^{-/-}$	×	×	-	(Alcamo et al., 2002)
	c-rel$^{-/-}$	✓	×	-	(Weih and Caamaño, 2003)
	Relb$^{-/-}$	×	×	-	(Weih and Caamaño, 2003)
	Ikk$\alpha^{-/-}$	✓$^{\$\$}$	✓ B follicles$^{\$\$}$ × GC$^{\$\$}$	🡻 CXCL13 🡻 CCL21 🡻 CCL19	(Dejardin et al., 2002; Kaisho et al., 2001a)
	aly/aly	×	×	-	(Weih and Caamaño, 2003; Karrer et al., 2000; Miyawaki et al., 1994; Koike et al., 1996)
Chemokines & receptors	*Cxcl13$^{-/-}$*	✓	× B follicles ✓ GC**	× CXCL13	(Ansel et al., 2000)
	Cxcr5$^{-/-}$	✓	× B follicles ✓ GC**	✓ CXCL13	(Förster et al., 1996)
	Plt/plt	×$^{\pounds\pounds}$	✓ B follicles	× CCL21 × CCL19	(Nakano et al., 1998; Luther et al., 2000)
	Ccr7$^{-/-}$	×$^{\pounds}$	✓ B follicles ✓ GC$^{\pounds}$	-	(Förster et al., 1999)

Table 1.3 Overview of splenic architecture in various mouse models.

** The segregation of B/T cells in the spleen of Lt$\beta^{-/-}$ mice is more pronounced than in Lt$\alpha^{-/-}$ but not equivalent to WT. CCL19 mRNA expression slightly increased in Lt$\beta^{-/-}$ mice compared with Lt$\alpha^{-/-}$, may contribute to more discrete B/T cell areas.*

$^{\$}$ Splenic CCL19/21 mRNA in Tnf$^{-/-}$ and TnfrI$^{-/-}$, not reduced as much as Lt$\alpha^{-/-}$ mice.

*** Aberrant location of GC formation in TnfrI$^{-/-}$, Cxcl13$^{-/-}$ and Cxcr5$^{-/-}$ mice.*

$^{\$\$}$ BM chimeras, Rag2$^{-/-}$ host.

$^{\pounds}$ Ccr7$^{-/-}$ mice exhibited disorganised spleens, with randomly located T cells and aberrantly located B cell follicles and GCs.

$^{\pounds\pounds}$ Disrupted T cell localisation to white pulp.

1.5. Secondary Lymphoid Organ Development

1.5.1. Lymph Node Development

Development of SLO occurs during embryogenesis and begins with development of the mesenteric LN (mLN), followed by development of the LNs from head to tail (Mebius, 2003) (Figure 1.3). LN development proceeds along four main stages; i) formation of lymphatic endothelium and differentiation of mesenchymal precursors into primed stromal cells, ii) maturation of primed stromal cells into lymphoid tissue organiser (LTo) cells, iii) interaction of LTo cells and lymphoid tissue inducer (LTi) cells, and iv) recruitment of lymphocytes.

LTo cells were first identified during the investigation of PP development. At embryonic day 15.5 (E15.5), clusters of cells expressing VCAM-1 were identified (Adachi et al., 1997) and mice deficient in LTα or IL-7Rα, lacked these structures and did not develop PPs (Yoshida et al., 1999; Adachi et al., 1998; Adachi et al., 1997), indicating that these VCAM-1^+ cells were critical to PP development. Various studies identified that this population of VCAM-1^+ mesenchymal stromal cells also expressed ICAM-1, MAdCAM-1, RelB and RANKL, and showed that these cells were capable of interacting with LTi cells via expression of LTβR, and following this interaction were capable of producing adhesion molecules and chemokines (Adachi et al., 1997; Adachi et al., 1998; Yoshida et al., 1999; Hashi et al., 2001; Honda et al., 2001; Bénézech et al., 2010). Subsequently, LTo cells have been identified in LNs and shown to express CXCL13 and CCL19/21, in addition to the markers previously described (Cupedo et al., 2004).

LN development is dependent on the presence of LTi cells. Mebius *et al*, were the first to describe LTi cells, with the following surface marker expression: CD3$^-$

$CD4^+LT\beta^+CXCR5^+$ (Mebius et al., 1997). Further characterisation of these cells has been performed by various studies, demonstrating that LTi cells also express IL-7Rα, Integrin $\alpha_4\beta_7$, CCR7, RANK/RANK-L and RORγt (Mebius et al., 1996; Mebius et al., 1997; Kim et al., 2000; Dougall et al., 1999) (Table 1.5). Mice lacking LTi cells, such as *Rorγ*$^{-/-}$ mice, fail to develop any peripheral LNs (Kurebayashi et al., 2000).

LTo	***LTi***
$VCAM\text{-}1^{high}$	$CD3^-CD4^+$
$ICAM\text{-}1^{high}$	$IL\text{-}7R\alpha^+$
CXCL13	$CXCR5^+$
$MAdCAM\text{-}1^+$	Integrin $\alpha_4\beta_7$
$LT\beta R^+$	$LT\alpha_1\beta_2$
CCL19/21	CCR7
$RANK\text{-}L^{high}$	RANK/RANK-L

Table 1.4 Surface markers identifying lymphoid tissue inducer (LTi) cells and lymphoid tissue organiser (LTo) cells.

Figure 1.3 Ontogeny of lymphoid tissue development

Diagram depicting the timing of lymphoid tissue development during embryogenesis. The mesenteric lymph node (mLN) is the first to develop, with the inguinal LN developing around E16. The PPs develop around E17.

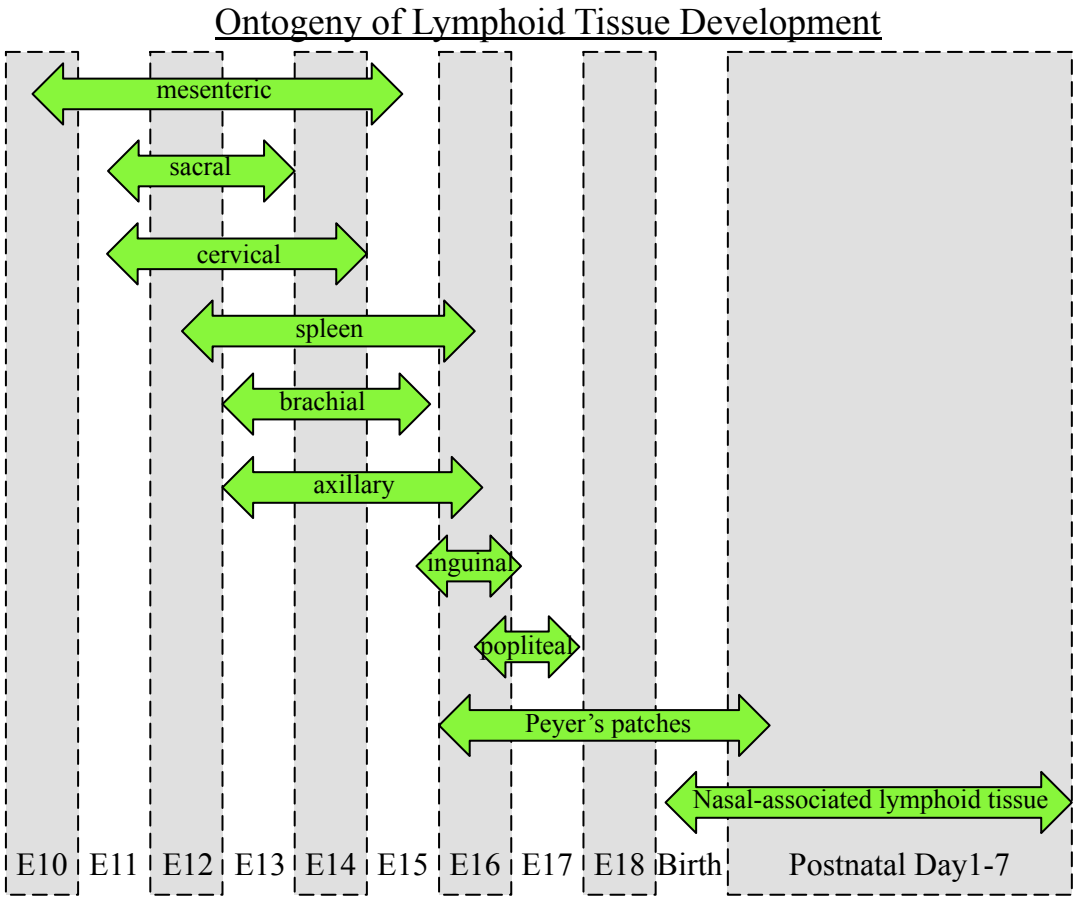

Adapted from Mebius, 2003, Nat Rev Immunol
Spleen: Mebius, 2005, Nat Rev Immunol

Figure 1.3

Figure 1.4 Lymph node development

LN development proceeds along four main stages; (1) Formation of lymphatic endothelium and differentiation of mesenchymal precursors into primed stromal cells, (2) maturation of primed stromal cells into LTo, (3) interaction of LTo and LTi cells, and (4) recruitment of lymphocytes.

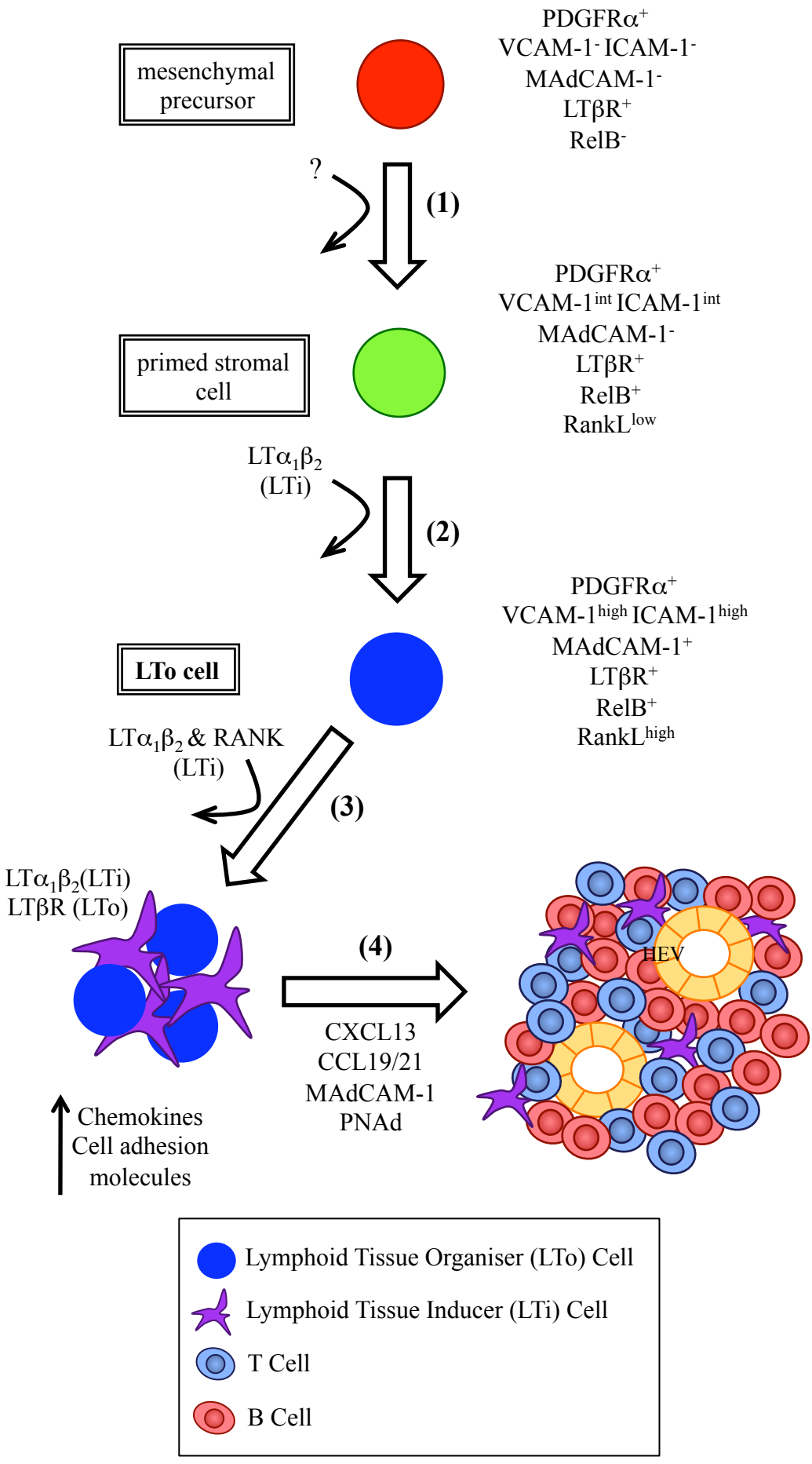
Lymph Node Development
mesenchymal precursor
PDGFRα+
VCAM-1- ICAM-1-
MAdCAM-1-
LTβR+
RelB-
?
(1)
primed stromal cell
PDGFRα+
VCAM-1int ICAM-1int
MAdCAM-1-
LTβR+
RelB+
RankLlow
LTα1β2
(LTi)
(2)
LTo cell
PDGFRα+
VCAM-1high ICAM-1high
MAdCAM-1+
LTβR+
RelB+
RankLhigh
LTα1β2 & RANK
(LTi)
(3)
LTα1β2(LTi)
LTβR (LTo)
(4)
HEV
CXCL13
CCL19/21
MAdCAM-1
PNAd
Chemokines
Cell adhesion molecules
Lymphoid Tissue Organiser (LTo) Cell
Lymphoid Tissue Inducer (LTi) Cell
T Cell
B Cell

Figure 1.4

1.5.1.1. Formation of Lymphatic Endothelium and Differentiation of Mesenchymal Precursors into Primed Stromal Cells

The initial stage of LN development is closely linked to that of the lymphatic vasculature and the formation of the lymph sac at the site of future LN development. It was proposed in 1902, by Sabin, that the lymph sac forms from endothelial cells budding from the blood vasculature during embryogenesis[253]. More recent studies have shown that cells expressing specific lymphatic endothelium markers, such as VEGFR3 (Kaipainen et al., 1995), Prox-1 (Wigle and Oliver, 1999) and Lyve-1, bud from the cardinal vein to form the lymph sac in response to VEGFC signals (Karkkainen et al., 2004). Indeed, mice deficient in Prox-1 were not able to develop lymph sacs. Interestingly however, they were able to develop primitive LN anlage and further work by Vondenhoff *et al*, indicated that the earliest stages of lymph node development did not depend on lymph sac formation (Vondenhoff et al., 2009).

It has been proposed that mesenchymal precursors, identified as $CD45^{-}ICAM\text{-}1^{-}VCAM\text{-}1^{-}MAdCAM\text{-}1^{-}LT\beta R^{+}RelB^{-}PDGFR\alpha^{+}$, give rise to LN stromal cells in a two-step maturation process (Bénézech et al., 2010) (Figure 1.4). The first step involves upregulation of ICAM-1 and VCAM-1 expression giving rise to a 'primed' stromal cell population, described as $CD45^{-}ICAM\text{-}1^{int}VCAM\text{-}1^{int}MAdCAM\text{-}1^{-}LT\beta R^{+}RelB^{+}PDGFR\alpha^{+}$. This step was shown to be independent of LTβR signalling and LTi cell presence, as in $Lt\beta R^{-/-}$ mice, and in $Ror\gamma^{-/-}$ mice lacking LTi cells, this population of cells was still present. The second maturation step involves further upregulation of ICAM-1 and VCAM-1, and induced expression of MAdCAM-1, producing a unique LTo cell population (see below) (Bénézech et al., 2010).

1.5.1.2. Maturation of Primed Stromal Cells into LTo Cells

Benezech *et al*, proposed a model for LTo cell maturation in LN development, whereby following LTβR engagement, ICAM-1^{int}VCAM-1^{int} 'primed' stromal cells are able to mature into ICAM^{hi}VCAM^{hi} LTo cells (Bénézech et al., 2010). The maturation of LTo cells is dependent on LTβR, as *Ltβr*$^{-/-}$ mice lack this cell population. The appearance of LTi cells in the inguinal LN between E15-E17 corresponds with the maturation of LTo cells, indicating that LTi cells are providing the lymphotoxin signal crucial for LTo cell maturation (Bénézech et al., 2010) (Figure 1.4).

1.5.1.3. Interaction of LTo and LTi Cells

The interaction of LTo and LTi cells is a critical event in LN development. Mice lacking LTi cells, such as the *Rorγ*$^{-/-}$ mice, do not develop LNs (Sun et al., 2000; Kurebayashi et al., 2000) and it is the expression of LT$\alpha_1\beta_2$ by LTi cells that is essential for crosstalk with LTβR expressing LTo cells. Interestingly, a recent study provided evidence that clustering of LTi cells with LTo cells, via LTo cell expression of CXCL13, occurred independently of LT and was instead induced by retinoic acid (RA) (van de Pavert et al., 2009). In addition to LT$\alpha_1\beta_2$-LTβR signalling between LTi and LTo cells, signalling via the RANKL-RANK axis is also crucial for LN development (Randall et al., 2008). Mice lacking RANKL, RANK or TRAF-6, the critical component of downstream RANK signalling, do not develop LNs (Naito et al., 1999; Kong et al., 1999; Kim et al., 2000; Dougall et al., 1999). It has been well described that LTi cells express RANK, as well as, RANKL, and that LTo cells

express RANKL. The expression of RANKL on LTo cells promotes differentiation and survival of LTi cells, whilst also inducing upregulation of $LT\alpha_1\beta_2$ on the surface of LTi cells (Yoshida et al., 2002; Cupedo et al., 2004). These steps initiate a positive feedback loop, where more LTi cells are recruited to the LN anlage with subsequent further stimulation and maturation of LTo cells. This interaction is likely to be important for providing LTo cells with sustained signalling through LTβR, potentially leading to activation of the NF-κB transcription factors and induction of *Nfkb2* and *Relb* transcription, thus resulting in activation of the alternative NF-κB signalling pathway. Activation of this pathway leads to expression of high levels of chemokines such as CCL19, CCL21 and CXCL13 (Guo et al., 2007). These chemokines are responsible for the recruitment of mature lymphocytes to the LN anlagen. (Figure 1.4)

1.5.1.4. Recruitment of Peripheral Lymphocytes

After sufficient LTo/LTi cell clustering, differentiation of HEVs occurs within mesenteric and peripheral LNs, allowing the influx of lymphocytes. Initially, HEVs express the cell addressin molecule MAdCAM-1 (Mebius et al., 1996), allowing entrance only of cells expressing Integrin $\alpha_4\beta_7$, such as LTi cells and γδ T cells (Mebius et al., 1997; Mebius et al., 1998; Yoshida et al., 2001). From postnatal day three, MAdCAM-1 expression is downregulated and PNAd expression is upregulated, this allows for the entrance of mature B and T lymphocytes (Mebius et al., 1996). The recruitment of lymphocytes to the LN anlage and their role in providing a constant source of surface LT, enables further differentiation of stromal cells to form specialised B and T cell areas. The molecules responsible for the demarcation of B and T zones include, CXCL13, CCL19 and CCL21. LTi cells express the receptors for these molecules (CXCR5 and CCR7, respectively), with B lymphocytes

expressing CXCR5, and T lymphocytes expressing CCR7. The differential expression of chemokines by the stromal cells, and of their receptors on B and T lymphocytes, allows organisation into specific B and T cell areas within the developing LN. Moreover, in order to sustain LN development and organisation postnatally, LN stromal cells require stimulation by newly immigrated IL-7Rα^+ T and natural killer (NK) cells (Coles et al., 2006).

1.5.2. Peyer's Patch Development

The formation of PPs follows a sequence of developmental steps similar to LN development, but with several key differences. Three main steps have been identified by immunohistochemical analysis (Figure 1.5).

The first step occurs around E15.5 with clustering of VCAM-1$^+$ICAM-1$^+$ LTo cells (Adachi et al., 1997; Yoshida et al., 1999), the phenotype of which is reflected in a stromal cell population identified in LN development (Cupedo et al., 2004). The differentiation of LTo cells from resident stromal cells is promoted by lymphoid tissue initiator cells (LTint). LTint are identified as CD4$^-$CD3$^-$IL7Rα^-c-kit$^+$CD11c$^+$, they express LT and are present in the gut from E15.5, depletion of these cells results in a drastic decrease in PP development (Veiga-Fernandes et al., 2007). In addition to the interaction of LTint and LTo cells via LT$\alpha_1\beta_2$/LTβR axis, signalling via the tyrosine kinase receptor, RET, expressed on LTint, and its ligand, ARTN, expressed on LTo cells, is also thought to play a key role in PP anlagen formation. Interestingly, in *Ret*$^{-/-}$ mice, normal numbers of LTint were observed in the gut at E15.5, but were unable to form clusters and PP anlage development was blocked, indicating that signalling via RET enables migration and aggregation of LTint (Veiga-Fernandes et

al., 2007). Importantly, the identification of LTint in LN anlagen has not been described to date.

The second stage of PP development involves the accumulation of LTi cells within the LTo cell clusters at around E17.5. LTi cells express Integrin $\alpha_4\beta_7$, allowing them to interact with MAdCAM-1 expressing LTo cells, thereby stimulating further clustering of the latter (Adachi et al., 1997; Yoshida et al., 1999). In addition, the expression of $LT\alpha_1\beta_2$ on LTi cells is upregulated by exposure to IL-7 inducing further recruitment of LTi cells to the PP anlagen (Yoshida et al., 2002). A key difference between PP and LN development is the requirement for the IL-7/IL-7Rα axis in PP development, which is dispensable for LN formation; *Il7rα*$^{-/-}$ mice lack PPs but do develop most LNs (Adachi et al., 1998). This differs from LN development where formation depends on RANK-L/RANK expression, not on IL-7 expression. PP development occurs independently of RANK-L/RANK expression (Kim et al., 2000; Kong et al., 1999).

The final stage of PP development occurs around E18.5 and involves compartmentalisation and recruitment of mature lymphocytes. This proceeds through the same mechanism as for LN development; LTi cell signal via LTβR to LTo cells and induction of chemokines and cell adhesion molecules ensues, enabling recruitment of mature lymphocytes. Initially, at E18.5 aggregates of $CD11c^+$ cells (most likely reflecting the LTint population, described by Veiga-Fernandes (Veiga-Fernandes et al., 2007)) and LTi cells are present, forming the basis of future B cell follicles (Hashi et al., 2001). Mature B and T lymphocytes are present in the PP anlagen at this stage but are not organised into distinct areas, this begins from postnatal day one onwards. The compartmentalisation of the PP anlagen is not

dependent on T lymphocytes, as *SCID* mice, lacking the latter, still exhibit a degree of compartmentalisation in the PP anlagen (Hashi et al., 2001).

Figure 1.5 Peyer's patch development

Peyer's patch development proceeds through three main steps; (1) LTint promotion of LTo cell clustering around E15.5, (2) Interaction of LTo and LTi cells around E17.5, as seen in LN development, (3) recruitment of mature lymphocytes around E18.5. Finally, B and T cells are organised into specific areas from postnatal day one onwards.

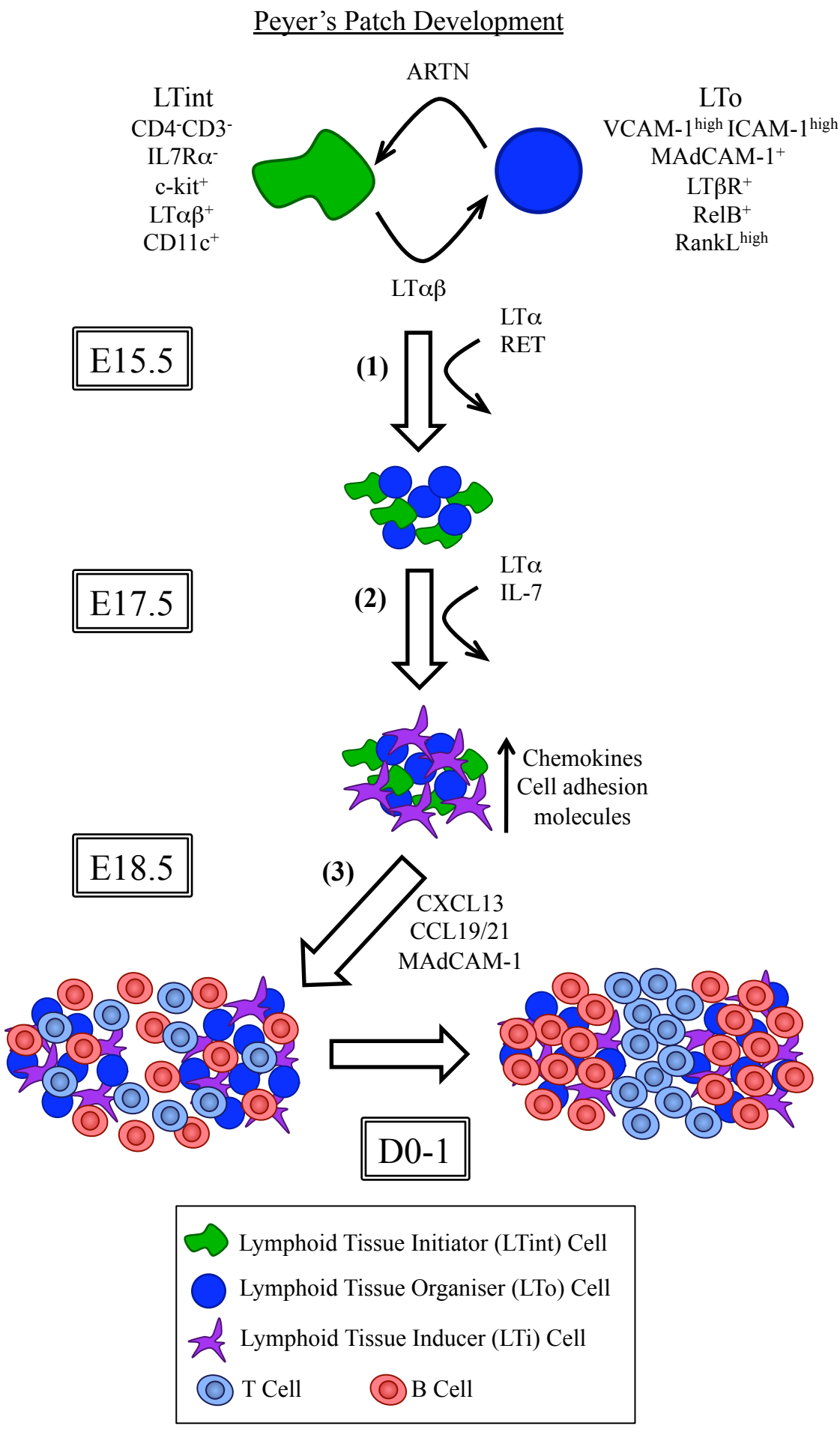
Peyer's Patch Development
ARTN
LTint
CD4-CD3-
IL7Rα-
c-kit+
LTαβ+
CD11c+
LTo
VCAM-1high ICAM-1high
MAdCAM-1+
LTβR+
RelB+
RankLhigh
LTαβ
E15.5
(1)
LTα
RET
E17.5
(2)
LTα
IL-7
Chemokines
Cell adhesion
molecules
E18.5
(3)
CXCL13
CCL19/21
MAdCAM-1
D0-1
Lymphoid Tissue Initiator (LTint) Cell
Lymphoid Tissue Organiser (LTo) Cell
Lymphoid Tissue Inducer (LTi) Cell
T Cell
B Cell

Figure 1.5

1.6. Tertiary Lymphoid Organs

Tertiary lymphoid organs (TLOs) differ from SLOs in that they develop postnatally and are inducible, and are located predominately at mucosal sites. Induction of TLOs can occur under steady-state, inflammatory or autoimmune conditions and formation of TLOs can, to a certain extent, be reversible. Of particular importance and interest is the development of intestinal tertiary lymphoid tissues, which includes cryptopatches (CPs) and isolated lymphoid follicles (ILFs). The formation of these structures involves intricate interactions between haematopoietic and stromal cell compartments, in much the same way as in LN and PP development.

1.6.1. Isolated Lymphoid Follicle Structure and Function

1.6.1.1. Structure

ILFs are located throughout the small intestine and colon, and consist of organised clusters of B and T lymphocytes, and DCs (Figure 1.2. C). Hamada *et al*, were the first to identify murine ILFs and defined them as aggregates of $B220^+$ B cells present along the mucosa of the intestine. Accompanying the B cells, various other cell types were identified including, c-kit^+IL7-Rα^+ LTi-like cells, $CD3^+$ T cells, and $CD11c^+$ DCs (Hamada et al., 2002). The B cells present within ILFs have been characterised by several studies, to be predominately B-2 B cells, based on expression of CD23 and lack of CD5 (Hamada et al., 2002; Wang et al., 2006; Lorenz et al., 2003), and display a mature phenotype, co-expressing IgM and IgD (Wang et al., 2006). Functionally, ILF B cells preferentially differentiate to produce IgA plasma

cells, rather than IgG or IgM, and their cytokine profile demonstrates IL-4 and IL-10 production, differing from that of splenic and PP B cells (Wang et al., 2006).

Recruitment of B lymphocytes to the gut utilises various chemokines and cell adhesion molecules. ILF B cells express Integrin $\alpha_4\beta_7$ and are able to migrate into the intestine in response to MAdCAM-1, expressed on vessels associated with ILFs (Wang et al., 2008). Indeed, mice lacking β_7 failed to develop the normal number of intestinal ILFs and the use of blocking antibodies to $\alpha_4\beta_7$ or MAdCAM-1 resulted in ablation of B cell aggregation (Wang et al., 2008). Additionally, ILF B cells express CCR6 and expression is increased compared with equivalent B cells from the spleen (McDonald et al., 2007). CCR6 is the only receptor for CCL20 (Liao et al., 1997); a chemokine expressed by colonic epithelium (Tanaka et al., 1999) and is important for the localisation of B cells to the intestine and subsequent aggregation into ILFs (McDonald et al., 2007; Williams, 2006).

Stromal cells play a key role in tertiary lymphoid tissue structure and organisation and this is highlighted by several studies investigating the ILF stromal cell compartment. The accumulation of VCAM-1^+ICAM-1^+ LTo cells into clusters marks the initial stages of LN and PP development, Taylor *et al*, identified VCAM-1^+ cells situated in CPs and ILFs, and proposed these cells to reflect the LTo cells seen in LN and PP development. Within the intestine, the expression of FDCM1, CD157 (BP-3) and VCAM-1 by ILF stromal cells, was dependent on functional NIK, thereby requiring activation of the alternative NF-κB pathway for their expression. RANKL is also expressed, but independently of NIK (Taylor et al., 2007). Additionally, ILF stromal cells express CCL20 (McDonald et al., 2007) and VCAM-1, and vessels associated with ILFs express MAdCAM-1 and CD31 (Wang et al., 2008).

1.6.1.2. Function

The organised follicular structure of intestinal ILFs and the presence of B cells exhibiting preferential class-switching to IgA plasma cells, along with the presence of T cells and antigen-presenting DCs alludes to a role as sites for induction of mucosal immunity. The function of PPs as important sites of mucosal immunity is well understood, however, a study by Yamamoto *et al*, demonstrated that mice treated *in-utero* with antagonistic LTβR-Ig, to ablate PP development, were still able to produce Ag-specific intestinal IgA (Yamamoto et al., 2000). Mice treated this way demonstrated a significant increase in intestinal ILF formation, in a potentially compensatory mechanism for the loss of PP development (Kweon et al., 2005). This data suggests that ILFs are able to function as inductive sites for producing Ag-specific intestinal IgA.

1.6.2. Isolated Lymphoid Follicle Development

The formation of ILFs is thought to follow developmental steps similar to those of LNs and PPs. LTβR signalling during secondary lymphoid tissue development revolves around the expression of $LT\alpha_1\beta_2$ on LTi cells. The initial clustering of these cells is critical for LN development and it is suggested that this is mirrored in ILF development, by the formation of ILF precursor structures termed cryptopatches (CPs) (Eberl, 2005) (Figure 1.6).

CPs owe their name to the location in the intestinal crypt at the base of villi. CPs were first described by Kanamori *et al*, as being composed of clusters of $Lin^-c\text{-}kit^+$ lymphoid cells and DCs (Kanamori et al., 1996) and are distinguished from ILFs by their lack of B and T cells (Hamada et al., 2002). It has been shown that $Lin^-c\text{-}kit^+$

lymphoid cells present in CPs present with LTi cell-like characteristics, including expression of IL-7Rα, and RORγt, whilst lacking lineage markers such as CD3, B220, CD11b, CD11c and Gr-1 (Saito et al., 1998; Eberl and Littman, 2004). Eberl suggested the model of CP development into ILFs (Eberl, 2005), a model that does not recognize CPs and ILFs as distinct structures but as structures representative of a spectrum of stages in intestinal lymphoid tissue development (Pabst et al., 2005; Bouskra et al., 2008; Ivanov et al., 2006). Studies of a variety of mutant mouse models have elucidated that CP development is dependent on LTα, LTβ, LTβR and RORγt, as mice deficient in any of these molecules fail to develop CPs and subsequent ILFs (Taylor et al., 2004; Pabst et al., 2005; Eberl and Littman, 2004; McDonald et al., 2010). Thus demonstrating that LTi-like cells and the $LT\alpha_1\beta_2$-LTβR signalling axis are essential for the development of intestinal lymphoid tissue, as well as for LN and PP development. The development of CPs occurs independently of NIK, CCR6, Integrin $\alpha_4\beta_7$ and lymphocytes, as CP structures have been observed in *aly/aly* mice (expressing a non-functional form of NIK), *Ccr6*$^{-/-}$ mice (Lügering and Kucharzik, 2006), $\beta_7^{-/-}$ mice (Wang et al., 2008) and mice lacking lymphocytes, such as *Rag*$^{-/-}$ and *SCID* mice (Hamada et al., 2002) (Table 1.5).

The transition of CPs to ILFs is defined by the recruitment of B cells to the structure, a process that is dependent on NIK (Hamada et al., 2002), B cell expression of CCR6 (Lügering and Kucharzik, 2006), Integrin $\alpha_4\beta_7$ (Wang et al., 2008), and CXCR5 (Velaga et al., 2009) and, by definition, lymphocytes, a situation opposing that of CP development (Table 1.5). To date there are no mouse models where the development of ILFs has been observed in the absence of CP development, supporting the theory that ILFs develop from CPs. Moreover, the common dependence of CP and ILF development on LTα, LTβ, LTβR and RORγt further

supports this hypothesis. In addition, it has been shown that it is LTα-sufficient B cells and LTβR expressing stromal cells, that are required for ILF formation, as LTα-sufficient B cells transferred into LTα-deficient mice results in ILF formation, and in *Ltβr*$^{-/-}$ mice receiving WT BM ILFs fail to develop (Lorenz et al., 2003; Taylor et al., 2004). Interestingly, ILF ontogeny differs from that of PPs in the timing during embryogenesis when LTβR signalling is required. PPs require LTβR signalling between E14-17, and blockage at this point results in a lack of PP development with a corresponding, and potentially compensatory, development of large numbers of ILFs (Kweon et al., 2005).

Additionally, LTβR signalling is important in the formation of other tertiary lymphoid tissues such as in aged *ApoE*$^{-/-}$ mice, where LTβR signalling is responsible for the formation of aortic tertiary lymphoid organs and LTβR signal blockage disrupted these structures (Gräbner et al., 2009).

Importantly, it has been shown that ILF formation and maturation is dependent on gut flora (Hamada et al., 2002; Lorenz et al., 2003), in a NOD1 dependent manner (Bouskra et al., 2008). NOD1 binds Peptidoglycan from Gram-negative bacteria. The number of ILFs present in the colon of WT mice housed under Germ-free conditions was severely reduced compared with WT mice residing in specific pathogen free (SPF) conditions, a similar reduction of ILFs was observed in mice deficient for NOD1 (Bouskra et al., 2008). However, in mice deficient for TLR2/4, or MyD88, the molecule involved in downstream signalling of TLRs, induction of ILFs was comparable with WT mice (Bouskra et al., 2008). Interestingly, in mice lacking AID (activation-induced cytidine deaminase), where the intestinal bacterial load is increased due to lack of IgA production in the gut, an increase in

number and size of ILFs was observed, a phenotype which was rescued following treatment with antibiotics to reduce bacterial load (Fagarasan et al., 2002).

The interaction of intestinal stromal cells, resident and migratory haematopoietic cells and gut commensal bacteria, clearly plays an important role in ILF development. Ivanov proposes a model for CP transition to ILFs that follows DC activation by intestinal bacteria, resulting in the recruitment of B cells and some T cells into CP structures. This recruitment could occur via several mechanisms; direct action of CP-derived DCs on B and T cells; the activation of CP stromal cells by DCs; the indirect activation of stromal cells via stimulation of LTi-like cells, with all of these mechanisms resulting in direct recruitment of B and T cells or alterations in chemokine expression allowing B and T migration to the CPs (Ivanov et al., 2006).

	Mouse model	LNs	PPs	CPs	ILFs	Refs
TNF & TNFR superfamily	*Lt$\alpha^{-/-}$*	×	×	×	×	(Ivanov et al., 2006; De Togni et al., 1994; Hamada et al., 2002; Banks et al., 1995; Taylor et al., 2004; Lorenz et al., 2003)
	Lt$\beta^{-/-}$	× peripheral LNs ≈75% have mLNs	×	×	×	(Alimzhanov et al., 1997; Pabst et al., 2005)
	LtβR$^{-/-}$	×	×	×	×	(Fütterer et al., 1998; Ivanov et al., 2006; Taylor et al., 2004; Lorenz et al., 2003)
	Tnf$^{-/-}$	✓	↓	✓	✓	(Pasparakis et al., 1997; Ivanov et al., 2006)
	Tnfr$^{-/-}$	✓	↓(small)	✓	✓	(Neumann et al., 1996; Ivanov et al., 2006; Lorenz et al., 2003)
	Rankl$^{-/-}$	×	✓	?	?	(Kong et al., 1999; Kim et al., 2000; Ivanov et al., 2006)
	Rank$^{-/-}$	×	✓	?	?	(Dougall et al., 1999)
NF-κB components	*Rela$^{-/-}$ TnfrI$^{-/-}$*	×	×	?	?	(Alcamo et al., 2002)
	Nfkb1$^{-/-}$	✓	↓No.			(Paxian et al., 2002; Weih and Caamaño, 2003)
	Nfkb2$^{-/-}$	✓ ×*	✓×*	✓*	✓	(Carragher et al., 2004; Paxian et al., 2002; Weih and Caamaño, 2003) This study
	p100Δ	✓	✓	✓	↑No.	(Ishikawa et al., 1997) This study.
	Rela$^{-/-}$ TnfrI$^{-/-}$	×	×	?	?	(Alcamo et al., 2002)
	Relb$^{-/-}$	×	×	?	×	(Weih et al., 1995; Yilmaz et al., 2003; Weih and Caamaño, 2003) This study.
	c-rel$^{-/-}$	✓	✓	?	?	(Weih and Caamaño, 2003)
	Ikk$\alpha^{-/-}$	?	×	?	?	(Matsushima et al., 2001)
	aly/aly	×	×	✓	×	(Shinkura et al., 1999; Miyawaki et al., 1994; Ivanov et al., 2006; Hamada et al., 2002; Taylor et al., 2004; Karrer et al., 2000)
	Nik$^{-/-}$	×	×	?	?	(Yin et al., 2001)
Chemokines & receptors	*Cxcl13$^{-/-}$*	✓	× (0-2 formed)	?	?	(Ansel et al., 2000)
	Cxcr5$^{-/-}$	✓	×	×$^{\$}$	×$^{\$}$	(Velaga et al., 2009; Förster et al., 1996; Ansel et al., 2000)
	Ccr6$^{-/-}$			✓	×	(McDonald et al., 2007)
Other	*Traf6$^{-/-}$*	×	✓	?	?	(Kong et al., 1999)
	Plt/plt	✓	✓	?	?	(Nakano et al., 1998)
	Ret$^{-/-}$		↓	?	?	(Veiga-Fernandes et al., 2007)
	β7$^{-/-}$			✓	×	(Wang et al., 2008)
	Il7R$^{-/-}$	✓	×	↓	✓(small)	(Ivanov et al., 2006; Adachi et al., 1998; Hamada et al., 2002)
	ROR$\gamma^{-/-}$	×	×	×	×	(Kurebayashi et al., 2000; Sun et al., 2000; Eberl et al., 2004; Ivanov et al., 2006; Eberl and Littman, 2004)
	Rag$^{-/-}$	✓	✓(small)	✓(large)	×	(Hamada et al., 2002; Ivanov et al., 2006)

Table 1.5 Overview of the development of secondary and tertiary lymphoid tissue in various mouse models.

** The LNs and PPs that develop in Nfkb2$^{-/-}$ mice are reduced in size and number and consist of mainly of T lymphocytes with no B cell follicles.*

Figure 1.6 Isolated lymphoid follicle development

The initial clustering of LTi cells is critical for LN development and it is suggested that this is mirrored in isolated lymphoid follicle (ILF) development, by the formation of ILF precursor structures, termed cryptopatches. Recruitment of B cells to CP structures defines the transition from CP to ILF.

Development of Isolated Lymphoid Follicles

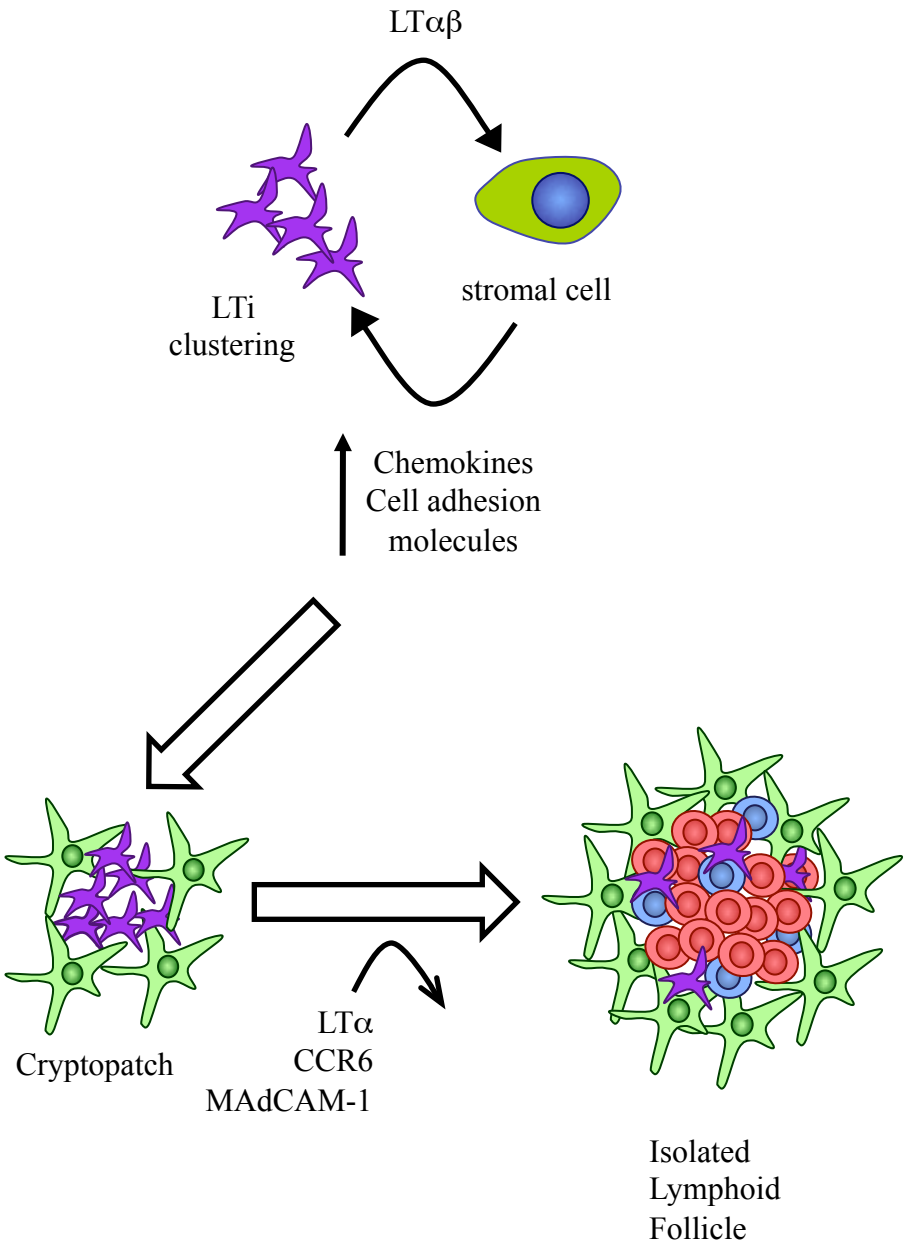

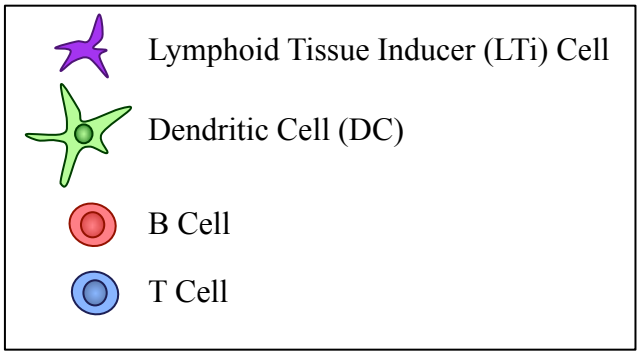

Figure 1.6

1.7. Innate Immunity

The innate immune system is an evolutionary ancient system for defence against pathogenic microorganisms. The innate immune system utilises recognition molecules that are germ-line encoded, thus enabling genetic inheritance and these molecules have therefore evolved by natural selection to be specific for recognition of infectious microorganisms. This contrasts with the adaptive immune system, where B and T cell receptors are generated by random somatic mutations to generate a diverse repertoire of receptors capable of recognising a vast array of antigens, whether they are pathogenic, innocuous or self-antigens. Due to the somatic generation of the B and T cell receptors, the range of specificities produced in an individual's life cannot be passed on to offspring, no matter how beneficial they may be (Medzhitov and Janeway, 2000; Medzhitov, 2010; Iwasaki and Medzhitov, 2010).

1.7.1. PAMPs and PRRs

The innate immune system utilises recognition molecules that are designed to identify groups of microorganisms, based on pathogen-associated molecular patterns (PAMPs). PAMPs are highly conserved invariant structures shared by molecules expressed by particular groups of microorganisms, for example LPS is produced by all Gram-negative bacteria, and the PAMP Lipoteichoic acid, is produced by Gram-positive bacteria. Other types of molecules recognised as PAMPs include Peptidoglycan, Mannans, bacterial DNA and single/double-stranded RNA. The receptors for PAMPs are pattern recognition receptors (PRRs) and are expressed by cells of the innate immune system (Medzhitov and Janeway, 2000).

There are three main structural groups of PRRs: secreted, cytosolic and transmembrane. Secreted PRRs, including collectins and ficolins, act as opsonins, binding to microbial surfaces and inducing activation of complement pathways and label the microbe for phagocytosis. Cytosolic PRRs include RIG-1-like receptors (RLRs), which are capable of recognising ssRNA and dsRNA associated with viral pathogens, and nucleotide-binding domain and leucine-rich repeat-containing receptors (NLRs), which can detect pathogens and stress signals. Transmembrane PRRs include, C-type lectins and Toll-like receptors (TLRs), of which TLRs are the most studied and well characterised (Iwasaki and Medzhitov, 2010).

1.7.2. Toll-like Receptors

TLRs are a family of receptors capable of recognising particular PAMPs (Table 1.6). Toll receptors were first discovered in *Drosophila* before the identification of mammalian homologues termed Toll-like Receptors (TLRs). The Toll family of receptors in *Drosophila* were shown to be involved in fly embryogenesis (Hashimoto et al., 1988) and, importantly, ligation of Toll receptors induced the activation of NF-κB, a transcription factor known to be involved in the production of inflammatory molecules (Belvin and Anderson, 1996). Studies of *Drosophila* with a loss-of-function mutation in the *Toll* gene demonstrated increased susceptibility to fungal infections, indicating the need for Toll receptors in innate immunity (Lemaitre et al., 1996). The first mammalian TLR identified, later designated TLR4, was shown to induce NF-κB signalling and production of cytokines and costimulatory molecules involved in adaptive immune responses (Medzhitov et al., 1997; Rock et al., 1998). To date, at least ten mammalian TLRs have been identified (Table 1.6).

TLRs are expressed by various cell types including cells of the innate immune system, such as macrophages and DCs. The assessment of TLR expression by such cells, has been hindered by the lack of effective antibodies to detect TLRs and by differences in expression between freshly isolated cells and *in-vitro* derived cells (Boonstra et al., 2003). However, all freshly isolated murine splenic DCs express TLR1, 2, 4, 6, 8 and 9, with plasmacytoid DCs lacking expression of TLR3 and $CD8a^+$ DCs lacking expression of TLR5 and TLR7 (Edwards et al., 2003).

TLR	*PAMP*
TLR1/TLR2	Lipoteichoic acid Lipoproteins (Gram+ bacteria)
TLR2/TLR6	
TLR4	LPS (Gram- bacteria)
TLR5	Flagellin
TLR3	dsRNA
TLR7	ssRNA
TLR9	dsDNA

Table 1.6 Toll-like Receptors (TLRs) and their respective Pathogen-associated Molecular Patterns (PAMPs).

1.8. Dendritic Cells

1.8.1. Dendritic Cells in Innate and Adaptive Immunity

Interaction between the innate and adaptive immune systems is central to the promotion of efficient pathogen recognition, leading to initiation of antigen-specific immune responses and development of immunological memory. An important aspect of this crosstalk is mediated through TLR ligation-induced upregulation of co-stimulatory molecules on APCs, which then enables interaction and activation of cells of the adaptive immune system.

The key cells involved in this innate control of adaptive responses are DCs. DCs are APCs, involved in presentation of antigenic peptides by MHC molecules to T cells. TLR stimulation of splenic DCs induces up-regulation of CCR7 (Sallusto et al., 1998; Dieu et al., 1998), a receptor critical for migration of DCs to T cell areas in the spleen and LNs, this results in interaction of DCs with T cells and subsequent T cell activation. Activation of T cells requires two signals: i) recognition of the TCR cognate antigen presented by MHC molecules on APCs; ii) co-stimulatory signalling via CD28, expressed on T cells, and CD80 or CD86, expressed on activated APCs. Ligation of the TCR without the second co-stimulatory signal results is T cell anergy. The expression of CD80/CD86 on DCs is upregulated upon activation and maturation, and the main pathway controlling this occurs by TLR recognition of PAMPs (Medzhitov, 2001; Kaisho et al., 2001b; Michelsen et al., 2001; Weatherill et al., 2005). In this way, T cells require signalling through TCR engagement with microbe-derived peptide presented on MHC and co-stimulatory signalling from TLR activation-induced CD80/CD86 expression on DCs. This is the fundamental link between the innate and adaptive immune systems.

1.8.2. Dendritic Cell Origin and Homeostasis

The origin of the vast heterogenous populations of DCs is complicated. In its most basic form, monocyte, macrophage and dendritic cell precursors (MDPs) give rise to monocytes and common DC precursors (CDPs) (Figure 1.7). Monocytes are able to migrate to areas of inflammation and differentiate into subsets of macrophages and inflammatory DCs. CDPs are able to generate plasmacytoid DCs (PDCs) and precursors of conventional DCs (pre-cDCs), both of which are released from the BM into the blood. The blood-borne pre-cDCs migrate to lymphoid tissues, before

undergoing proliferation, differentiation and maturation into mature cDCs (Liu et al., 2009), a process controlled by regulatory T cells (T regs), Flt3 and LTbR (Geissmann et al., 2010).

Under steady state conditions the peripheral DC pool needs to be maintained in order to allow efficient and rapid responses to antigenic challenge. This homeostasis of DCs occurs by continual seeding of the periphery by pre-cDCs and by local proliferation, a process regulated by LTβR. In mice deficient for LTβR, LTα or LTβ, a reduction in splenic DC numbers was observed, with a preferential decrease in $CD11c^{high}CD8\alpha^-$ DCs (Wu et al., 1999; Abe et al., 2003; De Trez et al., 2008; Wang et al., 2005). DC subsets express LTβR and *in vitro* bone marrow DC cultures revealed that DC numbers were increased following treatment with agonist LTβR antibody (Kabashima et al., 2005). There are two known ligands for LTβR: $LT\alpha_1\beta_2$ and LIGHT, these are expressed by B and T lymphocytes and it could be that these cell types are responsible for providing the LTβR signalling that DCs require for their homeostasis (Kabashima et al., 2005). In addition to this, it has also been shown that ligation of RANK expressed on DCs increases survival, but is not necessary for maturation (Josien et al., 2000), stimulation of CD40 expressed on DCs contributes to their survival and maturation (Caux et al., 1994; Miga et al., 2001; Mackey et al., 1998) and a component of the signalling pathway downstream of CD40, TRAF6, has been shown as necessary for the development of splenic $CD8\alpha^-$ cDCs (Ardavín, 2003; Kobayashi et al., 2003).

The involvement of LTβR, RANK and CD40 in DC homeostasis, survival and maturation and the fact that activation of the classical and alternative NF-κB pathways occurs following ligation of these receptors, indicates that these signalling pathways play a significant role in DC biology. Analysis of mice lacking different

NF-κB subunits revealed the relative contribution of these pathways. Considering the classical pathway, mice deficient in p50, p65 or c-Rel, demonstrate normal proportions of $CD11c^{high}CD8\alpha^{+}$ and $CD11c^{high}CD8\alpha^{-}$ DCs in the spleen (Ouaaz et al., 2002). In contrast, mice with non-functional NIK (*aly/aly*) or *Relb*$^{-/-}$ mice, exhibiting a block in alternative NF-κB signalling, a selective defect in splenic $CD11c^{high}CD8\alpha^{-}$ DCs is observed (De Trez et al., 2008; Wu et al., 1998). Interestingly however, Ouaaz *et al*, revealed defects in DC maturation and survival in mice doubly deficient in p50-RelA and p50-cRel (Ouaaz et al., 2002). Furthermore, RANKL deficient mice do not exhibit defects in DC development (Kong et al., 1999), suggesting a degree of redundancy in the system. Critically, it appears that LTβR signalling through the alternative NF-κB pathway maintains splenic $CD11c^{high}CD8\alpha^{-}$ DC homeostasis.

Regarding the mechanism by which the alternative NF-κB pathway is involved in DC biology, Speirs *et al*, demonstrated that p100 is able to inhibit RelB activation in stimulated DCs by acting as a negative regulator of RelB. The consequence of removing this control mechanism, as in *Nfkb2*$^{-/-}$ mice, is that DCs present with elevated expression of activation markers, but normal cytokine production levels and possess an increased capacity to stimulate $CD4^{+}$ T cells (Speirs et al., 2004).

Taken together, these studies expose mechanisms by which the alternative NF-κB pathway is involved in DC homeostasis and activation.

1.8.3. Dendritic Cell Subtypes

There are many different subtypes of DCs, which vary in their origin, migration/recruitment, anatomical location and function. These subsets include classical DCs (cDCs), monocyte-derived DCs, resident DCs such as Langerhan cells

within the skin, migratory DCs and recruited or inflammatory DCs. Here we focus on cDCs which can be identified by their high expression of CD11c. Within the spleen the two main subtypes are determined based on CD8α expression: $CD11c^{high}CD8\alpha^{+}$ and $CD11c^{high}CD8\alpha^{-}$ cDCs (Leenen et al., 1998; Shortman and Liu, 2002).

Within the gut, two significant subsets of DCs are present, with distinct functions in intestinal immunity (See Section 1.8.4); non-migratory CX_3CR1^{+} DCs (Schulz, Jung et al., 2000; Schulz et al., 2009), and migratory $CD103^{+}$ DCs (del Rio et al., 2010; Schulz et al., 2009). In addition, $CD103^{+}$ DCs have been identified in mLNs and investigation into the origins of this subset revealed that the majority are migratory LP-derived $CD103^{+}$ DCs (Jaensson et al., 2008).

1.8.4. Mucosal Dendritic Cells

The intestinal mucosa is a pivotal site for defence against potentially pathogenic organisms and DCs play an important role in maintaining host defences. Many subsets of mucosal DCs have been identified based on surface expression of different molecules; of particular interest is expression of CD103 and CX_3CR1.

CD103, also termed Integrin $\alpha_{E,}$ combines with β_7 in a heterodimeric complex ($\alpha_E\beta_7$) and is able to interact with E-cadherin, a molecule expressed by mucosal epithelial cells (Agace et al., 2000; Cepek et al., 1994). CD103 is a typical marker for intraepithelial T cells, but is also expressed on a subset of effector memory $CD8^{+}$ T cells, T regs and lamina propria (LP) T cells (Lehmann et al., 2002; Uss et al., 2006; Agace et al., 2000; Annunziato et al., 2006) and, of particular interest, on mucosal $CD11c^{high}$ DCs (Jaensson et al., 2008). $CD103^{+}$ DCs are present in the mLN, colonic LP and PPs (Annacker et al., 2005). Functional analysis has been performed on the specific $CD11c^{high}CD103^{+}$ and $CD11c^{high}CD103^{-}$ DC populations and demonstrated

that $CD103^+$ DCs are able to induce expression of gut-homing molecules on T cells, such as CCR9 (Annacker et al., 2005) and Integrin $\alpha_4\beta_7$, whereas $CD103^-$ DCs do not exhibit this capacity (Jaensson et al., 2008). Furthermore, $CD103^+$ LP-DCs are capable of migrating to the draining mLN in order to present antigen to T cells (Schulz et al., 2009) and are proficient at generating $Foxp3^+$ T regs from naïve T cells (Coombes et al., 2007; Siddiqui and Powrie, 2008). Together these studies demonstrate that $CD103^+$ DCs play a distinct role in presentation of gut-derived antigens to T cells within the mLN, inducing gut-homing capability of the T cells, along with induction of Tregs, thereby producing a tolerogenic gut environment. In contrast, $CD103^-$ DCs promote the generation of IFNγ-producing T cells and secrete high levels of IL-6 and TNFα following stimulation, demonstrating enhanced phagocytic qualities compared with their $CD103^+$ counterparts (del Rio et al., 2008). Therefore, this subset of DCs appears capable of promoting pro-inflammatory responses.

Intestinal CX_3CR1^+ DCs are a population of non-migratory, tissue resident DCs (Schulz et al., 2009), present in the intestine and responsible for extending dendrites into the lumen to sample antigens (Chieppa et al., 2006; Niess et al., 2005; Rescigno et al., 2001b; Rescigno et al., 2001a). These DCs are not able to migrate to the draining mLN to interact with T cells and also have a reduced capacity to induced expression of gut-homing molecules on T cells, indicating they play a different role in intestinal immunity from $CD103^+$ DCs.

Together, these studies demonstrate that specific subsets of DCs are present in the gut and that each has distinct functions in intestinal immunity.

Figure 1.7 Dendritic cell origin

Monocyte, macrophage and dendritic cell precursors (MDPs) give rise to monocytes and common DC precursors (CDPs). Monocytes are able to migrate to areas of inflammation and differentiate into subsets of macrophages and inflammatory DCs. CDPs are able to generate plasmacytoid DCs (PDCs) and precursors of conventional DCs (pre-cDCs), both of which are released from the bone marrow into the blood. The blood-borne pre-cDCs migrate to lymphoid tissues, before undergoing proliferation, differentiation and maturation into mature cDCs, a process controlled by regulatory T cells, Flt3 and LTβR.

Dendritic Cell Origin

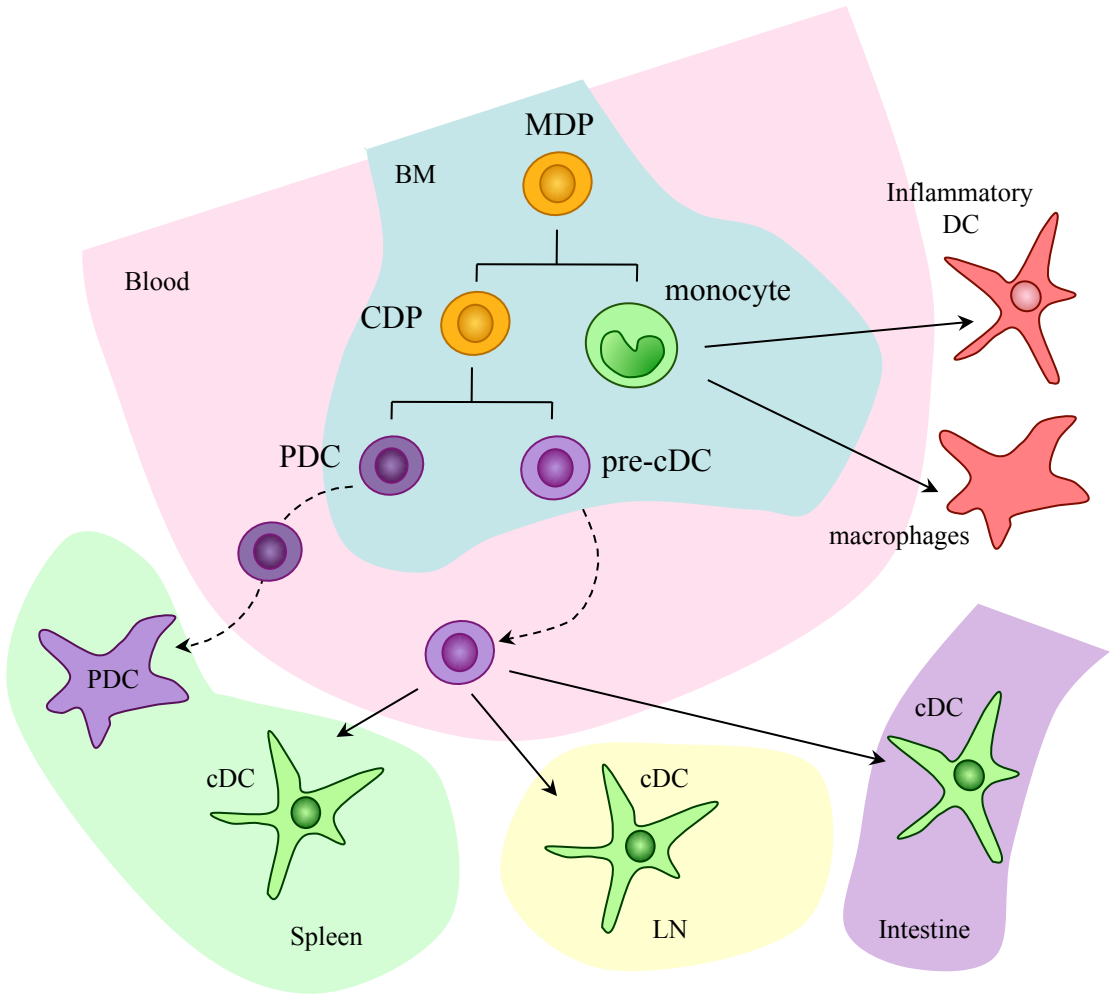

Adapted from Geissmann et al, 2010, Science

Figure 1.7

1.9. NF-κB Signalling Pathways

The family of Rel/NF-κB transcription factors play a role in a wide range of immune system processes, including generation of immune responses, lymphocyte survival, recruitment and homeostasis, lymphoid tissue development and control of cell cycle and transformation. There are two main activation pathways involving signal transduction through NF-κB: the Classical and Alternative pathways (Figure 1.9).

1.9.1. Rel/NF-κB Family of Transcription Factors

The Rel/NF-κB family of transcription factors consists of five, structurally related, members: RelA, RelB, c-Rel, NF-κB1 (the precursor p105 and the active protein p50) and NF-κB2 (the precursor p100 and the active protein p52) (Figure 1.8). The five Rel/NF-κB proteins share the highly conserved Rel-homology domain (RHD), which enables DNA binding, dimerisation of family members and binding with inhibitors of NF-κB (IκBs). The Rel/NF-κB proteins are able to form homo- and/or heterodimers with any other member of the family, except for RelB, which can only dimerise with p52 and p50. These dimers are retained in the cytoplasm in an inactive form often associated with IκBs. Each of the Rel/NF-κB proteins contains a nuclear localisation signal (NLS), allowing the translocation of dimers into the nucleus following activation. In addition to the NLS, the family members RelA, RelB and c-Rel also contain a transcriptional activation domain; therefore only dimers containing these proteins are capable of inducing gene transcription.

The structure of NF-κB1 (p105/p50) and NF-κB2 (p100/p52) differs from the other members of the Rel/NF-κB family. These proteins are transcribed as a precursor protein with a series of ankyrin repeats at the C-terminus and in this respect the structure resembles that of IκBs, enabling p105 and p100 to act as inhibitors of NF-κB activation (Basak et al., 2007). Indeed, it is the presence of these ankyrin repeats and the accompanying glycine-rich hinge region that allows for folding of the protein and concealment of the NLS, resulting in sequestration of p105- and p100-associated dimers in the cytoplasm (Ghosh et al., 1998). The carboxy terminal region of p105 and p100 are degraded by the proteosome to produce the active proteins, p50 and p52 respectively (See Section 1.9.4).

1.9.2. Inhibitors of NF-κB and IκB Kinases

IκBs are capable of masking the NLS exhibited by all five Rel/NF-κB family members, thus inhibiting nuclear translocation and induction of gene transcription. The IκB family consists of IκBα, IκBβ, IκBε, (Figure 1.8) and Bcl-3 and, as previously described, the precursor forms of NF-κB1 and NF-κB2, (p105 and p100, respectively) can also act as IκBs. Degradation of IκBs is required in order for signal transduction to proceed through the classical and alternative NF-κB pathways. IκB degradation requires IκB kinases (IKKs): IKKα, IKKβ and IKKγ (aka NEMO). IKKγ is a scaffold protein that forms the structure of the IKK complex (Ghosh and Karin, 2002).

Figure 1.8 Rel/NF-κB family of transcription factors and inhibitors of NF-κB

In mammals there are five members of the Rel/NF-κB family of transcription factors: RelA, c-Rel, RelB, NF-κB1 (p105/p50) and NF-κB2 (p100/p52). All five members share a highly conserved Rel-homology domain (RHD). Only RelA, c-Rel and RelB have transcriptional activation domains. NF-κB1 and NF-κB2 are transcribed as the inactive precursors p105 and p100, respectively, with a series of ankyrin repeats at the C-terminal. These proteins can act as inhibitiors of NF-κB by dimerising with other members of the Rel/NF-κB family and retaining the complex in the cytoplasm. Phosphorylation and proteosomal degradation cleaves the ankyrin repeats from p105 and p100 to produce the active p50 and p52 proteins, respectively. The inhibitors of NF-κB (IκBs) possess similar ankyrin repeats as p105 and p100, and are responsible for the retention of Rel/NK-κB dimers in the cytoplasm. Three of the five members of the IκB family are depicted.

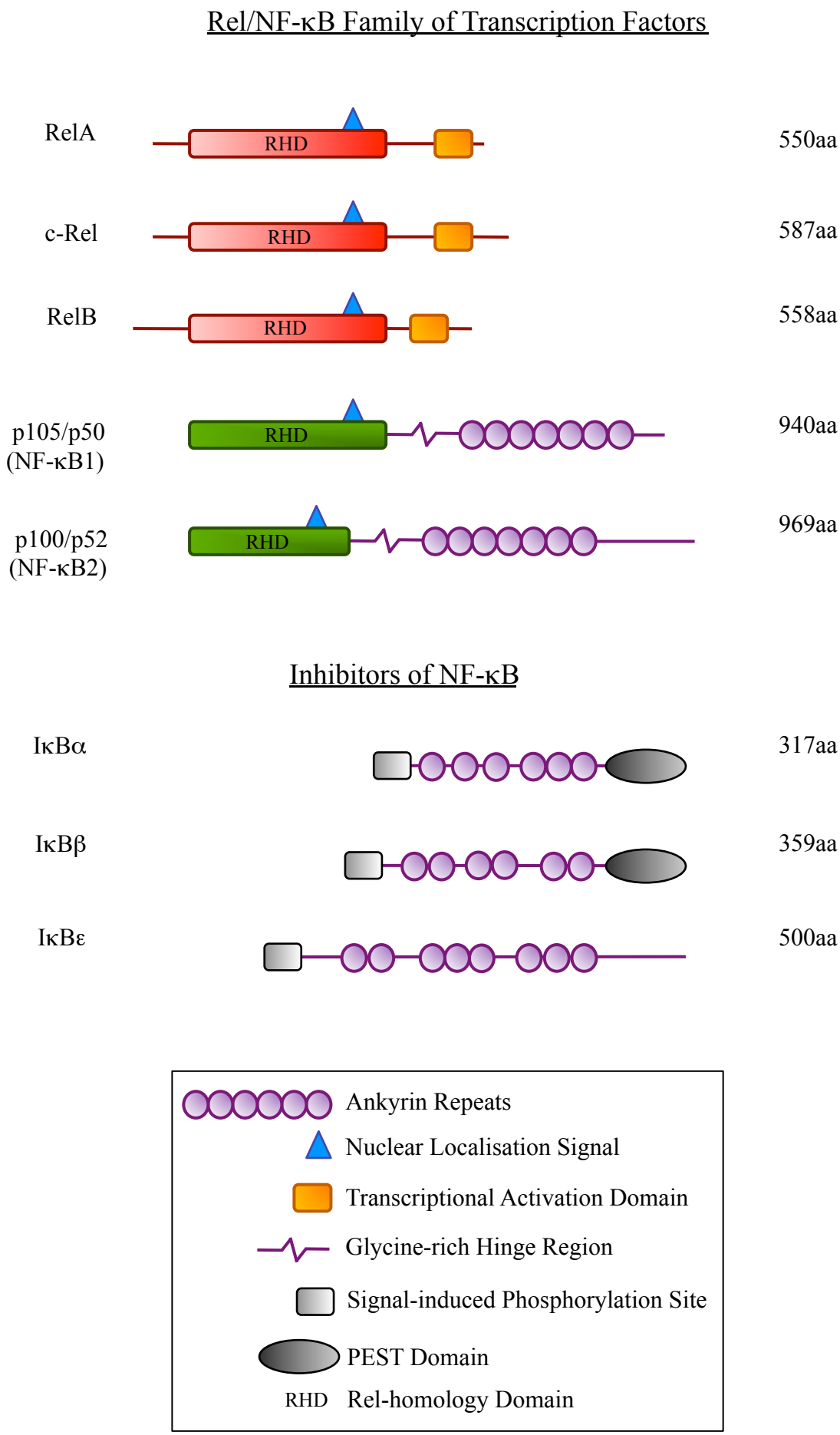
Rel/NF-κB Family of Transcription Factors
RelA
RHD
550aa
c-Rel
RHD
587aa
RelB
RHD
558aa
p105/p50
(NF-κB1)
RHD
940aa
p100/p52
(NF-κB2)
RHD
969aa
Inhibitors of NF-κB
IκBα
317aa
IκBβ
359aa
IκBε
500aa
Ankyrin Repeats
Nuclear Localisation Signal
Transcriptional Activation Domain
Glycine-rich Hinge Region
Signal-induced Phosphorylation Site
PEST Domain
RHD
Rel-homology Domain

Figure 1.8

1.9.3. The Classical NF-κB Pathway

The classical pathway is the most studied Rel/NF-κB activation pathway. It occurs downstream of signals such as TNFα and LPS, and revolves around nuclear translocation of RelA/p50 and c-Rel/p50 heterodimers (Figure 1.9). These heterodimers are retained in the cytoplasm by IκBs and the degradation of IκBs is controlled by a trimeric complex of IKKs (consisting of IKKα, IKKβ and IKKγ). The IKK complex phosphorylates IκB, thereby labelling it for proteosomal degradation. This reveals the NLS enabling the RelA/p50 and c-Rel/p50 heterodimers to translocate into the nucleus.

Activation of the classical NF-κB pathways results in transcription of target genes including cytokines, chemokines, cell adhesion molecules and enzymes (Figure 1.9). The classical NF-κB pathway plays a key role in cell proliferation, apoptosis and pro-inflammatory responses (Beinke and Ley, 2004); Ghosh, 1998, p08739}.

1.9.4. The Alternative NF-κB Pathway

The alternative NF-κB pathway is focussed on the activation and processing of NF-κB2 p100, followed by subsequent nuclear translocation of predominantly p52/RelB, but also p52/RelA heterodimers (Dejardin et al., 2002), and this pathway occurs downstream of several TNF receptor family members, such as LTβR, BAFF-R, CD40, RANK and TNF-R2 but not TNF-R1 (Dejardin et al., 2002; Müller and Siebenlist, 2003; Claudio et al., 2002; Coope et al., 2002; Weih and Caamaño, 2003) (Figure 1.9). Ligation of these receptors induces activation of both the classical and alternative NF-κB pathways (Bonizzi and Karin, 2004). The alternative pathway has been implicated in various immune processes, including development and

organisation of secondary lymphoid organs, lymphocyte survival and proliferation, and promotion of adaptive immune responses.

The central feature of the alternative pathway is the degradation of NF-κB2 p100 to p52 and this process is dependent on specific IKKs. Several studies have investigated the mechanism of NF-κB2 activation using mouse embryonic fibroblasts (MEFs) and have revealed that the production of p52 cannot occur in the absence of NF-κB-inducing kinase (NIK) or IKKα (Müller and Siebenlist, 2003; Claudio et al., 2002; Senftleben et al., 2001; Yilmaz et al., 2003), but occurs independently of IKKβ and IKKγ (Dejardin et al., 2002; Müller and Siebenlist, 2003; Yilmaz et al., 2003; Weih and Caamaño, 2003). NIK is responsible for activation of IKKα, a process that is required for the phosphorylation of p100, enabling ubiquitination and proteosomal degradation (Xiao et al., 2001; Silverman and Maniatis, 2001; Senftleben et al., 2001; Yilmaz et al., 2003). This degradation entails proteolytic cleavage of the p100 C-terminal ankyrin repeats at the glycine-rich hinge region (Heusch et al., 1999). The predominant heterodimers that form in the alternative pathway are p100/RelB (Dejardin et al., 1998; Yilmaz et al., 2003) and it is through association with p100 that RelB is retained in the cytoplasm (Coope et al., 2002).

Interestingly, continuous induction of p100 processing requires *de novo* protein synthesis of p100 within 24 hours of receptor ligation, as treatment of MEFs with cycloheximide, an inhibitor of protein synthesis, prevented proteolysis of p100 and generation of p52 (Coope et al., 2002; Müller and Siebenlist, 2003). As previously explained the classical pathway is dependent on IKKβ and IKKγ, and in MEFs lacking IKKβ or IKKγ, no new p100 protein is produced, but that which is present is degraded to p52 following LTβR ligation (Dejardin et al., 2002), indicating that the classical pathway is required for *de novo* p100 synthesis, but not for p100

processing. This data correlates with evidence that the classical NF-κB pathway induces transcription of *Nfkb2* (Liptay et al., 1994).

Other components involved in activation of the alternative pathway are tumour necrosis factor receptor-associated factors (TRAFs), intracellular proteins involved in signal transduction downstream of members of the TNF receptor family, IL-1 receptor and TLRs (Wajant et al., 2001). It has been demonstrated that TRAF3 association with BAFF-R and LTβR (Xu and Shu, 2002; Kuai et al., 2003) acts as a negative regulator of NIK (Liao et al., 2004). The interaction of TRAF3 and NIK induces continuous degradation of NIK, a situation that can be reversed following ligation of receptors, such as CD40 and BAFF, inducing degradation of TRAF3, thereby ablating NIK degradation and increasing cytoplasmic levels, and allowing processing of p100 (Liao et al., 2004). Furthermore, it has been demonstrated that TRAF3 acts as a negative regulator of CD40 signalling (Hostager and Bishop, 1999; He et al., 2004), which has been shown to proceed via the alternative NF-κB pathway (Coope et al., 2002). In addition, it has been postulated that TRAF6 functions downstream of RANK, as *Rank*$^{-/-}$ and *Traf6*$^{-/-}$ mice exhibit similar phenotypes, with a defect in osteoclast differentiation and a lack of peripheral LNs, whilst retaining PP development (Dougall et al., 1999; Kim et al., 2000; Naito et al., 1999).

Expanding on the role of the alternative NF-κB pathway in lymphocyte survival and proliferation, truncations of the C-terminal region of p100 have been associated with various lymphomas (Rayet and Gélinas, 1999) and the alternative pathway has been shown to be involved in cell transformation by oncogenic viruses, such as HTLV-1 (human T-cell leukaemia virus type 1) (Lanoix et al., 1994) and the LMP-1 (latent membrane protein 1) (Saito et al., 2003; Atkinson, 2003, p13785; Eliopoulos et al., 2003; Luftig et al., 2004) from Epstein Barr virus. These two viruses

are able to induce p100 processing via different mechanisms; HTLV-1 depends on the classical IKK complex (IKKα-IKKβ-IKKγ) and occurs independently of NIK (Lanoix et al., 1994); LMP-1 requires presence of a TRAF binding site in it's cytoplasmic tail and induces p100 processing independently of IKKγ (Luftig et al., 2004). In addition, the alternative NF-κB pathway has been shown to be involved in the transcription of various factors involved in cell cycle progression, such as cyclin-D1 and skp2. Heterodimer complexes of p52/Bcl3 upregulate *Cyclin-D1* gene expression (Westerheide et al., 2001; Rocha et al., 2003) and p52/RelB complexes upregulate *Skp2* gene expression (Schneider et al., 2006), thereby promoting proliferation.

1.9.5. κB DNA binding sites

The nuclear translocation of heterodimers formed during activation of the alternative NF-κB pathway, mainly p52/RelB, induce transcription of specific genes. Bonizzi *et al*, demonstrated that RelB containing complexes specifically bind to κB binding sites in the promoter regions of genes encoding CXCL13, CCL19 and CCL21 (Bonizzi et al., 2004). Stimulation of stromal cells and bone marrow-derived DCs (BMDCs) with agonistic LTβR antibody resulted in nuclear translocation of p52/RelB heterodimers, in an IKKα-depedent manner, and induced upregulation of CXCL13, CCL19 and CCL21 chemokine expression (Bonizzi et al., 2004).

Figure 1.9 NF-κB activation pathways

The classical NF-κB pathway occurs downstream of receptors such as TNFR and TLR4, and revolves around nuclear translocation of RelA/p50 and c-Rel/p50 heterodimers, by degradation of IκBs which retain these complexes in the cytoplasm. Activation of the classical NF-κB pathway results in transcription of target genes including cytokines, chemokines, cell adhesion molecules and enzymes.

The alternative NF-κB pathway occurs downstream of receptors such as LTβR, CD40, BAFF-R and RANK, and centres around degradation of p100 to p52 and subsequent nuclear translocation of predominantly p52/RelB heterodimers. Activation of this pathway results in transcription of chemokines, cytokines and cell adhesion molecules.

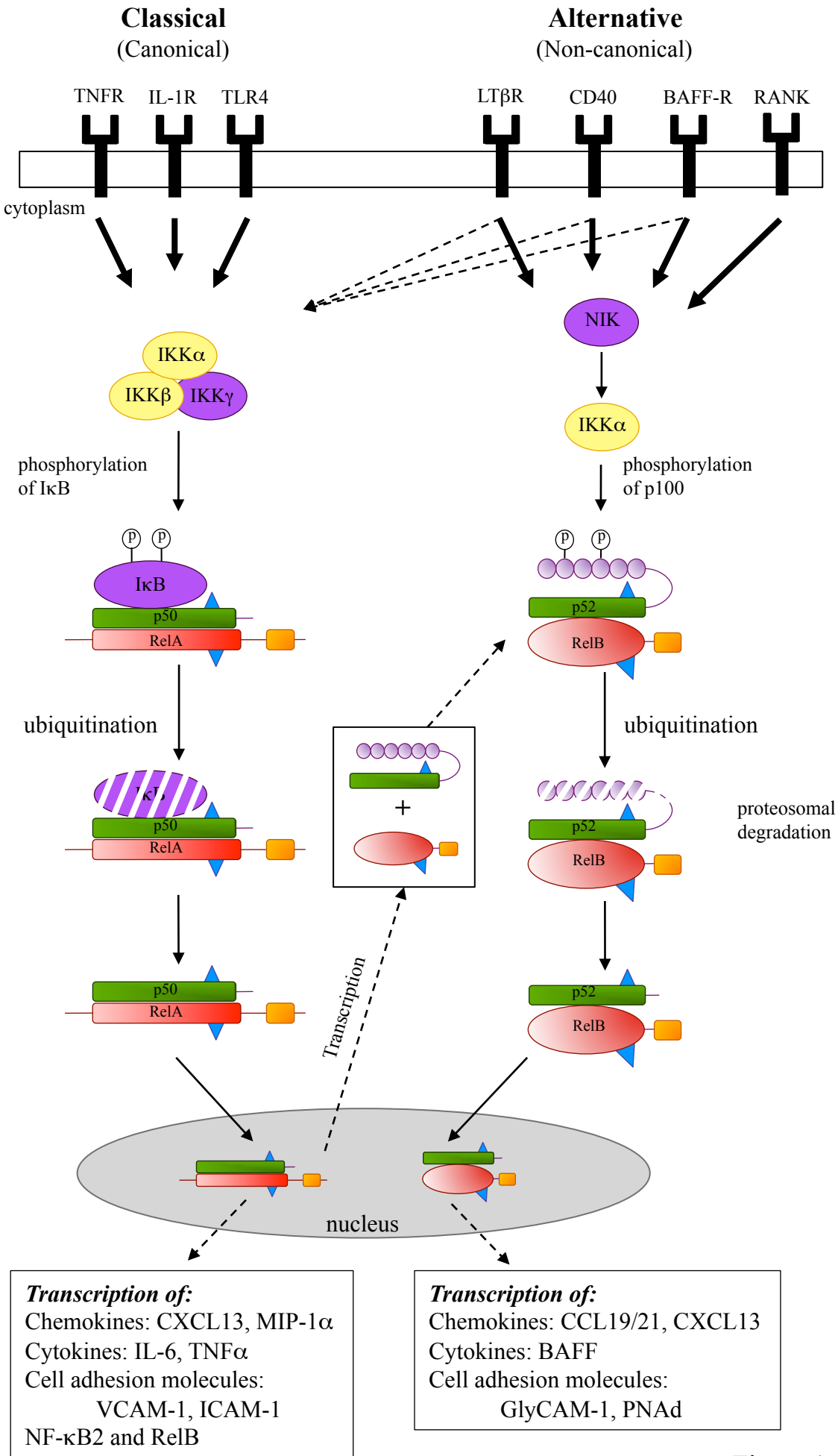
Classical
(Canonical)
Alternative
(Non-canonical)
TNFR
IL-1R
TLR4
LTβR
CD40
BAFF-R
RANK
cytoplasm
IKKα
IKKβ
IKKγ
NIK
IKKα
phosphorylation
of IκB
phosphorylation
of p100
P
P
IκB
p50
RelA
p52
RelB
ubiquitination
ubiquitination
κ
p50
RelA
+
p52
RelB
proteosomal
degradation
p50
RelA
p52
RelB
Transcription
nucleus
Transcription of:
Chemokines: CXCL13, MIP-1α
Cytokines: IL-6, TNFα
Cell adhesion molecules:
VCAM-1, ICAM-1
NF-κB2 and RelB
Transcription of:
Chemokines: CCL19/21, CXCL13
Cytokines: BAFF
Cell adhesion molecules:
GlyCAM-1, PNAd

Figure 1.9

1.9.6. Receptors that Activate the Alternative NF-κB Pathway

The alternative NF-κB pathway occurs downstream of several TNF receptor family members, including LTβR, BAFF-R, CD40 and RANK. These receptors are expressed by a variety of cell types and can consequently induce different gene expression patterns.

1.9.6.1. LTβR

The most extensively analysed receptor-induced activation of the alternative NF-κB pathway is activation via LTβR. LTβR is expressed by stromal cells, such as MEFs and by DCs (Kabashima et al., 2005). Several studies have elucidated the mechanism by which p100 processing occurs downstream of LTβR. Treatment of WT MEFs with an agonistic LTβR monoclonal antibody induced p100 processing to p52. This p100 degradation did not occur in MEFs with a naturally occurring non-functional mutation in NIK (*aly/aly*), or in MEFs lacking IKKα, but did occur in MEFs lacking RelA, IKKβ, IKKγ or NF-κB1 (Dejardin et al., 2002; Müller and Siebenlist, 2003; Yilmaz et al., 2003). These results suggested that p100 processing to p52 was dependent on the alternative NF-κB pathway and not the classical pathway. In addition, it was shown that LTβR ligation promotes nuclear translocation of p52, RelB and RelA and that at six hours post ligation the predominant heterodimers located in the nucleus are p52/RelB dimers and this nuclear translocation was dependent on IKKα, but not IKKβ (Dejardin et al., 2002). However, LTβR stimulation does not only induce the alternative NF-κB pathway, but also activates the classical pathway and the gene expression patterns differ depending on the pathway activated (Dejardin et al., 2002; Lo et al., 2006). When WT MEFs were stimulated

with agonistic LTβR, expression of VCAM-1 mRNA was upregulated, this was not observed in MEFs lacking a component of the classical pathway, such as RelA or IKKβ, but was present in *aly/aly* and *Ikkα*$^{-/-}$ MEFs (Dejardin et al., 2002). Conversely, expression levels of the chemokines CCL19/21 and CXCL13, and BAFF, were increased in splenocytes from WT mice treated with agonistic LTβR antibody. This increase was inhibited in mice with a non-degradable form of IKKα, therefore with no alternative NF-κB signalling. Together this data demonstrates that LTβR signalling proceeds through the classical and alternative pathways and in support of this Müller *et al*, demonstrated that following LTβR ligation DNA binding of complexes containing RelA were observed initially, with subsequent DNA binding of RelB containing heterodimers (Müller and Siebenlist, 2003). Thus indicating that LTβR engagement initially activates the classical pathway, followed later by prolonged activation of the alternative pathway.

1.9.6.2. BAFF-R

The B cell activating factor (BAFF) is a member of the TNF family and is required for proliferation and survival of mature B cells (Schneider et al., 1999). BAFF is present as a membrane-bound and secreted protein and binds to three receptors: BAFF-R, BCMA (B cell maturation antigen) and TACI (transmembrane activator and CAML interactor). Two of these receptors, BCMA and TACI, are also able to bind the proliferation-inducing ligand, APRIL (Do and Chen-Kiang, 2002). APRIL does not bind to BAFF-R, therefore the only known ligand for BAFF-R is BAFF (Thompson et al., 2001). Claudio *et al*, investigated the involvement of NF-κB pathway components on the survival, proliferation and maturation of B cells in

response to BAFF. They showed that treatment of mature splenic B cells and immature BM B cells with BAFF induced processing of p100 to p52 and that this processing was ablated in B cells from *aly/aly* mice and in B cells expressing a mutated BAFF-R (A/WySnJ mice (Thompson et al., 2001)) (Claudio et al., 2002). It was also shown that BAFF induced nuclear translocation of p52/RelB heterodimers and DNA binding occurred in splenic B cells in a NIK-dependent manner. This data shows that BAFF is able to induce p100 degradation and nuclear translocation of p52/RelB heterodimers, dependent on NIK and this process occurs downstream of BAFF-R.

In vivo, the two NF-κB activation pathways have been shown to be involved in B cell maturation and survival, by evidence that mice doubly deficient for NF-κB1 and NF-κB2 showed increased apoptosis of splenic B cells, due to decreased expression of anti-apoptotic genes, such as *Bcl2*. The effect in single *Nfkb1*$^{-/-}$ and *Nfkb2*$^{-/-}$ mice revealed that B cell development was dependent on NF-κB2 and not NF-κB1. Moreover, in *aly/aly* mice and mice expressing a mutated form of BAFF-R, maturation of bone marrow B cell precursors was not markedly impaired (Claudio et al., 2002).

1.9.6.3. CD40

CD40 is a member of the TNFR superfamily and is involved in B cell activation and differentiation. CD40 is expressed on B cells, as well as other APCs, and it's ligand, CD40-L, is expressed on activated T cells (Grewal and Flavell, 1998). The potential for involvement of the alternative NF-κB pathway in signalling downstream of CD40 was postulated following the observation that *aly/aly* mice present with defects in B cell function (Karrer et al., 2000; Yamada et al., 2000).

Coope *et al*, demonstrated, using CD40-transfected 293 cells, that CD40 engagement by either anti-CD40 antibody or CD40-L induced processing of p100 to p52 and that this processing did not occur following treatment with TNFα or IL-1α (stimulators of the classical, but not the alternative NF-κB pathway). Subsequent nuclear translocation of p52 was observed and the entire process was dependent on functional NIK. Furthermore, CD40 treatment of splenic B cells induced p100 degradation and nuclear translocation of p52/RelB heterodimers (Coope et al., 2002).

1.9.6.4. RANK

RANK is a member of the TNFR superfamily and is involved in osteoclast differentiation and LN development (Wong et al., 1999; Dougall et al., 1999; Kong et al., 1999). RANK is the receptor for RANKL (also known as TRANCE). RANKL is expressed by activated T cells (Josien et al., 1999; Anderson et al., 1997; Wong et al., 1999), whereas RANK is expressed by DCs (Josien et al., 1999; Anderson et al., 1997; Wong et al., 1999; Wong et al., 1997), and osteoclast progenitors (Wong et al., 1999; Lacey et al., 1998). RANK plays a role in the promotion of DC survival following lgation with RANK-L (Josien et al., 2000). In addition, RANK signalling is required for osteoclastogenesis and LN development, but is dispensable for the development of PPs; *Rank*$^{-/-}$ and *Rankl*$^{-/-}$ mice exhibit a block in osteoclast differentiation and lack peripheral LNs, whilst retaining development of PPs (Dougall et al., 1999; Kong et al., 1999). Importantly, LTi cells express both RANK and RANKL (Kim et al., 2000). Additionally, mice lacking TRAF6 present with a phenotype similar to *Rank*$^{-/-}$ and *Rankl*$^{-/-}$ mice, indicating that signalling downstream of RANK involves TRAF6 (Naito et al., 1999).

1.9.7. The alternative NF-κB pathway and lymphoid tissue development

The alternative NF-κB pathway is activated downstream of several TNFR family members known to be important in lymphoid tissue development and organisation of the spleen, therefore indicating a significant role for alternative NF-κB signalling in these processes. Several mouse models with deficiencies in components of the NF-κB pathway have been developed and analysed for the formation of lymphoid tissue and splenic architecture (Table 1.5).

Of the classical pathway, three models are of interest: *Nfkb1*$^{-/-}$, *c-rel*$^{-/-}$ and *Rela*$^{-/-}$*TnfrI*$^{-/-}$. *Nfkb1*$^{-/-}$ and *c-rel*$^{-/-}$ mice both develop LNs and PPs, although PP numbers in *Nfkb1*$^{-/-}$ are decreased (Paxian et al., 2002; Weih and Caamaño, 2003). The normal development of lymphoid tissues in these mice suggests a non-essential role for the classical NF-κB pathway. Deletion of RelA is embryonic lethal at E15 (Beg et al., 1995), due to TNFα-induced liver degeneration, therefore, *Rela*$^{-/-}$ mice were crossed with *TnfrI*$^{-/-}$ mice to allow full term survival (Alcamo et al., 2001). Interestingly, *Rela*$^{-/-}$*TnfrI*$^{-/-}$ mice do not develop LNs or PPs and lack demarcation of B and T zones in the spleen, contrary to *TnfrI*$^{-/-}$ mice (Alcamo et al., 2001). This phenotype is similar to that seen in *LtβR*$^{-/-}$ (Fütterer et al., 1998) and *Relb*$^{-/-}$ (Weih et al., 2001) mice, and considering that LTβR signalling initially activates nuclear translocation of p52/RelA heterodimers, followed by p52/RelB heterodimers, this is a possible explanation for the defects in lymphoid tissue development and splenic organisation associated with RelA deficiency (Dejardin et al., 2002).

The key components of the alternative NF-κB pathway are NF-κB2/p100, RelB, NIK and IKKα. The phenotype of *Nfkb2*$^{-/-}$ mice differs from that of *Relb*$^{-/-}$ and *aly/aly* (non-functional NIK) mice in that the former develops LNs and PPs, whereas

the latter do not (Paxian et al., 2002; Weih et al., 1995; Carragher et al., 2004; Shinkura et al., 1999; Miyawaki et al., 1994). Ordinarily, RelB is retained in the cytoplasm in association with p100, in *Nfkb2*$^{-/-}$ mice no p100 is present, therefore there is no negative control of RelB-induced gene transcription suggesting a possible explanation for LN and PP development. However, the LNs and PPs that do develop are disorganised, with few B cells present and no B cell follicles. In the LN, this is linked to a defect in CXCL13 expression and a decrease in CCL19/21 expression (Carragher et al., 2004). In addition, B/T cell segregation in the spleen can be observed, but no B cell follicles form (Caamaño et al., 1998; Franzoso et al., 1998). In contrast to *Nfkb2*$^{-/-}$ mice, *Relb*$^{-/-}$ and *aly/aly* mice lack all LNs and PPs, and when the spleen is analysed, no B/T cell segregation can be seen and, similar to *Nfkb2*$^{-/-}$ mice, a defect in B cell follicle formation is observed (Weih et al., 2001; Karrer et al., 2000; Miyawaki et al., 1994).

Removal of p100 as a negative regulator of RelB-induced gene transcription results in a decrease in lymphocyte homing chemokines, the reverse situation involves constitutive activation of p100 (p100Δ mouse model), resulting in increased p52/RelB heterodimerisation and nuclear translocation. In p100Δ mice, an increase in splenic CXCL13 and CCL21 can be observed, with ectopic MAdCAM-1 expression in the red pulp and increased VCAM-1 and ICAM-1 expression. The splenic architecture is not disrupted with regards to B/T cll segregation, but an increase in MZ B cells has been shown (Guo et al., 2007) (Table 1.5).

1.10. Aims

The $LT\alpha_1\beta_2$-LTβR axis is critical for the development of clearly demarcated B and T cell areas in the spleen through the expression of area-specific chemokines. The spleens of LTβR and LTα deficient mice show no organisation of B and T zones due to a lack of homing chemokines, such as CXCL13 and CCL19/21. We aim to analyse the affect of introducing constitutively active NF-κB2 p100 into an LTα-deficient environment with the hypothesis that this will mimic continuous LTβR signalling and therefore rescue expression of homing chemokines and recovery of splenic organisation.

It is well established that the alternative NF-κB pathway plays a significant role in SLO development through its involvement in signalling downstream of various TNFR superfamily members. This thesis aims to expand on this area by investigating the role of this pathway in the development of TLOs, by utilising a mouse model where NF-κB2/p100 is constitutively active, the p100Δ mouse model. The tertiary lymphoid tissue system we focus on is the formation of colonic ILFs. With the aim to address the following points:

- The affect of constitutively active NF-κB2/p100 on the formation of colonic lymphoid aggregates and the similarity of these aggregates to ILFs within the following parameters:
    - Cellular composition and organisation, and stromal structure
    - Investigation into which cellular compartment constitutively active NF-κB2/p100 plays a significant role: haematopoietic or stromal

- Assessment of alterations in proportion and cell number for cell subtypes such as B and T cells, and dendritic cells.
- Alterations in activation or maturation status seen in the lymphoid organs (spleen, mLN) and colon of p100Δ mice.

The $LT\alpha_1\beta_2$-LTβR axis is critical for the development of clearly demarcated B and T cell areas in the spleen through the expression of area-specific chemokines. The spleens of LTβR and LTα deficient mice show no organisation of B and T zones due to a lack of homing chemokines, such as CXCL13 and CCL19/21. We aim to analyse the affect of introducing constitutively active NF-κB2/p100 into an LTα-deficient environment with the hypothesis that this will mimic continuous LTβR signalling. With the view to analyse the following areas:

- Demarcation of B and T cell areas in the spleen
- Expression of homing chemokines and stromal markers (e.g. CCL21, CXCL13, Gp38)
- Recovery of aspects of splenic micro-architecture, such as the marginal zone.
- Development of lymph nodes

2. Materials and Methods

2.1. Mice

Details of all mouse strains are found in Table 2.1. These strains were bred and maintained under specific pathogen-free (SPF) conditions in the Biomedical Service Unit at the University of Birmingham according to Home Office and local ethics committee regulations.

Strain	*Background*	*CD45 Isotype*
C57Bl/6 (WT)	C57Bl/6	CD45.2
p100Δ	C57Bl/6	CD45.2
LTα$^{-/-}$	C57Bl/6	CD45.2
p100ΔLTα$^{-/-}$	C57Bl/6	CD45.2
Relb$^{-/-}$	C57Bl/6	CD45.2
p100ΔRelb$^{-/-}$	C57Bl/6	CD45.2
Rag$^{-/-}$ *(BoyJ)*	C57Bl/6	CD45.1

Table 2.1 Mouse strains.

2.1.1. Generation of p100Δ Mouse Model

Ishikawa, *et al*, generated the p100Δ mouse model (Ishikawa et al., 1997). The *Nfkb2* gene was disrupted by the introduction of a stop sequence, KpnI and SalI at amino acid 451, located between the glycine rich region and the first ankyrin repeat. This resulted in transcription of the p52 molecule that is only 450 amino acids in length and no production of the full-length p100 precursor protein (Figure 2.1). The p100Δ mice have high levels of p52/RelB heterodimers in the nucleus of many different cell types.

Figure 2.1 Generation of p100Δ mouse model

Ishikawa et al, (1997) J. Exp. Med.

A. Targeting strategy of the ankyrin-encoding region of the nfkb2 gene.
The relevant part of the mouse nfkb2 gene structure is shown at the top. Exons 13–19, encoding residues 332–690, are indicated by closed boxes. Targeting vector pPNT/IκBδ and the targeted allele are shown at the middle and bottom, respectively. Open boxes indicate the SV40 polyadenylation recognition sequences, PGK-neo and PGK-tk cassettes. The position of KpnI and SpeI sites are indicated by K and S, respectively. The diagnostic restriction fragments used for Southern blot analysis are indicated at the top (wild-type allele) and bottom (targeted allele). The DNA fragments used as 5′ external (H) and internal (B) probes are indicated at the bottom.

B. Genotype analysis of mice generated from p100+/− heterozygote intercrosses.
Tail DNAs were digested with KpnI and SpeI, and subjected to Southern blot analysis using the 5′ external probe H indicated in A. The 8.5-kb band indicates the wild-type allele, while the 7.2-kb band represents the targeted allele.

C. Absence of p100 in homozygous mutant mice.
Protein extracts from control (+/+) and homozygous (−/−) mutant thymocytes labeled with [35S]methionine for 8 h in the presence of PMA (20 ng/ml) and PHA (5 μg/ml) were immunoprecipitated with an anti-p52 antiserum. p100 and p52 proteins are indicated by the arrows.

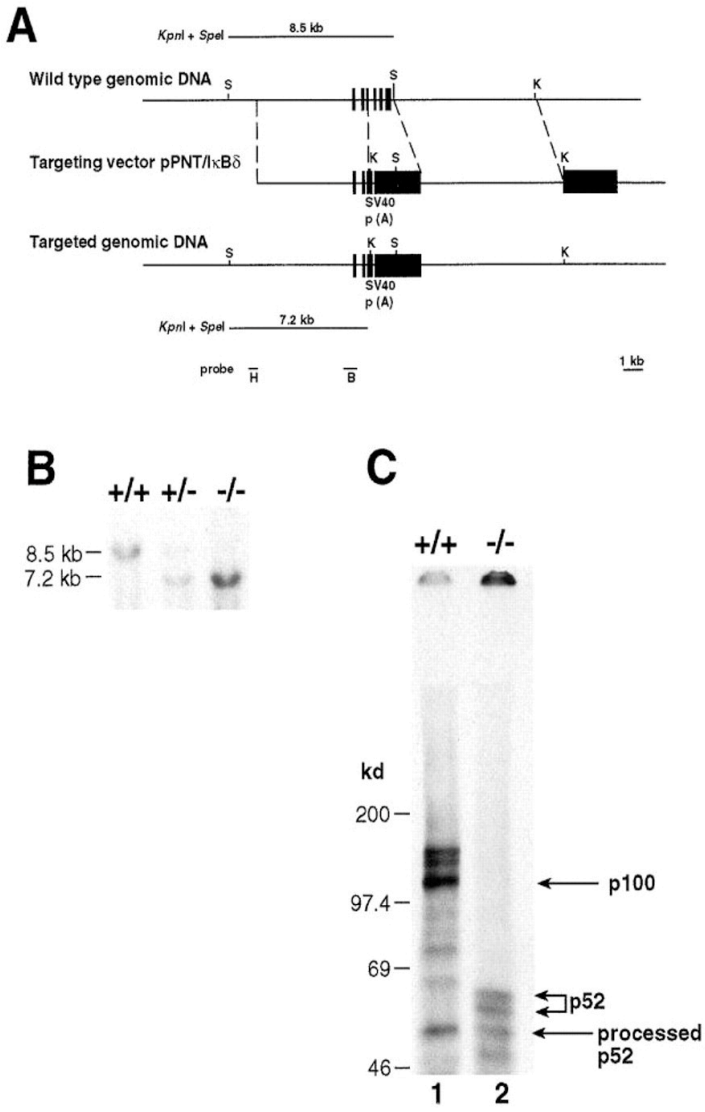

Ishikawa H et al. J Exp Med
1997;186:999-1014

JEM

Figure 2.1

2.1.2. Genotyping

Heterozygous p100Δ mice ($p100\Delta^{+/ki}$) were bred due to postnatal lethality of $p100\Delta^{ki/ki}$ at three weeks of age. $p100\Delta^{ki/ki}$ are designated p100Δ within this thesis. When crossing the p100Δ strain with $Relb^{-/-}$ the parents were heterozygous for p100Δ ($p100\Delta^{+/ki}$) and either heterozygous or knockout for RelB ($Relb^{+/-}$ *or* $Relb^{-/-}$). Once established the *p100ΔLTα* stain bred parents heterozygous for p100Δ ($p100\Delta^{+/ki}$) and knockout for LTα ($LT\alpha^{-/-}$). Ear clippings from the p100Δ, *p100ΔRelb* and *p100ΔLTα* colonies were taken at ten days of age, providing tissue for genotyping. The tissue was digested in 100μl DNA extraction buffer (Table 2.2) for 20 minutes at 95°C on a thermoshaker (Eppendorf, Thermomixer). Following this incubation 100μl 40mM Tris HCl was added to precipitate out the DNA. The extracted DNA solution could then be used directly in the PCR reaction mix.

2.1.2.1. PCR Reaction Mix

The primers used to genotype the p100Δ and *p100ΔRelb* colonies are listed in Table 2.3. The PCR reaction mix per sample was as follows: 1μl each primer, 16μl ReddyMix (containing inert red dye, Taq DNA polymerase, 1.5mM $MgCL_2$ and dNTPs) (Thermo Scientific, UK) and 2μl sample DNA solution.

2.2. Medium and Supplements

All dissected tissues and cells were handled in RF10 medium, prepared as shown in Table 2.5.

DNA Extraction Buffer 10x			
Reagents	*Conc*	*Volume*	*Supplier*
NaOH 10N	1M	1,250µl	Sigma-Aldrich, UK
EDTA	500mM	200µl	AccuGENE (BioWhittaker)
H_2O	-	48,550µl	-

Table 2.2 Reagents required for DNA extraction buffer 10x.
Solution is used at 1x concentration.

		Primer Name	*Primer Sequence*
p100	*Primers*	p100 Forward	ATCAATAAACACGACCGGAG
		p100 Reverse	CAACTAACAGATCCAGGCAC
		SV40 Forward	ATGAATGGGAGCAGTGGTGG
		SV40 Reverse	GGTGTAAATAGCAAAGCAAGCAAG
	Cycle	45 seconds 94°C; 45 seconds 60°C; 1 minute 72°C: 33x	

Table 2.3 p100Δ primers and PCR cycle details.

		Primer Name	*Primer Sequence*
RelB	*Primers*	RelB 273	GTGGTGCCCGGGAATAGGATTGCTG
		RelB 106	CCATTTTGCTCTGGGTCTGTGTCTG
		RelB 4	CATCGACGAATACATTAAGGAGAACGG
		HHNEO	AAATGTGTCAGTTTCATAGCCTGAAGAACG
	Cycle	1 minute 95°C; 1.5 minutes 60°C; 1 minute 72°C: 35x	

Table 2.4 RelB primer and PCR cycle details.

RF10 Medium			
Medium and supplements	*Volume*	*Final concentration*	*Supplier*
RPMI	500ml	-	Sigma-Aldrich, UK
L-glutamine	5ml	1%	Sigma-Aldrich, UK
Penicillin Streptomycin	10ml	2%	Sigma-Aldrich, UK
Heat-inactivated foetal bovine serum	50ml	10%	Hyclone

Table 2.5 Supplements required for RF10 medium.

Digestion Buffer		
Reagents	*Concentration*	*Supplier*
Collagenase/Dispase	2.5 mg/ml	R&D Systems, Minneapolis, MN
DNase I	100 μg/ml	Sigma- Aldrich, UK
RPMI	-	Sigma- Aldrich, UK

Table 2.6 Reagents required for enzyme digestion buffer 1x.

Conjugate	*Antibody*	*Clone*	*Conc.*	*Dilution*		*Supplier*
				Confocal	*FACs*	
FITC	CD3ε	145-2C11	0.5mg/ml	1/100	1/100	e-bioscience
	CD8α	53-6.7	0.5mg/ml	-	1/200	e-bioscience
	CD11c	N418	0.5mg/ml	1/150	1/100	e-bioscience
	CD31	N418	0.5mg/ml	1/100	-	e-bioscience
	CD45.2	104	0.5mg/ml	1/100	-	e-bioscience
	CD103	2E7	0.5mg/ml	1/100	1/100	e-bioscience
	CD169	3D6.112	0.1mg/ml	1/50	-	AbD Serotec
	F4/80	BM8	0.5mg/ml	1/100	-	e-bioscience
	FDCM1	4E3	0.5mg/ml	1/100	-	e-bioscience
	FoxP3	FJK-16s	0.5mg/ml	1/50	1/200	e-bioscience
	IgD	11-26c	0.5mg/ml	1/300	-	e-bioscience
	Ki67	SP6	0.2mg/ml	1/400	-	Abcam
	VCAM-1	429	0.5mg/ml	1/100	-	e-bioscience
PE	CD3ε	145-2C11	0.2mg/ml	-	1/50	BD Pharmingen
	CD86	GL1	0.2mg/ml	-	1/200	e-bioscience
PE Cy5.5	B220	RA3-6B2	0.2mg/ml	-	1/200	e-bioscience
PerCP Cy5.5	CD11b	M1/70	0.2mg/ml	-	1/3500	e-bioscience
APC	CD4	GK1.5	0.2mg/ml	-	1/400	e-bioscience
	CD11c	N418	0.2mg/ml	-	1/300	e-bioscience
Biotin	B220	RA3-6B2	0.5mg/ml	1/200	-	e-bioscience
	CD69	H1-2F3	0.5mg/ml	-	1/500	e-bioscience
	MAdCAM-1	MECA-367	0.5mg/ml	1/100	-	e-bioscience
Purified	CCL21	polyclonal	0.1mg/ml	1/100	-	R&D Systems
	CXCL13	polyclonal	0.1mg/ml	1/50	-	R&D Systems
	IgA	C10-1	o.5mg/ml	1/200	-	BD Pharmingen
Other	CD4-647*	GK1.5	0.5mg/ml	1/200	-	e-bioscience
	Gp38/Podoplanin	8.1.1	Supernatant	1/2	-	**
	IgM-Rhodamine Red	-	1.5mg/ml	1/400	-	Jackson ImmunoResearch Laboratories

Table 2.7 Primary antibodies for immunofluorescent staining for confocal microscopy and FACs analysis.

* CD4 was directly conjugated using the Alexa Fluor 647 mAb Labeling Kit (Invitrogen, Carlsbad, CA).
** (Supernatant) Kind gift from A. Farr, University of Washington, Seattle, WA.

2.3. Isolation of Spleen, mLN and Colon

Spleen, mLN and colon were dissected from mice of varying ages from postnatal day 10 (P10) to P21 and all the attached fat was removed. The fat attached to the mLN and colon was removed by microdissection. All dissected tissues were stored in RF10 medium (Table 2.5) during handling.

2.3.1. Freezing of Tissues

To freeze the spleen, the tissue was placed on a section of aluminium foil and place on a Petri dish on dry ice. Once frozen the spleen was wrapped in the foil and transferred to -80^{o}c freezer for storage.

To freeze the colon, the tissue first had all luminal contents removed. This was done carefully to avoid damaging the tissue. Once cleaned the tissue was placed on aluminium foil with the cecum in the centre and the rest of the colon coiled around the outside. The tissue was frozen on dry ice and stored at -80^{o}c.

2.3.1.1. Cryostat Sectioning of Frozen Tissues

The tissue was removed from storage (-80^{o}C) and placed in the cryostat. A circle of wet filter paper (Whatman) was placed on a chuck and left to freeze followed by a large drop of OCT compound (Tissue Tek). The tissue was added to the compound with the flat side facing upwards. The chuck was then placed in the chuck holder and 5µm sections were cut and collected onto either a 4-spot microscope slide (C.A Hendley Lts, Essex, UK) for the spleen or an extra-adhesive microscope slide (Surgipath, UK) for the colon. The slides were left to air dry for at least 40 minutes

then fixed in cold (4°C) acetone (Sigma-Aldrich, Poole, UK) for 20mins at 4°C. Fixed slides were stored at -20°C.

2.3.1.2. Immunofluorescent Staining of Cryostat Sections

Slides were removed from -20°C and air-dried for approximately 30 minutes. After hydration in PBS (Sigma-Aldrich, Poole, UK) for 5 minutes, a blocking solution of 10% goat serum (Sigma-Aldrich, Poole, UK) in 1% BSA/PBS was added to each section and incubated for 10 minutes. The antibodies used are listed in Table 2.7. The blocking solution was aspirated and the primary antibody solution was added and incubated for one hour. The secondary antibodies were cross-absorbed with 10% normal mouse serum (NMS) (Sigma-Aldrich, Poole, UK) in 1% BSA/PBS. After primary antibody incubation, the slides were washed in PBS for 10 minutes, and then the secondary antibody solution was added and incubated for 30 minutes. If tertiary and quaternary antibodies were used then the same process was followed as for the secondary antibodies. All secondary and tertiary antibodies are listed in Table 2.8. After all antibody incubations and a final wash in PBS, the slides were mounted using Vectashield (VectorLaboratories) with or without the nuclei stain DAPI. A cover slip was added, excess Vectashield was blotted off and the slides were sealed with nail varnish. Finally, all stained slides were stored at -20°C. Confocal images were acquired using a Zeiss LSM 510 laser scanning confocal head with a Zeiss Axio Imager Z1 microscope (Zeiss, Oberkochen, Germany). Digital images were recorded in four separately scanned channels with no overlap in detection of emissions from the respective fluorochromes. Confocal micrographs were stored as digital arrays of 2048 x 2048 pixels with 8-bit sensitivity; detectors were routinely set so that intensities in each channel spanned the 0–255 scale optimally.

Antibody	*Conc.*	*Dilution*		*Supplier*
		Confocal	*FACs*	
Streptavidin Alexa Fluor 488	1mg/ml	1/300	-	Invitrogen
Streptavidin Alexa Fluor 555	1mg/ml	1/300	-	Invitrogen
Streptavidin Alexa Fluor 647	1mg/ml	1/300	-	Invitrogen
Streptavidin Alexa Fluor APC	1mg/ml	-	1/600	Invitrogen
Donkey anti Goat IgG 555	2mg/ml	1/100	-	Invitrogen
Rabbit anti FITC	1mg/ml	1/200	-	R & D Systems
Goat anti Rabbit IgG FITC	1mg/ml	1/200	-	Southern Biotech
Goat anti Hamster IgG- biotin	1.5mg/ml	1/100	-	Vector Labs
Goat anti Rat IgG- biotin	1mg/ml	1/100	-	Southern Biotech

Table 2.8 Secondary and tertiary antibodies.

2.3.1.3. Assessment of Colonic B cell Aggregate Number and Size

Colonic B cell aggregates were enumerated following immunofluorescence staining of colon sections with anti-IgM and visualisation on a fluorescence microscope. Three separate sections of colon where assessed for at least three mice of each genotype in each age group (WT postnatal day 10, n=2).

Quantification of B cell aggregate size was performed following immunofluorescence staining of colon sections with anti-IgM. Pictures of at least six aggregates per colon section were collected using fluorescence microscopy and image software ImageJ was used to measure aggregate size. Three mice per genotype were analysed.

2.3.1.4. Assessment of B and T cell Segregation in the Spleen

Confocal images of spleen sections were analysed using LSM software. The Region of Interest (ROI) was highlighted and the software calculated the area in μm^2. The ROI in this instance was the T cell area, marked by positive staining of anti-CD4.

At least six images were taken for each section of spleen, for three individual mice for each genotype was assessed.

Assessment of B and T cell segregation was determined by calculation of the number of $B220^+$ pixels present in the T cell area; the number of $B220^+$ pixels corresponding with the number of B cells. Between each confocal image the same settings were used for each fluorescence channel. Saturated pixels were excluded from the analysis. This data was presented as the mean number of $B220^+$ pixels per μm^2 of T zone area.

2.4. Preparation of Single Cell Suspensions

2.4.1. Spleen

The spleen was isolated and placed in RF10 medium. The spleen was cut into small fragments and mechanically forced through a nylon cell strainer (70μm, BD Falcon). The cell suspension was transferred to a falcon tube in 15 ml RF10 and centrifuged (7 minutes, 1400rpm, 4^oC). The supernatant was removed and 5 ml of red cell lysis buffer was added and incubated on ice for 5 minutes. After this time, 5 ml RF10 medium was added to prevent further action of the lysis buffer and centrifuged (7 minutes, 1400rpm, 4^oC). The supernatant was discarded and the cell pellet was resuspended in 5 ml RF10. Cell counts were performed using a haemocytometer.

2.4.2. Mesenteric lymph node and colon

The mLN was dissected and all fat was removed using a dissecting microscope. The mLN was then placed in 1 ml RF10 and roughly teased apart. The

colon was isolated and placed in RF10 media on ice. The luminal contents were removed and the colon was cut longitudinally and into small pieces, using a dissecting microscope.

The treatment of mLN and colon for enzymatic digestion was the same, as follows. Samples were centrifuged (7 minutes, 1400rpm, 4^{o}C) and resuspended in 500µl collagenase/Dispase and DNase solution (Table 2.6) and incubated at 37^{o}C on a thermocycler for 20 minutes, agitated frequently with pipetting. Following this incubation, 100µl 0.02% EDTA (Sigma-Aldrich, Poole, UK) was added to each sample before centrifugation, followed by addition of 500µl RF10 (7 minutes, 1400rpm, 4^{o}C). The supernatant was removed and the pellet resuspended in 1 ml RF10, each sample was then filtered through a 70µm cell strainer. Filtered samples were centrifuged as before and the cell pellets were resuspended in 1 ml RF10. Cell counts were performed using a haemocytometer.

2.4.2.1. Immunofluorescent staining of single cell suspensions

A 96-well v-bottomed plate was used to stain cells for flow cytometric analysis with approximately 500,000 cells per well. The cells were washed in 180µl 0.1% BSA/PBS and centrifuged (1 minute, 2500rpm, 4^{o}C), supernatant discarded. The cells were then resuspended in 50µl 0.1% BSA/PBS plus the required primary antibodies and incubated (20 minutes, in the dark, at 4^{o}C). After the primary antibody incubation, the cells were washed twice with 180µl 0.1% BSA/PBS. If secondary antibodies were used, they were added in 50µl 0.1% BSA/PBS and incubated for 20 minutes in the dark at 4^{o}C. The samples were then washed twice with 180µl 0.1% BSA/PBS and resuspended in 100µl PBS ready for flow cytometric analysis.

In the case of staining for DC and macrophages populations the single cell suspensions were first incubated with Fc block (supernatant of 2.4G2 hybridoma) for 30 minutes before addition of primary and secondary antibodies. In addition, the incubation time for primary antibodies was extended to 30 minutes to allow optimal DC staining.

Four-color flow cytometric analysis was performed using a FACSCalibur (BD Biosciences, San Jose, CA) with forward/side scatter gates set to exclude non-viable cells. Gates were applied appropriately according to the expression profile of the molecules being assayed. Data were analysed with FlowJo software (Tree Star, Ashland, OR).

2.5. Preparation of cDNA from Tissue Samples

The preparation of cDNA from spleen samples involved the acquisition of 20mm thick cryostat sections from frozen tissues. The samples were collected in DNase/RNase free eppendorfs (BioSphere® Micro Tube, SARSTEDT) and stored at -80^{o}C. High-purity cDNA was generated from purified mRNA using μMacs One-Step cDNA synthesis kit, according to the manufacturer's instructions (Miltenyi Biotec, Auburn, CA).

2.5.1. Real time RT-PCR

Real-time PCR was performed using IQ SYBR Green Supermix (Bio-Rad, Hercules, CA) with primers specific for *β-actin, Ccl21, Ccl19, Cxcl13, and Madcam-1* (Table 2.9). PCRs were conducted in triplicate in 10μl volumes containing

200nM primers. After an initial denaturation step (95˚C for 10 min), cycling was performed at 95˚C for 15 seconds, 60˚C for 20 s, and 72˚C for 5 seconds (45 cycles). Specific amplification was verified by melt curve analysis. mRNA transcript levels of each gene were analyzed using Applied Biosystem's SDS software (Applied Biosystems, Foster City, CA) by setting thresholds determining the cycle number at which the threshold was reached (Ct). The C_t of the β-actin was subtracted from the Ct of the target gene, and the relative amount was calculated as $2^{-\Delta Ct}$. Means of triplicate reactions (multiplied 1000-fold) are represented, data shown are representative of two separate experiments.

	Primer Sequence	
Gene	*Forward*	*Reverse*
β-actin	CGTGAAAAGATGACCCAGATCA	TGGTACGACCAGAGGCATACAG
Cxcl13	CATAGATCGGATTCAAGTTACGCC	TCTTGGTCCAGATCACAACTTCA
Ccl21	CTTCCTCAGGGTTTGCACAT	GCTGCCTTAAGTACAGCCAGAA
Ccl19	CCTTAGTGTGGTGAACACAACA	GGGGTCTAATGATGCGGAA
Madcam-1	CTCCTTTGCCCTGCTACTGG	ACAGTGGTGTGCCCTCAGC

Table 2.9 Primers used for real time RT-PCR.

2.6. Preparation of Blood Serum Samples

Cardiac punctures were performed on anaesthetised mice by qualified technicians in the Biomedical Services Unit, University of Birmingham. Blood samples were collected into 1.5ml eppendorf tubes and the blood was allowed to clot. Samples were then centrifuged at 4000rpm for 5 minutes. The serum supernatant was removed and placed in a clean eppendorf and stored at -20^{o}C. 200μl of each sample was sent to RBM Inc, USA, where the test, *Rodent MAP v2.0 – Antigens* (Multi-Analyte Profile of 58-biomarkers, Table 2.10) performed.

Apo A1 (Apolipoprotein A1)	IP-10 (Inducible Protein-10) (aka CXCL10)
CD40	KC/GROalpha (Melanoma Growth Stimulatory Activity Protein)
CD40 Ligand	LIF (Leukemia Inhibitory Factor)
CRP (C Reactive Protein)	Lymphotactin
EGF (Epidermal Growth Factor)	M-CSF (Macrophage-Colony Stimulating Factor)
Endothelin-1	MCP-1 (Monocyte Chemoattractant Protein-1) (aka CCL2)
Eotaxin	MCP-3 (Monocyte Chemoattractant Protein-3) (aka CCL7)
Factor VII	MCP-5 (Monocyte Chemoattractant Protein-5)
FGF-9 (Fibroblast Growth Factor-9)	MDC (Macrophage-Derived Chemokine)
FGF-basic (Fibroblast Growth Factor-basic)	MIP-1alpha (Macrophage Inflammatory Protein-1alpha) (aka CCL3)
Fibrinogen	MIP-1beta (Macrophage Inflammatory Protein-1beta) (aka CCL4)
GCP-2 (Granulocyte Chemotactic Protein-2)	MIP-1gamma (Macrophage Inflammatory Protein-1gamma) (aka CCL9)
GM-CSF (Granulocyte Macrophage-Colony Stimulating Factor)	MIP-2 (Macrophage Inflammatory Protein-2) (aka CXCL14)
GST-alpha (Glutathione S-Transferase alpha)	MIP-3beta (Macrophage Inflammatory Protein-3beta) (aka CCL19)
Haptoglobin	MMP-9 (Matrix Metalloproteinase-9)
IFN-gamma (Interferon-gamma)	MPO (Myeloperoxidase)
IgA (Immunoglobulin A)	Myoglobin
IL-10 (Interleukin-10)	OSM (Oncostatin M)
IL-11 (Interleukin-11)	RANTES (Regulation Upon Activation, Normal T-Cell Expressed and Secreted)
IL-12p70 (Interleukin-12p70)	SAP (Serum Amyloid P)
IL-17 (Interleukin-17)	SCF (Stem Cell Factor)
IL-18 (Interleukin-18)	SGOT (Serum Glutamic-Oxaloacetic Transaminase)
IL-1alpha (Interleukin-1alpha)	TIMP-1 (Tissue Inhibitor of Metalloproteinase Type-1)
IL-1beta (Interleukin-1beta)	Tissue Factor
IL-2 (Interleukin-2)	TNF-alpha (Tumor Necrosis Factor-alpha)
IL-3 (Interleukin-3)	TPO (Thrombopoietin)
IL-4 (Interleukin-4)	VCAM-1 (Vascular Cell Adhesion Molecule-1)
IL-5 (Interleukin-5)	VEGF (Vascular Endothelial Cell Growth Factor)
IL-6 (Interleukin-6)	vWF (von Willebrand Factor)
IL-7 (Interleukin-7)	

Table 2.10 Table of biomarkers in *Rodent MAP v2.0 – Antigens* (RBM Inc, USA)

2.7. Foetal Liver Cell Reconstitution Studies

2.7.1. Preparation of Foetal Liver Cells

Owing to the fact that p100Δ mice survive to around 3 weeks of age, harvesting of bone marrow cells was difficult, therefore to increase the number of cells recovered, foetal liver cells (FLCs) from E15 embryos were used instead. At E15 the liver is the major site for haematopoiesis.

Female mice at day 15 of gestation were sacrificed and the embryos removed. The livers of each embryo were dissected using a dissecting microscope and kept individually in RF10. Each liver was passed through a 70μm cell strainer into 5 ml RF10 to produce a single cell suspension of FLCs. The samples were centrifuged (7 minutes, 2500rpm, 4^{o}C) and washed once in 5 ml 1% BSA/PBS. The supernatant was removed and the cell pellets were resuspended gently in 1 ml 10% DMSO/FCS, avoiding generation of air bubbles. The samples were then transferred quickly to a pre-cooled (-80^{o}C) container lined with isopropanol (Sigma-Aldrich, Poole, UK). The container plus samples was placed back in the -80^{o}C freezer until the following day, when the samples were transferred to liquid nitrogen for storage.

When the FLC samples were ready for use they were thawed by addition of 500μl RF10, with gentle agitation using a 1ml pipette. Once thawed the cell suspensions were placed in 30ml RF10 in a falcon tube and left on ice for 20 minutes, followed by centrifugation (7 minutes, 2500rpm, 4^{o}C) and resuspension in 1ml RF10 ready for cell counting. Cell counts were performed using a haemocytometer, with the addition of Trypan Blue (Sigma-Aldrich, Poole, UK) to identify dead cells.

2.7.2. Foetal Liver Cell Reconstitutions

WT mice (age 8-11wks) were lethally irradiated and reconstituted with either 100% p100Δ, 50:50 WT:p100Δ or 100% p100Δ FLCs. Three months following reconstitution the mice were sacrificed and tissues were isolated and frozen. This work was carried out in collaboration with Dr Elena Vigorito at the Babraham Institute, Cambridge.

2.8. Statistical Analysis

All experiments were analysed using nonparametric, two-tailed Mann-Whitney U-test, unless otherwise indicated. Confidence interval was set at 95%.

3. NF-κB2 Involvement in Tertiary Lymphoid Tissue Development in the Colon

3.1. Introduction

Isolated lymphoid follicles (ILFs) are located throughout the small intestine and colon, and consist of an organised cluster of B and T lymphocytes, and DCs. ILFs develop postnatally and can be identified in C57Bl6 mice from around postnatal day 25 (P25) (Hamada et al., 2002). It has been proposed that ILFs develop from precursor structures termed cryptopatches (CPs) (Eberl, 2005). CPs are composed of a cluster of LTi-like cells ($CD3^-CD4^+$IL-$7R\alpha^+ROR\gamma t^+$) (Saito et al., 1998; Eberl and Littman, 2004) and DCs (Kanamori et al., 1996). The transition of a CP to an ILF is defined by the recruitment of B cells to the structure and this process is dependent on B cells expressing CCR6 (McDonald et al., 2007), CXCR5 (Velaga et al., 2009), and Integrin $\alpha_4\beta_7$ (Wang et al., 2008). The expression of these receptors allows B cells to migrate to the intestine in response to CCL20 (ligand for CCR6), expressed by epithelial cells (Tanaka et al., 1999), CXCL13 (ligand for CXCR5), expressed by a subtype of DCs, and MAdCAM-1 (ligand for Integrin $\alpha_4\beta_7$), expressed by ILF-associated vessels (Wang et al., 2008). Furthermore, it has been shown that ILF B cells are predominately B-2 B cells, based on expression of CD23 and lack of CD5 expression (Hamada et al., 2002; Wang et al., 2006; Lorenz et al., 2003), and display a mature phenotype, co-expressing IgM and IgD (Wang et al., 2006).

Eberl suggested subdivision of ILFs into two types: immature and mature, the difference being that mature ILFs possess germinal centres (GCs) (Eberl and Sawa,

2010). Essentially, the formation of GCs allows for B cells to undergo Ig class-switching and it has been shown that ILF B cells preferentially differentiate into IgA producing plasma cells (Wang et al., 2006). Work by Yamamoto *et al*, demonstrated that mice treated *in-utero* with antagonistic LTβR-Ig, to ablate PP development, were still able to produce Ag-specific intestinal IgA (Yamamoto et al., 2000) and later it was discovered that in this model, increased numbers of ILFs developed in a potentially compensatory mechanism for the loss of PP development (Kweon et al., 2005).

The $LT\alpha_1\beta_2$-LTβR signalling axis is indispensable for SLO development and it has been postulated that it plays a similar role in tertiary lymphoid tissue development. In mice where LT expression is compromised, such as $Lt\alpha^{-/-}$ or $Lt\beta R^{-/-}$ mice, or in mice lacking LTi cells ($ROR\gamma t^{-/-}$ mice), CPs and ILFs fail to develop (Ivanov et al., 2006; De Togni et al., 1994; Hamada et al., 2002; Taylor et al., 2004; Lorenz et al., 2003). Moreover, signalling downstream of LTβR activates the alternative NF-κB pathway (Dejardin et al., 2002; Müller and Siebenlist, 2003). The p100Δ mouse model exhibits constitutive alternative pathway activation and the development of secondary lymphoid tissue in this model has previously been investigated (Ishikawa et al., 1997; Guo et al., 2007). In a novel approach to studying tertiary lymphoid tissue development, we utilise the p100Δ model to investigate the role of the alternative NF-κB pathway in the development of colonic ILFs.

3.2. Results

3.2.1. Early postnatal death of p100Δ mice

Previous studies have described the reduced body weight and early postnatal death of p100Δ mice (Ishikawa et al., 1997). Ishikawa *et al*, attributed this phenotype to gastric hyperplasia of the stomach epithelial layer, with occlusion of the lumen. We confirm this published data showing that p100Δ mice appear smaller than WT littermates at two weeks of age (Figure 3.1. A) and after birth they gain weight at a slower rate (Figure 3.1. B). The survival of p100Δ mice is noticeably reduced compared with WT littermates, with 100% death rate by four weeks of age (Figure 3.1. C). Constitutive activation of the alternative NF-κB pathway leads to early postnatal death.

3.2.2. Augmented formation of colonic B cell aggregates in p100Δ mice

Within the intestine tertiary lymphoid tissues encompass CPs and ILFs. Intestinal ILFs are inducible structures, which occur postnatally and are defined as a cluster of B lymphocytes. In C57Bl6 mice, ILFs remain largely absent until P25 (Hamada et al., 2002).

Figure 3.1 Reduced survival and body weight of p100Δ mice

A *Reduced size and body weight of p100Δ mice in comparison to WT littermates. (Postnatal day 15 and 18 n≥17, day 21 n≥8, for each genotype).* ***B*** *Limited postnatal survival of p100Δ mice (n=17 for each genotype).*

A

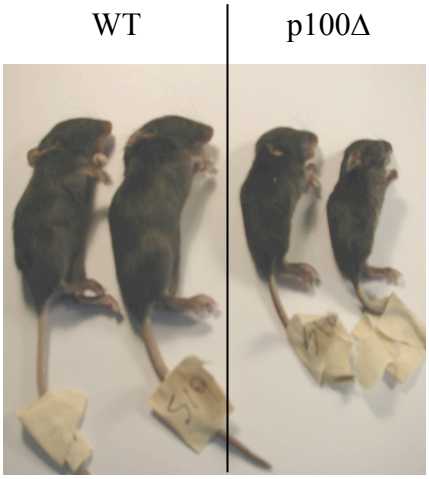
WT
p100Δ

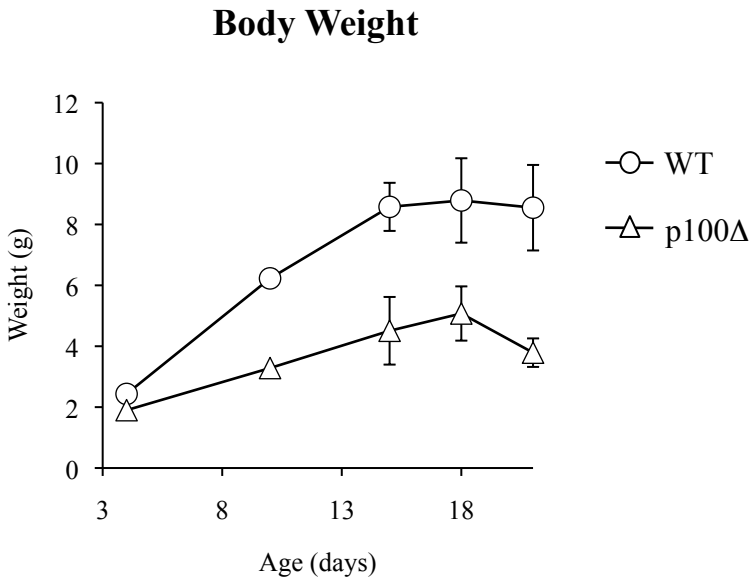
Body Weight
Weight (g)
12
10
8
6
4
2
0
3
8
13
18
Age (days)
WT
p100Δ

B

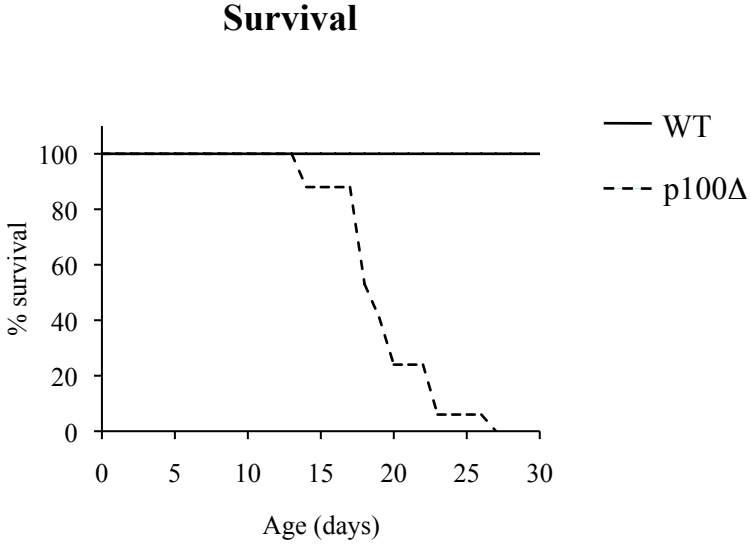
Survival
% survival
100
80
60
40
20
0
0
5
10
15
20
25
30
Age (days)
WT
p100Δ

Figure 3.1

Cryostat sections of colon were stained with immunofluorescently labelled antibodies to identify B cell aggregates. Figure 3.2, shows tilescan images (acquired using confocal microscopy) of WT and p100Δ colons stained with IgM (red) to identify B cell aggregates; sections were counterstained with nuclei dye DAPI (grey). p100Δ mice present with an increase in B cell aggregates in the colon (Figure 3.2. A).

B cell aggregates were enumerated following immunofluorescence staining of colon sections with anti-IgM and visualisation on a fluorescence microscope (Leica DM6000). Three separate sections of colon where assessed for each individual animal. A significant increase in colonic B cell aggregates in p100Δ mice was observed at P15 (WT, n=4, mean=4.9±2.8, p100Δ, n=4, mean=20.9±8.7, p=0.013) and P21 (WT, n=3, mean=1.5±1.3, p100Δ, n=6, mean=41.2±17.9, p=0.003) with respect to WT mice (Figure 3.2. B). Quantification of B cell aggregate size was performed following immunofluorescence staining of colon sections with anti-IgM and measurement of the IgM foci. At P21, p100Δ mice exhibit larger colonic B cell aggregate size compared with WT littermate controls (WT, n=3, mean=15611±2270, p100Δ, n=3, mean=37328±9031, p=0.100) (Figure 3.2. C).

Constitutive activation of NF-κB2 p100 leads to a significant increase in B cell aggregates in the colon. The structure and organisation of these aggregates was then assessed for their similarity to WT ILFs.

Figure 3.2 Augmented formation of colonic B cell aggregates in p100Δ mice

A *Immunofluorescence staining of colon sections showing DAPI nuclei staining (grey) and B cells stained with anti-IgM antibody (red). p100Δ mice display increased numbers of colonic B cell aggregates. Representative tilescans shown. Scale bar indicates 1mm.*

B *B cell aggregates per colon section were enumerated following immunofluorescence staining for IgM (as in A) and viewed by fluorescence microscopy. P10: WT n=3, p100Δ n=3. P15: WT n=4, p100Δ n=4. P21: WT n=4, p100Δ n=6. Graph shows mean number of B cell aggregates per colon, errors bars indicate standard deviation. Students T-test * p≤ 0.05, ** p≤ 0.02.*

C *The B cell aggregates in p100Δ colon at P21 show a trend to be larger in area than in WT littermates (n=3 for each genotype). Bar indicates mean.*

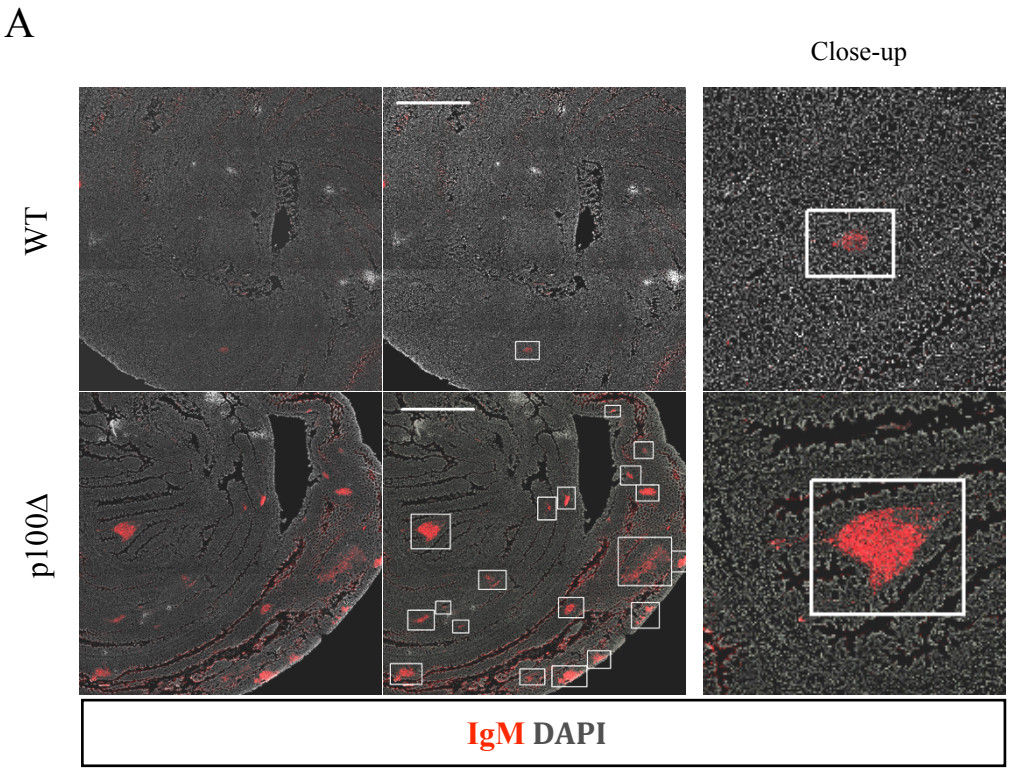
A
Close-up
WT
p100Δ
IgM DAPI
B
Colonic B cell Aggregates
Mean No. B cell aggregates (per colon)
70
60
50
40
30
20
10
0
8
10
12
14
16
18
20
22
Postnatal Age (days)
ns
*
**
WT
p100Δ
C
P21: Aggregate Size
B cell aggregate size (μm²)
5.0x10⁴
4.0x10⁴
3.0x10⁴
2.0x10⁴
1.0x10⁴
0
WT
p100Δ

Figure 3.2

Figure 3.3 Organisation of haematopoietic cells within p100Δ colonic B cell aggregates closely resembles WT ILFs

WT ILFs (A and B, left panel) typically consist of a $B220^+$ core (red) surrounded by $CD11c^+$ dendritic cells (green, 2^{nd} line), interspersed with $CD3^+$ T cells (green, 3^{rd} line). $F4/80^+$ macrophages (green, 4^{th} line) are located throughout the colonic tissue, but not within the ILF. The structure of p100Δ colonic B cell aggregates (A and B, right panel) closely resembles that of WT ILFs. Representative immunofluorescent confocal images are shown.

***A**, x10 magnification. Scale bar denotes 200μm.*
***B**, x40 magnification. Scale bar denotes 50μm.*

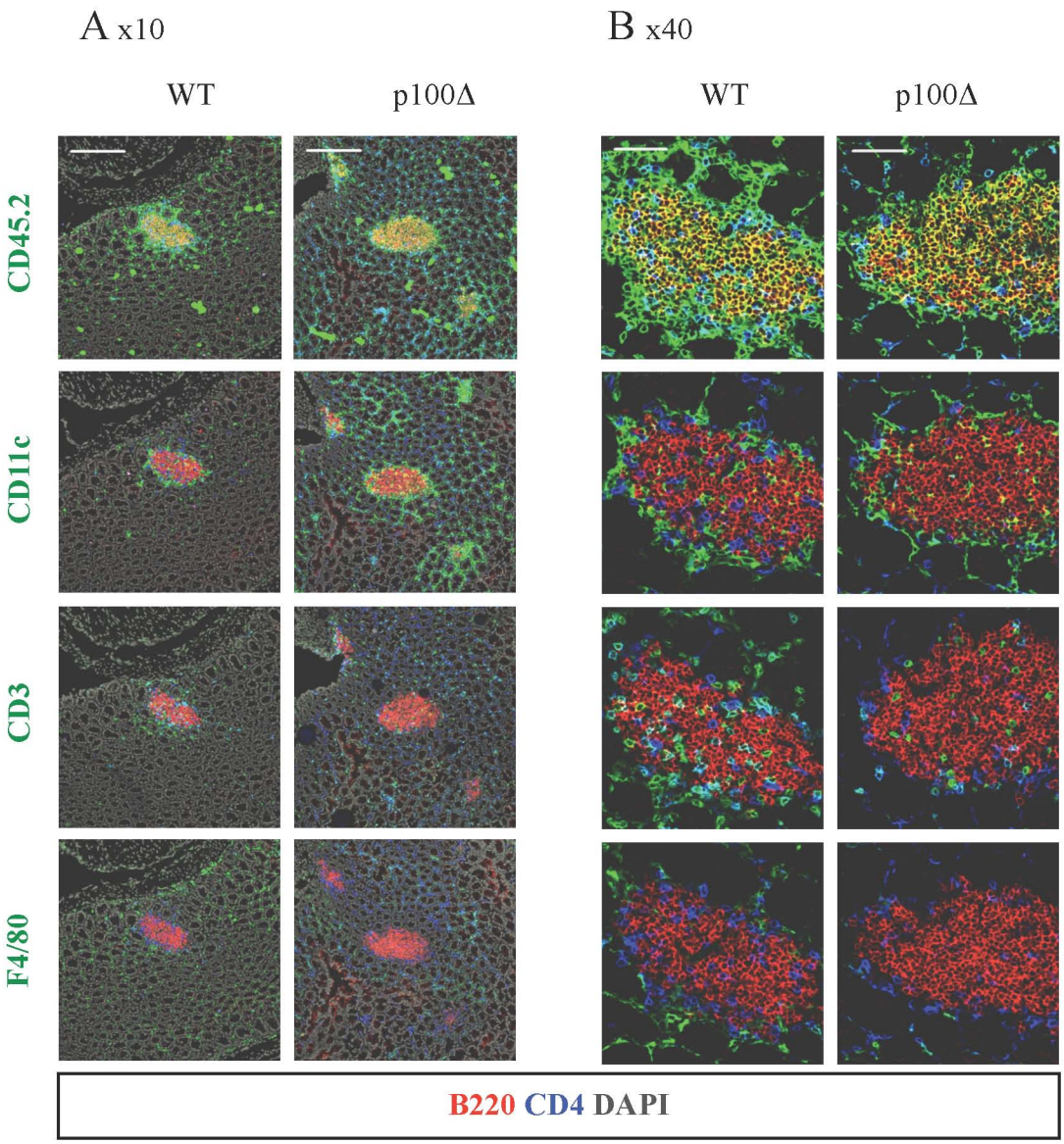
A x10
B x40
WT
p100Δ
WT
p100Δ
CD45.2
CD11c
CD3
F4/80
B220 CD4 DAPI

Figure 3.3

Figure 3.4 B cells constituting WT ILFs and p100Δ B cell aggregates display a mature phenotype and are capable of class switching

The phenotype of the B cells present was determined by staining with anti-IgM antibody (red), anti-IgD (green), anti-B220 (blue) and the nuclei stain DAPI (grey).

***A** Characteristically the B cells constituting WT ILFs exhibit a mature phenotype, $B220^{+}IgM^{+}IgD^{+}$ (A, merge, left panel, pale blue). In addition, $B220^{-}IgM^{+}$, $B220^{-}IgD^{+}$ (A, merge left panel, red and green respectively) and $B220^{-}IgA^{+}$ (**B**, left panel) cells are also present. This phenotype is mirrored in the p100Δ colon (A, right panel). Representative immunofluorescent confocal images are shown (x40 magnification). Scale bar denotes 50μm.*

A Mature B cells

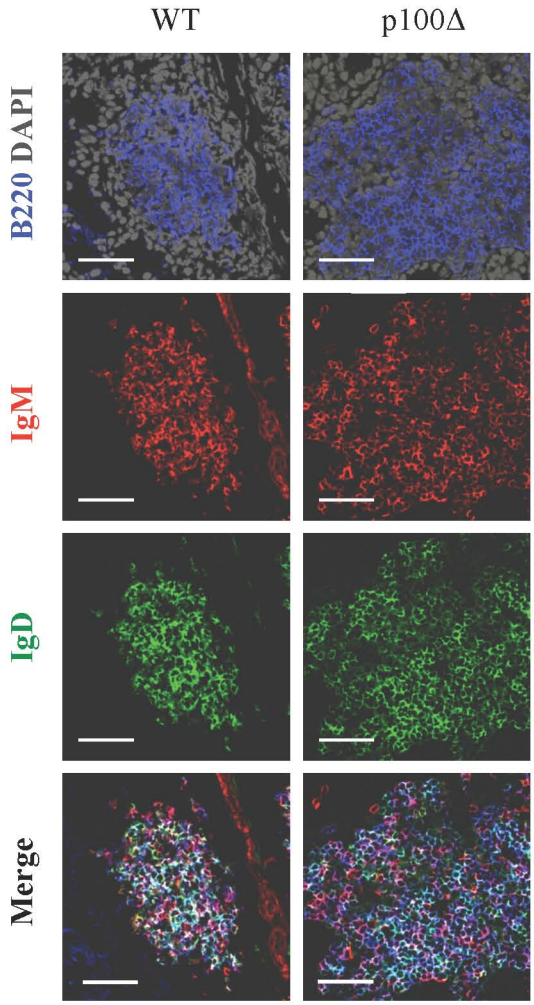

B IgA^+ cells

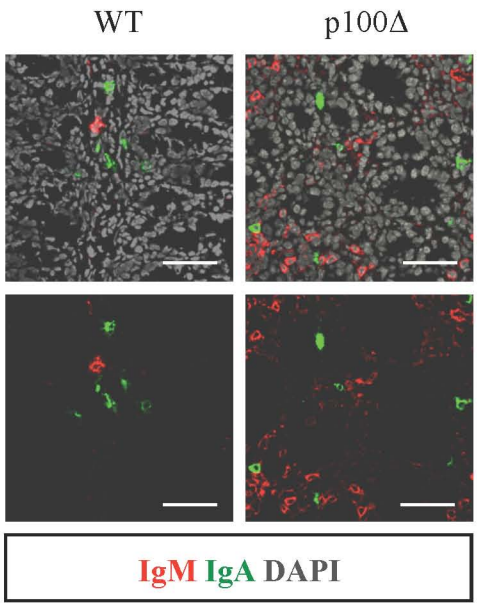

Figure 3.4

Figure 3.5 Presence of LTi-like cells and Tregs, and normal proliferation of colonic aggregate cells in p100Δ mice

A *Staining with anti-B220 (blue), anti-CD3 (green) and anti-CD4 (red) allows identification of* $CD3^+CD4^+$ *T cells (yellow cells) and* $CD3^-CD4^+$ *LTi-like cells (red, white circles) in both WT ILFs and p100Δ B cell aggregates.*

B *Regulatory T cells (white circles) were identified in both WT ILFs and p100Δ B cell aggregates by co-staining of anti-Foxp3 (green, nuclear stain) and anti-CD4 (red). Representative immunofluorescent confocal images are shown (x40 magnification).*

C *Ki67 staining identifies proliferating epithelial cells in the WT and p100Δ colon (dotted line), as well as proliferating cells within the WT ILFs and p100Δ B cell aggregates (arrow heads). B cells stained with anti-B220 (red) and T cells stained with anti-CD4 (blue).*

D *Close-up images of C (upper row).*

Scale bar represents 50mm. Top panel of A, B and C counterstained with DAPI.

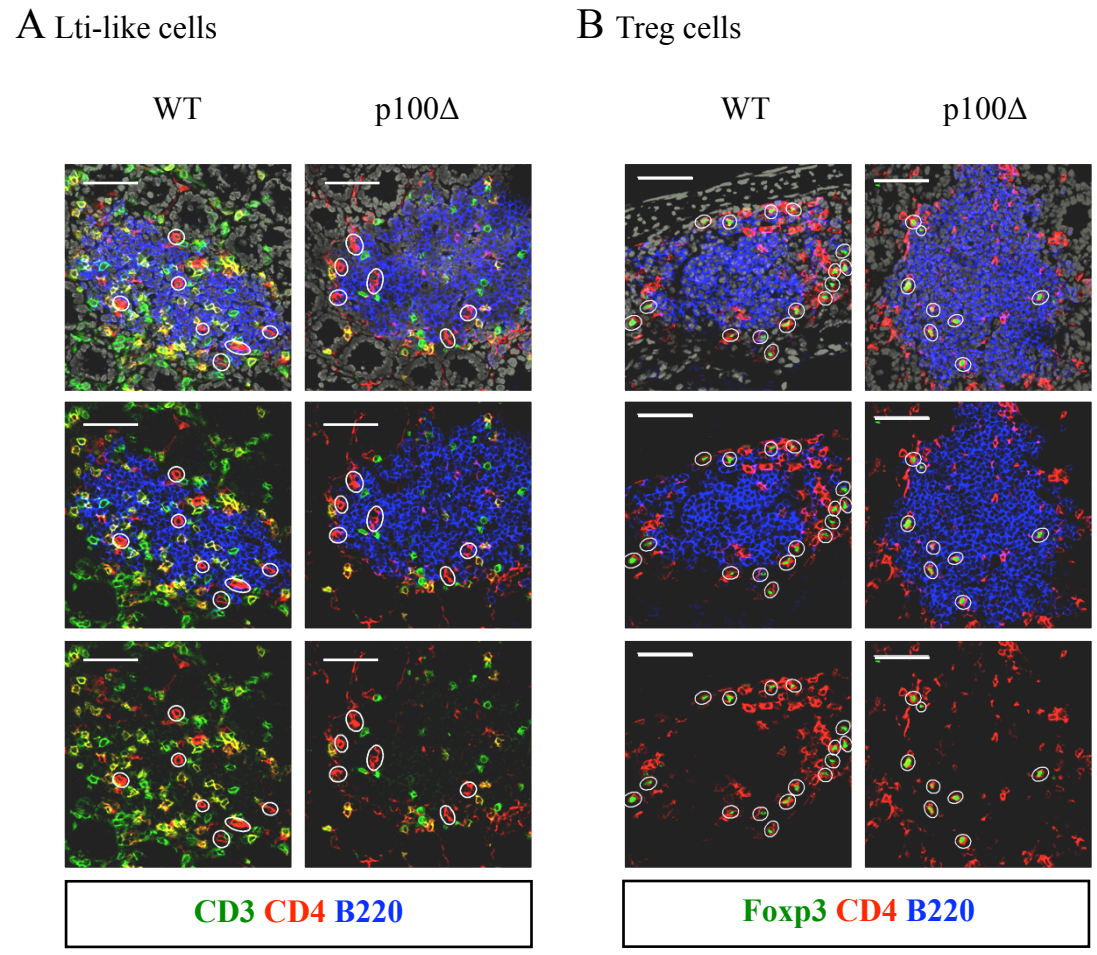
A Lti-like cells
WT
p100Δ
B Treg cells
WT
p100Δ
CD3 CD4 B220
Foxp3 CD4 B220
C Proliferating cells
WT
p100Δ
D
WT
p100Δ
Ki67 B220 CD4
Ki67 B220 CD4

Figure 3.5

3.2.3. Organisation of haematopoietic cells within p100Δ colonic B cell aggregates closely resembles WT ILFs

Intestinal WT ILFs consist of a central core of $B220^+$ B lymphocytes, surrounded by a ring of $CD11c^+$ DCs and interspersed with $CD3^+$ T cells (Hamada et al., 2002) (Figure 3.3. A & B, left panel). The B cell aggregates observed in the colon of p100Δ mice displayed a structure that closely resembles this phenotype (Figure 3.3. A & B, right panel). Interestingly, despite this normal cellular organisation within the B cell aggregates, areas adjacent to these regions display differences in cellular presence. A clear increase in $CD45^+$ haematopoietic cells can be seen in p100Δ mice and this increase is attributable to an increase in $CD11c^+$ DCs and, to a lesser extent, $CD3^+$ T cells (Figure 3.3. A, x10 magnification). In addition, $CD11c^+$ DCs and $CD3^+$ T cells appeared to be spread throughout the tissue in the p100Δ colons instead of being in and around the B cell aggregates, as in WT colons (Figure 3.3. A).

This data provides the first piece of evidence that the colonic B cell aggregates observed in p100Δ mice share characteristics analogous with ILFs.

3.2.4. B cells constituting WT ILFs and p100Δ B cell aggregates display a mature phenotype and are capable of class-switching

The defining characteristic of an ILF is the presence of B lymphocytes. Characterisation of these B cells was performed by confocal microscopy by staining sections of colon with anti-B220 to identify B cells and with anti-IgD and anti-IgM to define maturity. Mature peripheral B cells are $B220^+IgD^+IgM^+$ (Norvell and Monroe,

1996) and are able to undergo class switching, during which expression of B220 is lost, as is either IgM, IgD or both, resulting in their differentiation into antibody producing plasma cells (for example $B220^{-}IgD^{-}IgM^{+}$ or $B220^{+}IgD^{+}IgM^{-}$). The majority of B lymphocytes within WT ILF display a mature phenotype, $B220^{+}IgD^{+}IgM^{+}$ (individually blue, green and red respectively, coexpression: pale blue.) (Figure 3.4. A, left panel). The B cells constituting p100Δ B cell aggregates also display this mature phenotype (Figure 3.4. A, right panel). In addition, $B220^{-}IgD^{+}$ (green) and $B220^{-}IgM^{+}$ (red) plasma cells can be seen in both mice indicating that class switching is not affected in the colon of p100Δ mice.

The production of IgA antibody is crucial to effective gut immunity and there are several possible mechanisms explaining the presence of IgA secreting plasma cells in the intestine. Firstly, there is evidence that chemokines such as CCL25, CCL28 and MAdCAM-1 are key to IgA plasma cell localisation to the intestine (Bowman et al., 2002; Hieshima et al., 2004). Secondly, several groups have shown that *in situ* class switching of $B220^{+}IgM^{+}$ B cells to $B220^{-}IgA^{+}$ plasma cells and the presence of ILFs are an important source of IgA production in the gut (Fagarasan et al., 2001; Lorenz and Newberry, 2004; Eberl, 2005). In Figure 3.4, $B220^{-}IgA^{+}$ plasma cells (green) can be seen in WT and p100Δ mice in the vicinity of ILFs (Figure 3.4. B). It would be interesting and useful to investigate the origins and functional capabilities of these cells.

This data demonstrating that the mature B cell phenotype seen in WT ILF B cells is reflected in p100Δ B cell aggregates provides the second piece of evidence that the lymphoid structures in the colon of p100Δ mice are ILFs.

3.2.4.1. Presence of LTi-like cells and Tregs, and normal proliferation of colonic lymphoid aggregate cells in p100Δ mice

The critical role for and presence of LTi-like cells in ILF development has been well described (Eberl and Littman, 2004; Ivanov et al., 2006). Staining of colon sections with immunofluorescent antibodies against B220 (blue) to show B cell aggregates, CD3 (green) to label T cells and CD4 (red), allowed identification of LTi-like cells expressing high levels of CD4, but not CD3 or B220 (Figure 3.5. A. Red cells, bottom panel). These cells are clearly present in both WT ILFs and p100Δ B cell aggregates. To rule out the chance of these cells being CD4 expressing DCs, staining was performed with CD3 and CD11c combined in the FITC channel alongside staining for CD4 and B220 and clear LTi-like cells were observed in both WT ILFs and p100Δ B cell aggregates (Figure 9.5).

Regulation of immune responses in the gut is critical due to the exposure of intestinal cells to a broad range of commensal and pathogenic bacteria and the incidence of $CD4^+$ regulatory T cells within the gut is indispensible for this regulation. T regulatory cells are identifiable by their expression of the transcription factor Foxp3 (Hori et al., 2003). Figure 3.5, shows the presence of $CD4^+Foxp3^+$ T regulatory cells, with characteristic punctate nuclear Foxp3 staining, within WT ILFs and p100Δ B cell aggregates (Figure 3.5. B). This data demonstrates that regulatory T cells are present in the colon of p100Δ mice, as they are in WT mice. In this figure the number of Tregs appears reduced in p100Δ B cell aggregates, therefore assessment of Treg numbers in the colon would be beneficial to expand this study.

The question of whether the increase in the number of B cell aggregates and their size (P21) in p100Δ mice is a result of increased homing of B cells to the colon

or due to increased proliferation of B cells *in situ* was assessed by immunofluorescence staining for the proliferation marker Ki67. $Ki67^+$ staining of epithelial villus cells can be seen in the colon of both WT and p100Δ mice (Figure 3.5. C. Dotted line). In addition, $Ki67^+$ lymphocytes can be seen in the B cell aggregates (Figure 3.5. C. Arrows). There was no difference in Ki67 expression in p100Δ aggregates compared with WT ILFs. This indicates that the large number of B cell aggregates in the colon of p100Δ mice is not due to an increase in B cell proliferation *in situ*, but more likely due to enhanced homing/recruitment of B cells to the colon. With respect to the T cell population within the WT ILFs and p100Δ B cell aggregates, there is no obvious difference in proliferation.

The identification of LTi-like cells and Tregs within WT ILFs and the presence of analogous populations in the p100Δ B cell aggregates provides the third piece of evidence supporting the hypothesis that these aggregates are ILFs.

3.2.5. Stromal cells of p100Δ colonic B cell aggregates express the same markers as WT ILF stromal cells

The micro-architecture of secondary lymphoid tissues relies heavily on the expression of chemokines and cell adhesion molecules by stromal cells to orchestrate lymphocyte recruitment and organisation. CXCL13 is responsible for homing of $CXCR5^+$ B cells to B cell follicles in the white pulp of the spleen. In mice lacking NF-κB2, expression of CXCL13 is downregulated in secondary lymphoid tissues, resulting in disrupted micro-architecture (Carragher et al., 2004) and in the p100Δ mouse model it has been previously described that CXCL13 mRNA is slightly but not significantly increased (Guo et al., 2007). With regards to tertiary lymphoid tissue

development, CXCL13 and expression of its receptor CXCR5 on B cells is essential for ILF formation (Velaga et al., 2009). In addition, the cell adhesion molecule, VCAM-1, has been shown to be expressed by ILF stroma (Taylor et al., 2007). Immunofluorescence staining was used to assess the expression of CXCL13 and VCAM-1 by intestinal stromal cells. $CXCL13^+$ and $VCAM\text{-}1^+$ stromal cells can be seen localised within the WT ILFs and p100Δ B cell aggregates, and there are no obvious differences in the localisation of these markers between the two genotypes (Figure 3.6. A). However, with respect to CXCL13 expression, there is a potential increase in staining intensity, indicating an increase in protein expression, in the colonic B cell aggregates in p100Δ mice, corresponding with previously published data that *Cxcl13* is a downstream gene target of NF-κB2 (Liptay et al., 1994).

In order for lymphocytes to migrate to secondary and tertiary lymphoid tissue organogenesis, a suitable vascular network is required. The vascular structures associated with ILFs express MAdCAM-1 and CD31 (Wang et al., 2008). Several studies have demonstrated the requirement for MAdCAM-1 expression and that of its receptor, Integrin $\alpha_4\beta_7$, in the development of ILFs (Miles et al., 2008; Wang et al., 2008; Gorfu et al., 2009). In Figure 3.6, expression of $MAdCAM\text{-}1^+$ and $CD31^+$ vascular structures can be A consistent increase in CD31 staining was visible across different sections of colon from individual p100Δ mice and across all p100Δ mice investigated.

The data presented here shows clearly that intestinal stromal cells within and around the colonic B cell aggregates in p100Δ mice possess all the defining features observed in WT ILFs, further supporting the hypothesis that these structures are ILFs.

Figure 3.6 Stromal cells of p100Δ colonic B cell aggregates express markers comparable to WT ILF stroma

A *Stromal cells present in WT ILFs and p100Δ B cell aggregates express the B cell homing chemokine CXCL13 (green, top panel) and the adhesion molecule VCAM-1 (green, bottom panel). B cells stained with anti-B220 (red).*

B *Staining for tissue vasculature with anti-CD31 (green) and anti-MAdCAM-1 (blue) shows co-expression of these markers on vascular endothelium (pale blue cells, merge, white circles). B cells stained with anti-IgM (red).*

Tissue counterstained with DAPI (grey). Representative immunofluorescent confocal images are shown (x40 magnification). Scale bar denotes 50μm.

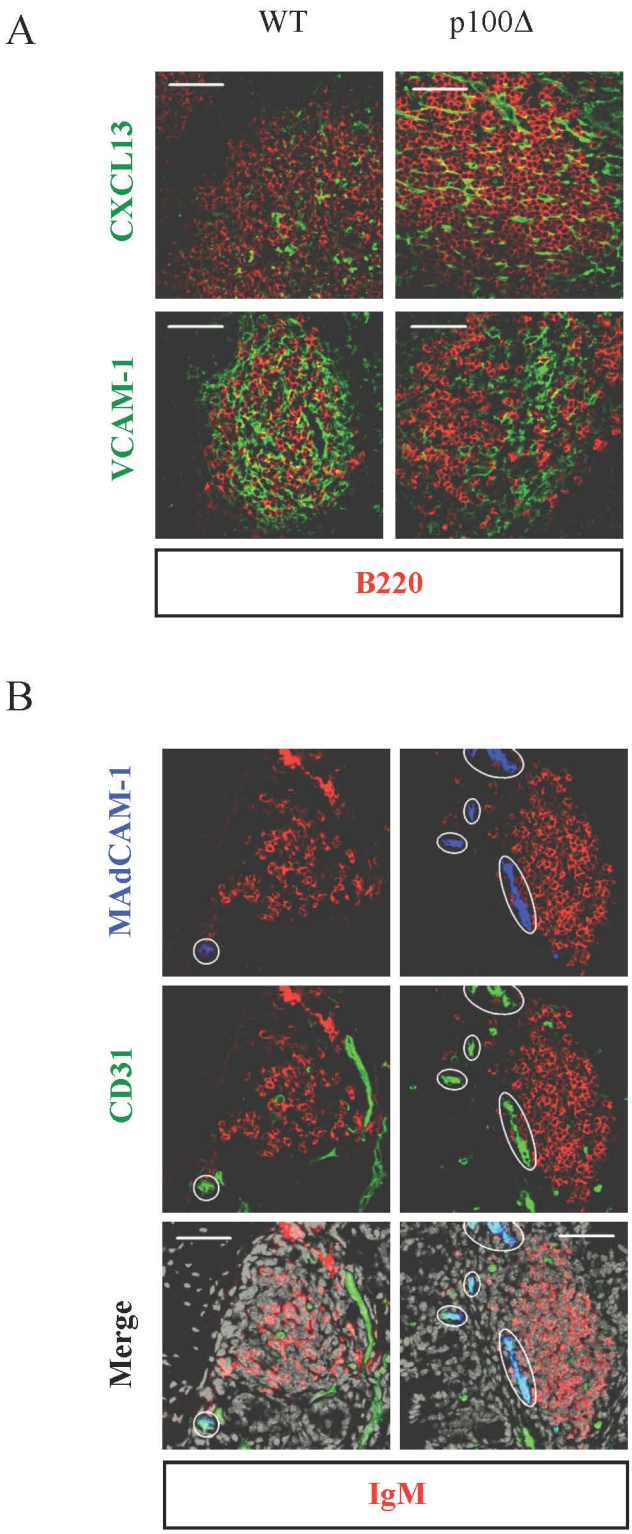

Figure 3.6

3.2.6. WT and p100Δ foetal liver cell reconstitutions

In order to dissect the haematopoietic versus stromal cell contribution to the increase in colonic ILF formation observed in p100Δ mice, foetal liver cell (FLC) reconstitutions were performed. Host WT mice were used to provide a normal stromal environment and following lethal irradiation, these mice were injected with either 50:50 mix of WT and p100Δ FLCs or 100% p100Δ FLCs, to reconstitute their immune system (positive control mice received 100% WT FLCs). In this way the development of colonic ILFs was assessed in a situation where haematopoietic cells express constitutively active NF-κB2 in a normal stromal environment. Three months post-transfer the colons of the reconstituted mice were harvested and ILF formation was assessed by confocal microscopy.

Figure 3.7, shows enumeration of B cell aggregates, as previously described (Chapter 3.2.2, Materials and Methods 2.2.1.3). Mice receiving 100% p100Δ FLCs presented with a significant increase in colonic B cell aggregates compared with those receiving 100% WT FLC (100% WT, n=4, mean=10.3±10.9, 100% p100Δ, n=3, mean=73.8±44.1, p=0.004) (Figure 3.7. A). Interestingly, mice receiving 50:50 WT:p100Δ FLCs developed B cell aggregates in similar numbers to that seen in mice receiving 100% WT FLC (50:50 WT:p100Δ, n=5, mean=13.3±6.6, p=0.617). The organisation of the B cell aggregates formed in these chimeric mice resembles WT ILF structures (Figure 3.7. B). The aggregates consist of a $B220^+$ B cell core (red), surrounded with $CD11c^+$ DCs (green, middle panel) and interspersed with $CD3^+$ T cells (green, lower panel). LTi-like cells ($CD3^-CD4^+$, blue cells, bottom panel) can be seen within these structures and there is no obvious difference between the different chimeric animals. In addition, the majority of B cells present with a mature

phenotype, $B220^{+}IgD^{+}IgM^{+}$ (Figure 3.7. C, pale blue cells, bottom panel). Furthermore, $B220^{-}IgD^{+}$ (green) and $B220^{-}IgM^{+}$ (red) plasma cells can be seen in both mice indicating that class switching is not affected in the colons of the reconstituted animals.

This data demonstrates that haematopoietic cells with constitutive activation of NF-κB2 p100 are able to significantly increase ILF formation in the colon of WT host mice. The observation that mice receiving 50:50 WT:p100Δ FLC developed ILFs in similar numbers to that seen in mice receiving 100% WT FLC, may be due to a reduction in cell survival of p100Δ derived lymphocytes when in competition with WT derived cells (Appendix, Figure 9.4), or due to a competitive defect in lymphocyte homing to the intestine.

Figure 3.7 Mice receiving 100% p100Δ foetal liver cells show an increase in colonic B cell aggregates with ILF characteristics

WT mice were lethally irradiated and reconstituted with either 100% WT foetal liver cells (FLC), 50:50 WT:p100Δ FLC or 100% p100Δ FLC.

***A** Colonic B cell aggregates were enumerated by staining colon sections with fluorescently labelled anti-B220 and visualised using fluorescence microscopy. Graph shows number of B cell aggregates per colon. Bar indicates mean. Students T-test, ** $p \leq 0.02$, ns= not significant.*

***B** Colon sections were stained for $CD11c^+$ DCs (green, upper panel), $CD3^+$ T cells (green, lower panel), $B220^+$ B cells (red) and $CD4^+$ T cells (blue). Scale bar denotes 50μm.*

***C** The phenotype of the B cell present in the aggregates was determined by staining with anti-IgM antibody (red), anti-IgD (green), anti-B220 (blue) and the nuclei stain DAPI (grey). The majority of B cells present within the aggregates have a mature phenotype, $B220^+IgM^+IgD^+$ (A, merge, left panel, pale blue). In addition, $B220^-IgM^+$, $B220^-IgD^+$ (A, merge left panel, red and green respectively) and $B220^-IgA^+$ (B, left panel) plasma cells are also present. Scale bar denotes 50μm.*

A

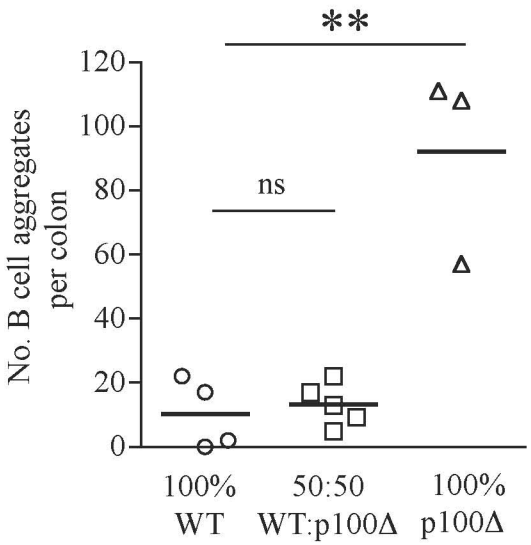
**
ns
No. B cell aggregates per colon
120
100
80
60
40
20
0
100% WT
50:50 WT:p100Δ
100% p100Δ

B

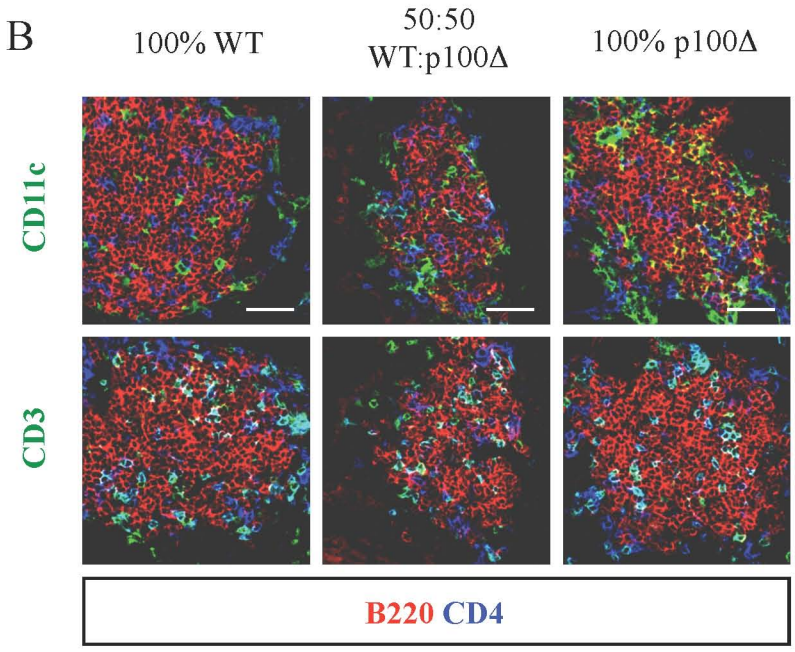
100% WT
50:50 WT:p100Δ
100% p100Δ
CD11c
CD3
B220 CD4

Figure 3.7

C

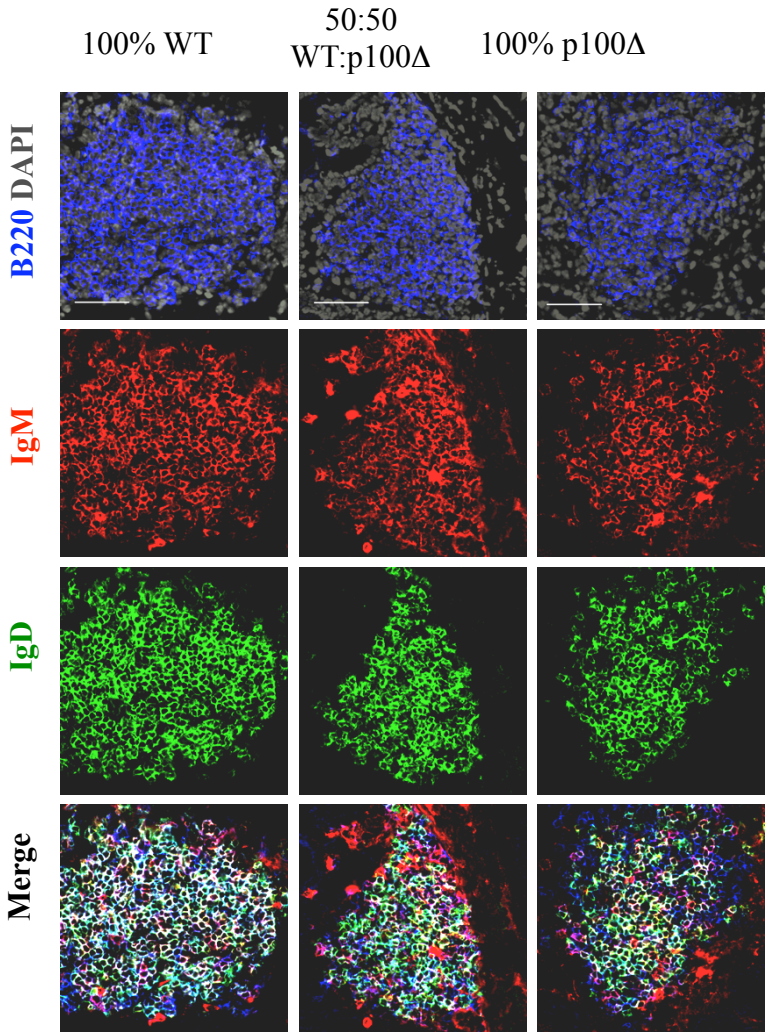

Figure 3.7

Figure 3.8 The B cell aggregate stroma in mice receiving 100% p100Δ FLC express ILF stromal markers

A *Stromal cells present in WT ILFs and p100Δ B cell aggregates express the B cell homing chemokine CXCL13 (green, top panel) and the adhesion molecule VCAM-1 (green, bottom panel). B cells stained with anti-B220 (red).*

B *Staining for tissue vasculature with anti-CD31 (green) and anti-MAdCAM-1 (blue) shows co-expression of these markers on vascular endothelium (pale blue cells, merge, white circles). B cells stained with anti-IgM (red) and tissue counterstained with DAPI (grey).*

Representative immunofluorescent confocal images are shown (x40 magnification). Scale bar denotes 50μm.

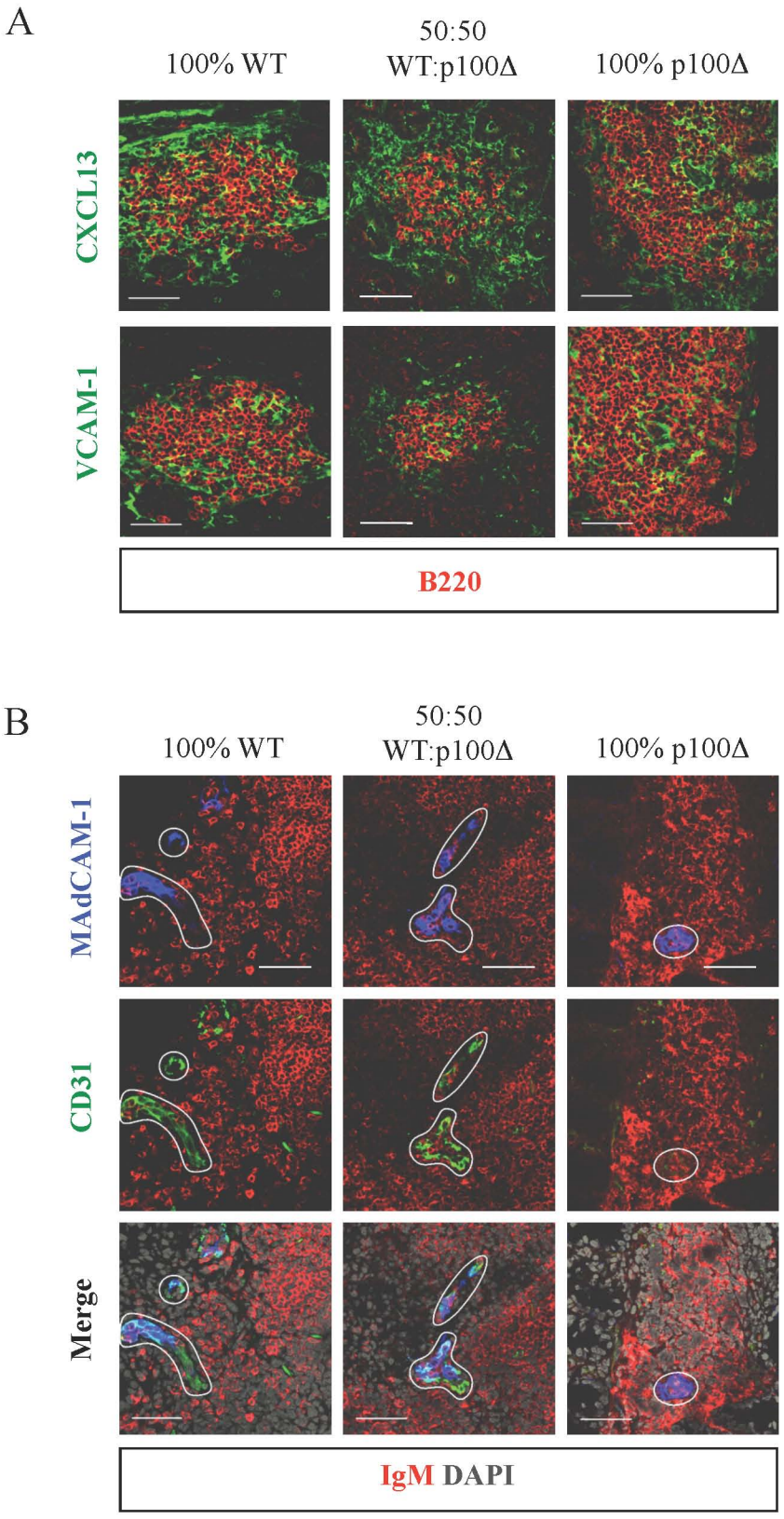
A
100% WT
50:50
WT:p100Δ
100% p100Δ
CXCL13
VCAM-1
B220
B
100% WT
50:50
WT:p100Δ
100% p100Δ
MAdCAM-1
CD31
Merge
IgM DAPI

Figure 3.8

3.2.6.1. Expression of stromal markers in colonic ILFs in mice receiving 100% p100Δ foetal liver cells

Following analysis of the presence of ILFs in chimeric mice, the characteristics of the ILF stroma was assessed using confocal microscopy. CXCL13 and VCAM-1 expression can be seen in the colonic B cell aggregates found in mice receiving 100% WT, 50:50 mix of WT and p100Δ or 100% p100Δ FLCs (Figure 3.8. A) and there are no obvious differences in the expression of these markers.

In Figure 3.8, expression of MAdCAM-1^+ and $CD31^+$ vascular structures can be seen in the vicinity of B cell aggregates in 100% WT FLC, 50:50 mix of WT and p100Δ and 100% p100Δ FLCs reconstituted colon (Figure 3.8. B).

This data demonstrating the ability of p100Δ haematopoietic cells to drive an increase in colonic ILF formation, does not completely rule out a role for the stroma. The ILF formation in these reconstitution experiments was assessed three months post transfer, whereas p100Δ mice develop augmented ILF formation from two weeks of age. It would be interesting and useful to perform further reconstitution experiments for analysis at 2-3 weeks post transfer to evaluate this further. Nevertheless, the important role of haematopoietic cells in augmenting ILF development is clear and therefore further characterisation of this cell compartment was undertaken.

3.2.7. Characterisation of lymphocyte subsets in p100Δ mice

3.2.7.1. Differences in spleen, mLN and colon absolute cell number in p100Δ mice

When absolute cell counts were performed following digestion of the spleen, mLN and colon of WT and p100Δ mice, a reduction in splenic cell numbers was observed in p100Δ mice (WT n=9, median=46.4 $x10^6$, p100Δ n=9, median=9.1 $x10^6$, p=0.001) and no difference was seen in total mLN cell numbers (WT n=7, median=5.2 $x10^6$, p100Δ n=7, median=6.5 $x10^6$, p=0.535), when compared with WT mice (Figure 3.9). Compared to WT, there is an increase in the size of mLN of p100Δ mice size relative to their reduced size/weight. Importantly, an approximate two-fold increase in total colonic cell numbers was observed in p100Δ mice compared with WT mice (WT n=9, median=650,000, p100Δ n=9, median=1.35 $x10^6$, p=0.0009) (Figure 3.9). This increase correlates with the observation of a significant increase in colonic ILF formation in p100Δ mice.

3.2.7.2. Assessment of B and T cell populations in the spleen, mLN and colon of p100Δ mice

The significant increase in ILF formation observed in the colon of p100Δ mice prompted an investigation of lymphocyte populations within this tissue and in comparison with the draining lymph node of the gut, the mLN, and the spleen.

Single cell suspensions of WT and p100Δ splenocytes were prepared and stained with immunofluorescently labelled anti-B220, to identify B cells, and anti-CD3, to identify T cells, and analysed by flow cytometry. Within the spleen there was

no significant difference in the proportion of B cell (WT n=9, median=65.3, p100Δ n=9, median=62.9, p=0.34) and T cell (WT n=9, median=10.9, p100Δ n=9, median=17.7, p=0.09) populations between WT and p100Δ mice (Figure 3.10. A). However, due to the reduced total cell number in the spleen, the B and T cell counts were significantly lower in the spleen of p100Δ mice compared with WT mice (B cells: WT n=9, median=30.3 $x10^6$, p100Δ n=9, median=5.7 $x10^6$, p=0.008. T cells: WT n=9, median=5.4 $x10^6$, p100Δ n=9, median=1.9 $x10^6$, p=0.001) (Figure 3.10. B.).

Similar to the spleen, there was no difference in the proportion of B cells (WT n=10, median=32.6, p100Δ n=9, median=38.3, p=0.100) or T cells (WT n=7, median=42.9, p100Δ n=7, median=46.0, p=0.620) in the mLN of p100Δ mice compared with WT mice (Figure 3.10. A). In contrast to the spleen, there was ~~also~~ no difference in B cell (WT n=7, median=2.4 $x10^6$, p100Δ n=7, median=2.6 $x10^6$, p=0.867) or T cell (WT n=7, median=2.4 $x10^6$, p100Δ n=7, median=2.9 $x10^6$, p=0.383) number in the mLN (Figure 3.10. B).

With respect to the colon, the proportion of B and T lymphocytes was not altered between p100Δ mice and WT mice (B cells: WT n=7, median=47.1, p100Δ n=7, median=47.9, p=0.243. T cells: WT n=7, median=13.9, p100Δ n=7, median=16.4, p=0.356) (Figure 3.10. A). Due to the overall increase in cells isolated from the colon of p100Δ mice, a significant increase in the number of B cells (WT n=7, median=166,640, p100Δ n=7, median=484,110 p=0.010) and T cells (WT n=7 median=75,498, p100Δ n=7, median=225,000 p=0.002) was observed in p100Δ mice compared with WT mice (Figure 3.10. B).

In summary, this data demonstrates an increase in lymphocytes in the colon in p100Δ mice and that the majority of these infiltrating cells are $B220^+$ B cells,

approximately 40%, with a small but significant population of $CD3^+$ T cells, approximately 15%.

3.2.7.3. Profile of T cell subsets in the spleen, mLN and colon of WT and p100Δ mice

To further characterise the T cell population in the tissues of p100Δ mice, $CD3^+$ T cells were analysed for their CD4/CD8 profile. Typically, in the WT mouse, peripheral T cells are skewed towards a $CD4^+$ instead of a $CD8^+$ phenotype. Within the spleen of p100Δ mice there is a decrease in the proportion of $CD8^+$ T cells (WT n=3, median=24.0, p100Δ n=6, median=19.0, p=0.024), with a slight, but not significant, reciprocal increase in $CD4^+$ T cells (WT n=3, median=57.0, p100Δ n=6, median=63.0, p=0.095), compared with WT (Figure 3.12. A). When considering cell counts, total $CD4^+$ and $CD8^+$ T cell numbers are reduced in p100Δ spleen compared with WT ($CD4^+$: WT n=3, median=7.7 $x10^6$, p100Δ n=6, median=580,685, p=0.024. $CD8^+$: WT n=3, median=3.3 $x10^6$, p100Δ n=6, median=128,505, p=0.024) (Figure 3.12. B). In the mLN of p100Δ mice, the proportion of $CD4^+$ T cells was increased compared with WT (WT n=3, median=62.6, p100Δ n=6, median=68.8, p=0.024), but no difference was seen in the $CD8^+$ T cell population (WT n=3, median=28.8, p100Δ n=6, median=22.3, p=0.095) (Figure 3.12. A).

Importantly, when proportions of CD4+ and CD8+ T cells were analysed in the colon of p100D mice, the T cell population was skewed in favour of a CD4+ T cell phenotype, with a slight, but not significant, reduction in CD8+ T cells (WT n=3, median=17.1, p100D n=6, median=10.7, p=0.381) and a significant, reciprocal increase in CD4+ T cells (WT n=3, median=23.8, p100D n=6, median=53.8,

p=0.024) compared with WT (Figure 3.12. A) When considering cell counts, CD4+ T cells (WT n=3, median=19,087, p100D n=6, median=124,666, p=0.046), but not CD8+ T cells (WT n=3, median=16,531, p100D n=6, median=35,002, p=0.548), were greatly increased in number in p100D mice compared with WT (Figure 3.12. B).

Figure 3.9 Differences in absolute cell number from spleen, mLN and colon of WT and p100Δ mice

*Isolation of total cells from WT (o) and p100Δ (Δ) mice, show that p100Δ mice display a reduction in spleen cellularity, an increase in colonic cell number and no difference in mLN cell number. Data from five independent experiments. *** p≤ 0.01, ns= not significant.*

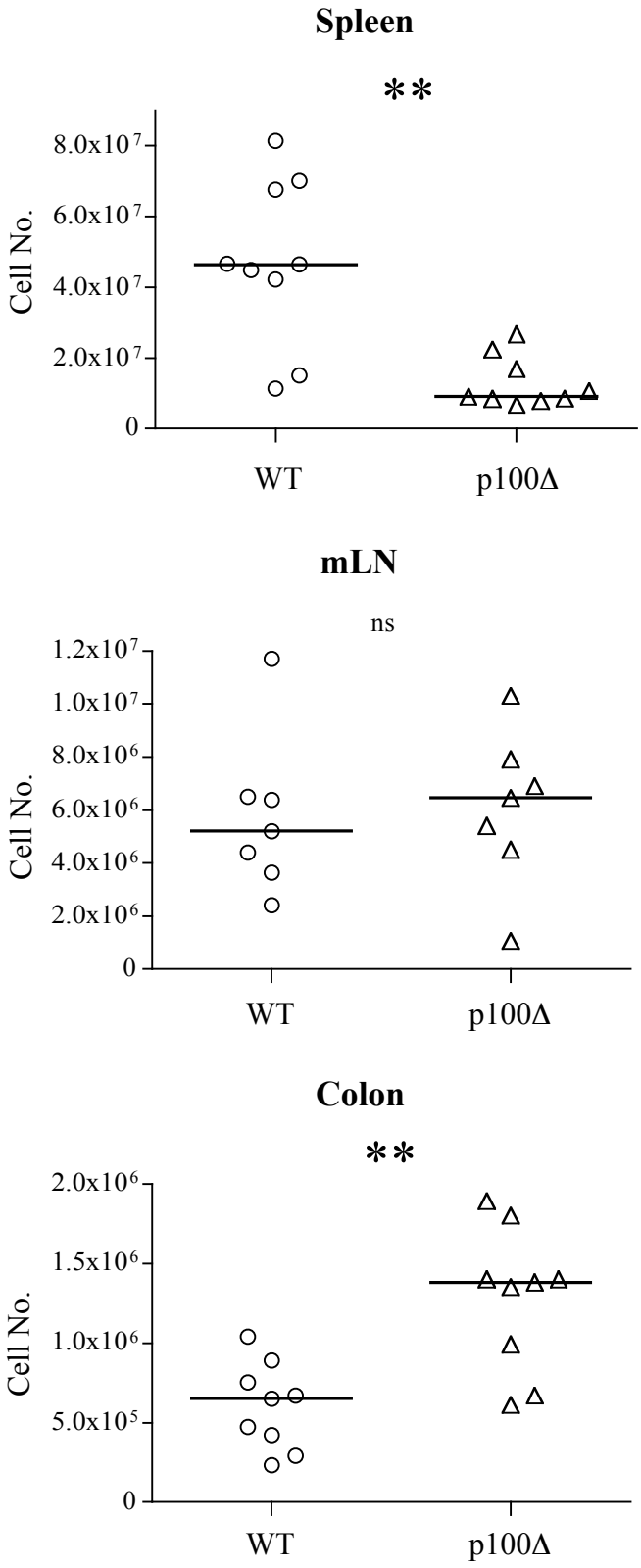
Spleen
**
8.0x10^7
6.0x10^7
4.0x10^7
2.0x10^7
0
Cell No.
WT
p100Δ
mLN
ns
1.2x10^7
1.0x10^7
8.0x10^6
6.0x10^6
4.0x10^6
2.0x10^6
0
Cell No.
WT
p100Δ
Colon
**
2.0x10^6
1.5x10^6
1.0x10^6
5.0x10^5
0
Cell No.
WT
p100Δ

Figure 3.9

Figure 3.10 Evaluation of B and T lymphocyte proportions and cell numbers in the spleen, mLN and colon

A *Single cell suspension from spleen, mLN and colon were stained for flow cytometry with anti-B220 (B cells) and anti-CD3 (T cells). Representative FACs plots are shown. Graphs showing proportion of B and T lymphocytes, in the spleen, mLN and colon of WT and p100Δ mice.*

B *Graphs showing the total cell count for $B220^+$ B cells and $CD3^+$ T cells (data from at least three independent experiments, total n≥7 for each genotype).*

** p≤0.05, ** p≤ 0.02, ns= not significant. Bar indicates median.*

B B and T lymphocytes: Absolute cell number

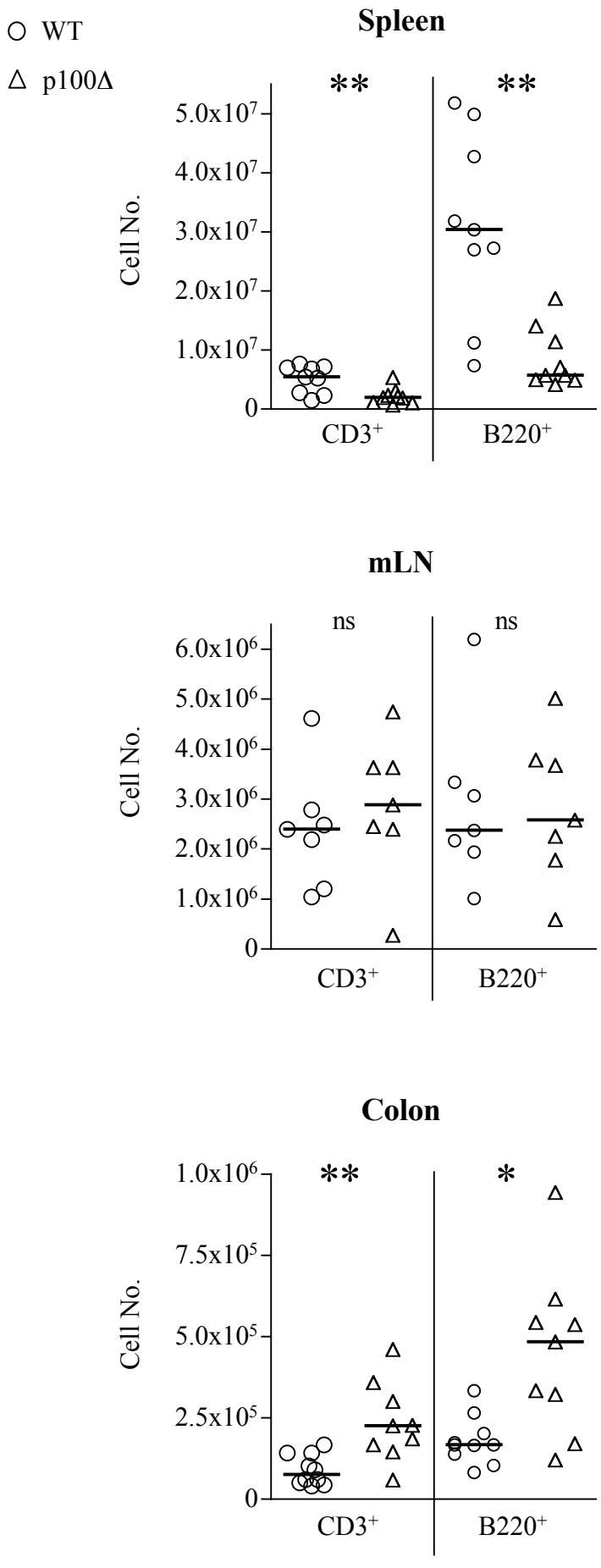

Figure 3.10

Figure 3.11 Analysis of activation status of B and T lymphocytes

*Single cell suspensions from spleen, mLN and colon were stained with fluorescently labelled CD3 and B220 antibodies, to identify T and B cell populations, respectively. The marker CD69 was used to assess the activation status of these cells. Graph shows percentage of cells expressing CD69, bar indicates median. Results from at least two independent experiments. ns= not significant, * $p \leq 0.05$.*

○ WT

△ p100Δ

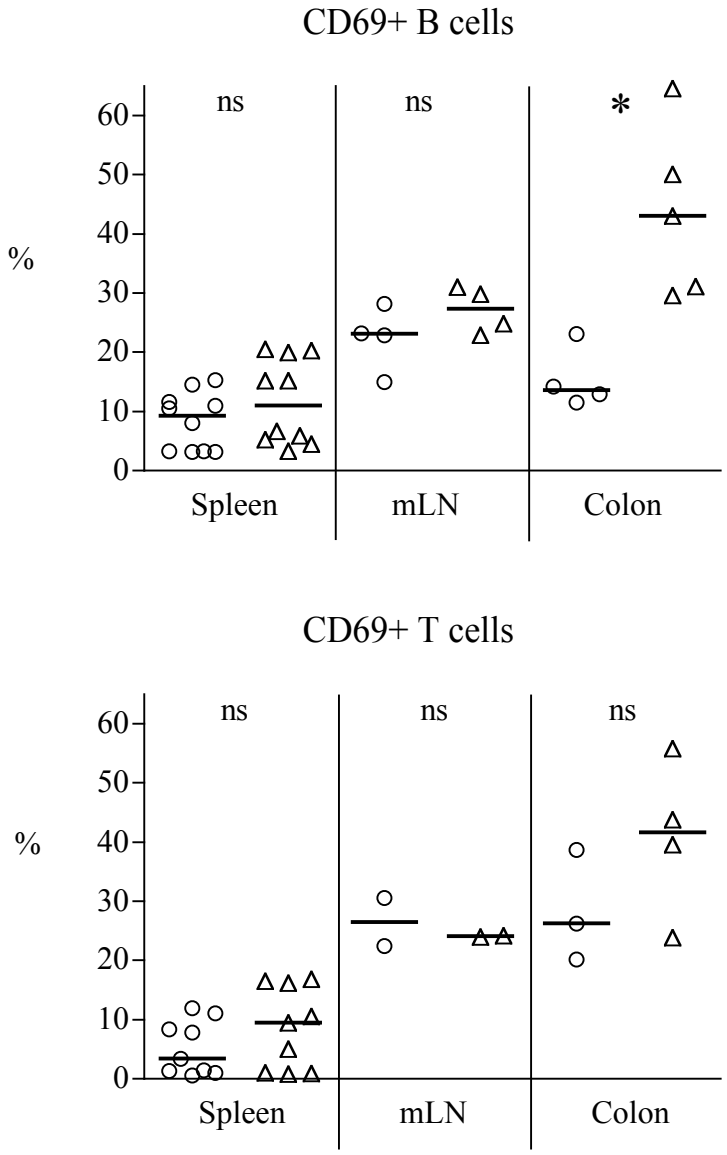

Figure 3.11

Figure 3.12 Evaluation of $CD4^+$/$CD8^+$ T lymphocyte proportions and cell numbers in the spleen, mLN and colon

A *Single cell suspension from spleen, mLN and colon were stained for flow cytometry with anti-CD3 (T cells), anti-CD4 and anti-CD8. The CD4/CD8 profile of the $CD3^+$ gate is shown. Representative FACs plots are shown. Graphs showing proportion of $CD4^+$ and $CD8^+$ T cells, in the spleen, mLN and colon of WT and p100Δ mice.*

B *Graphs showing the total cell count for $CD3^+CD4^+$ and $CD3^+CD8^+$ T cells (data from two independent experiments, total n≥3 for each genotype).*

** p≤0.05, *** p≤ 0.01, ns= not significant. Bar indicates median.*

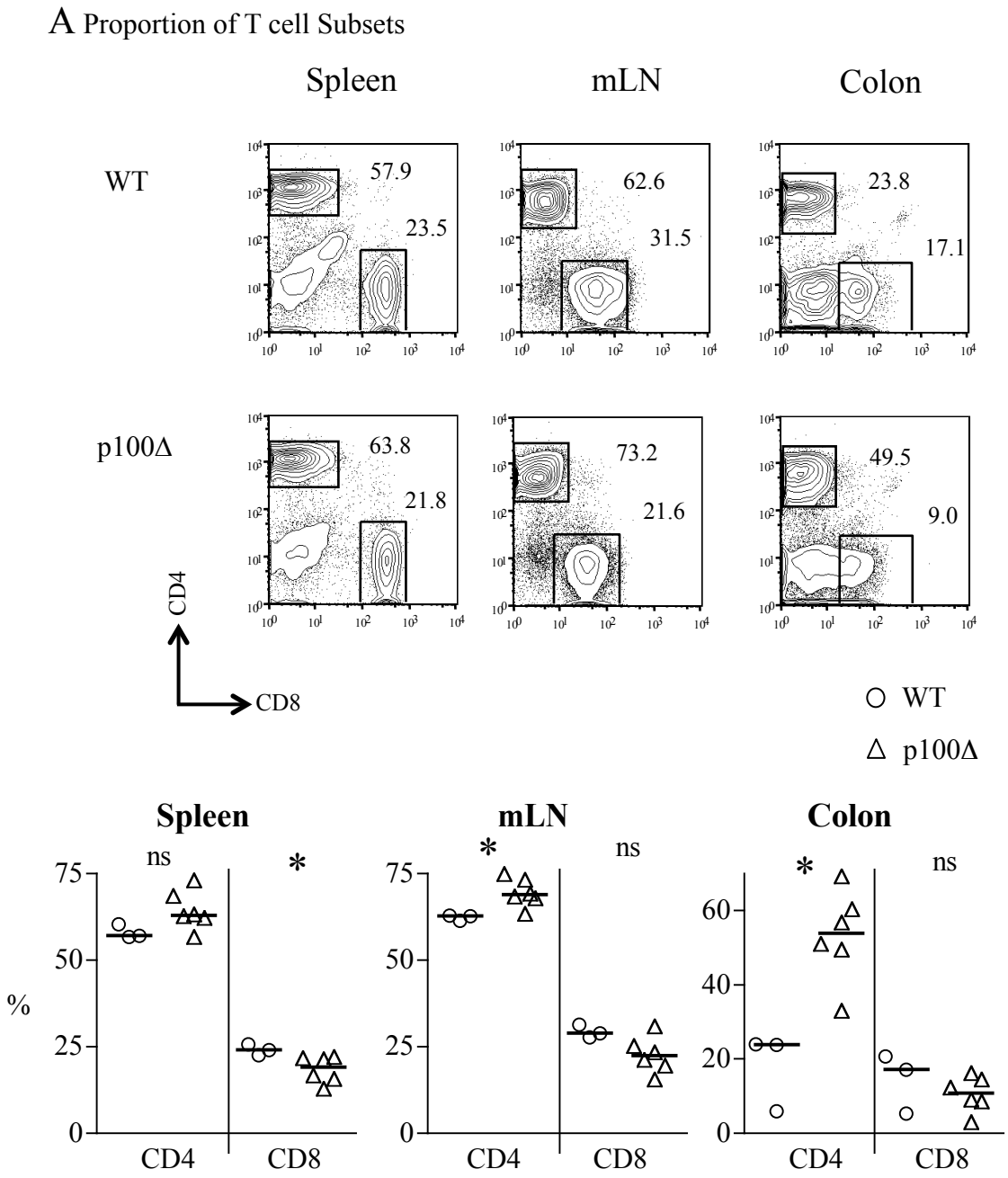
A Proportion of T cell Subsets
Spleen
mLN
Colon
WT
p100Δ
57.9
23.5
62.6
31.5
23.8
17.1
63.8
21.8
73.2
21.6
49.5
9.0
CD4
CD8
WT
p100Δ
Spleen
mLN
Colon
ns
*
%
75
50
25
0
60
40
20
CD4
CD8
B Absolute Cell Number
Cell No.
8.0x10^6
6.0x10^6
4.0x10^6
2.0x10^6
2.0x10^5
1.5x10^5
1.0x10^5
5.0x10^4

Figure 3.12

3.2.8. RelB-dependent, p52-independent development of ILFs

Previous data in this study has shown that p100Δ mice exhibit a dramatic increase in ILF formation in the colon. Downstream signalling analysis of the alternative NF-κB pathway by other groups has shown that p100 predominately heterodimerises with the RelB subunit within the cytoplasm. In addition, RelB is also able to heterodimerise with NF-κB1/p50. Following receptor ligation and degradation of p100 to p52, this p52/RelB heterodimer is able to translocate to the nucleus and induce transcription of target genes, such as *Ccl19* and *Cxcl13*. In order to assess the relative contribution of p52 and RelB to the expression of their target genes and subsequently to the colonic phenotype observed in p100Δ mice, these mice were crossed with $Relb^{-/-}$ mice and ILF formation was analysed.

3.2.8.1. Further manipulation of the NF-κB2 activation pathway and ILF development

Figure 3.13 A, shows enumeration of B cell aggregates in the colon of WT, p100Δ, $Relb^{-/-}$, $Nfkb2^{-/-}$, $p100\Delta Relb^{+/-}$ and $p100\Delta Relb^{-/-}$ mice, by immunofluorescence staining with anti-B220 to identify the B cells. In mice deficient in RelB, no ILF structures could be found and, conversely, in mice lacking NF-κB2, normal levels of ILF formation were seen. In the p100Δ mouse model, it could be expected that due to the presence of excessive p52 in the cytoplasm, an increase in p52/RelB heterodimers would be formed and translocate to the nucleus and induce transcription of genes controlling the colonic phenotype observed. When one allele of *Relb* is removed from this system, the number of ILFs formed was similar to that observed in WT mice. When both *Relb* alleles are removed, ILF formation was prevented (Figure 3.13. A).

Figure 3.13 B, illustrates the lymphocyte aggregates formed within the colon of the mice indicated. A small number of B cells are observed within the colon of *p100ΔRelb*$^{-/-}$ mice and within CPs (clusters of CD3^{-}CD4^{+} LTi-like cells (blue)), however, no organised B cell follicle is formed.

In conclusion, *Relb*$^{-/-}$ mice lack colonic ILFs, whereas *Nfkb2*$^{-/-}$ mice develop ILFs in similar numbers to WT mice, therefore ILF formation is dependent on RelB, but independent of NF-κB2. Removal of RelB from the p100Δ mouse model ablates ILF formation, indicating that constitutive activation of NF-κB2 p100 alone is not sufficient to drive ILF development; the p52 protein must be able to dimerise with RelB to elicit an effect.

Figure 3.13 ILF formation is dependent on RelB but independent of p52

A *Colonic ILFs were enumerated by staining colon sections with fluorescently labelled anti-B220 and visualised using fluorescence microscopy. WT n=4, p100Δ n=6, p100ΔRelb$^{+/-}$ n=4, p100ΔRelb$^{-/-}$ n=4, Relb$^{-/-}$ n=2, Nfkb2$^{-/-}$ n=3.*

B *Colon sections were stained for haematopoietic cells (anti-CD45, green, 1st line), dendritic cells (anti-CD11c, green, 2nd line), T cells (anti-CD3, green, 3rd line), macrophages (anti-F4/80, green, 4th line), B cells (anti-B220, red) and CD4^{+} cells (anti-CD4, blue).*

Representative immunofluorescent confocal images are shown (x40 magnification). Scale bar represents 50μm. ND= Not Detected.

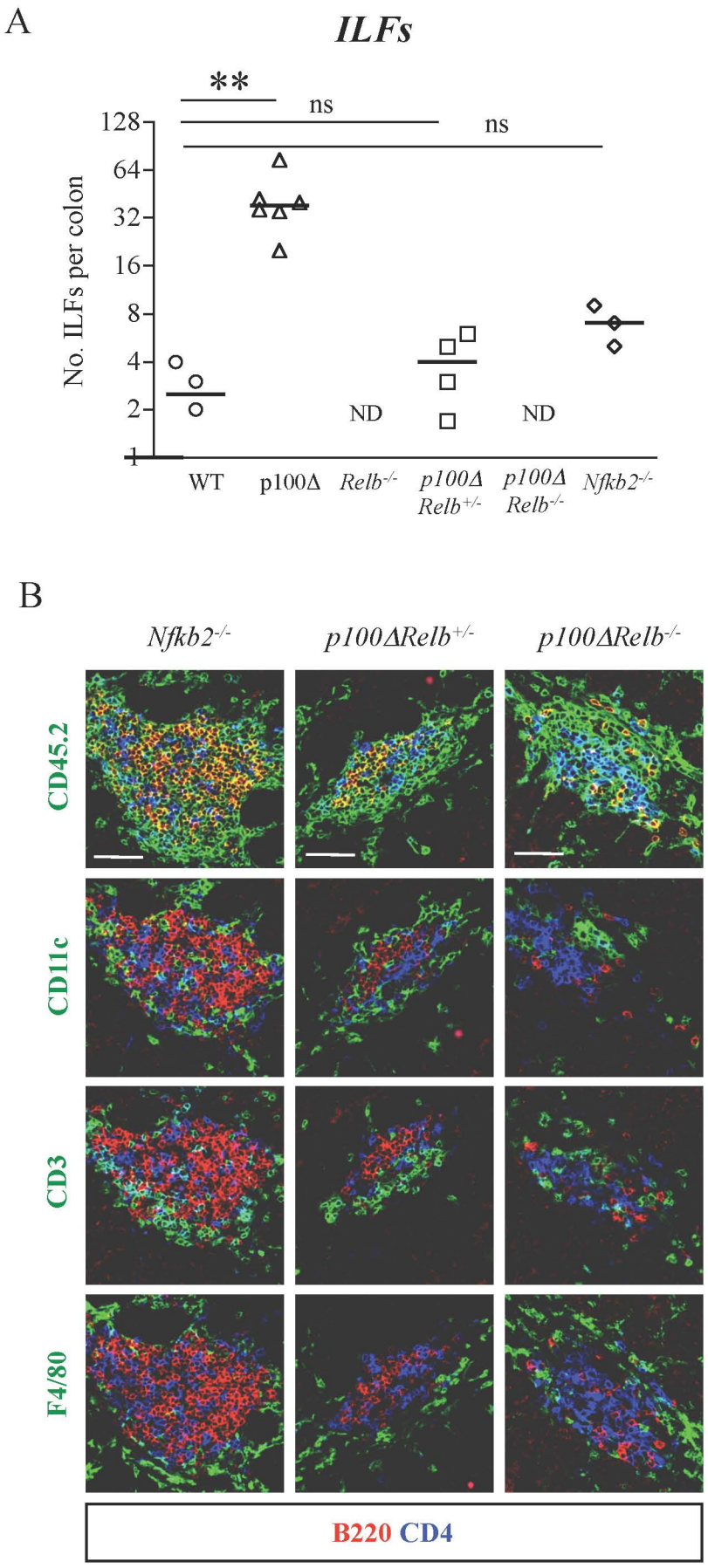
A
ILFs
**
ns
ns
128
64
32
16
8
4
2
1
No. ILFs per colon
ND
ND
WT
p100Δ
Relb-/-
p100Δ Relb+/-
p100Δ Relb-/-
Nfkb2-/-
B
Nfkb2-/-
p100ΔRelb+/-
p100ΔRelb-/-
CD45.2
CD11c
CD3
F4/80
B220 CD4

Figure 3.13

Figure 3.14 Characterisation of B cell phenotype and the stromal cell compartment of colonic lymphoid tissue in different NF-κB mouse models

A *Colon sections from p100ΔRelb$^{+/-}$, p100ΔRelb$^{-/-}$ and Nfkb2$^{-/-}$ mice were frozen and cryostat sections were stained with fluorescently labelled antibodies to B220 (blue), IgM (red) and IgD (green), counter stained with nuclei stain DAPI. Mature B cells express B220, IgM and IgD (pale blue cells, bottom panel).*

B *Staining with fluorescent antibodies to CXCL13 (green, left panel), VCAM-1 (green, right panel) and B220 (red) show minimal expression of CXCL13 in the three mouse strains, with slightly stronger staining for VCAM-1.*

C *Staining for tissue vasculature with anti-CD31 (green) and anti-MAdCAM-1 (blue) shows co-expression of these markers on vascular endothelium (pale blue cells, merge, white circles). B cells stained with anti-IgM (red) and tissue counterstained with DAPI (grey).*

Representative immunofluorescent confocal images are shown (x40 magnification). Scale bar denotes 50 μm.

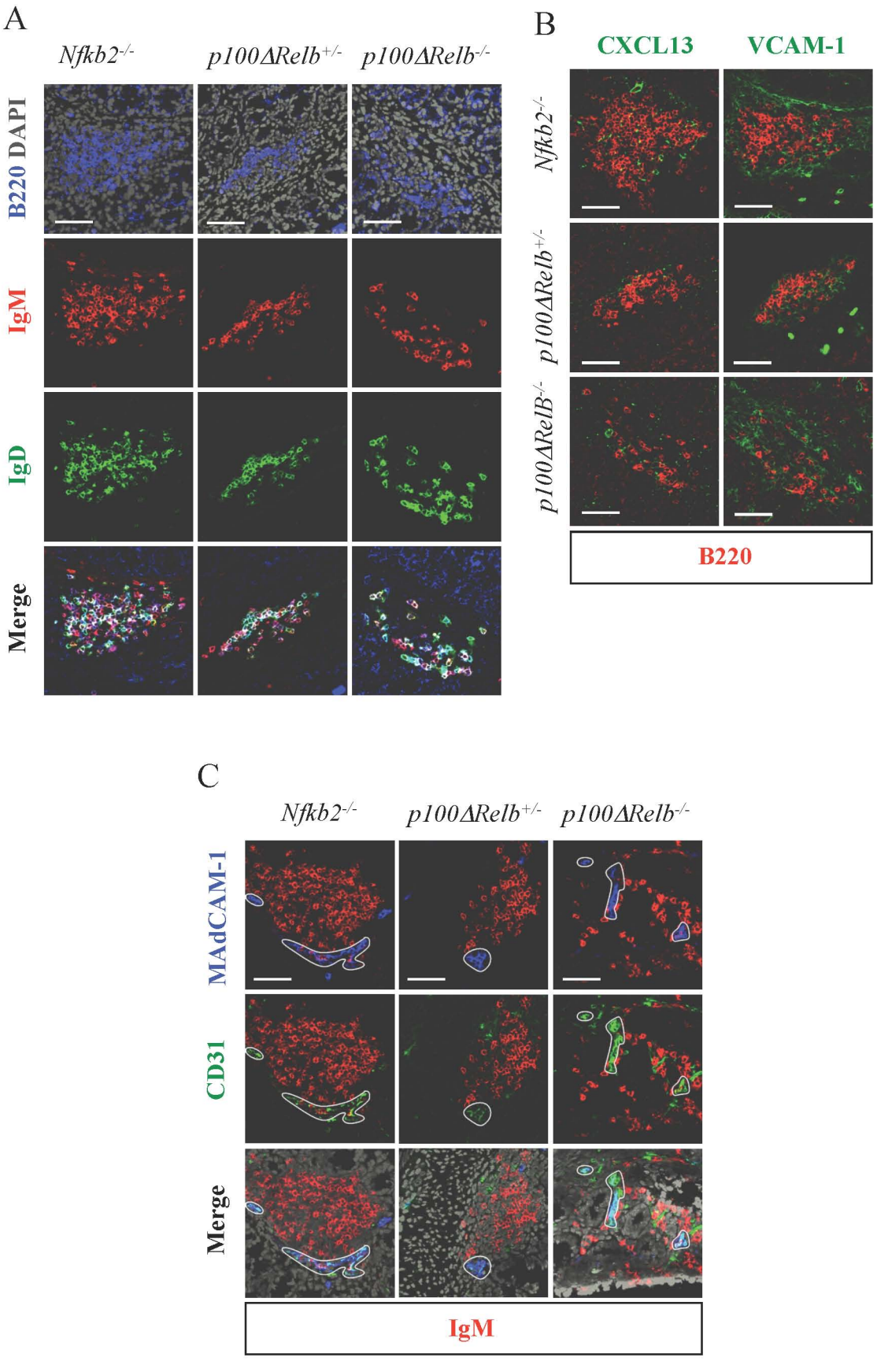
A
Nfkb2-/-
p100ΔRelb+/-
p100ΔRelb-/-
B220 DAPI
IgM
IgD
Merge
B
CXCL13
VCAM-1
Nfkb2-/-
p100ΔRelb+/-
p100ΔRelB-/-
B220
C
Nfkb2-/-
p100ΔRelb+/-
p100ΔRelb-/-
MAdCAM-1
CD31
Merge
IgM

Figure 3.14

3.2.8.2. Haematopoietic cell organisation in colonic lymphoid tissues of *Nfkb2*$^{-/-}$, *p100ΔRelb*$^{+/-}$ and *p100ΔRelb*$^{-/-}$ mice

The cellular organisation of the ILFs seen was evaluated by confocal microscopy. The ILFs present in the colon of *Nfkb2*$^{-/-}$ mice exhibit the expected structure, a B220^{+} B cell core, surrounded by CD11c^{+} DCs and interspersed with CD3^{+} T cells (Figure 3.13. B, left column). The ILFs observed in *p100ΔRelb*$^{+/-}$ varied in size (data not shown), and although the ILF pictured is small it still shows an organised structure as previously described (Figure 3.13. B, second column). The lymphoid structures in *p100ΔRelb*$^{-/-}$ colon resemble cryptopatches in their cellular composition and structure. A cluster of CD3^{-}CD4^{+} LTi-like cells can be seen (Figure 3.13. B, right column, third row, blue cells), along with CD11c^{+} DCs (Figure 3.13. B, right column, second row, green cells). A few B220^{+} B cells can be seen within the cryptopatch, but they are not arranged into an organised structure.

The majority of B lymphocytes within ILFs display a mature phenotype, B220^{+}IgD^{+}IgM^{+}. When considering the *Nfkb2*$^{-/-}$ mice, the majority of the B cells within ILFs display this mature phenotype (Figure 3.14. A, left panel). However, there appears to be more B220^{-}IgD^{+} (green) and B220^{-}IgM^{+} (red) plasma cells when compared with WT ILF (Figure 3.14. A, and Figure 3.3. A. WT ILF). The majority of B cells present in *p100ΔRelb*$^{+/-}$ ILFs also display a mature phenotype (Figure 3.14. A, second column). Assessment of the few B cells present in *p100ΔRelb*$^{-/-}$ CPs shows that nearly all possess a mature phenotype and that fewer B220^{-}IgD^{+} and B220^{-}IgM^{+} plasma cells can be seen (Figure 3.14. A, third column).

3.2.8.3. Expression of stromal cell markers in colonic lymphoid tissues of *Nfkb2*$^{-/-}$, *p100ΔRelB*$^{+/-}$ and *p100ΔRelB*$^{-/-}$ mice

To check the phenotype of the stromal cells constituting the lymphoid tissues present in the colon of *Nfkb2*$^{-/-}$, *p100ΔRelb*$^{+/-}$ and *p100ΔRelb*$^{-/-}$ mice, immunoflorescence staining was used to assess the expression of CXCL13 and VCAM-1. Carragher *et al*, have published that *Nfkb2*$^{-/-}$ mice show a reduction in CXCL13 expression, but normal levels of VCAM-1, in lymph nodes at P7-14 (Carragher et al., 2004). Consistent with this data, P14 colon from *Nfkb2*$^{-/-}$ mice show reduced CXCL13 expression within ILFs (Figure 3.14. B, left column). In addition, the expression of CXCL13 and VCAM-1 in *p100ΔRelb*$^{+/-}$ and *p100ΔRelb*$^{-/-}$ colon was low and difficult to detect by confocal microscopy (Figure 3.14. B, middle and right column, respectively).

Carragher *et al*, further showed that MAdCAM-1 expression is reduced by postnatal day seven in *Nfkb2*$^{-/-}$ LN. In contrast to this data, Figure 3.14, shows expression of MAdCAM-1^{+} vasculature in *Nfkb2*$^{-/-}$ colon (Figure 3.14. C, left column). Furthermore, co-localisation of CD31 with MAdCAM-1 within the colon can be observed in these mice (Figure 3.14. C, left column, merge).

3.3. Discussion

The dependence of secondary and tertiary lymphoid tissue development on LTβR signalling and the subsequent involvement of the alternative NF-κB pathway downstream of LTβR, has been well documented (Fütterer et al., 1998; Ivanov et al., 2006; Taylor et al., 2004; Lorenz et al., 2003; Alimzhanov et al., 1997; Pabst et al., 2005; De Togni et al., 1994; Hamada et al., 2002; Banks et al., 1995; Weih et al., 1995; Yilmaz et al., 2003; Weih and Caamaño, 2003; Shinkura et al., 1999; Miyawaki et al., 1994; Fagarasan et al., 2000; Karrer et al., 2000). Studies investigating the effect of constitutive activation of this pathway on secondary lymphoid tissue, namely the spleen, have previously been published (Ishikawa et al., 1997; Guo et al., 2007) and this chapter expands on this by studying the effects on the development of tertiary lymphoid tissue, in particular the formation of colonic ILFs.

This chapter presents the striking finding that in the colon of p100Δ mice there is a significant increase ILF formation by two weeks of age, with supporting data confirming that these structures are indeed ILFs. The augmented development of ILFs in these mice is dependent on constitutive activation of p100 in haematopoietic cells, but the contribution of stromal cells is not excluded. p100Δ mice present with increased absolute cell numbers in the colon, with an increase in both the B and T cell compartments and within the T cell population an increase in the proportion of $CD4^+$ T cells was observed. We also show that ILF development is dependent on RelB and that removal of RelB from p100Δ mice abrogates of ILF formation.

The development of ILFs in C57/Bl6 mice has been described to commence at around P25 (Hamada et al., 2002). There are inevitable variations on this timescale from one animal facility to the other, as the resident commensal bacteria will likely

differ. It is demonstrated in this chapter that small numbers of ILFs were present in the colon of C57/Bl6 mice from P10 and that by P15 a significant increase in B cell aggregates in the colon of p100Δ mice was observed (Figure 3.2. B).

Several pieces of evidence are presented indicating that the p100Δ colonic B cell aggregates are ILFs. The first is that the cellular organisation of p100Δ B cell aggregates closely resembles that of WT ILFs, with a core of $B220^+$ B cells, surrounded by $CD11c^+$ DCs and interspersed with $CD3^+$ T cells (Figure 3.3). Secondly, the majority of B cells constituting WT ILFs present with a mature phenotype, $B220^+IgM^+IgD^+$, a comparable profile is seen in p100Δ B cell aggregates (Figure 3.4). Thirdly, identification of LTi-like cells and Tregs within WT ILF and p100Δ B cell aggregates was observed (Figure 3.5. A and B) and enumeration and functional analysis of these cell populations would be beneficial in understand the phenotype observed. Finally, the presence of similar chemokine and cell adhesion molecule expression, namely that of CXCL13, VCAM-1 and MAdCAM-1, between WT ILFs and p100Δ B cell aggregates was observed (Figure 3.6). Together these findings provide extensive evidence that p100Δ colonic B cell aggregates are ILFs and that p100Δ mice present with a significant increase in colonic ILF numbers.

The significant increase in ILF formation in the colon of p100Δ mice could arise due to various phenomena. Two main explanations revolve around the development of cryptopatches and their transition into ILFs. Eberl, *et al*, suggested the link between CP development and subsequent formation into ILFs following the recruitment of B cells (Eberl, 2005; Eberl and Sawa, 2010). One possible explanation for the increase in ILF development in p100Δ mice could stem from augmented CPs development. The presence and enumeration of CPs in the colon of p100Δ mice was

attempted by confocal microscopy, however this proved difficult to accurately assess. CPs consist of a cluster of $CD3^{-}CD4^{+}$ LTi-like cells, and $CD11c^{+}$ DCs, but lacking presence of B220 expressing B cells (Kanamori et al., 1996; Hamada et al., 2002). The CD4 antibody used was conjugated to a fluorochrome emitting in the far-red range and therefore not visible by eye, thus $CD4^{+}$ clusters could not be counted. $CD11c^{+}$ cells were visible by eye (antibodies were conjugated to FITC), however DCs are located throughout the colon and clusters of DCs were hard to define and therefore not reliable for CP enumeration. In an attempt to address these issues, p100Δ mice were crossed onto the *Rag*$^{-/-}$ background to remove the complication of lymphocyte presence. It has been reported that *Rag*$^{-/-}$ mice develop CPs as normal (Hamada et al., 2002; Ivanov et al., 2006). Initial data from *p100ΔRag*$^{-/-}$ and *Rag*$^{-/-}$ mice indicated no difference in colonic CP number, however the *p100ΔRag*$^{-/-}$ mice suffered from a failure to thrive that was more severe than p100Δ mice complicating the phenotype observed (data not shown). As a result, it is currently unclear whether p100Δ mice exhibit normal or increased numbers of CPs in their colon; if more CPs were present this could go some way to explain the increase in ILFs. Conversely, if there were normal numbers of CPs, then it may be that a higher proportion of the CPs present are induced to develop into ILFs. The increased CP transition into ILFs would be dependent on increased haematopoietic cell recruitment and this could be driven by the haematopoietic cells themselves preferentially migrating to the colon, by colonic stromal cells expressing chemokines and cell adhesion molecules, or by a combination of both. Additionally, commensal bacteria and TLR stimulation may also have an affect by inducing upregulation of chemokines for example, or by stimulation DCs.

The migration of B cells to the intestine involves various chemokine and cell adhesion molecules, such as CCL20 (McDonald et al., 2007; Williams, 2006), CXCL13 (McDonald et al., 2010) and MAdCAM-1 (Wang et al., 2008). The presence of CXCL13 and MAdCAM-1 can be observed in the colon of p100Δ mice (Figure 3.6), but the level of expression has not been assessed. The presence of CCL20 has not been confirmed in this study. Guo, *et al*, have shown that in the spleen of p100Δ mice the expression of CXCL13 is slightly increased and MAdCAM-1 expression is significantly increased compared to levels in WT mice (Guo et al., 2007). If this were reflected in the colon, it may be that increased levels of these chemokines could result in accumulation of B cells. Interestingly however, Guo *et al*, also demonstrated that p100Δ splenic B cells show reduced localisation to CXCL13 *in vitro* (Guo et al., 2007). Peripheral B cells may not reflect this defect but if they did it is possible that B cell recruitment to the colon is influenced more by migration towards chemokines such as CCL20. There is a positive increase in expression of CCR6, the receptor for CCL20, by p100Δ T cells from the spleen, mLN and colon. However, this shift is not seen in the B cell population (Appendix Figure 1. A).

The role of chemokine/cell adhesion molecule expression by stromal cells and the expression of reciprocal receptors on haematopoietic cells is clearly important in ILF development. The contribution of stromal and haematopoietic cells to the colonic phenotype observed in p100Δ mice was investigated using FLC transfers.

Mice receiving 100% p100Δ FLCs developed more colonic ILFs than those receiving WT FLCs or a 50:50 mix (Figure 3.7. A). This data points to a predominately haematopoietic cell driven phenotype, but does exclude a role for the stroma. The mice in the FLC transfer experiments were sacrificed three months post-transfer and no earlier time points were investigated. There are at least two possible

scenarios; i) it could have taken three months for the difference in ILF numbers to become significant or, ii) it was significant from an earlier age, potentially equivalent to the age at which p100Δ mice exhibit significantly more ILFs. In the first scenario, a role for stromal cells and haematopoietic could be envisaged; the recruitment or preferential migration of p100Δ lymphocytes to the colon, could have induced priming and activation of the stroma thereby allowing more CP transition to ILFs, generating a positive feedback loop, the 'activation' of the stroma being the potential reason for the delay in increased ILF formation. In the second scenario, if increased ILF formation was occurring soon after FLC transfer, the role of the stroma is much diminished and the haematopoietic cells could be considered the major contributor. Earlier time points post-FLC transfer would need to be investigated to ascertain which of these two scenarios is occurring. Interestingly, transfer of whole splenocytes from p100Δ mice, and the harvesting of host mice six weeks post-transfer, no increased ILF formation is seen (data not shown), this could be for two reasons: i) mice were harvested too early to see significant differences, ii) a cell population present in the foetal liver but not in the adult spleen is responsible for inducing increased ILF formation.

In order to clarify the relative contribution of stromal and haematopoietic cells to the induction of augmented ILF formation in p100Δ mice, a time course experiment following FLC transfer may elucidate differences in the onset and development of ILFs. An additional, and similar, time course following splenocyte transfer would help narrow down the potential cell type responsible for driving augmented p100Δ ILF formation.

An additional explanation for the increase in ILF formation in p100Δ mice is the potential contribution of commensal bacteria and subsequent stimulation of TLRs

and NLRs (NOD-like receptors). Bouskra, *et al*, demonstrated that TLRs and NOD2 are most likely required for the maturation of ILFs, but not for induction, while NOD1 is required for the induction of ILFs (Bouskra et al., 2008). A possible scenario could be envisaged where the intestinal APCs of p100Δ mice are hyper-reactive to commensal bacteria. This development of ILFs in response to gut flora is recapitulated in the DSS-induced colitis model, where an increase in ILF formation was observed (Spahn et al., 2002; Jungbeck et al., 2008), the same occurred in the T cell transfer model of murine colitis (Leithäuser et al., 2001) and in human Crohn's disease and colitis (Sitohy et al., 2008; Nascimbeni et al., 2005; Yeung et al., 2000). It is possible that the increase in ILF development in p100Δ mice reflects the initial stages of colitis but that the early postnatal death limits disease progression and by the time of death p100Δ mice do not exhibit symptoms of colitis such as diarrhoea or intestinal epithelial hyperplasia.

Corresponding to the increase in colonic ILFs in p100Δ mice, an increase in the number of B and T lymphocytes was observed in the colon (Figure 3.10). Interestingly, there was no difference in proportion of these cell populations, indicating that they were increased by similar levels, i.e. it is not just an influx of B cells into the colon to form ILFs, but also an increase in T cells. Flow cytometric analysis does not take into account the location of the cells present. Colonic B cells are located predominately in ILFs, but the T cells can be located within the epithelium or lamina propria, not just within ILFs. Interestingly, within the colon of p100Δ mice, the proportion of $CD4^+$ and $CD8^+$ T cells was altered, with an increase in the proportion of $CD4^+$ T cells and no change in the proportion of $CD8^+$ T cells when compared to WT counterparts (Figure 3.12). It could be that the $CD4^+$ cells in the

colon are activated and therefore proliferate to expand the population or that there is increased recruitment of $CD4^+$ T cells from the periphery, via altered chemokine expression by colonic stromal cells or receptors levels on the T cells. Flow cytometric analysis revealed a positive, but non-significant, shift in CD69 expression by $CD3^+$ T cells isolated from the colon of p100Δ mice relative to WT colonic T cells (Figure 3.11). This analysis would need to be repeated and expanded to include other activation markers in order to verify the results.

The alternative NF-kB pathway centres around activation of predominately p52/RelB heterodimers (Dejardin et al., 1998; Yilmaz et al., 2003). ILF formation is dependent on RelB, and therefore dependent on the alternative NF-κB pathway, as demonstrated in this chapter by the lack of ILF formation in *Relb*$^{-/-}$ mice. Moreover, the removal of RelB from p100Δ mice, as in *p100ΔRelb*$^{-/-}$ mice, results in a lack of ILF formation, presumably through alteration of heterodimer formation. When there is no alternative NF-κB pathway activation there is no ILF development, when there is constitutive activation of this pathway there is augmented ILF formation. In *p100ΔRelb*$^{-/-}$ mice, with a lack of RelB and excess p52 available, the compensatory heterodimers that form could be p52/RelA, p52/c-Rel and p52/p52. p52 homodimers would operate as transcriptional repressors due to their lack of transcriptional activation domains, unless they are bound to Bcl-3 (Ghosh et al., 1998; Brown et al., 1994; Bours et al., 1993). The relative formation of these different complexes has not been assessed but it would be of importance to investigate this in order to assess the contribution to gene expression and ILF development.

In summary, p100Δ mice present with a significant increase in the number of colonic ILFs, it is currently unclear whether this increase stems from augmented development of CPs or from an increase in the number of CPs transitioning into ILFs. This colonic phenotype is dependent on RelB containing complexes, as in *p100ΔRelb*$^{-/-}$ mice development of ILFs is inhibited. It is clear that the migration of lymphocytes to the colon of p100Δ mice is dramatically enhanced compared with WT mice, and the presence of CXCL13, VCAM-1 and MAdCAM-1 has been established but the relative levels of expression have not. FLC transfer experiments indicate that constitutive activation of NF-κB2 p100 in haematopoietic cells is sufficient to drive the increase in ILF formation, however possible involvement of stromal cells in this phenotype has not been excluded.

4. Characterisation of Dendritic Cell Populations in p100Δ Mice

4.1. Introduction

The role of DCs and macrophages in intestinal immunity is not fully understood, with diverse subpopulations eliciting differential effects and producing various combinations of chemokines and cytokines. cDCs are identified by their high expression of CD11c and within the spleen, the two main subtypes are determined based on CD8α and CD11b expression: $CD11c^{high}CD8\alpha^{+}(CD11b^{-})$ and $CD11c^{high}CD8\alpha^{-}(CD11b^{+})$ cDCs (Leenen et al., 1998). cDCs are also present in non-lymphoid tissues, particularly at mucosal sites. Within the intestine a subpopulation of lamina propria (LP) DCs express CD103 and these $CD11c^{high}CD103^{+}$ LP-DCs are capable of migrating to the draining LN of the gut (mLN) (Schulz et al., 2009) and inducing expression of gut homing markers on T cells (Annacker et al., 2005; Jaensson et al., 2008), as well as stimulating the generation of Treg cells (Coombes et al., 2007; Siddiqui and Powrie, 2008). This anti-inflammatory phenotype is contrasted by $CD11c^{high}CD103^{-}$ intestinal DCs, which induce a pro-inflammatory response by secreting IL-6 and TNFα, and by influencing T cells to generate IFNγ (Coombes et al., 2007). mLN populations of DCs include $CD11c^{high}CD8\alpha^{+}$ and $CD11c^{high}CD8\alpha^{-}$ DCs, as well as $CD11c^{high}CD103^{+}$ and $CD11c^{high}CD103^{-}$ DCs (Coombes et al., 2007; Iwasaki and Kelsall, 2001). The assessment of these DC subpopulations in p100Δ mice was performed to gain insight into the nature of the altered colonic phenotype in these mice, demonstrated by the augmented development of ILFs.

The importance of LTβR signalling in the regulation of DC homeostasis can be shown by the fact that i) DC subsets express LTβR and *in vitro* bone marrow DC

cultures revealed that DC numbers were increased following treatment with agonist LTβR (Kabashima et al., 2005), ii) splenic CD11c^{high}CD8α^{-} DCs are preferentially decreased in mice deficient for LTβR, LTα or LTβ, indicating that LTβR is involved in the regulation of this subset of DCs (Wu et al., 1999; Abe et al., 2003; De Trez et al., 2008; Wang et al., 2005), iii) ligation of LTβR induces signalling through both the classical and the alternative NF-κB activation pathways. Mice deficient in individual components of the classical pathway, such as *Rela*$^{-/-}$ *cRel*$^{-/-}$ *and p50*$^{-/-}$ mice, demonstrated intact populations of splenic cDCs (Ouaaz et al., 2002). Additionally, mice deficient in NF-κB2 also displayed normal splenic DC development (Kobayashi et al., 2003). Conversely, mice with ineffective alternative pathway signalling, either due to a lack of LTβR signalling (De Trez and Ware, 2008; Kabashima et al., 2005), or due to a lack of RelB (Wu et al., 1998; Kobayashi et al., 2003) have a selective defect in development of splenic CD11c^{high}CD8α^{-} DCs. Interestingly however, Ouaaz *et al*, revealed defects in DC maturation and survival in mice doubly deficient in p50-RelA and p50-cRel (Ouaaz et al., 2002).

Considering the effect of LTβR signalling on the homeostasis of DCs and the critical contribution of this cell type to mucosal immunity, analysis of populations of DCs was undertaken in p100Δ mice to understand what affect constitutive activation of the alternative NF-κB pathway has on their development, mobilisation and activation.

4.2. Results

4.2.1. Increase in dendritic cells and CD11c$^-$CD11b$^+$ cells in p100Δ mice

During the characterisation of ILFs in the colon of p100Δ mice, an apparent increase in the numbers of CD11c$^+$ DCs was noted throughout the colon. Flow cytometric analysis was performed in order to verify and enumerate this observation.

Classical DCs (cDCs) are defined by high expression of CD11c and myeloid cells, including monocytes and granulocytes are classified as CD11c$^-$CD11b$^+$, and both are visible in the spleen, mLN and colon of WT and p100Δ mice (Figure 4.1. A). In the spleen of p100Δ mice, a significant increase in the proportion of CD11c^{high} DCs (WT n=5, median=1.06, p100Δ n=5, median=1.95, p=0.008) and CD11c$^-$CD11b$^+$ cells (WT n=5, median=4.15, p100Δ n=5, median=8.32, p=0.008) was observed when compared with WT spleen (Figure 4.1. B). Taking into account the decrease in total splenocyte numbers in p100Δ mice, a decrease in cDC cell numbers was observed compared with WT (WT n=5, median=585,297, p100Δ n=5, median=430,920, p=0.008) and no difference in cell numbers was observed for the CD11c$^-$CD11b$^+$ population (WT n=5, median=2.2 x10^6, p100Δ n=5, median=1.7 x10^6, p=0.222) (Figure 4.1. C). In contrast, the cDC and CD11c$^-$CD11b$^+$ proportions (cDC: WT n=5, median=2.18, p100Δ n=6, median=1.65, p=0.537. CD11c$^-$CD11b$^+$ cells: WT n=5, median=1.57, p100Δ n=6, median=1.85 p=0.792) and cell numbers (cDC: WT n=5, median=73,828, p100Δ n=6, median=18,195, p=0.247. CD11c$^-$CD11b$^+$ cells: WT n=5, median=58,729, p100Δ n=6, median=38,801 p=0.178) were similar in the mLN of WT and p100Δ mice (Figure 4.1. B and C).

When the colon is considered, p100Δ mice exhibited an increase in proportion and total cell number for cDCs with respect to WT mice (Proportions of cDCs: WT n=5, median=0.53, p100Δ n=6, median=1.74, p=0.004. cDC Cell Number: WT n=5, median=615, p100Δ n=6, median=7,225, p=0.004) (Figure 4.1. B and C). For $CD11c^{-}$ $CD11b^{+}$, no difference in proportion was observed (WT n=5, median=1.01, p100Δ n=6, median=4.17, p=0.662) (Figure 4.1. B), but due to increased total colon cell number, a significant increase in $CD11c^{-}CD11b^{+}$ cell numbers was seen (WT n=5, median=1,852, p100Δ n=6, median=17,543, p=0.004) (Figure. 4.1. C).

When the cDC population is divided based on the expression of CD11b, two distinct populations can be observed; $CD11c^{high}CD11b^{-}$ and $CD11c^{high}CD11b^{+}$. In the spleen and colon the proportion of $CD11c^{high}CD11b^{-}$ (Spleen: WT n=5, median=0.58, p100Δ n=5, median=1.13, p=0.008. Colon: WT n=5, median=0.23, p100Δ n=5, median=0.89, p=0.009) and $CD11c^{high}CD11b^{+}$ DCs (Spleen: WT n=5, median=0.48, p100Δ n=6, median=0.65, p=0.030. Colon: WT n=5, median=0.22, p100Δ n=6, median=0.72, p=0.004) is elevated in p100Δ mice compared with WT counterparts (Figure 4.2. A). The reduction in absolute splenic cell number in p100Δ mice correlates with a reduction in $CD11c^{high}CD11b^{-}$ (WT n=5, median=336,378, p100Δ n=6, median=284,760, p=0.032) and $CD11c^{high}CD11b^{+}$ (WT n=5, median=248,919, p100Δ n=5, median=124,461, p=0.004) DC cell number despite the increase in proportion (Figure 4.2. B). In the colon, the cell number for both these cDC subpopulations is elevated in p100Δ mice with respect to WT mice ($CD11c^{high}CD11b^{-}$ DCs: WT n=5, median=307, p100Δ n=6, median=3,718, p=0.004. $CD11c^{high}CD11b^{+}$ DCs, WT n=5, median=297, p100Δ n=6, median=3,000, p=0

.004) (Figure 4.2. B).

In summary, the spleen and colon of p100Δ mice exhibit an increase in cDC and macrophage populations, and within the cDCs, both $CD11b^-$ and $CD11b^+$ DCs are increased.

4.2.2. Expression of CD103 by dendritic cells in the spleen, mLN and colon

Expression of CD103 on DCs allows identification of functionally distinct DC populations. $CD11c^{high}CD103^+$ LP-DCs, and not $CD11c^{high}CD103^-$ LP-DCs, are capable of migrating from the intestine to the draining mLN, to prime naïve T cells and induce expression of gut-homing receptors on these T cells (Jaensson et al., 2008; Schulz et al., 2009; Johansson-Lindbom et al., 2005). $CD11c^{high}CD103^+$ LP-DCs have been shown to derive from proliferating precursors that circulate in the blood and continually migrate into the gut (Jaensson et al., 2008). The observation that p100Δ mice have an increase in colonic cDCs prompted investigation of CD103 expression by this population.

Figure 4.1 Analysis of dendritic cell and CD11b^{+} populations in the spleen, mLN and colon of WT and p100Δ mice

A *Preparations of single cell suspensions from spleen, mLN and colon of WT and p100Δ mice were stained with fluorescently labelled antibodies to CD11c and CD11b, and analysed by flow cytometry. Classical dendritic cells (cDCs) were classified as CD11c^{high}. Within the spleen, CD11c^{-} cells were subdivided based on intermediate or high expression of CD11b. Representative FACs plots of two independent experiments are shown. Graphs depict proportion of indicated cell populations, from two independent experiments (n≥5 for each genotype). Lower graph shows separation of CD11c^{-}CD11b^{+} splenic cells into CD11b^{intermedate} and CD11b^{high} populations.*

B *Graphs depicting cDC and macrophage cell number for the different tissues, from two independent experiments (n≥5 for each genotype).*

*Bar indicates median.*** p<0.001 ** p<0.02, ns= not significant.*

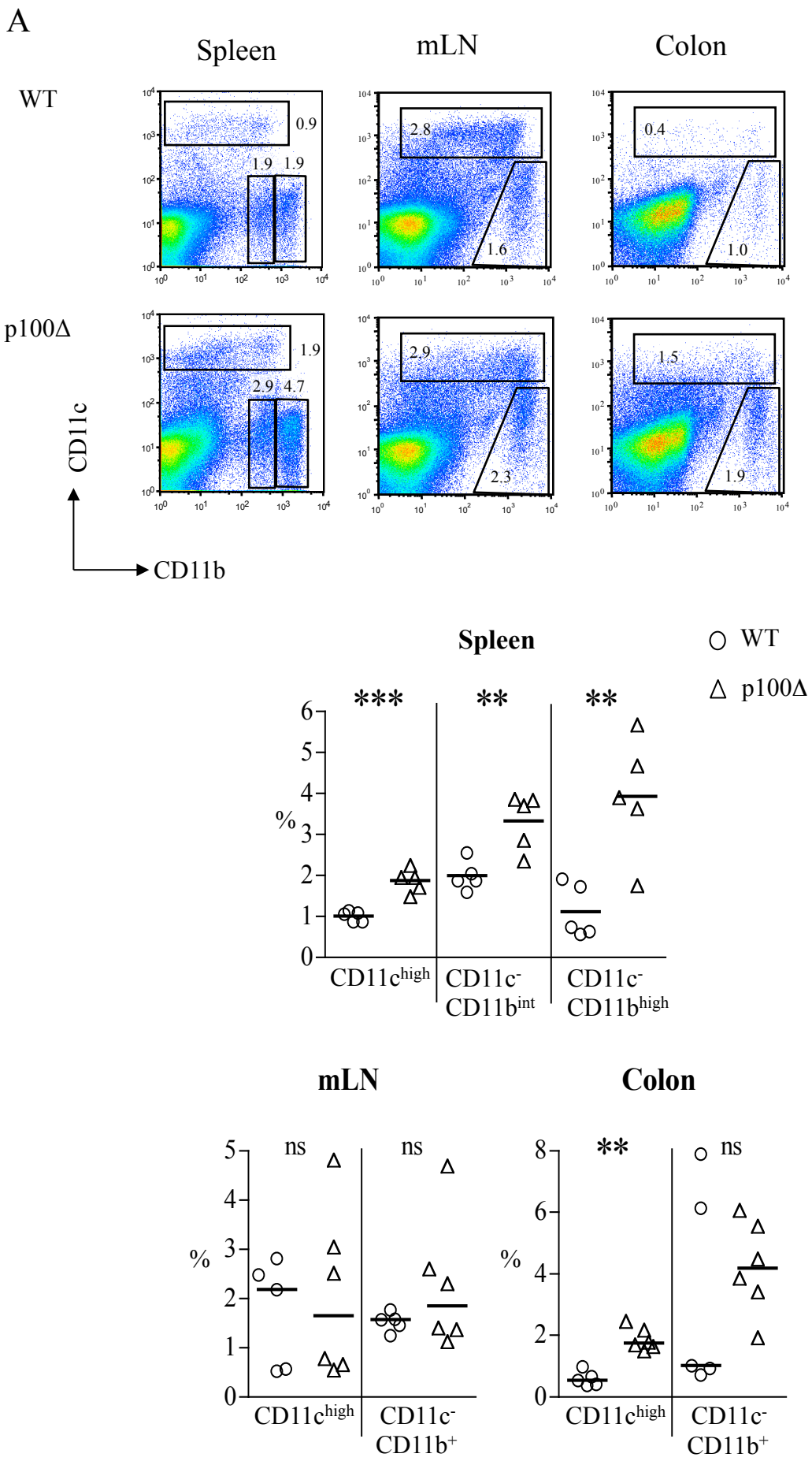
A
Spleen
mLN
Colon
WT
p100Δ
0.9
1.9
1.9
2.8
1.6
0.4
1.0
1.9
2.9
4.7
2.9
2.3
1.5
1.9
CD11c
CD11b
Spleen
WT
p100Δ
***
**
**
%
CD11c^high
CD11c^- CD11b^int
CD11c^- CD11b^high
mLN
Colon
ns
ns
**
ns
%
CD11c^high
CD11c^- CD11b^+
CD11c^high
CD11c^- CD11b^+

Figure 4.1

B

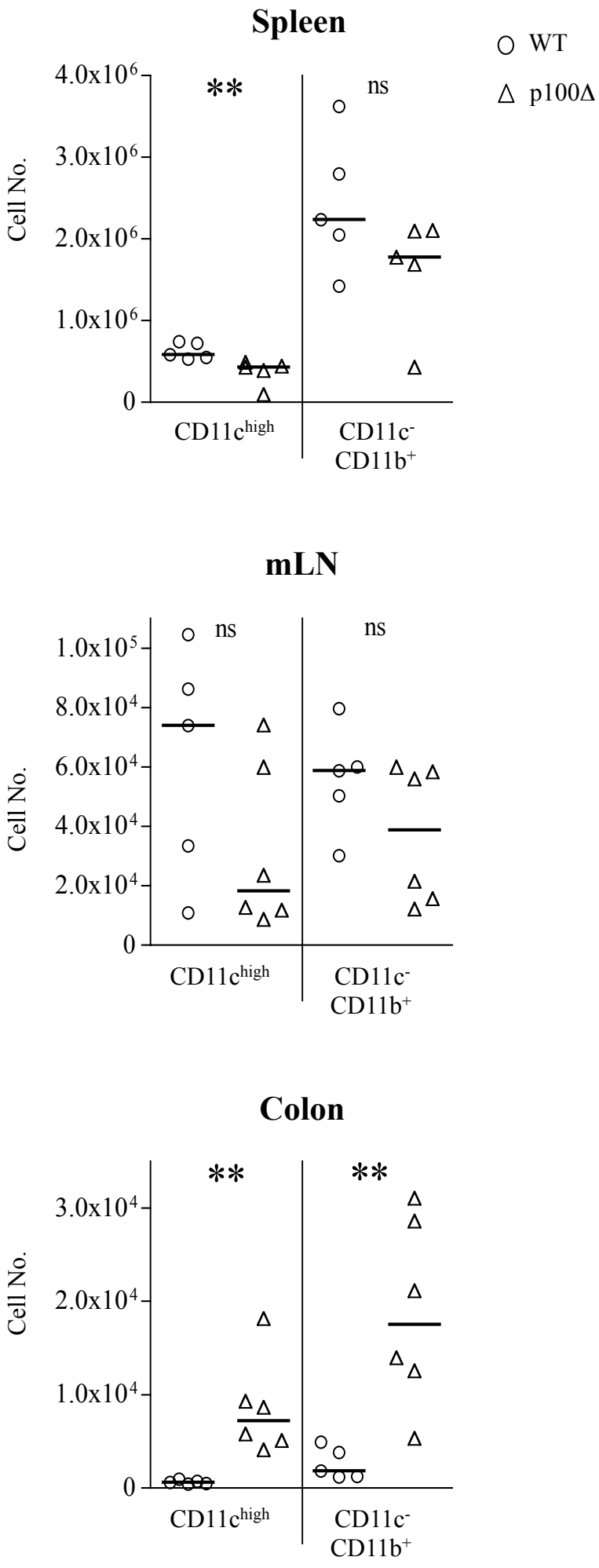
Spleen
WT
p100Δ
4.0x10^6
3.0x10^6
2.0x10^6
1.0x10^6
0
Cell No.
**
ns
CD11c^high
CD11c^- CD11b^+
mLN
1.0x10^5
8.0x10^4
6.0x10^4
4.0x10^4
2.0x10^4
0
Cell No.
ns
ns
CD11c^high
CD11c^- CD11b^+
Colon
3.0x10^4
2.0x10^4
1.0x10^4
0
Cell No.
**
**
CD11c^high
CD11c^- CD11b^+

Figure 4.1

Figure 4.2 Analysis of CD11b expression by CD11c^{high} dendritic cells in the spleen and colon of WT and p100Δ mice

Flow cytometric analysis of single cell suspensions of cells isolated from the spleen and colon from WT and p100Δ mice. Classical DCs were defined as CD11c^{high} and subdivided according to CD11b expression, revealing two populations: CD11c^{high}CD11b^{-} and CD11c^{high}CD11b^{+}.

***A** Representative FACs plots. Graphs depicting proportion of CD11c^{high} CD11b$^{-/+}$ dendritic cells.*

***B** Graphs depicting cell number of CD11c^{high} CD11b$^{-/+}$ dendritic cells.*

*Results of two independent experiments, bar indicates median. (n≥5 for each genotype). ** p<0.02, * p<0.05.*

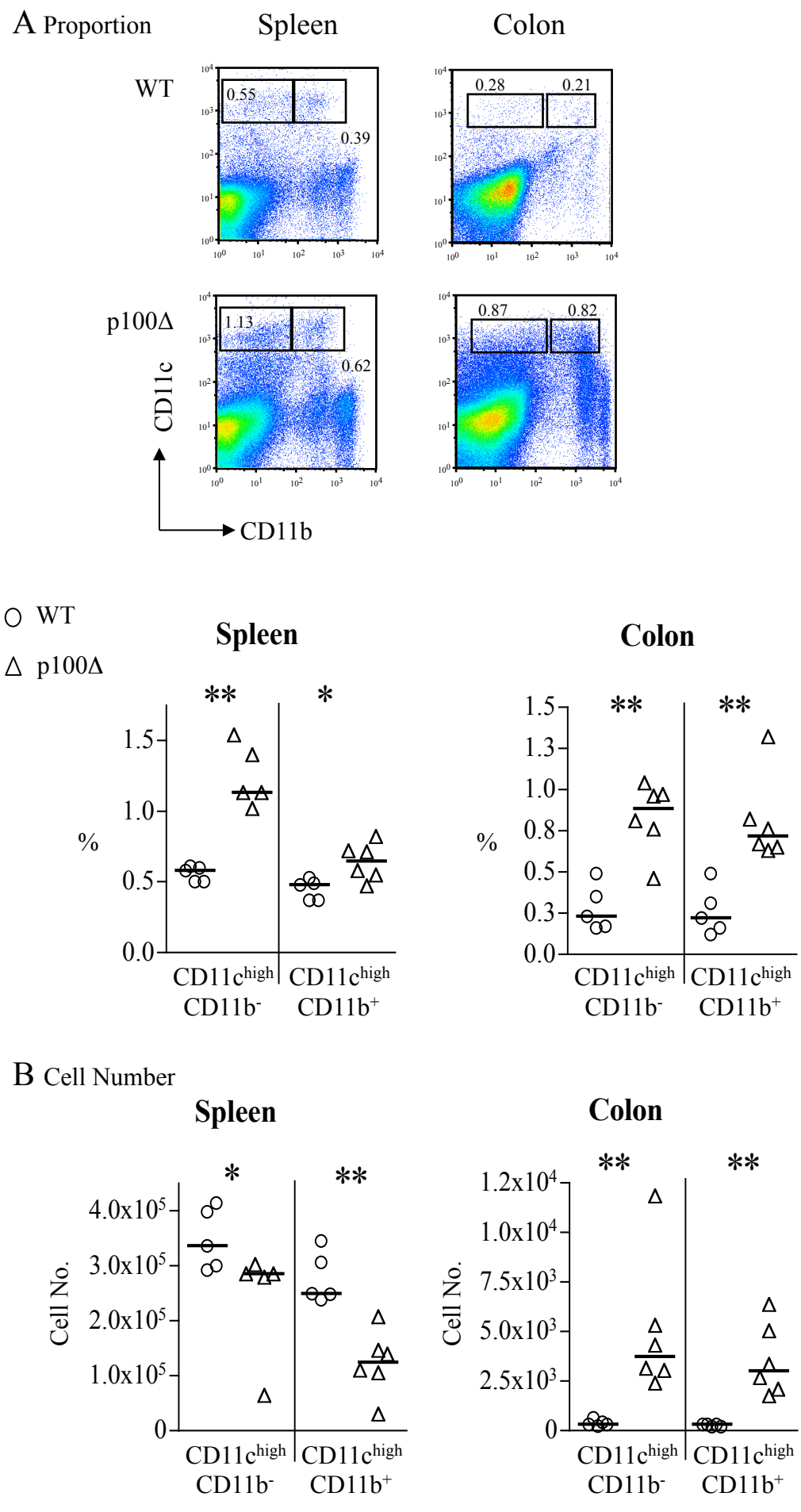
A Proportion
Spleen
Colon
WT
p100Δ
0.55
0.39
0.28
0.21
1.13
0.62
0.87
0.82
CD11c
CD11b
○ WT
△ p100Δ
Spleen
Colon
**
*
**
**
%
1.5
1.0
0.5
0.0
1.3
0.8
0.3
CD11c^high CD11b^-
CD11c^high CD11b^+
B Cell Number
Cell No.
4.0x10^5
3.0x10^5
2.0x10^5
1.0x10^5
0
1.2x10^4
1.0x10^4
7.5x10^3
5.0x10^3
2.5x10^3

Figure 4.2

$CD103^+$ DCs are normally found in mucosal-draining LNs, such as the mLN, however, we observed $CD11c^{high}CD103^+$ DCs in the spleen of WT (≈0.2% of total splenocytes) and the proportion of this population was significantly increased in p100Δ mice (≈0.7% of total splenocytes, p=0.004) (Figure 4.3. B). The proportion of $CD11c^{high}CD103^-$ DCs in the spleen of p100Δ mice did not differ significantly from that observed in WT mice (WT n=5, median=0,78, p100Δ n=6, median=0.96, p=0.052) (Figure 4.3. B). The majority of splenic $CD11c^{high}CD103^+$ DCs in both WT and p100Δ mice were $CD11b^-$ (≈90%) (Appendix, Figure 8.2). The cell numbers for splenic $CD11c^{high}CD103^-$ DCs in p100Δ mice was reduced by approximately half, compared with WT (WT n=5, median=428,076, p100Δ n=6, median=177,117, p=0.004) and due to the reduction in p100Δ absolute splenocyte number, no difference in cell numbers for $CD11c^{high}CD103^+$ DCs was observed (WT n=5, median=129,210, p100Δ n=6, median=151,250, p=0.177) (Figure 4.3. C). Within the mLN, the only difference seen between WT and p100Δ mice was the three-fold decrease in $CD11c^{high}CD103^-$ DC cell number (WT n=5, median=35,323, p100Δ n=6, median=7,785 p=0.017) (Figure 4.3. B and C). The proportion of $CD11c^{high}CD103^+$ DCs co-expressing CD11b in the mLN was lower than in the spleen, for both WT and p100Δ mice (≈70% in WT, ≈50% in p100Δ) (Appendix, Figure 9.2). However, it is important to note that there is much variation in the proportions and cell numbers in this population between individual animals, as well as between WT and p100Δ mice, due to variations in digestion of tissues and extraction of cells.

When considering the colon, p100Δ mice displayed an approximate two-fold increase in the proportion of $CD11c^{high}CD103^-$ (WT n=5, median=0.11, p100Δ n=5, median=0.5 p=0.008) and $CD11c^{high}CD103^+$ (WT n=5, median=0.27, p100Δ n=5, median=0.84 p=0.032) DCs when compared with WT mice. This is reflected in the

cell counts where few, if any, $CD11c^{high}CD103^{-}$ DCs are found in the colon of WT mice, with an approximately 10-fold increase in this population in p100Δ mice (WT n=5, median=120, p100Δ n=5, median=1632, p=0.008) (Figure 4.3. C). Compared with $CD11c^{high}CD103^{-}$ DCs, a greater number of $CD11c^{high}CD103^{+}$ DCs are found in the colon of WT mice (n=5), an increase from 120 to 400 cells, but in p100Δ mice (n=5) this population expands from 1,300 to around 3,000 cells (p=0.008) (Figure 4.3. C). Approximately 60% of colonic $CD11c^{high}CD103^{+}$ DCs co-express CD11b, in WT and p100Δ mice (Appendix, Figure 9.2).

To summarise, there is a significant increase in $CD11c^{high}CD103^{-}$ and $CD11c^{high}CD103^{+}$ DCs in the colon of p100Δ mice, as well as an increase in these two populations in the spleen. CD103 is used as a marker for cDCs capable of migrating from the intestine to the draining mLN and spleen, the increase in colonic $CD11c^{high}CD103^{+}$ DCs and their subsequent potential migration to the spleen may account for the expansion of this population in the latter. Additionally, although the proportion of $CD11c^{high}CD103^{+}$ DCs in the mLN of p100Δ mice is not significantly higher than in WT mLN, an increase is observed nonetheless, potentially equating to increased migration of these cells from the intestine.

4.2.3. Activation of dendritic cell subsets in the spleen, mLN and colon of WT and p100Δ mice

Due to the increase in proportion of DC populations in the spleen and colon of p100Δ mice, the activation status of DC populations from p100Δ mice was investigated to assess potential functional differences. Following ~~antigen~~ stimulation,

DCs upregulate co-stimulatory molecules, such as CD86, thereby allowing CD86 to be used as a useful marker for DC activation.

Within the splenic cDC population in p100Δ mice an increase in CD86 MFI was seen with respect to WT mice (WT n=4, mean=48.3±8.0, p100Δ n=4, mean=105.6±37.6, p=0.02). Within the colon no difference was observed (WT n=4, mean=102.5±36.6, p100Δ n=4, mean=115.3±34.7, p=0.63). Strikingly, in the mLN, cDCs from p100Δ mice displayed a marked upregulation of CD86 (WT n=4, mean=138.5±45.7, p100Δ n=4, mean=344.8±41.2, p=0.0005) (Figure 4.4).

The cDC population was further subdivided into $CD11b^{+}$ or $CD11b^{-}$ cDCs. The increased expression of CD86 by splenic cDCs from p100Δ mice is accounted for by upregulation of CD86 by $CD11c^{high}CD11b^{+}$ DCs (WT n=4, mean=21.6±5.5, p100Δ n=4, mean=128.5±71.8, p=0.03), rather than $CD11c^{high}CD11b^{-}$ DCs (WT n=4, mean=70.7±11.4, p100Δ n=4, mean=91.5±18.2, p=0.10) (Figure 4.4). The CD86 expression of these two cDC populations in the colon was similar between WT and p100Δ mice ($CD11c^{high}CD11b^{+}$ DCs: WT n=4, mean=123.0±40.1, p100Δ n=4, mean=124.2±48.4, p=0.970. $CD11c^{high}CD11b^{-}$ DCs: WT n=4, mean=101.9±34.7, p100Δ n=4, mean=117.9±34.6, p=0.539). Finally, in the mLN, the majority of CD86 expression in the cDC population in p100Δ mice is accounted for by increased CD86 expression in the $CD11c^{high}CD11b^{-}$ DC (WT n=4, mean=166.0±33.3, p100Δ n=4, mean=454.0±98.7, p=0.002), with a less dramatic upregulation of CD86 by $CD11c^{high}CD11b^{+}$ DCs (WT n=4, mean=116.5±60.6, p100Δ n=4, mean=263.0±42.5, p=0.007) (Figure 4.4).

When the cDC profile is switched to assess CD103 expression, a slight, but not significant, upregulation of CD86 was seen in the $CD11c^{high}CD103^{+}$ (Spleen: WT n=4, mean=105.6±35.1, p100D n=4, mean=150.2±43.1, p=0.160. Colon: WT n=4,

mean=121.6±41.0, p100D n=4, mean=161.0±41.7, p=0.226) and $CD11c^{high}CD103^{-}$ (Spleen: WT n=4, mean=35.1±8.1, p100D n=4, mean=60.7±26.3, p=0.112. Colon: WT n=4, mean=39.9±29.1, p100D n=4, mean=70.3±11.4, p=0.101) DC populations in the spleen and colon of p100Δ mice, when compared with WT mice. The largest difference, was again observed in the mLN, where p100Δ mice demonstrated upregulation of CD86 in both subpopulations of DCs ($CD103^{+}$ cDCs: WT n=4, mean=237.0±64.8, p100D n=4, mean=472.0±78.5, p=0.004. $CD103^{-}$ cDCs: WT n=4, mean=56.7±8.2, p100D n=4, mean=153±43.5, p=0.007) (Figure 4.4). Others markers of activation which would be useful to assess with regards to DC biology include CD80 and MHCII.

In summary, the largest differences in DC activation status can be seen in the mLN, with all of the DC subsets investigated expressing higher levels of CD86 in p100Δ mice when compared with WT counterparts.

Figure 4.3 Analysis of $CD103^{+}$/$CD103^{-}$ dendritic cell populations in the spleen, mLN and colon of WT and p100Δ mice

A *Preparations of single cell suspensions from spleen, mLN and colon of WT and p100Δ mice were stained with fluorescently labelled antibodies to CD11c and CD103 and analysed by flow cytometry. Classical dendritic cells (cDCs) were classified as* $CD11c^{high}$ *and this population was subdivided according to CD103 expression, revealing two distinct populations;* $CD11c^{hi}CD103^{-}$ *and* $CD11c^{hi}CD103^{-}$ *cDCs. FACs plots representative of two independent experiments are shown.*

B *Graphs depicting proportion of* $CD11c^{hi}CD103^{-}$ *and* $CD11c^{hi}CD103^{-}$ *cDCs for the different tissues, from two independent experiments (n≥5 for each genotype).*

C *Graphs depicting* $CD11c^{hi}CD103^{-}$ *and* $CD11c^{hi}CD103^{-}$ *cDC cell number for the different tissues, from two independent experiments, bar indicates median (n≥5 for each genotype).*

*** p<0.02, * p<0.05, ns= not significant.*

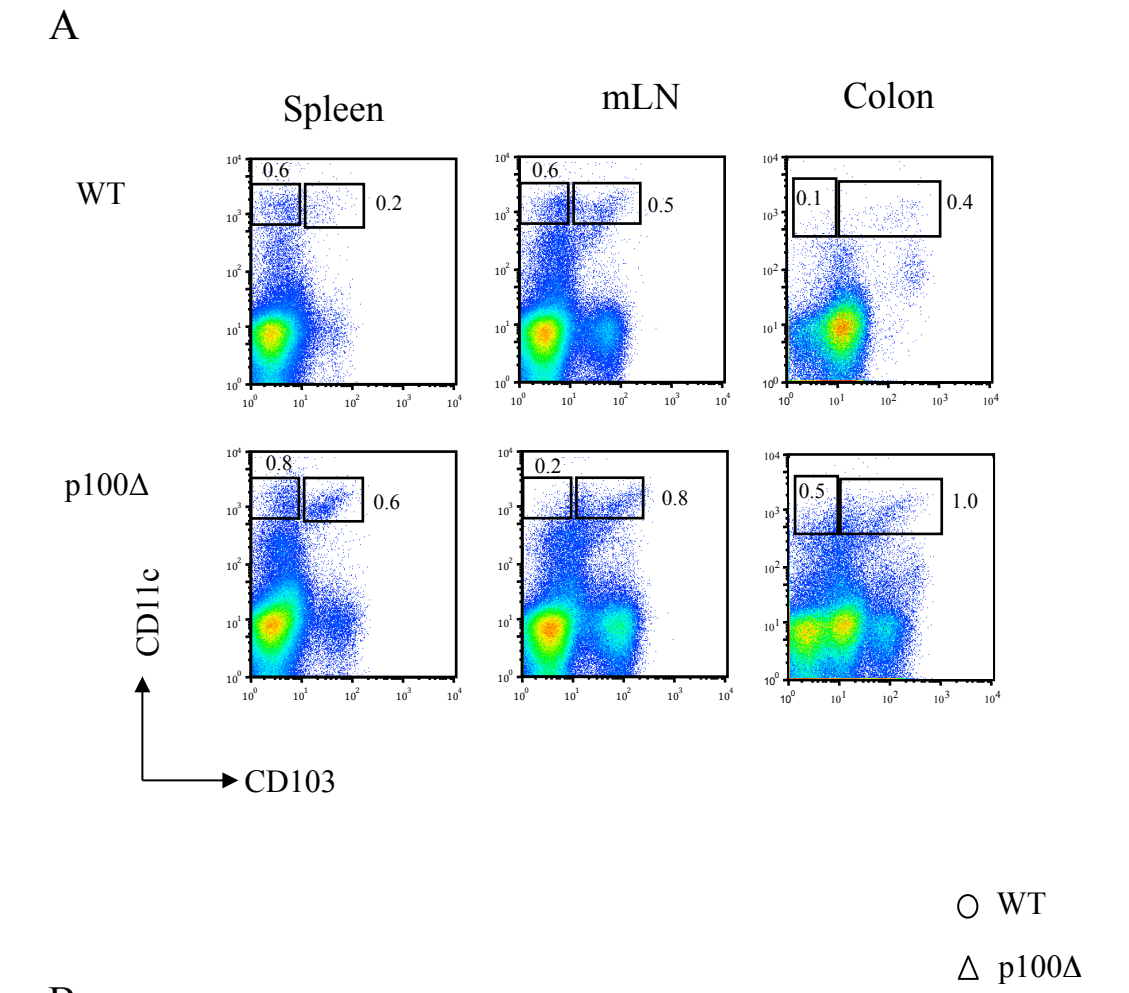
A
Spleen
mLN
Colon
WT
p100Δ
0.6
0.2
0.6
0.5
0.1
0.4
0.8
0.6
0.2
0.8
0.5
1.0
CD11c
CD103
WT
p100Δ
B
Spleen
mLN
Colon
%
ns
**
ns
ns
**
*
CD11chi CD103-
CD11chi CD103+

Figure 4.3

C

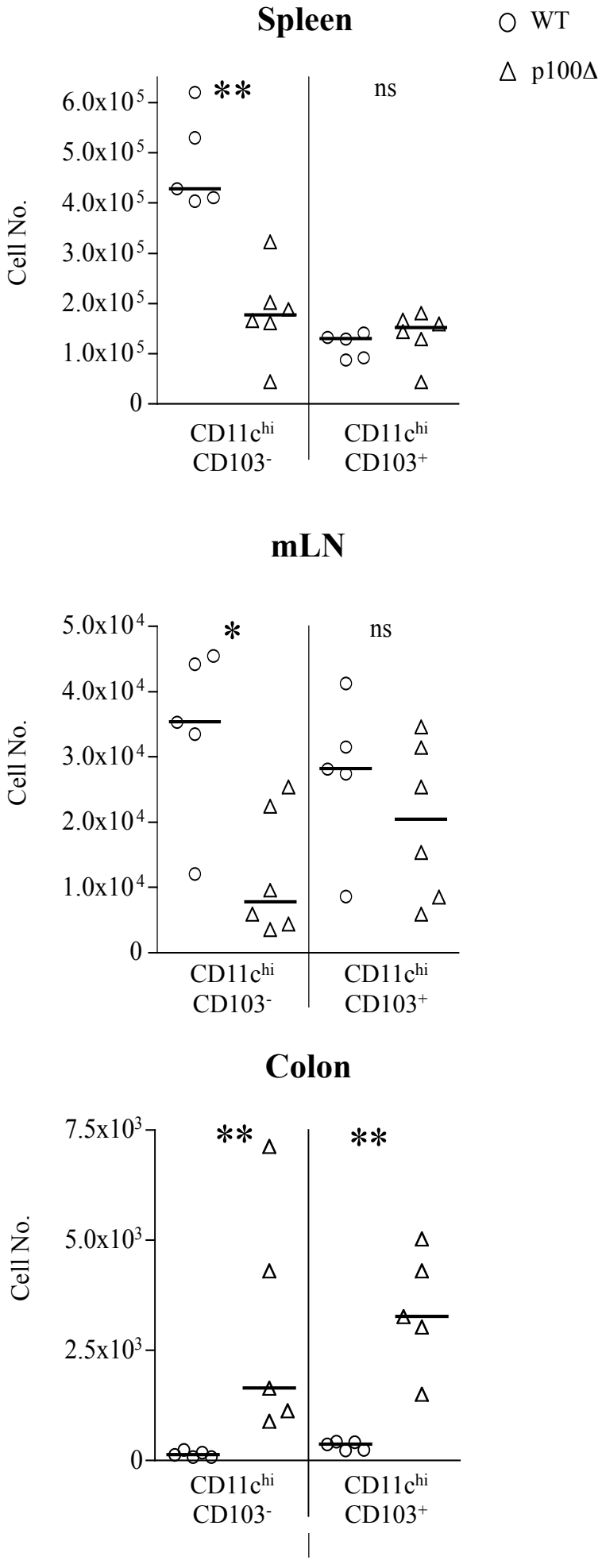
Spleen
WT
p100Δ
**
ns
6.0x10^5
5.0x10^5
4.0x10^5
3.0x10^5
2.0x10^5
1.0x10^5
0
Cell No.
CD11c^hi CD103^-
CD11c^hi CD103^+
mLN
*
ns
5.0x10^4
4.0x10^4
3.0x10^4
2.0x10^4
1.0x10^4
0
Cell No.
CD11c^hi CD103^-
CD11c^hi CD103^+
Colon
**
**
7.5x10^3
5.0x10^3
2.5x10^3
0
Cell No.
CD11c^hi CD103^-
CD11c^hi CD103^+

Figure 4.3

Figure 4.4 Activation of dendritic cell subsets in the spleen, mLN and colon of WT and p100Δ mice

*Single cell suspensions of spleen, mLN and colon were stained with fluorescently labelled antibodies against CD11c, CD11b, CD103, CD3, and the activation marker CD86 was used to assess DC activation. Graphs show mean fluorescence intensity (MFI) and standard deviation error bars for CD86 expression by the DC populations described. Classical dendritic cells (cDCs), defined as $CD11c^{high}$. The cDC population was further sub-divided into $CD11c^{high}CD11b^{+}$ and $CD11c^{hghi}CD11b^{-}$ DCs. Two additional DC populations were identified as $CD11c^{high}CD103^{+}$ and $CD11c^{high}CD103^{-}$. Results of two independent experiments (n=4 for each tissue and genotype). ***p<0.001 ** p<0.02, * p<0.05, ns= not significant.*

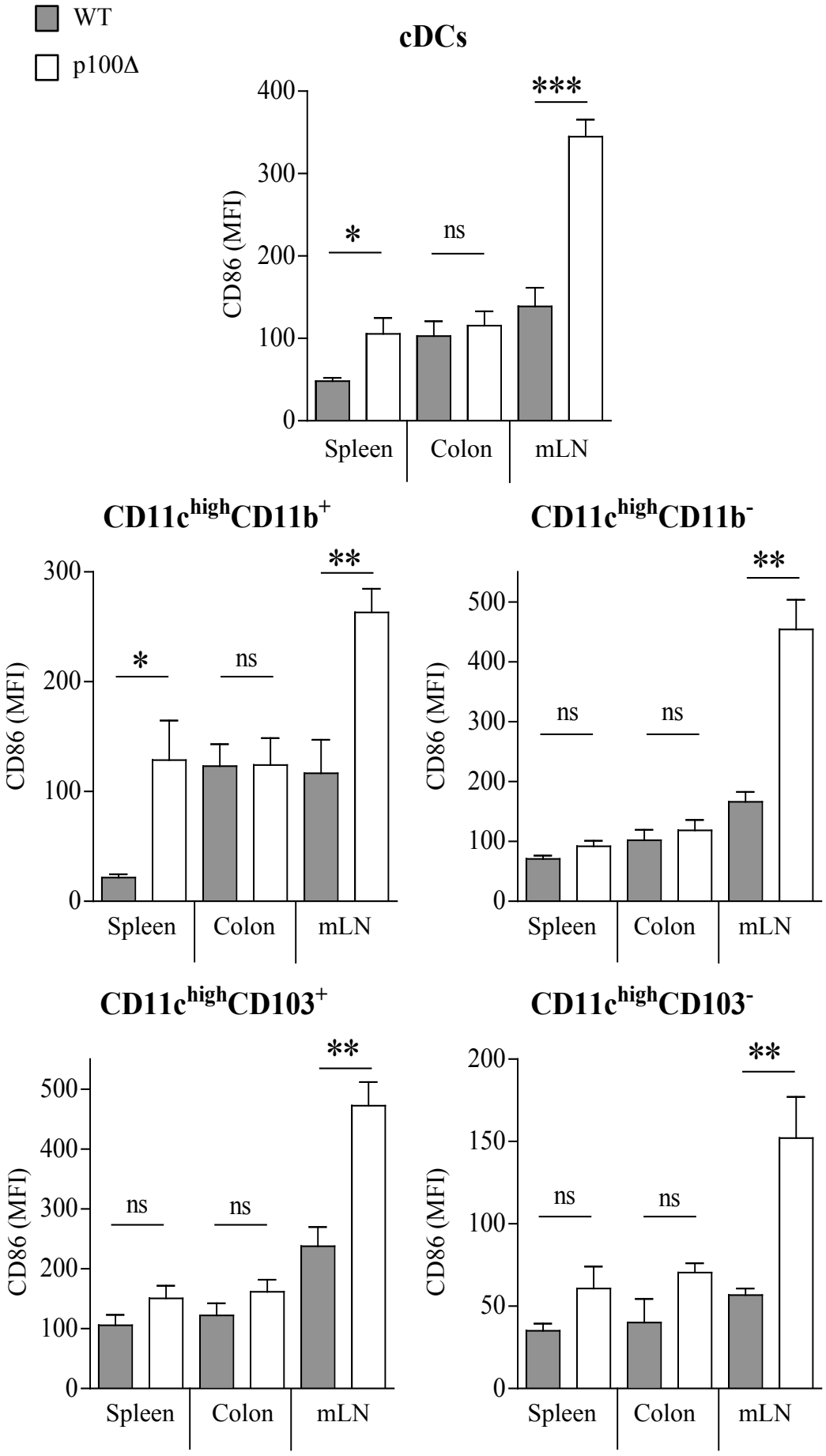
WT
p100Δ
cDCs
CD86 (MFI)
400
300
200
100
0
*
ns
***
Spleen
Colon
mLN
CD11c^high CD11b^+
300
200
100
0
*
ns
**
Spleen
Colon
mLN
CD11c^high CD11b^-
500
400
300
200
100
0
ns
ns
**
Spleen
Colon
mLN
CD11c^high CD103^+
500
400
300
200
100
0
ns
ns
**
Spleen
Colon
mLN
CD11c^high CD103^-
200
150
100
50
0
ns
ns
**
Spleen
Colon
mLN

Figure 4.4

4.2.4. Analysis of CD103 expression by non-cDC populations

CD103 expression is not restricted to DC populations, particular subsets of T cells also express CD103 (Uss et al., 2006), such as intraepithelial T cells (Annunziato et al., 2006) and LP T cells (Agace et al., 2000). The $CD11c^{-}CD103^{+}$ population of cells visible in spleen, mLN and colon, were investigated further.

In the spleen there is a 2.5-fold increase in the proportion of $CD11c^{-}CD103^{+}$ cells in p100Δ mice over that seen in WT mice (WT n=5, median=1.0, p100D n=6, median=2.6, p=0.004), although no change in absolute cell numbers was documented (WT n=5, median=656,708, p100D n=6, median=515,650, p=0.247), as p100Δ mice have a lower splenocyte count compared with WT (Figure 4.5. B). Within the mLN, the proportion of $CD11c^{-}CD103^{+}$ cells in p100Δ mice (n-6) was increased to 15%, compared with 7% in WT mice (n=5) (Figure 4.5. B, p=0.004). However, this did not correspond to an increase in absolute cell number (WT n=5, median=250,947, p100D n=6, median=316,758, p=0.691) (Figure 4.5. C).

Interestingly, when investigating the colon, a decrease of 30% was observed in the proportion of $CD11c^{-}CD103^{+}$ cells in p100Δ mice compared with WT mice (WT n=5, median=70.5, p100D n=6, median=43.1, p=0.028) (Figure 4.5. B). However, when converted to cell numbers, a significant increase in $CD11c^{-}CD103^{+}$ cells was seen in p100Δ mice compared with cells isolated from the colon of WT mice (WT n=5, median=84,600, p100D n=6, median=171,314 p=0.016) (Figure 4.5. C).

Within the colon the $CD11c^{-}CD103^{+}$ population can be subdivided based on level of expression of CD103 (Figure 4.5. D). In the colon of p100Δ mice an increase in the proportion of $CD11c^{-}CD103^{high}$ cells with a concomitant decrease in $CD11c^{-}CD103^{int}$ cells when compared with WT mice. In addition, the side scatter (SSC) and forward scatter (FSC) plots for the individual $CD11c^{-}CD103^{high}$ and $CD11c^{-}CD103^{int}$

populations differ. The $CD11c^{-}CD103^{high}$ cells exhibit a profile similar to lymphocytes and the $CD11c^{-}CD103^{int}$ cells exhibit a wider SSC/FSC profile, demonstrating larger size and granularity. This data suggests that these two populations are unique and further investigation into their phenotype and function would be advantageous.

In summary, an increase in the proportion of $CD11c^{-}CD103^{+}$ cells was seen in the spleen and mLN of p100D mice compared with WT mice and an increase in $CD11c^{-}CD103^{+}$ cell number was observed in the colon of p100D mice. Further flow cytometric analysis was performed to characterise this population.

Figure 4.5 Analysis of CD103 expression on non-cDC populations

A *Single cell suspensions from spleen, mLN and colon of WT and p100Δ mice were stained with fluorescently labelled antibodies to CD11c and CD103 and analysed by flow cytometry. This figure focuses on the* $CD11c^{-}CD103^{+}$ *cell population. FACs plots representative of two independent experiments are shown.*

B *Graph depicting proportion of* $CD11c^{-}CD103^{+}$ *for the different tissues, from two independent experiments (n≥5 for each genotype).*

C *Graph depicting* $CD11c^{-}CD103^{+}$ *cell number for the different tissues, from two independent experiments (n≥5 for each genotype).*

D *Within the colon the* $CD11c^{-}CD103^{+}$ *population can be divided based on the level of CD103 expression. Two populations can be observed:* $CD11c^{-}CD103^{int}$ *and* $CD11c^{-}CD103^{high}$*. The side scatter (SSC) and forward scatter (FSC) profile for each subpopulation is shown.*

*** $p<0.02$, * $p<0.05$, ns= not significant.*

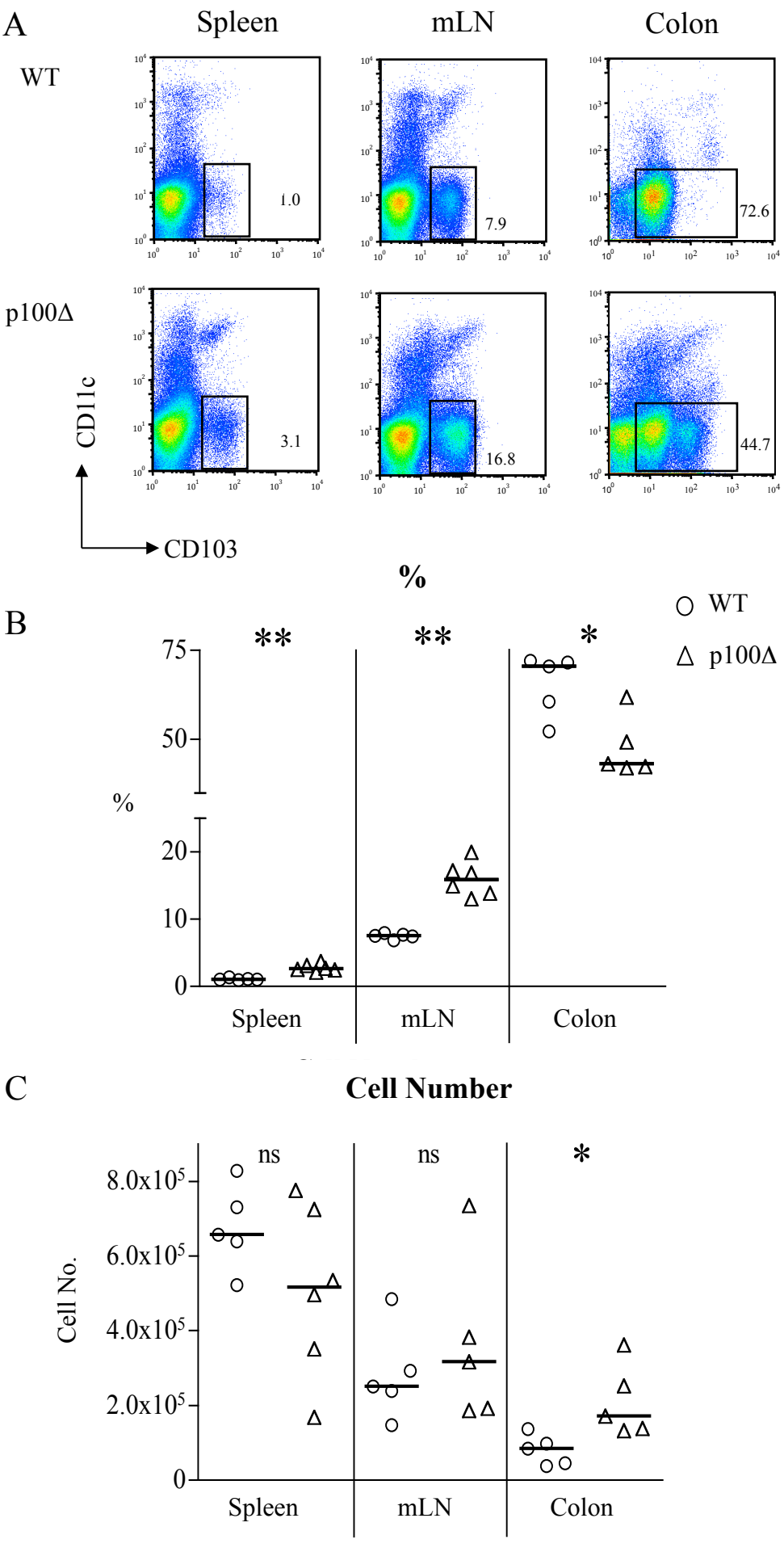
A
Spleen
mLN
Colon
WT
p100Δ
1.0
7.9
72.6
3.1
16.8
44.7
CD11c
CD103
%
B
WT
p100Δ
**
**
*
75
50
20
10
0
%
Spleen
mLN
Colon
C
Cell Number
ns
ns
*
8.0x10^5
6.0x10^5
4.0x10^5
2.0x10^5
0
Cell No.
Spleen
mLN
Colon

Figure 4.5

D

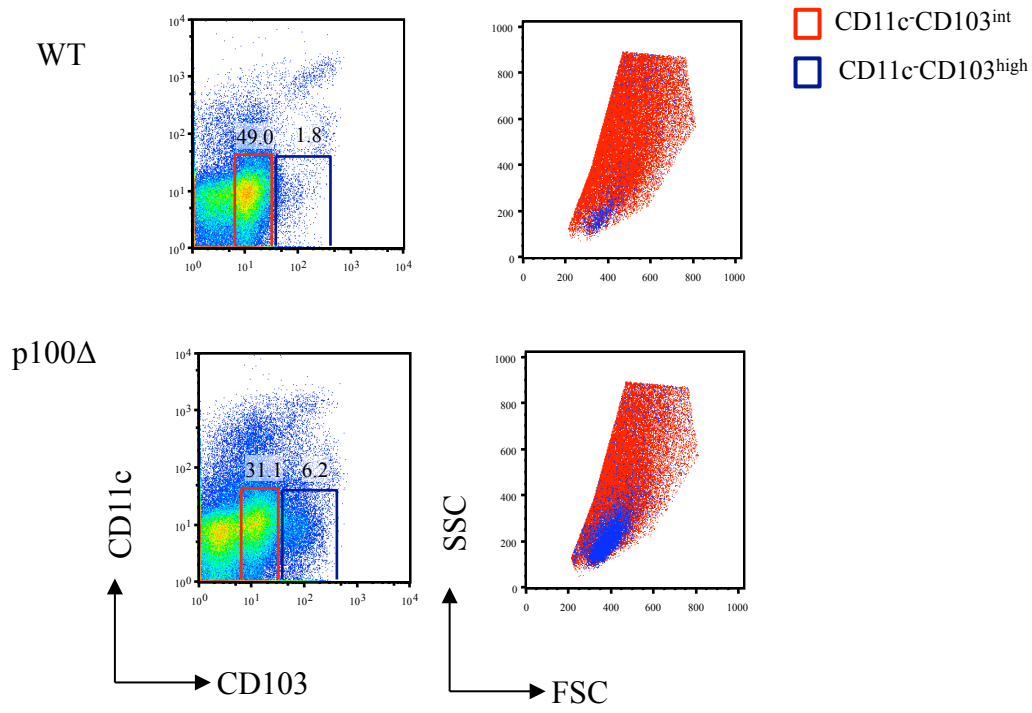
WT
p100Δ
49.0
1.8
31.1
6.2
CD11c
CD103
SSC
FSC
CD11c-CD103int
CD11c-CD103high

Figure 4.5

4.2.5. Characterisation of $CD11c^{-}CD103^{+}$ cells in the spleen, mLN and colon of WT and p100Δ mice

In order to analyse any differences in $CD11c^{-}CD103^{+}$ subpopulations between WT and p100Δ mice, single cell suspensions from spleen, mLN and colon where stained with fluorescently labelled antibodies to CD11c, CD11b, CD103 and CD3, and analysed by flow cytometry.

In Figure 4.6, it can be seen that within the spleen approximately 60% of $CD11c^{-}CD103^{+}$ cells are $CD3^{+}$ T cells ($CD11b^{-}$) in both WT (n=5) and p100Δ (n=6) mice (Figure 4.6. A). Interestingly, when the $CD11c^{-}CD11b^{-}CD3^{+}$ T cell population is gated on, a larger proportion of T cells are $CD103^{+}$ in p100Δ mice with respect to WT mice (increased from 20% in WT, to 36% in p100Δ) (Figure 4.6. C). Within the mLN, approximately 90% of the $CD11c^{-}CD103^{+}$ cells are $CD3^{+}$ T cells ($CD11b^{-}$) in both WT (n=5) and p100Δ (n=6) mice (Figure 4.6. A). Similar to the spleen, when the $CD11c^{-}CD11b^{-}CD3^{+}$ T cell population is gated on, a larger proportion of T cells are $CD103^{+}$ p100Δ mice compared with WT mice (increased from 23% in WT, to 44% in p100Δ) (Figure 4.6. B).

In the colon the $CD11c^{-}CD103^{+}$ population is subdivided into $CD11c^{-}CD103^{int}$ and $CD11c^{-}CD103^{high}$ cells. Consistent with the SSC/FSC profile reflecting that the classical lymphocyte profile, the $CD11c^{-}CD103^{high}$ cells from WT and p100Δ mice consist mainly of $CD3^{+}CD11b^{-}$ T cells (Figure 4.6. C). Whereas, the $CD11c^{-}CD103^{int}$ cells represent a heterogeneous population with regards to CD3 and CD11b expression. This is consistent between WT and p100Δ mice (Figure 4.6. C). A greater proportion of $CD3^{+}$ colonic T cells from p100Δ mice express CD103 when compared to $CD3^{+}$ colonic T cells isolated from WT mice (Figure 4.6. D).

4.2.6. Blood serum levels of monocyte and macrophage chemotactic factors and IL-10

Monocytes and macrophages response to chemotactic gradients in the same way lymphocytes respond to chemokines such as CXCL13 and CCL21. There are many chemotactic proteins able to promote mobilisation and recruitment of monocytes and macrophages and they can be secreted into the blood under steady-state and inflammatory conditions, such as monocyte chemotactic protein (MCP) -1, MCP-3 and MCP-5, and macrophage inflammatory protein (MIP) -1γ. Blood serum levels of MCP-1, MCP-5 and MIP-1γ were increased in p100Δ mice, as was the level of IL-10, when compared to WT blood serum levels (Figure 4.7).

Figure 4.6 Characterisation of $CD11c^{-}CD103^{+}$ cells in the spleen, mLN and colon of WT and p100Δ mice

Preparations of single cell suspensions from spleen, mLN and colon of WT (n=3) and p100Δ (n=2) mice were stained with fluorescently labelled antibodies to CD11c, CD11b, CD103 and CD3, and analysed by flow cytometry. Representative FACs plots are shown.

***A** Spleen and mLN: Cells were gated on $CD11c^{-}CD103^{+}$ and the CD11b/CD3 profile was analysed.*

***B** Spleen and mLN: CD103 histogram for T cells (gated on $CD11c^{-}C11b^{-}CD3^{+}$).*

***C** Colon: Cells were gated on $CD11c^{-}CD103^{-}$ $CD11c^{-}CD103^{int}$ and $CD11c^{-}CD103^{high}$. The CD11b/CD3 profile was analysed for these populations.*

***D** Spleen and mLN: CD103 histogram for T cells (gated on $CD11c^{-}C11b^{-}CD3^{+}$).*

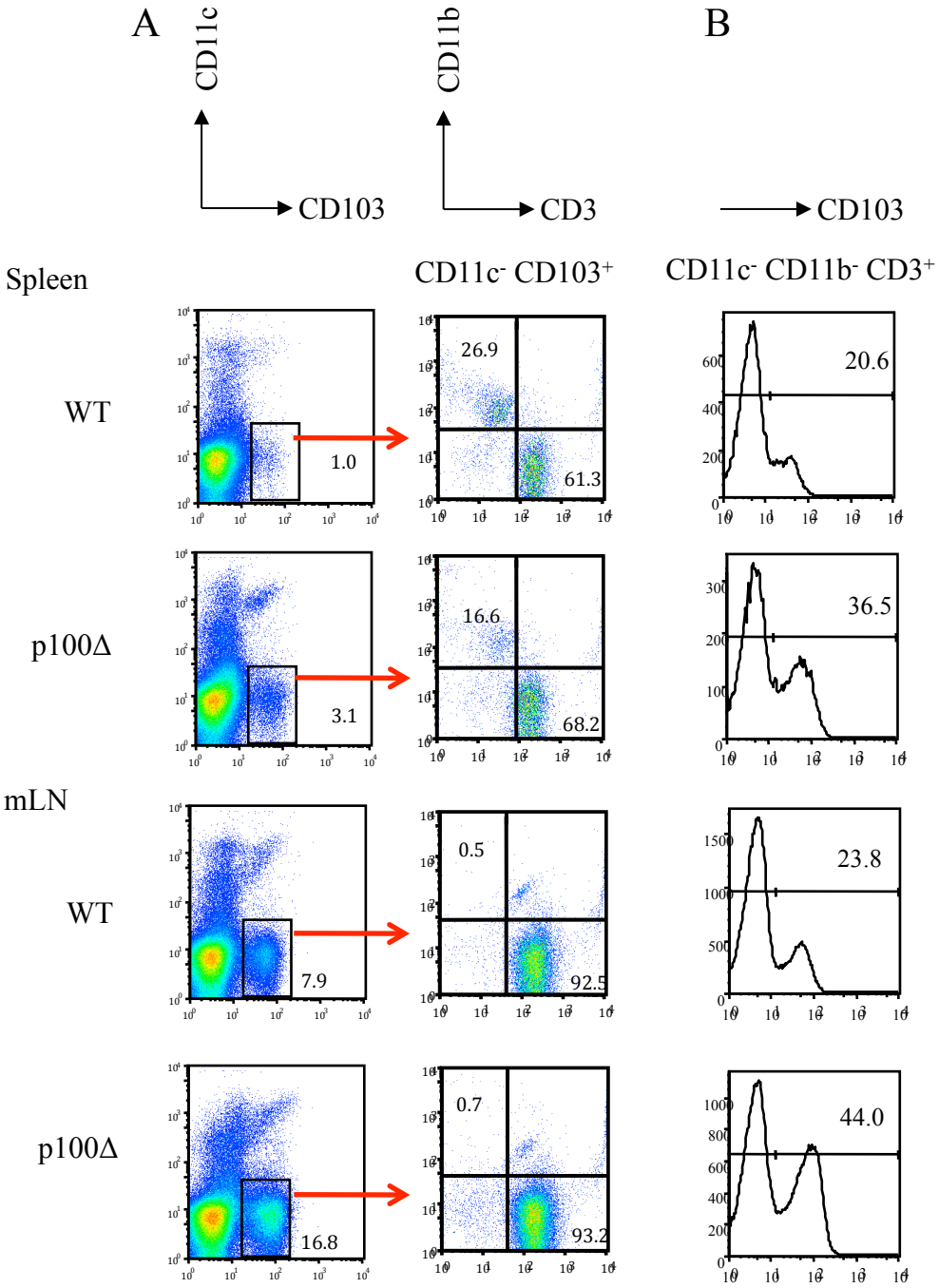
A
CD11c
CD103
CD11b
CD3
B
CD103
Spleen
CD11c- CD103+
CD11c- CD11b- CD3+
WT
1.0
26.9
61.3
20.6
p100Δ
3.1
16.6
68.2
36.5
mLN
WT
7.9
0.5
92.5
23.8
p100Δ
16.8
0.7
93.2
44.0

Figure 4.6

C

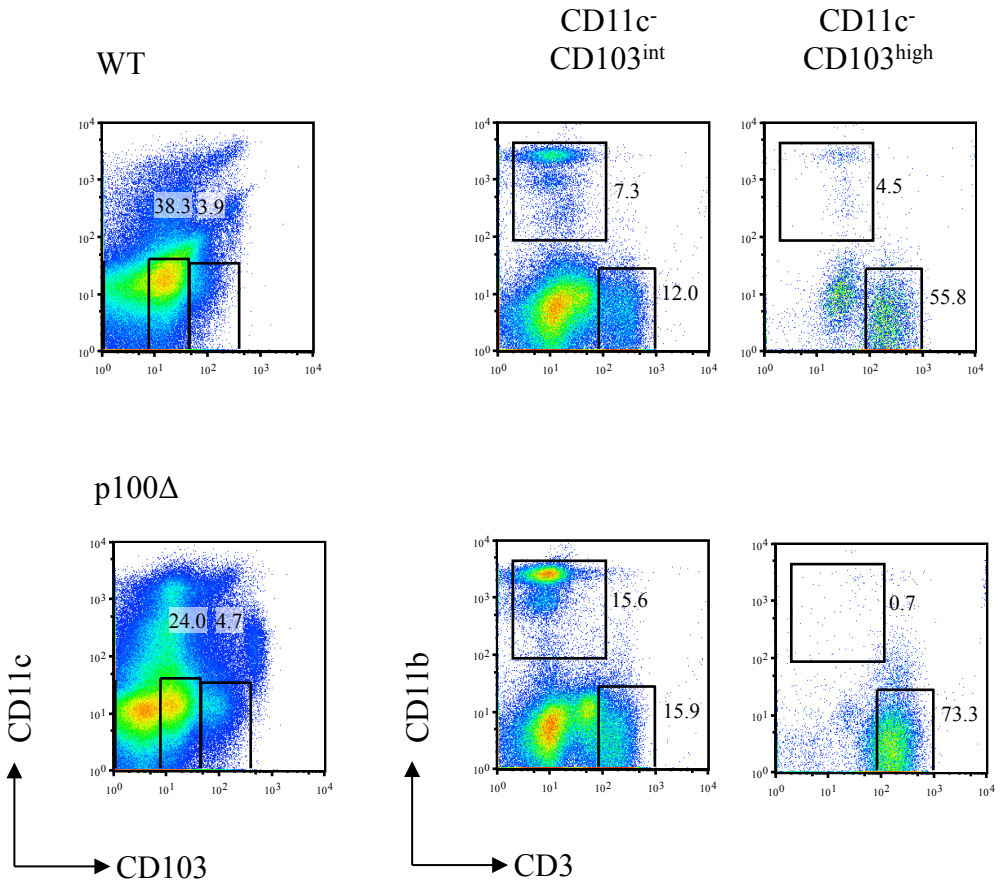

D CD11c- CD11b- CD3+

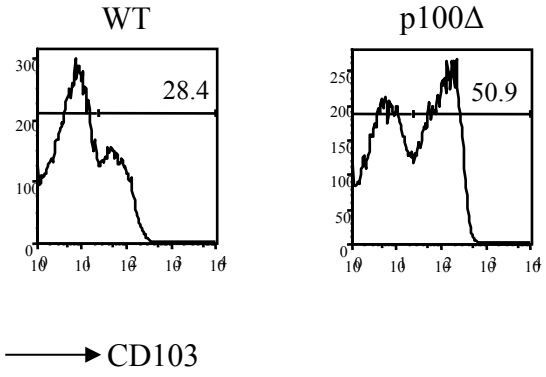

Figure 4.6

Figure 4.7 Serum levels of monocyte and macrophage chemokines

*Blood serum collected from WT and p100Δ mice. Graph shows serum levels of MCP-1, MCP-3 and MCP-5 (monocyte chemotactic protein), IL-10 and MIP-1γ (macrophage inflammatory protein) (WT n=4, p100Δ n=2). Results from one experiment. Mean values are shown, bars represent standard deviation. Students T-test, *p≤0.05, **p≤0.01, ns=not significant.*

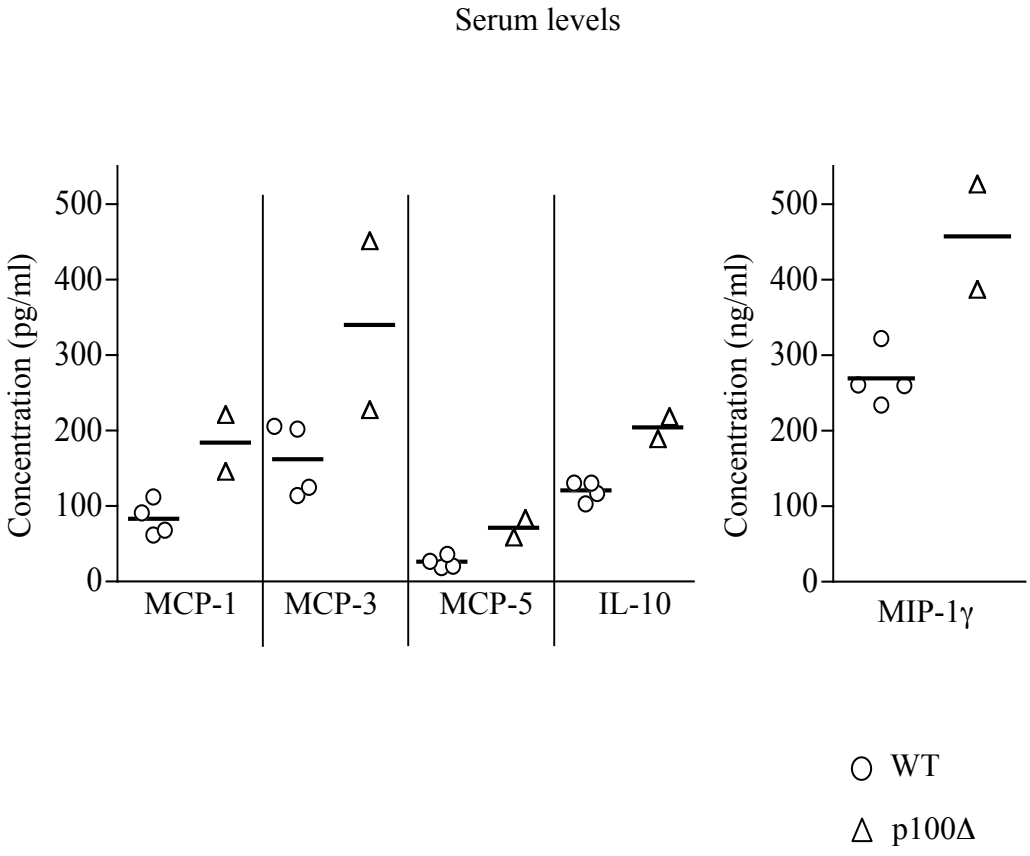
Serum levels
Concentration (pg/ml)
500
400
300
200
100
0
MCP-1
MCP-3
MCP-5
IL-10
Concentration (ng/ml)
500
400
300
200
100
0
MIP-1γ
WT
p100Δ

Figure 4.7

4.3. Discussion

Two distinct populations of splenic DCs that have been well characterised in the spleen: $CD11c^{high}CD8\alpha^{-}CD11b^{+}$ and $CD11c^{high}CD8\alpha^{+}CD11b^{-}$ DCs (Leenen et al., 1998; Shortman and Liu, 2002), and the proportion of both of these DC subsets was increased in the spleen and colon of p100Δ mice (Figure 4.1). Within the mLN, the expression of CD103 on gut-derived $CD11c^{high}$ cells identifies DCs capable of migrating from the intestine to the mLN (Annacker et al., 2005; Schulz et al., 2009), and this population of DCs was increased in the colon of p100Δ mice (Figure 3.3). Intraepithelial and LP-T lymphocytes also express CD103 (Lehmann et al., 2002; Uss et al., 2006; Agace et al., 2000; Annunziato et al., 2006) and in the colon of p100Δ mice an increase in expression of CD103 was observed on $CD3^{+}$ T cells, as well as on $CD3^{+}$ T cells from the spleen and mLN (Figure 3.6). In addition to the identification of these DC subsets, the activation status of each was analysed and revealed increased CD86 expression by all the aforementioned DC subsets in the mLN of p100Δ mice and by $CD11c^{high}CD11b^{+}$ DCs from the spleen (Figure 4.4). Finally, blood serum levels of chemoattractant proteins, MCP-1, MCP-5 and MIP-1γ, in addition to the regulatory cytokine, IL-10, were elevated in p100Δ mice (Figure 4.7).

The subdivision of cDCs based on CD8α/CD11b expression denotes two distinct populations within the spleen. Within the $CD11c^{high}$ cDC population, both these subsets are increased in proportion in the spleen and colon of p100Δ mice (Figure 4.2), with no preferential increase in either class. If both sets are functioning normally, it is unlikely that any alteration in the cytokine milieu has occurred, although it is not known if the populations of $CD8\alpha^{+}CD11b^{-}$ and $CD8\alpha^{-}CD11b^{+}$ DCs in the colon posses the same functional characteristics as the respective populations in

the spleen. Although functional studies have not been performed, the maturation phenotype has been assessed by expression of CD86. In this regard, both $CD11b^-$ and $CD11b^+$ cDCs from the mLN of p100Δ mice demonstrated an increased activation status (Figure 4.4). This data suggests that an immune response is occurring in this tissue and as the mLN is the draining LN of the gut this implies that stimulation of DCs has occurred at this location, with subsequent migration to the draining LN. Conversely, it is the $CD11b^+$ DC population, not the $CD11b^-$ population, in the spleen of p100Δ mice where an increased maturation status can be seen (Figure 4.4), implying that the phenotype in this tissue may be skewed towards a pro-inflammatory environment. Providing further complication to the situation, the proportion of $CD11b^-$ and $CD11b^+$ cDCs was increased in the colon of p100Δ mice to a similar extent (Figure 4.2), but no alteration in activation status was observed (Figure 4.4). To fully understand the contribution of these DC subtypes to the p100Δ phenotype, expansion of activation markers investigated, such as CD80 and MHCII, as well as functional DC analysis is critical.

LTβR is involved in the homeostasis of $CD11c^{high}CD11b^+CD8\alpha^-$ DCs, but not $CD11c^{high}CD11b^-CD8\alpha^+$ DCs (Kabashima et al., 2005; Geissmann et al., 2010), therefore constitutive activation of signalling downstream of LTβR could account for the increase in $CD11c^{high}CD11b^+CD8\alpha^-$ cDCs, but not for $CD11c^{high}CD11b^-CD8\alpha^+$ DCs. This indicates that in this situation alternative processes may be giving rise to the increase in $CD11c^{high}CD11b^-CD8\alpha^+$ DCs.

Similar to $CD11b^+CD8\alpha^-$ and $CD11b^-CD8\alpha^+$ cDCs, the subpopulations of $CD103^-$ and $CD103^+$ intestinal cDCs present with differing functions, with $CD103^-$ cDCs driving a pro-inflammatory response and $CD103^+$ cDCs inducing a tolerogenic environment (Annacker et al., 2005; Jaensson et al., 2008; Schulz et al., 2009;

Coombes et al., 2007; Siddiqui and Powrie, 2008). The proportion of both $CD103^-$ and $CD103^+$ cDC populations were increased in the colon of p100Δ mice (Figure 3.3), suggesting that the balance between a tolerogenic and pro-inflammatory environment is not disturbed. Whereas, in the spleen of p100Δ mice, only the $CD11c^{high}CD103^+$ DCs population was increased in proportion (Figure 3.3). The majority of splenic $CD103^+$ cDCs do not express CD11b and therefore correlate with the $CD11b^-$ DC subset (Appendix Figure 2), data that is supported by Annacker *et al* (Annacker et al., 2005). Therefore, the $CD103^+$ and $CD11b^-$ splenic DC populations presented in this chapter should not be regarded as distinct populations. The activation status of $CD103^-$ and $CD103^+$ cDCs was increased only in the mLN of p100Δ mice and both populations demonstrate similar relative increases in CD86 expression (Figure 4.4). Therefore no individual population was preferentially affected by constitutive activation of p100. As with the $CD8\alpha^+CD11b^-$ and $CD8\alpha^-CD11b^+$ DC subsets, functional analysis would need to be performed to determine whether this is altered.

In compliance with the observed increases in cDC and $CD11c^-CD11b^+$ cell populations in the tissues of p100Δ mice, increased blood serum levels of chemoattractant proteins for monocytes, macrophages and DCs were detected (Figure 4.7). Despite the fact that these analyses need to be repeated, this suggests a possible explanation for the augmented mobilisation of these cell types. It is important to note that the serum levels of these chemoattractant proteins may not reflect the levels present within specific tissues. In addition, increased serum IL-10 levels were observed (Figure 4.7) and may be associated with expansion of the ~~macrophages~~ $CD11c^-CD1b^+$ cell population in the colon of p100Δ mice, even though this expansion is not statistically significant (Figure 4.1). The population of $CD11c^-CD11b^+$ cell could include granulocytes and macrophages. Recent work investigating colonic

lamina propria macrophages demonstrates that they exhibit an anti-inflammatory M2-like phenotype, expressing increased IL-10 and MCP-1 compared with splenic macrophages (Takada et al., 2010). Indeed, serum levels of not only IL-10 but also MCP-1 are increased in p100Δ mice (Figure 3.7). In contrast, splenic macrophages present with a pro-inflammatory M-1 phenotype, producing more TNFα than lamina propria counterparts (Takada et al., 2010). The population of splenic ~~macrophages~~ $CD11c^{-}CD1b^{+}$ cells in p100Δ mice is significantly increased (Figure 4.1), and if this population consisted of predominately splenic macrophages capable of producing TNFα this may correlate with data published by Ishikawa *et al*, where they showed increased TNFα mRNA in the spleen of p100Δ mice (Ishikawa et al., 1997).

The majority of IELs are $CD8^{+}$, and approximately 90% express CD103, whilst greater than 50% of LP-lymphocytes are $CD4^{+}$ and only around 40-50% express CD103 (Agace et al., 2000). Analysis of $CD103^{+}$ non-DCs in this chapter revealed that in the spleen and mLN, of WT and p100Δ mice, the majority of $CD11c^{-}$ $CD103^{+}$ cells were $CD3^{+}$, whereas in the colon only around 40-50% were $CD3^{+}$, with a potential increase in the proportion of $CD11c^{-}CD103^{+}CD3^{+}$ cells in p100Δ mice (Figure 4.6). Importantly, in Chapter 3 the proportions of $CD4^{+}$ and $CD8^{+}$ T cells in the colon of WT and p100Δ mice showed an increase only in the $CD4^{+}$ T cell population in p100Δ mice, leaving the proportion of $CD8^{+}$ T cells unchanged (Figure 3.12). Together this data suggests that the increase in $CD103^{+}CD3^{+}$ T cells in the colon of p100Δ mice is likely to occur within the $CD4^{+}$ lamina propria T cell population as opposed to the $CD8^{+}$ IEL. Further flow cytometric analysis would confirm the phenotype of this colonic $CD103^{+}CD3^{+}$ T cell population and parallel immunofluorescence staining of colon sections would provide data on the *in situ* localisation.

5. Constitutive NF-κB2 Signalling in LTα-deficient Mice

5.1. Introduction

The importance of $LT\alpha_1\beta_2$/LTβR signalling in the development and organisation of the spleen has been well described. The chemokines responsible for localisation of B and T lymphocytes to their respective areas include CXCL13, responsible for B cell recruitment (Förster et al., 1999; Cyster et al., 1999) and produced by FDCs (Ansel et al., 2000) in the B cell follicles, and CCL19/21, responsible for T cell and DC localisation and produced by T zone stromal cells and DCs (Luther et al., 2000). In addition to expression of CCL19/21, stromal cells of the T zone also express the transmembrane mucin-type protein, Gp38/Podoplanin, expression of which is dependent on LTβR signalling (Ngo et al., 2001; Withers et al., 2007). *Cxcl13* and *Ccl19/21* are target genes of the alternative NF-κB pathway (Bonizzi et al., 2004)·(Dejardin et al., 2002) and without signalling via this pathway efficient organisation of B and T cell areas in the spleen cannot be achieved (Franzoso et al., 1998; Caamaño et al., 1998; Weih and Caamaño, 2003; Dejardin et al., 2002; Kaisho et al., 2001a; Karrer et al., 2000; Miyawaki et al., 1994; Koike et al., 1996).

Lt$\alpha^{-/-}$ mice present with a disorganised splenic architecture, with absence of B/T cell segregation, failure of B cell follicle formation and a lack of expression of chemokines associated with migration of B and T cells to their correct locations (Alexopoulou et al., 1998; De Togni et al., 1994; Matsumoto et al., 1996; Kuprash et al., 2002; Koni et al., 1997; Ngo et al., 1999). Moreover, mice deficient in alternative NF-κB signalling, such as *Relb*$^{-/-}$ or *aly/aly* mice, B/T segregation in the spleen is ablated as a result of reduced or absent CXCL13 and CCL19/21 expression (Weih et

al., 2001; Fagarasan et al., 2000). Corroborating this, constitutive activation of the alternative pathway, as in the p100Δ mouse model, results in increased expression of CXCL13 and CCL21, and no defects in splenic B/T segregation (Guo et al., 2007).

We hypothesised that introduction of constitutive activation of the alternative NF-κB pathway into an LTα-deficient environment, with subsequent recovery of chemokine expression, could rescue the disorganised splenic phenotype observed in *Lt*$\alpha^{-/-}$ mice.

5.2. Results

5.2.1. Similar body weight for p100Δ and *p100ΔLtα*$^{-/-}$ mice

The body weight of p100Δ and *p100ΔLtα*$^{-/-}$ mice at approximately three weeks of age does not differ (p=0.471) and the body weight of *Ltα*$^{-/-}$ mice at the same age is slightly increased compared with WT mice (Figure 5.1. A, p=0.013).

Ligation of LTβR activates both the classical and alternative NF-κB pathways. The major ligand of LTβR is $LT\alpha_1\beta_2$, with LIGHT being the minor ligand. In the *p100ΔLtα*$^{-/-}$ mouse model, signalling via the alternative pathway is constitutively active, but membrane bound $LT\alpha_1\beta_2$ ligation of LTβR does not occur and therefore only minimal classical pathway activation is assumed to take place. The absence of LTα ligation of LTβR does not rescue the reduced body weight observed in p100Δ mice, indicating that this phenotype is controlled mainly through the alternative NF-κB pathway.

5.2.2. Rescue of splenic B and T cell segregation in *Ltα*$^{-/-}$ mice with constitutive activation of NF-κB2 p100

The effect of introducing constitutive activation of the alternative NF-κB pathway into *Ltα*$^{-/-}$ mouse background was investigated by the generation of *p100ΔLtα*$^{-/-}$ mice. Cryostat sections of the spleens from these mice were stained and analysed by confocal microscopy.

Analysis of spleen sections from WT, p100Δ, *Ltα*$^{-/-}$ and *p100ΔLtα*$^{-/-}$ mice demonstrated normal B and T cell organisation in WT and p100Δ mice, but a lack of

B/T cell segregation in the white pulp of *Lt*$\alpha^{-/-}$ mice. In the spleen of *p100ΔLt*$\alpha^{-/-}$ mice the segregation of B and T cells was clearly restored in 100% of mice analysed (Figure 5.1. B).

In order to enumerate the extent of B/T cell segregation in the spleen, the T-zone in the confocal images was highlighted for further analysis. Initially, the measurement of T-zone size (μm^2) was recorded. There was no difference in T-zone size between WT and p100Δ mice (p=0.229), a significant decrease in size was observed between WT and *Lt*$\alpha^{-/-}$ mice (p=0.004) (Figure 5.1. C). Considering that the T-zone in *Lt*$\alpha^{-/-}$ mice constitutes the entire white pulp, it can be said that a reduction in total white pulp area was observed in *Lt*$\alpha^{-/-}$ mice. No significant difference in T-zone size was seen between WT and *p100ΔLt*$\alpha^{-/-}$ mice (Figure 5.1. C, p=0.060).

Following assessment of T-zone size, the segregation of B and T cells was ascertained. This was evaluated by calculating the mean number of $B220^+$ pixels within the T cell area, with $B220^+$ pixels corresponding to the presence of B cells. The higher the value, the more B cells present and thus correlating to reduced segregation of B and T cells. p100Δ mice exhibited a similar number of $B220^+$ pixels in the T-zone as WT mice (p=0.629), demonstrating normal B/T cell segregation (Figure 5.1. C). *Lt*$\alpha^{-/-}$ mice had significantly more $B220^+$ pixels in the T-zone when compared with WT mice (Figure 5.1. C, p=0.021), indicating a reduction in B/T cell segregation, this is supported by the confocal images of spleen sections (Figure 5.1. B). Analysis of *p100ΔLt*$\alpha^{-/-}$ mice showed a significant reduction in $B220^+$ pixels in the T-zone compared with WT mice (p=0.007) and compared with *Lt*$\alpha^{-/-}$ mice (p=0.004), indicating a more organised splenic organisation with respect to B and T cell areas (Figure 5.1. C).

In summary, p100Δ mice demonstrated normal demarcation of B and T cell areas in the spleen, whereas *Ltα*$^{-/-}$ mice showed no segregation of these two areas. Importantly, the introduction of constitutively active NF-κB2 p100 into *Ltα*$^{-/-}$ mice, as *p100ΔLtα*$^{-/-}$ mice, appears to rescue the formation of proper of B- and T- cell areas within the spleen.

5.2.3. Expression of T-zone chemokines in *Ltα*$^{-/-}$ and *p100ΔLtα*$^{-/-}$ spleen

The expression of chemokines by specialised splenic stromal cells is necessary for recruitment of B and T lymphocytes to their specific areas. Stromal cells in the T zone express Gp38/Podoplanin and CCL21 (Ngo et al., 2001; Withers et al., 2007), and *Ccl21* is a target gene for the alternative NF-κB pathway (Bonizzi et al., 2004), (Dejardin et al., 2002). To further dissect the differences in splenic microarchitecture and organisation, chemokine expression was assessed by confocal microscopy.

Identification of T-zone stroma was achieved by staining for Gp38/Podoplanin and CCL21. Gp38/Podoplanin staining was observed in 100% of WT and p100Δ mice, but not in *Ltα*$^{-/-}$ mice, as expected (Figure 5.2 A and B, first colomn). Importantly, Gp38/Podoplanin staining was detectable in *p100ΔLtα*$^{-/-}$ mice, indicating recovery of expression of this glycoprotein by T-zone specific stromal cells (Figure 5.2. B first column). CCL21 staining was observed in 100% of WT and p100Δ mice, but absent from *Ltα*$^{-/-}$ mice (Figure 5.2. A and B, second column). Interestingly, CCL21 expression was recovered in some, but not all, *p100ΔLtα*$^{-/-}$ mice: 60% of mice demonstrated positive CCL21 staining (Figure 5.2. A).

Splenic mRNA levels of *Ccl21* were relatively similar in WT and p100Δ mice, reduced in *Ltα*$^{-/-}$ mice and restored in *p100ΔLtα*$^{-/-}$ mice. Surprisingly, the relative mRNA levels of *Ccl19* in the spleen of p100Δ mice was elevated compared with WT, contrary to that published by Guo, *et al*, where they showed a reduction in *Ccl19* mRNA in the spleen (Guo et al., 2007). Levels in *Ltα*$^{-/-}$ mice were reduced compared with WT, and *p100ΔLtα*$^{-/-}$ mice demonstrated slightly elevated levels with respect to WT mice (Figure 5.3).

5.2.4. Development of B cell follicles in *Ltα*$^{-/-}$ and *p100ΔLtα*$^{-/-}$ spleen

The development of B cell follicles is dependent on LT, TNF and the expression of the chemokine CXCL13, which is produced by FDCs. In mice lacking TNF or LTα, few FDCs are found in the spleen and subsequently CXCL13 expression is severely reduced (Ngo et al., 1999) and in mice lacking CXCL13, FDCs and B cell follicles fail to develop (Ansel et al., 2000). Figure 5.2, shows CXCL13 expression (green, third column) and presence of FDCM1^{+} FDCs (green, fourth column) in WT and p100Δ mice. *Ltα*$^{-/-}$ and *p100ΔLtα*$^{-/-}$ mice lack both these markers (Figure 5.2. B). Splenic mRNA levels of *Cxcl13* were elevated in p100Δ mice compared with WT mice and as expected levels were reduced in *Ltα*$^{-/-}$ mice. The level in the spleen of *p100ΔLtα*$^{-/-}$ mice was similar to that observed in *Ltα*$^{-/-}$ mice (Figure 5.3). Surprisingly, there was one *p100ΔLtα*$^{-/-}$ mouse in which B cell follicle formation was restored, as was the expression of CXCL13 (Figure 5.4. C).

Constitutive signalling through the alternative NF-κB pathway in *Ltα*$^{-/-}$ mice results in the rescue of B/T cell segregation in the spleen, but does not restore the formation of B cell follicles, except in one *p100ΔLtα*$^{-/-}$ mouse.

Figure 5.1 Rescue of splenic B and T cell segregation in $Lt\alpha^{-/-}$ mice with constitutive activation of NF-κB2 p100

A *Body weights of WT, p100Δ, $Lt\alpha^{-/-}$ and p100Δ$Lt\alpha^{-/-}$ mice at approximately 3 weeks of age. Black line represents median.*

B *Cryostat sections of spleen from WT, p100Δ, $Lt\alpha^{-/-}$ and p100Δ$Lt\alpha^{-/-}$ mice were stained with fluorescently labelled antibodies to B220 (blue) and CD4 (red) to visualise the T cell zone and B cell follicles using confocal microscopy. Representative images are shown. The T cell zone of the white pulp was extracted and the area measured using LSM image software. At least six T cell areas per animal, for three individual animals were quantified.*

C *Using LSM image software the mean number of $B220^{+}$ pixels present in the T cell area was counted. Black line represents mean. Statistical analysis: Student's T-test.*

*$p<0.05$, **$p<0.01$, ***$p<0.001$.*

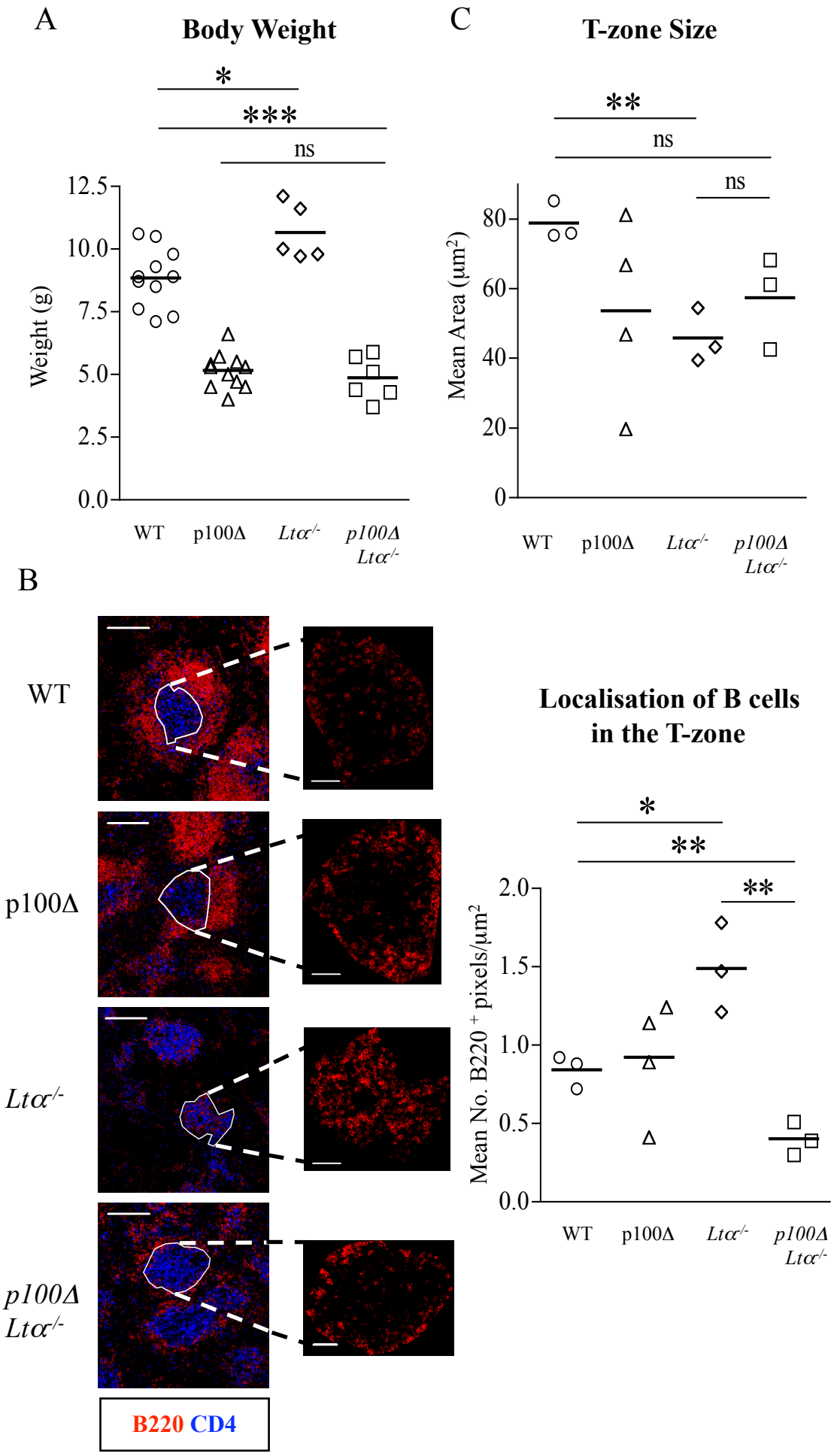
A
Body Weight
*
***
ns
Weight (g)
12.5
10.0
7.5
5.0
2.5
0.0
WT
p100Δ
Ltα-/-
p100Δ Ltα-/-
C
T-zone Size
**
ns
ns
Mean Area (µm2)
80
60
40
20
0
WT
p100Δ
Ltα-/-
p100Δ Ltα-/-
B
WT
p100Δ
Ltα-/-
p100Δ Ltα-/-
B220 CD4
Localisation of B cells in the T-zone
*
**
**
Mean No. B220+ pixels/µm2
2.0
1.5
1.0
0.5
0.0
WT
p100Δ
Ltα-/-
p100Δ Ltα-/-

Figure 5.1

Figure 5.2 Rescue of CCL21 and Gp38/Podoplanin expression in *p100ΔLtα*$^{-/-}$ mice

A *Overview of immunofluorescence analysis of p100ΔLtα*$^{-/-}$ *spleen. At least four individual animals per genotype were assessed. Consecutive cryostat sections of spleen were stained with fluorescent antibodies to CCL21 (T-zone chemokine), FDCM1 (marker for follicular DCs), Gp38 (stromal marker expressed by T zone stromal cells) (all green), B220 (red) and CD4 (blue)* (***B***)*, CXCL13 (B cell area chemokine) and CD169 (marker for marginal* metallophilic *macrophages) (both green), B220 (red) and CD4 (blue) (****C****).*

For x10 magnification scale bar denotes 200μm.
For x40 magnification scale bar denotes 50μm.

A

Marker	WT	p100Δ	*Ltα*$^{-/-}$	*p100Δ Ltα*$^{-/-}$
CCL21	4/4	4/4	0/4	3/5
FDCM1	4/4	4/4	0/4	1/3
Gp38	4/4	4/4	0/4	5/5
CXCL13	4/4	4/4	0/4	1/5
CD169	4/4	4/4	0/4	1/5
B cell follicles	4/4	4/4	0/4	1/5
B/T seg	4/4	4/4	0/4	5/5

B

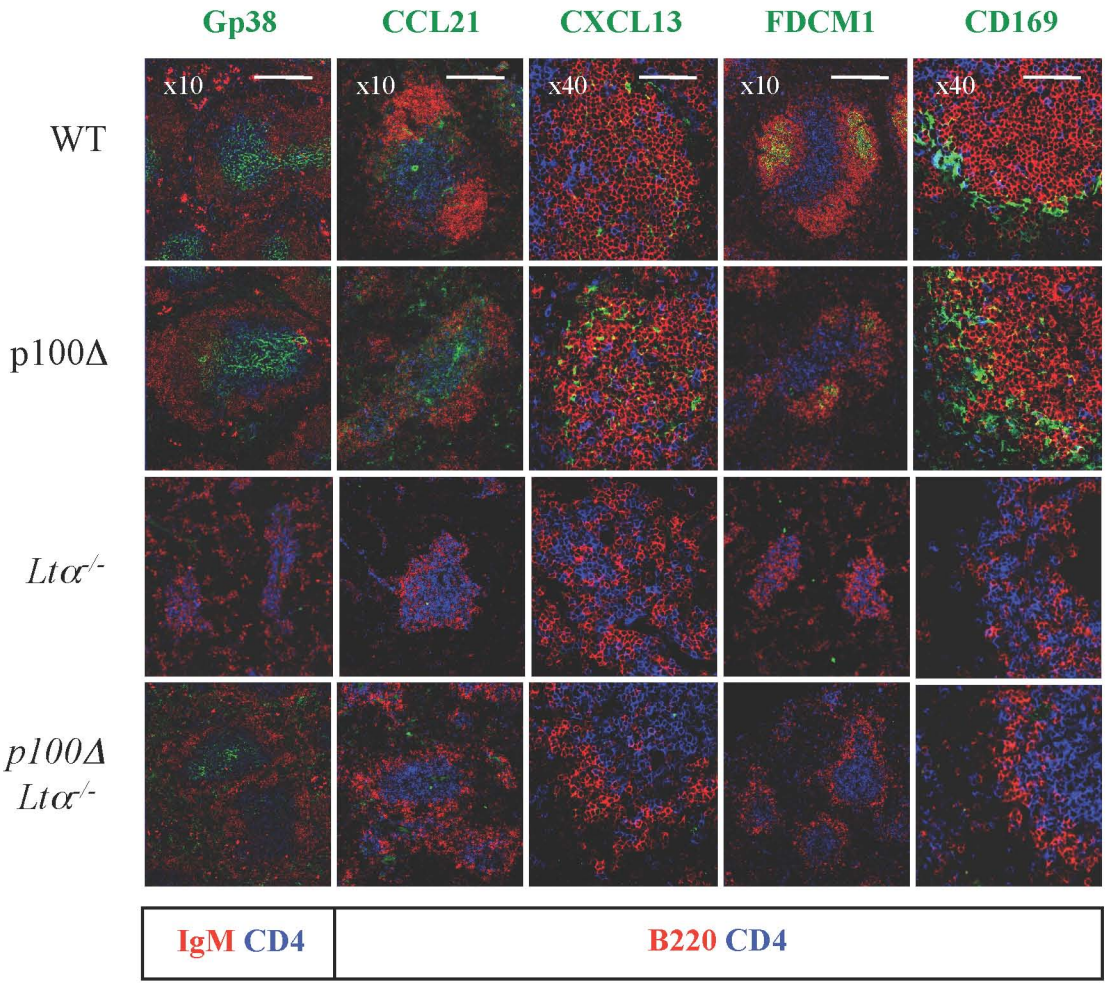

Figure 5.2

Figure 5.3 Splenic mRNA levels of *Cxcl13*, *Madcam-1*, *Ccl21* and *Ccl19*

Real-time RT-PCR analysis of Cxcl13, Madcam-1, Ccl21 and Ccl19 genes. Ratio of genes of interest to β-actin is shown. Error bars indicate SD from two independent samples.

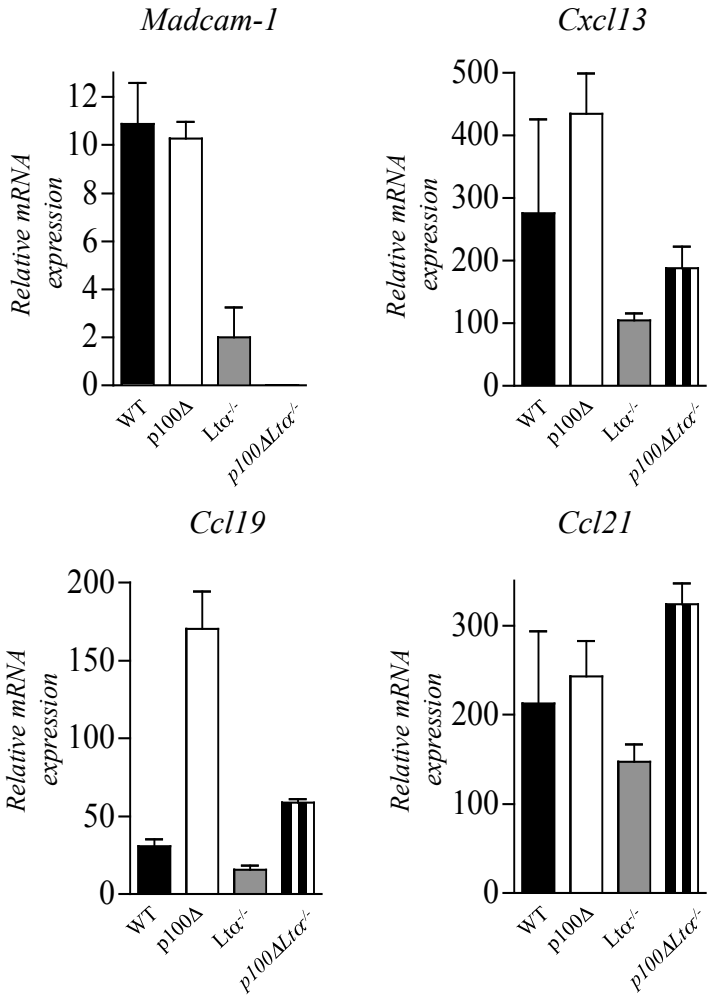
Madcam-1
Relative mRNA expression
12
10
8
6
4
2
0
WT
p100Δ
Ltα-/-
p100ΔLtα-/-
Cxcl13
Relative mRNA expression
500
400
300
200
100
0
WT
p100Δ
Ltα-/-
p100ΔLtα-/-
Ccl19
Relative mRNA expression
200
150
100
50
0
WT
p100Δ
Ltα-/-
p100ΔLtα-/-
Ccl21
Relative mRNA expression
300
200
100
0
WT
p100Δ
Ltα-/-
p100ΔLtα-/-

Figure 5.3

Figure 5.4 Effect of constitutive activation of NF-κB2 p100 on LN development in *Lt*$\alpha^{-/-}$ mice

A *Photograph showing presence of inguinal LNs (iLNs) in one p100ΔLt*$\alpha^{-/-}$ *mouse.*

B *Cryostat sections of iLNs from WT, p100Δ and one p100ΔLt*$\alpha^{-/-}$ *mouse found to have developed LNs, were immunofluorescently stained for follicular DCs (FDCM1, green), B cells (B220, red) and T cells (CD4, blue).*

C *Cryostat sections of spleen from the p100ΔLt*$\alpha^{-/-}$ *mouse that developed LNs, immunofluorescently stained for Gp38 (green), CD169 (green), CXCL13 (green), B220 (red) and CD4 (blue).*

Representative images are shown.
For x10 magnification scale bar denotes 200μm.
For x40 magnification scale bar denotes 50μm.

A *p100ΔLtα*$^{-/-}$

B iLN

C Spleen

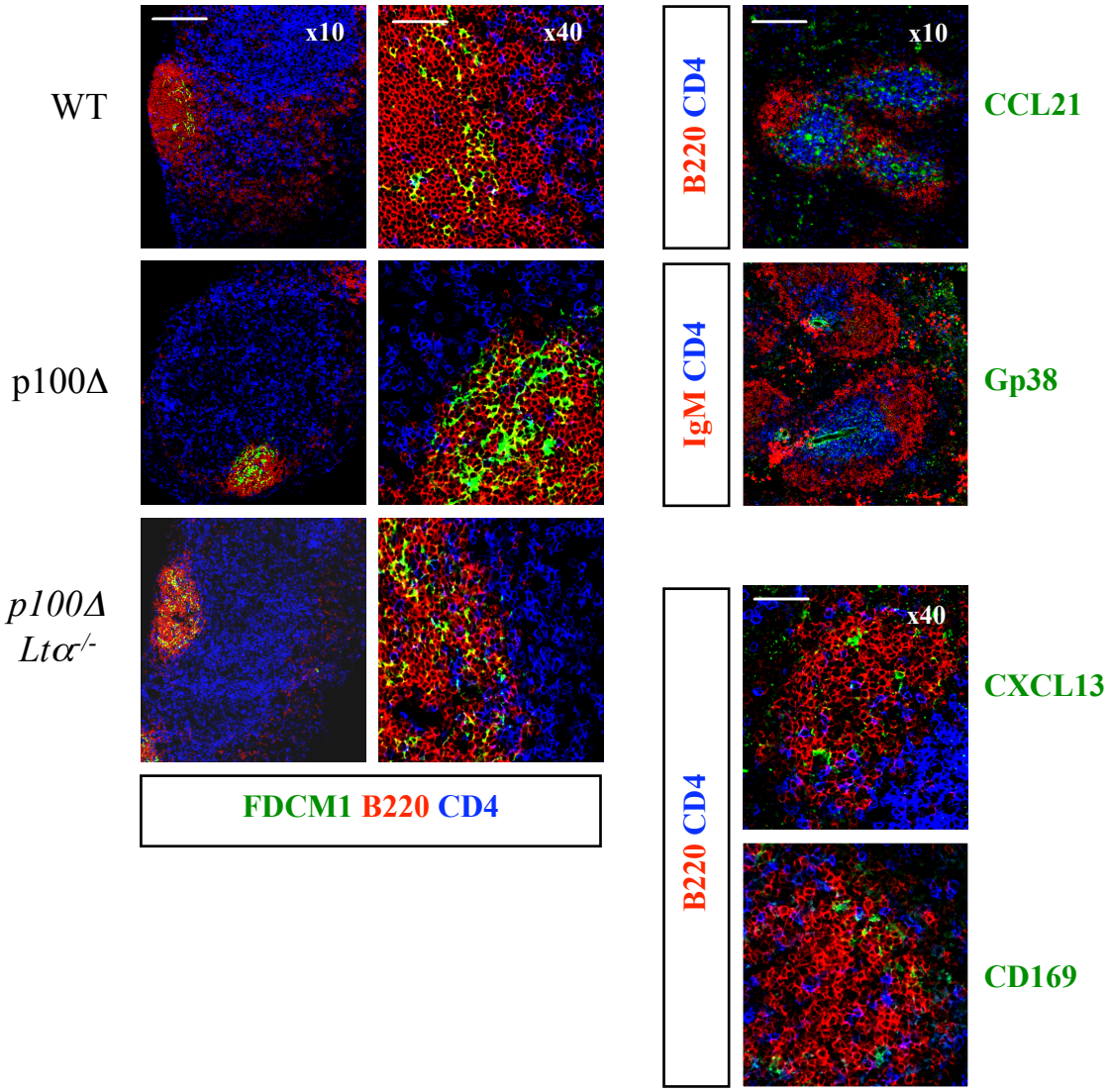

Figure 5.4

5.2.5. Marginal zone development in *Ltα*$^{-/-}$ and *p100ΔLTα*$^{-/-}$ spleen

Within the marginal sinus of the spleen reside two subpopulations of macrophages: marginal zone macrophages (MZMs) and marginal metallophilic macrophages (MMMs) (Figure 1.2. B). MMMs are located at the inner surface of the marginal sinus and express the marker CD169 (Oetke et al., 2006).

In Figure 5.2 B, (final column) positive CD169 staining can be seen in WT and p100Δ mice, showing the presence of MMMs. However, in p100Δ mice the staining appears more diffuse, with the emergence of B220^{+} B cells throughout and outside the MMM ring. In the spleens of both *Ltα*$^{-/-}$ and *p100ΔLtα*$^{-/-}$ mice, CD169^{+} MMMs were not found (Figure 5.2. B, final column). Interestingly, in the *p100ΔLTα*$^{-/-}$ mouse that did develop B cell follicles, faint but positive CD169 staining could be seen in the marginal sinus of the spleen (Figure 5.4. C). Cells lining the marginal sinus express MAdCAM-1, and WT and p100Δ mice presented with similar levels of splenic *Madcam-1* mRNA, while *Ltα*$^{-/-}$ and *p100ΔLtα*$^{-/-}$ mice present with minimal *Madcam-1* expression (Figure 5.3).

The splenic marginal zone does not develop in *Ltα*$^{-/-}$, and after introduction of constitutive activation of NF-κB2 p100, as in *p100ΔLtα*$^{-/-}$ mice, MZ development was not recovered in 80% of mice.

5.2.6. LN development in *Ltα*$^{-/-}$ mice with constitutive activation of NF-κB2 p100

LN development is dependent on LT, and mice lacking LTα or LTβR, LNs fail to develop (De Togni et al., 1994; Banks et al., 1995; Fütterer et al., 1998). Signalling downstream of LTβR occurs via the classical and alternative NF-κB

activation pathways (Dejardin et al., 2002). Strikingly, one of the five *p100ΔLtα*$^{-/-}$ mice analysed demonstrated recovery of inguinal and mesenteric LN development (Figure 5.4. A). This was the same animal in which B cell follicle, CXCL13 expression and CD169 expression in the marginal sinus was recovered (Figure 5.4. C).

Figure 5.4 A, shows the presence of inguinal LNs in one *p100ΔLtα*$^{-/-}$ mouse. Cryostat sections of inguinal and mesenteric LNs from WT, p100Δ and *p100ΔLtα*$^{-/-}$ mice were stained with fluorescently labelled anti-B220 (red), for B cells, anti-CD4 (blue), for CD4^{+} T cells and anti-FDCM-1 (green), for FDCs, or anti-CD3 (green) for T cells (Figure 5.4. B. inguinal LN only). The structure of the inguinal LN from the *p100ΔLtα*$^{-/-}$ mouse, showed normal architecture, with defined segregation of B and T cell areas, development of B cell follicles and presence of FDCs.

5.3. Discussion

The organisation of the white pulp of the spleen into distinct B and T cell areas depends on the expression of specific chemokines, an LTβR-dependent process (Mebius and Kraal, 2005). This chapter presents the dramatic rescue of B and T cell segregation in the spleen of *Lt*$\alpha^{-/-}$ mice with constitutive activation of the alternative NF-κB pathway (*p100ΔLt*$\alpha^{-/-}$ mice) (Figure 5.1), with the recovery of Gp38/Podoplanin expression in the T zone in all *p100ΔLt*$\alpha^{-/-}$ mice and recovery of T-zone associated CCL21 expression in 60% of animals (Figure 5.2). The rescue of B/T demarcation in these mice was not accompanied by development of B cell follicles, except in one instance (Figure 5.2 A, and Figure 5.4 C). In addition, four of the five *p100ΔLt*$\alpha^{-/-}$ mice examined did not recover development of peripheral LNs (Figure 5.1. A). Interestingly, the remaining *p100ΔLt*$\alpha^{-/-}$ mouse did develop iLNs and mLN, along with identification of B cell follicles in the spleen (Figure 5.4).

Specialised stromal cells and FDCs in the B cell area express CXCL13 (Ansel et al., 2000), and stromal cells of the T cell area express CCL21 (Luther et al., 2000) and Gp38/Podoplanin (Ngo et al., 2001), staining of these markers can be seen in the appropriate areas in WT and p100Δ mice, corresponding with normal demarcation of B and T cell areas. In *Lt*$\alpha^{-/-}$ mice, no expression of CXCL13, CCL21 or Gp38/Podoplanin is observed and the white pulp showed no organisation, with intermingling of B and T cells. Strikingly, the introduction of constitutive activation of NF-κB2 p100 into an LTα deficient environment, rescues the disorganisation in the spleen of *Lt*$\alpha^{-/-}$ mice, and this organisation correlates with recovery of expression of Gp38/Podoplanin and a degree of recovery of CCL21 expression (Figure 5.2).

The recovery of CCL21 protein expression in *p100ΔLtα*$^{-/-}$ mice was only evident in 60% of mice examined, although CCL21 mRNA was detectable to similar levels in mice that expressed the protein and those that did not (Figure 5.3). This spectrum of CCL21 protein expression recovery could suggest a requirement of a threshold level of nuclear translocation of NF-κB heterodimers, such as p52/RelB, for transcription of the gene, a threshold that may not be met in each individual mouse. Interestingly, in *p100ΔLtα*$^{-/-}$ mice lacking detectable CCL21 protein in the T zone, demarcation of B and T cell areas was still rescued; this could be due to the fact that 100% of *p100ΔLtα*$^{-/-}$ mice recovered Gp38/Podoplanin expression within the T zone. This indicates that constitutive activation of NF-κB2 p100 in an LTα deficient environment is sufficient to induce Gp38/Podoplanin expression, without $LT\alpha_1\beta_2$-induced LTβR signalling, suggesting that activation of the classical NF-κB pathway downstream of the LTβR may play a negligible role in the expression of this glycoprotein.

The dramatic rescue of B and T zone organisation in *p100ΔLtα*$^{-/-}$ mice was not accompanied by recovery of B cell follicle formation or the development FDC networks, and, as a result, CXCL13 expression was not recovered. The lack of FDC and B cell follicle development in *Ltα*$^{-/-}$ mice is reflected in *aly/aly* mice, comprising a non-functional form of NIK, and mice lacking NF-κB2 also present with defects in B cell follicle formation (Miyawaki et al., 1994; Koike et al., 1996; Karrer et al., 2000; Franzoso et al., 1998; Caamaño et al., 1998). Together these studies demonstrate that LTβR signalling through the alternative NF-κB pathway is required for FDC development and B cell follicle formation. The recruitment of B cells to the follicle requires the expression of CXCL13 by stromal cells and FDCs. Intriguingly, a recent paper has described the requirement for classical and alternative NF-κB

pathway activation in expression of CXCL13 by an established LN stromal cell line (Suto et al., 2009). Considering that in *p100ΔLtα*$^{-/-}$ mice, LTα-induced LTβR signalling via the classical NF-κB pathway is ablated, but alternative signalling is constitutive, owing to the knock-in *p100Δ* gene, this provides a possible explanation for the lack of recovery of CXCL13 expression. However, LIGHT is an alternative ligand for LTβR (Mauri et al., 1998) that in this situation appears unable to compensate for the lack of membrane bound $LT\alpha_1\beta_2$ in *p100ΔLtα*$^{-/-}$ mice with regards to CXCL13 expression.

In addition to its role in splenic organisation, LTβR plays a critical and well described role in LN development, with *Ltα*$^{-/-}$ and *LtβR*$^{-/-}$ mice lacking all LNs (Fütterer et al., 1998; Banks et al., 1995; De Togni et al., 1994). We observed the same phenotype in *Ltα*$^{-/-}$ mice, but strikingly in one of the five *p100ΔLtα*$^{-/-}$ mice examined, development of mLN and iLNs was clearly recovered (Figure 5.4). Moreover, the iLNs and mLN presented with well organised B and T cell areas and distinct B cell follicles, with presence of FDCM1^{+} FDCs. This data demonstrates that approximately 20% of *p100ΔLtα*$^{-/-}$ mice develop mature, fully organised iLNs and mLNs, however, it does not rule out the possibility that in those mice that do not develop mature LNs that rudimentary structures developed earlier in life and failed to fully mature. It would be of interest to study *p100ΔLtα*$^{-/-}$ mice younger than three weeks old, and during embryonic development.

iLN development has been investigated in *Ltα*$^{-/-}$ and *LtβR*$^{-/-}$ embryos at E15 and shown to be comparable with that in WT embryos (White et al., 2007; Bénézech et al., 2010). By E16-17, further iLN development in both *Ltα*$^{-/-}$ and *LtβR*$^{-/-}$ embryos was halted and the structures were difficult to identify (White et al., 2007; Bénézech et al., 2010). The process of LN development depends on maturation of LTo cells, a

two-step process. The first step occurs independently of $LT\alpha_1\beta_2$-LTβR signalling, and can therefore be observed in E15 *Ltα*$^{-/-}$ and *LtβR*$^{-/-}$ embryos, whereas the second step depends on LTβR signalling and LNs fail to develop further without this signal (White et al., 2007; Bénézech et al., 2010). It could be envisaged that introducing constitutive activation of NF-κB2 p100 in *Ltα*$^{-/-}$ mice, thereby compensating for the lack of LTα-induced LTβR signalling, enables development of LNs to a later stage than that observed in *Ltα*$^{-/-}$ mice. Splenic mRNA levels of *Cxcl13* and *Madcam-1* were not recovered in *p100ΔLtα*$^{-/-}$ mice (the individual mouse that developed LNs was not analysed) (Figure 5.3). It is possible that the lack of MAdCAM-1 and CXCL13 recovery could indirectly block maturation of LN anlage through prevention of lymphocyte recruitment and localisation, respectively, explaining the lack of mature LNs in the majority of adult *p100ΔLtα*$^{-/-}$ mice. Following early embryonic development, in the majority of *p100ΔLtα*$^{-/-}$ mice, the constitutively active NF-κB2 p100 may not be able to compensate for the lack of LTα, resulting in atrophy of LN anlagen and their inability to develop into fully mature LNs.

6. General Discussion

6.1. The role of NF-κB2 in ILF development

The role of NF-κB2 in the development of secondary lymphoid tissues, such as LNs and PPs, has been well described. Mice lacking alternative pathway signalling, such as *aly/aly* (Shinkura et al., 1999; Miyawaki et al., 1994; Fagarasan et al., 2000; Karrer et al., 2000) and *Relb*$^{-/-}$ (Weih et al., 1995; Yilmaz et al., 2003; Weih and Caamaño, 2003) mice, fail to develop LNs and PPs, and the LNs and PPs that develop in *Nfkb2*$^{-/-}$ mice are reduced in size and disorganised in their microarchitecture (Carragher et al., 2004; Paxian et al., 2002). The alternative pathway signals downstream of LTβR (Dejardin et al., 2002; Müller and Siebenlist, 2003; Yilmaz et al., 2003) and mice deficient in LTβR or components of the membrane bound ligand, $LT\alpha_1\beta_2$, fail to develop LNs and PPs (Fütterer et al., 1998). Additionally, alternative pathway signalling occurs downstream of several other TNF Receptor family members, including RANK and there is a critical role for RANKL-RANK interaction in LN development; *Rankl*$^{-/-}$ and *Rank*$^{-/-}$ mice do not develop peripheral LNs, whilst PP development is unaffected (Kong et al., 1999; Kim et al., 2000; Dougall et al., 1999).

6.1.1.1. CP development

The role of NF-κB2 in the development of tertiary lymphoid tissue, such as CPs and ILFs, is less well understood. The development of CPs is considered to be genetically programmed (Bouskra et al., 2008; Eberl, 2007) and is dependent on the $LT\alpha_1\beta_2$-LTβR signalling axis as these structures are not present in the intestine of

Ltβ$R^{-/-}$, *Lt*$\alpha^{-/-}$ and *Ltβ*$^{-/-}$ mice (Ivanov et al., 2006; Taylor et al., 2004; Lorenz et al., 2003; Pabst et al., 2005; Hamada et al., 2002). However, it is unclear whether the alternative NF-κB pathway plays a crucial role in CP development. *Aly/aly* mice do exhibit CPs in the intestine (Ivanov et al., 2006; Hamada et al., 2002; Taylor et al., 2004), but the presence of CP development in *Relb*$^{-/-}$ and *Nfkb2*$^{-/-}$ mice has not yet been investigated. We did observe CP-like structures in the colon of *Relb*$^{-/-}$ mice (data not shown) and in this thesis we present a lack of ILF development in these mice. Conversely initial analysis of *Nfkb2*$^{-/-}$ mice revealed the presence of colonic ILFs and as ILF formation has not been observed without the development of CPs, it can be assumed that CP development in *Nfkb2*$^{-/-}$ mice does occur. Accurate analysis and quantification of CP development in *Relb*$^{-/-}$ mice, *Nfkb2*$^{-/-}$ and p100Δ mice is needed to fully understand the contribution of the alternative pathway to this process. A useful tool to address this question is the *RORγt*^{YFP} knock-in mouse, in this system the gene encoding enhanced yellow fluorescent protein (EYFP) was inserted in the first exon of the gene encoding RORγt (Eberl et al., 2004). Eberl *et al*, demonstrated that RORgt was expressed exclusively by LTi cells in the embryo. The generation of *p100ΔRORγt*^{YFP} and *Relb*$^{-/-}$*RORγt*^{YFP} mice would enable reliable and accurate assessment of CP formation in these mice as YFP^{+} clusters, lacking B lymphocytes, within the colon could be enumerated by fluorescence microscopy.

6.1.1.2. ILF Formation

CPs are proposed to be the precursor structures for ILFs (Pabst et al., 2005; Eberl, 2005; Eberl, 2007; Eberl and Sawa, 2010), defined by the recruitment of B lymphocytes to the structure (Hamada et al., 2002). The presence of CPs has been described in *aly/aly* mice (Ivanov et al., 2006; Hamada et al., 2002; Taylor et al.,

2004) thus suggesting that CP development may occur independently of alternative pathway activation. It would be beneficial to assess the development of CPs in *Relb*$^{-/-}$ mice to corroborate this theory. It is then conceivable that in the colon of p100Δ mice CP numbers are equivalent to WT mice. Therefore, the augmented ILF formation observed in p100Δ mice would likely be due to an increase in the proportion of CPs maturing into ILFs, rather than an increase in CP development.

Similar to CP development, the formation of ILFs is dependent on the LT$\alpha_1\beta_2$-LTβR signalling axis; *Ltβr*$^{-/-}$, *Ltα*$^{-/-}$ and *Ltβ*$^{-/-}$ mice do not develop ILFs (Ivanov et al., 2006; Taylor et al., 2004; Lorenz et al., 2003; Pabst et al., 2005; Hamada et al., 2002). In contrast to CP development, ILFs do not develop in *aly/aly* mice (Ivanov et al., 2006; Hamada et al., 2002; Taylor et al., 2004). Together these findings indicate that LTβR signalling via the alternative NF-κB pathway is involved in ILF formation. In support of this, we demonstrate that constitutive activation of this pathway results in augmented ILF formation and initial analysis of *Relb*$^{-/-}$ mice revealed no colonic ILF formation.

Independent of the function of NF-κB2 in CP development, the significant increase in colonic ILF formation in p100Δ mice may elude to a role for alternative pathway signalling in recruitment of B cells to the intestine. The recruitment of B lymphocytes to the intestine, facilitating ILF formation, is dependent on interactions between specific ligands and receptors, for example LT$\alpha_1\beta_2$-LTβR (Lorenz et al., 2003; Taylor et al., 2004), CCL20:CCR6(Lügering and Kucharzik, 2006; Williams, 2006) and Integrin $\alpha_4\beta_7$:MAdCAM-1 (Wang et al., 2008). B lymphocytes lacking LTα, CCR6 or β_7 are unable to migrate to the intestine and subsequently ILF formation is prevented (Lorenz et al., 2003; Taylor et al., 2004; Lügering and Kucharzik, 2006; Wang et al., 2008). CCL20 (Tanaka et al., 1999; McDonald et al.,

2007) and MAdCAM-1 (Ando et al., 2005; Wang et al., 2008) are expressed by intestinal epithelium and we showed MAdCAM-1 expression in the colon of p100Δ mice (Figure 3.6. B). The expression level of MAdCAM-1 in the colon of p100Δ mice needs to be assessed. If expression is increased, as it is in the spleen (Guo et al., 2007), this could provide an explanation for the enhanced recruitment of B cells to the intestine. Additionally, a recent study has postulated that CXCR5 is required for normal development of CPs and ILFs, together termed solitary intestinal lymphoid tissue (SILT), showing that *Cxcr5*$^{-/-}$ mice do not develop SILT by four weeks of age, whereas WT mice did (Velaga et al., 2009). CXCR5 and its ligand CXCL13, are involved in the positive feedback loop that occurs following LTi cell interaction with stromal cells and as such are indispensible for normal LN and PP development. *Cxcr5*$^{-/-}$ and *Cxcl13*$^{-/-}$ mice developed no or few PPs, and those that did form were not fully developed and development of LNs was severely, but not fully, impaired (Förster et al., 1996; Ansel et al., 2000). Expression of CXCL13 by a LN stromal cell line has been shown to require activation of both the classical and alternative NF-κB pathways (Suto et al., 2009). In p100Δ mice, the classical pathway is assumed to occur normally whereas the alternative pathway is constitutively active. We demonstrated CXCL13 expression within the colon of p100Δ (Figure 3.6. A), if this expression is elevated compared to WT mice, potentially due to the persistent activation of NF-κB2 p100, this could shift the balance of intestinal lymphoid tissue towards ILFs rather than CPs by the recruitment of B cells, potentially explaining the augmented ILF development.

6.1.1.3. Haematopoietic and stromal cells function during ILF formation

Dissection of the contribution of haematopoietic and stromal cells to the colonic phenotype observed in p100Δ mice was investigated through the generation of WT mice reconstituted with p100Δ-derived FLCs (Chapter 2.7). Irradiated WT host mice received p100Δ FLCs, providing the situation where radiation resistant WT stromal cells are able to interact with haematopoietic cells in which the alternative NF-κB pathway is constitutively active.

These reconstitution experiments demonstrated that constitutively active NF-κB2 p100 in haematopoietic cells was sufficient to drive augmented ILF formation. The caveat being that the host mice were harvested three months post transfer, and as p100Δ mice demonstrate a significant increase in ILFs by 2-3 weeks of age, the two situations are difficult to compare. Two alternative scenarios could be occurring. In the first instance, augmented ILF formation in the chimeric mice may take several months to develop, in which case haematopoietic cells with constitutively active NF-κB2 p100 may need to 'induce' intestinal stromal cells to increase chemokine expression thereby resulting in recruitment of lymphocytes and promotion of ILF formation, accounting for the discrepancy in measurable increased ILF formation. In the second instance, augmented ILF formation may be discernible at three weeks post-transfer, in which case the role of the stroma may be less prominent, with the phenotype driven predominately by the haematopoietic cells. However, the situation with ILF formation in p100Δ mice may well vary from either of these two scenarios; within p100Δ mice, the alternative pathway is constitutively active in both haematopoietic cells and stromal cells and there may be a synergistic effect occurring between the two.

Supplementing previously published studies, this thesis expands on current information relating to ILF formation by demonstrating that constitutive activation of the alternative NF-κB pathway results in a significant increase in colonic ILF formation and with the suggested future experiments, including assessment of CP development in p100Δ mice, the understanding of CP and ILF development would be further enhanced. It is important to understand whether or not the alternative NF-κB pathway plays a role in CP development because if it does not and is only involved in maturation of CPs to ILFs then inhibition of this pathway could be used as a therapeutic tool to limit ILF formation. The question then remains: what role do ILFs play in disease?

6.1.2. Consequences of alterations in ILF formation

Regardless of the mechanism for increased ILF development in p100Δ mice, the resulting phenotype carries different potential outcomes. The limitation with the p100Δ mouse model is that the animals die prematurely, by 3-4 weeks of age, due to a currently unknown cause; this limits investigation of the long-term affect of increased colonic ILF numbers. Interestingly, the WT mice reconstituted with p100Δ FLCs, do develop increased numbers of ILFs, but do not present with signs of disease at the time of sacrifice three months post-transfer. The development of CPs and ILFs in the intestinal tract occurs under steady state conditions and can also be induced during inflammatory responses. Many studies have reported that during colitis an increase in lymphoid aggregates in the intestine can be observed (Spahn et al., 2002; Leithäuser et al., 2001), but the reason for this increase has not been elucidated. Numerous animal models of colitis have been established where colitis is induced

either chemically (Wirtz et al., 2007), by transfer of T cell subsets to immunodeficient hosts (Ostanin et al., 2009) or by genetic manipulation. Of particular interest is the chemically induced dextran sodium sulphate (DSS) colitis model (Wirtz et al., 2007). In this model animals are treated with DSS in either an acute or chronic model of colitis and present with inflammation in the colon. Interestingly, the presence of B and T cells is not required for DSS-induced colitis, as *SCID* mice develop colitis following DSS treatment (Dieleman et al., 1994). However, in WT mice the generation of lymphoid aggregates in the colon can be observed following DSS treatment and it was suggested that these structures resembled ILFs (Spahn et al., 2002).

The alternative NF-κB pathway is activated downstream of LTβR and the DSS-colitis model has been used by several groups to assess the role of LTβR signalling in the development of colitis. Jungbeck *et al*, used this acute colitis model to investigate the affect of inhibiting LTβR signalling on disease progression in $Lt\beta R^{-/-}$ mice. It was demonstrated that treatment of $Lt\beta R^{-/-}$ mice with DSS resulted in increased severity of intestinal inflammation when compared with WT mice (Jungbeck et al., 2008). Additionally, it was shown that mice lacking LTβ expression specifically on B lymphocytes presented with decreased intestinal inflammation, whereas mice with loss of LTβ on T cells showed disease severity comparable to $Lt\beta R^{-/-}$ mice; indicating that B cells play a role in promoting disease progression (Jungbeck et al., 2008). An additional study where acute DSS-colitis was induced in $Lt\alpha^{-/-}$ mice, demonstrated a more severe disease phenotype in these animals compared with WT colitic mice (Spahn et al., 2002). Together these studies indicate that LTβR signalling plays a role in the induction and progression of colitis. $Lt\beta R^{-/-}$ mice do not develop LNs or ILFs, a phenotype which could play a significant role in the

progression of colitis. The lack of LNs could mean that an effective immune response may not be mounted against the invading pathogens and the lack of PPs and ILFs, and subsequent lack of IgA, could mean there is an increase in bacterial load in the intestine of $Lt\beta R^{-/-}$ mice before colitis is induced thereby exacerbating the disease.

Considering these studies and relating them to the situation observed in p100Δ mice, where signalling downstream of LTβR is constitutively active instead of inhibited there are a number of points to discuss. Intestinal epithelial cells express LTβR (Browning and French, 2002) and in p100Δ mice the need for interaction of these stromal cells with LT expressing cells to induce LTβR signalling is ablated, as a result there is a potential premature expression of chemokine and cell adhesion molecules, such as MAdCAM-1, VCAM-1 and CXCL13, without the need for prior lymphocyte stimulation. As a result this could enable recruitment of lymphocytes into the colon, early than would be seen in WT mice, culminating in an increase in ILF formation. In the p100Δ model, MAdCAM-1 and VCAM-1, CXCL13 expression can be observed in the colon and quantification of this expression would reveal if levels were elevated. The association of MAdCAM-1 expression with colitis progression has been well described (Xu et al., 2007; Kang et al., 2007; Farkas et al., 2006; Stopfer et al., 2004; Teramoto et al., 2005) and elevated levels of MAdCAM-1 in the spleen of p100Δ mice has been previously reported (Guo et al., 2007), if levels were also increased in the colon this could be a sign of the beginning of colitis in these mice.

Two potential systems for induction of ILFs may occur in colitis models. Firstly, they may be induced simply as a response to bacterial stimuli, which in the case of colitis is increased as the epithelial barrier is disrupted, allowing influx of bacteria into the tissue. In this situation, ILF formation occurs as an immune response to limit infection. Alternatively, the host's immune system may respond

inappropriately to commensal bacteria, stimulating ILF development and progression of a pro-inflammatory response to harmless micro-organisms. These two situations are opposing in their function; the first protects against the infection induced by epithelial barrier decay, the second potential instigates epithelial barrier decay by promoting a pro-inflammatory 'attacking' environment. In mouse models where colitis occurs spontaneously, such as *Il-10*$^{-/-}$ mice, initiation of disease occurs from around two months of age (Sellon et al., 1998; Berg et al., 1996; Kühn et al., 1993). As p100Δ mice die by 3-4 weeks of age, assessment of colitis progression cannot be observed or analysed. However, when NF-κB2 p100 is constitutively active only in the haematopoietic cell compartment, as is the case when WT mice are reconstituted with p100Δ FLC, an environment is generated which does not spontaneously lead to inflammation; these mice do not develop signs of colitis. A set of interesting experiments could be pursued to ascertain the response of these mice to DSS treatment. Would the increased colonic ILF formation lead to protection against colitis or induce more severe disease?

6.1.3. The role of DCs in intestinal immunity

The significant increase in ILF formation in p100Δ mice was not the only interesting phenotype observed in the colon. A dramatic influx and or proliferation of DCs in the colon was noted and as DCs play a crucial role in maintaining gut immunity and initiating mucosal immune responses, investigation into the phenotypes of these cells was undertaken. The T cell transfer model of colitis results in increased total numbers of CD11c^{high} DCs in mLN and colon (Laffont et al., 2010). This model of colitis involves the transfer of naïve T cells into immunodeficent hosts, such as *Rag*$^{-/-}$ mice, and due to the lack of T regulatory cells these mice develop colitis

(Mottet et al., 2003). We observed a similar increase in CD11c^{high} DCs in the colon of p100Δ mice. Although, the cDC numbers were not increased in the mLN, it is conceivable that the potential inflammatory response occurring in the colon might not be observable in mLN due to the early death of p100Δ mice. Alterations in cell recruitment and retention might also play a role.

Within the spleen the CD11c^{high} DC population can be subdivided into two distinct, groups: CD8α^{+}CD11b^{-} and CD8α^{-}CD11b^{+} DCs.-*LtβR*$^{-/-}$ mice exhibit a defect in splenic CD11c^{high}CD8α^{-} DC numbers (Wu et al., 1999; Abe et al., 2003; De Trez et al., 2008; Wang et al., 2005), as do *aly/aly* and *Relb*$^{-/-}$ mice (De Trez et al., 2008; Wu et al., 1998). Therefore, it appears that LTβR signalling through the alternative NF-κB pathway maintains CD11c^{high}CD8α^{-} DC homeostasis. Interestingly, in p100Δ mice there is no preferential increase in either CD11c^{high}CD11b^{+}CD8α^{-} or CD11c^{high}CD11b^{-}CD8α^{+} DC populations (Figure 4.2. A), suggesting that constitutive activation of NF-κB2 p100 can override homeostatic control of CD11c^{high}CD11b^{-} CD8α^{+} DCs, a process that has not previously been described.

Many subsets of mucosal DCs have been identified based on surface expression of different molecules; of particular interest is CD103. LP CD103^{+} DCs are able to sample antigen, migrate to the mLN and present antigen to T cells (Schulz et al., 2009), thereby inducing upregulation of gut-homing receptors, such as CCR9 (Annacker et al., 2005). In p100Δ mice, there was an increase in CD103^{+} DCs in the colon (Figure 4.3. B and C); this was not observed in the mLN, potentially this could be due to retention of these cells in the colon or due to a reduced migration rate under steady-state conditions, by unknown mechanisms. This hypothesis is supported by FACs analysis of CD3^{+} T cells from the mLN of p100Δ mice, showing no change in CCR9 expression and no alteration in activation status, when compared to WT

counterparts (Appendix Figure 1). LP $CD103^+$ DCs located in the small intestine are derived from a blood-bourne DC precursor (Jaensson et al., 2008), it is possible that LP $CD103^+$ DCs from the colon are also derived from such a precursor. The role of the alternative NF-κB pathway in generation and/or release of pre-DCs into the blood from bone marrow has not been investigated neither has any potential role in homeostasis of $CD103^+$ DC subsets. However, it has been demonstrated that RelB is required for the survival and maturation of $CD8^-CD11b^+$ DCs, but not for $CD8^+CD11b^-$ DCs (Wu et al., 1998). Interestingly, lymphoid $CD8^+CD11b^-$ DCs have been proposed to be developmentally and functionally linked to peripheral $CD103^+$ DCs (Edelson et al., 2010). Considering that LTβR, CD40 and RANK signalling, and subsequent alternative pathway activation is involved in DC homeostasis, maturation and survival in the spleen, it would be interesting to extend this knowledge to the $CD103^+$ DC population in the colon and mLN. It could be envisaged that the alternative pathway plays a role in DC homeostasis either through increased generation of pre-DCs, by increasing their proliferation via factors such as Cyclin-D1, or by affecting proliferation of DC subsets within tissues by similar mechanisms and/or due to signalling downstream of LTβR, CD40 or RANK. If this were the case it would provide a possible explanation for the increase in DC populations in the spleen and mLN of p100Δ. The role of p100 as a negative regulator of RelB function through heterodimerisation and cytoplasmic retention is highlighted in DC biology (Speirs et al., 2004). In mice lacking p100 (*Nfkb2*$^{-/-}$ mice) RelB can be found in the nucleus of DCs before activation, this is not the case in WT DCs. Furthermore, *Nfkb2*$^{-/-}$ DCs present with elevated expression of activation markers, but normal levels of cytokine production and possess an increased capacity to stimulate $CD4^+$ T cells (Speirs et al., 2004). Considering that in p100Δ mice the p100 protein has been

replaced by p52, there will be no negative regulation of RelB activation, therefore with regards to DC maturation and activation the situation may be similar to that observed in *Nfkb2*$^{-/-}$ mice.

We demonstrate that the alternative NF-κB pathway plays a role in DC homeostasis, with potential affects on their survival, maturation and activation. This area of work would be of great interest to pursue in the future as it may deepen our understanding of DC biology.

6.1.4. The alternative NF-κB pathway and splenic organisation

It is well established that the alternative NF-κB pathway is involved in the organisation of the spleen through activation downstream of LTβR ligation and transcription of genes encoding chemokines and cell adhesion molecules, such as CXCL13, CCL19/21 and MAdCAM-1. Mice lacking LTβR (Fütterer et al., 1998), or components of the ligand $LT\alpha_1\beta_2$ (Kuprash et al., 2002; Banks et al., 1995; Alexopoulou et al., 1998; Matsumoto et al., 1997; Ngo et al., 1999; Alimzhanov et al., 1997), fail to develop an organised spleen where B and T cell areas are clearly demarcated. Moreover, these knock-out mouse models also fail to develop LNs, as do mice in which signalling through the alternative pathway is ablated, such as *Relb*$^{-/-}$ (Weih et al., 1995; Yilmaz et al., 2003; Weih and Caamaño, 2003) and *aly/aly* (Shinkura et al., 1999; Miyawaki et al., 1994; Fagarasan et al., 2000; Karrer et al., 2000) mice. We demonstrate that introducing constitutively active p100 into an LTα deficient environment results in the striking recovery of organised B and T cell areas within the white pulp of the spleen, but with only one out of five *p100dLtα*$^{-/-}$ mice developing B cell follicles (Figure 5.2 and 5.2). Our second significant finding was

the fact that the same animal that developed B cell follicles also developed mature and fully organised iLNs and mLN (Figure 5.4). This data confirms that splenic organisation and LN development are dependent on the $LT\alpha_1\beta_2$-LTβR signalling axis and demonstrates that this signalling critically occurs through the alternative NF-κB pathway.

In light of these findings it would be interesting to investigate the development of LNs in *p100dLtα*$^{-/-}$ mice during embryogenesis to elucidate at which point constitutively active NF-κB2 p100 can no longer compensate for the lack of LTβR ligation by $LT\alpha_1\beta_2$, thus further deepening our understanding of LN development.

In summary, this thesis presents compelling evidence that activation of the alternative NF-κB pathway plays a significant role in the promotion of colonic ILF formation, potentially through various roles in cell activation, survival, proliferation and migration, as well as through stimulation of chemokine expression by endothelial cells. This leads to the suggestion that this signalling pathway may also be involved in development of other tertiary lymphoid tissues.

Additionally, this thesis highlights the role of the alternative NF-κB pathway in the cellular organisation of adult spleen, through the expression of B- and T-zone specific chemokines and we show that this pathway is a crucial signalling pathway downstream of LTβR.

7. Future Directions

This thesis has demonstrated that constitutive activation of p100Δ results in an increase in colonic ILFs and as described in the general discussion there are several potential explanations for this increase.

1. Increased ILF numbers may result from an increase in CP number, therefore an accurate assessment of CP number is vital to address this theory.
2. During experimental models of inflammatory bowel disease increased ILF numbers are often observed. p100Δ mice die prematurely at three weeks of age and have reduced body weight compared with WT littermates, they do not present with any gross symptoms of colonic inflammation but this may be due to early death, therefore it would be useful to repeat the serum cytokine analysis and to assess the cytokine levels in colonic tissue.
3. Constitutive activation of NF-κB2/p100 in a specific cell type could be responsible for the increase in ILFs. To address this theory repeats of the FLC transfer, along with splenocyte transfers would help to deduce whether the cell or cells responsible are precursors (i.e. from the foetal liver) or have a more mature phenotype (i.e. from the spleen).
4. Dysregulation of the alternative NF-κB pathway has been shown to affect chemokine expression in the spleen and LNs, it may be that chemokine expression in the colon is altered and this affects the ILF formation, therefore analysis of chemokine levels in colon and assessment of the chemotactic potential of different p100Δ cell types would help to elucidate whether this

axis of lymphoid tissue development is involved in the augmented ILF development in p100Δ mice.

The second area addressed in this thesis where future work could noticeably improve understanding is the potential role of the alternative NF-κB pathway in DC biology. Isolation of DC subsets from the colon of p100Δ mice and assessment of their function would reveal whether this heterogeneous population of cells plays a role in the colonic phenotype observed. Additionally, p100Δ mice may have defects in DC development and maturation, investigation of which encompasses a large and very interesting area of potential future research.

8. References

Abe, K., Yarovinsky, F. O., Murakami, T., Shakhov, A. N., Tumanov, A. V., Ito, D., Drutskaya, L. N., Pfeffer, K., Kuprash, D. V., Komschlies, K. L., and Nedospasov, S. A. (2003). Distinct contributions of TNF and LT cytokines to the development of dendritic cells in vitro and their recruitment in vivo. Blood *101*, 1477-1483.

Adachi, S., Yoshida, H., Honda, K., Maki, K., Saijo, K., Ikuta, K., Saito, T., and Nishikawa, S. I. (1998). Essential role of IL-7 receptor alpha in the formation of Peyer's patch anlage. Int Immunol *10*, 1-6.

Adachi, S., Yoshida, H., Kataoka, H., and Nishikawa, S. (1997). Three distinctive steps in Peyer's patch formation of murine embryo. Int Immunol *9*, 507-514.

Agace, W. W., Higgins, J. M., Sadasivan, B., Brenner, M. B., and Parker, C. M. (2000). T-lymphocyte-epithelial-cell interactions: integrin alpha(E)(CD103)beta(7), LEEP-CAM and chemokines. Curr Opin Cell Biol *12*, 563-568.

Alcamo, E., Hacohen, N., Schulte, L. C., Rennert, P. D., Hynes, R. O., and Baltimore, D. (2002). Requirement for the NF-kappaB family member RelA in the development of secondary lymphoid organs. J Exp Med *195*, 233-244.

Alcamo, E., Mizgerd, J. P., Horwitz, B. H., Bronson, R., Beg, A. A., Scott, M., Doerschuk, C. M., Hynes, R. O., and Baltimore, D. (2001). Targeted mutation of TNF receptor I rescues the RelA-deficient mouse and reveals a critical role for NF-kappa B in leukocyte recruitment. J Immunol *167*, 1592-1600.

Alexopoulou, L., Pasparakis, M., and Kollias, G. (1998). Complementation of lymphotoxin alpha knockout mice with tumor necrosis factor-expressing transgenes rectifies defective splenic structure and function. J Exp Med *188*, 745-754.

Alimzhanov, M. B., Kuprash, D. V., Kosco-Vilbois, M. H., Luz, A., Turetskaya, R. L., Tarakhovsky, A., Rajewsky, K., Nedospasov, S. A., and Pfeffer, K. (1997). Abnormal development of secondary lymphoid tissues in lymphotoxin beta-deficient mice. Proc Natl Acad Sci USA *94*, 9302-9307.

Anderson, D. M., Maraskovsky, E., Billingsley, W. L., Dougall, W. C., Tometsko, M. E., Roux, E. R., Teepe, M. C., DuBose, R. F., Cosman, D., and Galibert, L. (1997). A homologue of the TNF receptor and its ligand enhance T-cell growth and dendritic-cell function. Nature *390*, 175-179.

Ando, T., Jordan, P., Wang, Y., Itoh, M., Joh, T., Sasaki, M., Elrod, J. W., Carpenter, A., Jennings, M. H., Minagar, A., and Alexander, J. S. (2005). MAdCAM-1 expression and regulation in murine colonic endothelial cells in vitro. Inflamm Bowel Dis *11*, 258-264.

Annacker, O., Coombes, J. L., Malmstrom, V., Uhlig, H. H., Bourne, T., Johansson-Lindbom, B., Agace, W. W., Parker, C. M., and Powrie, F. (2005). Essential role for CD103 in the T cell-mediated regulation of experimental colitis. J Exp Med *202*, 1051-1061.

Annunziato, F., Cosmi, L., Liotta, F., Lazzeri, E., Romagnani, P., Angeli, R., Lasagni, L., Manetti, R., Marra, F., Gerard, C., Petrai, I., Dello Sbarba, P., Tonelli, F., Maggi,

E., and Romagnani, S. (2006). CXCR3 and alphaEbeta7 integrin identify a subset of CD8+ mature thymocytes that share phenotypic and functional properties with CD8+ gut intraepithelial lymphocytes. Gut *55*, 961-968.

Ansel, K. M., Ngo, V. N., Hyman, P. L., Luther, S. A., Förster, R., Sedgwick, J. D., Browning, J. L., Lipp, M., and Cyster, J. G. (2000). A chemokine-driven positive feedback loop organizes lymphoid follicles. Nature *406*, 309-314.

Ardavín, C. (2003). Origin, precursors and differentiation of mouse dendritic cells. Nat Rev Immunol *3*, 582-590.

Azzali, G. (2003). Structure, lymphatic vascularization and lymphocyte migration in mucosa-associated lymphoid tissue. Immunol Rev *195*, 178-189.

Bajénoff, M., Egen, J. G., Koo, L. Y., Laugier, J. P., Brau, F., Glaichenhaus, N., and Germain, R. N. (2006). Stromal cell networks regulate lymphocyte entry, migration, and territoriality in lymph nodes. Immunity *25*, 989-1001.

Banks, T. A., Rouse, B. T., Kerley, M. K., Blair, P. J., Godfrey, V. L., Kuklin, N. A., Bouley, D. M., Thomas, J., Kanangat, S., and Mucenski, M. L. (1995). Lymphotoxin-alpha-deficient mice. Effects on secondary lymphoid organ development and humoral immune responsiveness. J Immunol *155*, 1685-1693.

Basak, S., Kim, H., Kearns, J. D., Tergaonkar, V., O'Dea, E., Werner, S. L., Benedict, C. A., Ware, C. F., Ghosh, G., Verma, I. M., and Hoffmann, A. (2007). A fourth IkappaB protein within the NF-kappaB signaling module. Cell *128*, 369-381.

Beg, A. A., Sha, W. C., Bronson, R. T., Ghosh, S., and Baltimore, D. (1995). Embryonic lethality and liver degeneration in mice lacking the RelA component of NF-kappa B. Nature *376*, 167-170.

Beinke, S., and Ley, S. C. (2004). Functions of NF-kappaB1 and NF-kappaB2 in immune cell biology. Biochem J *382*, 393-409.

Belvin, M. P., and Anderson, K. V. (1996). A conserved signaling pathway: the Drosophila toll-dorsal pathway. Annu Rev Cell Dev Biol *12*, 393-416.

Bénézech, C., White, A., Mader, E., Serre, K., Parnell, S., Pfeffer, K., Ware, C. F., Anderson, G., and Caamaño, J. H. (2010). Ontogeny of Stromal Organizer Cells during Lymph Node Development. J Immunol .

Berg, D. J., Davidson, N., Kühn, R., Müller, W., Menon, S., Holland, G., Thompson-Snipes, L., Leach, M. W., and Rennick, D. (1996). Enterocolitis and colon cancer in interleukin-10-deficient mice are associated with aberrant cytokine production and CD4(+) TH1-like responses. J Clin Invest *98*, 1010-1020.

Berlin, C., Berg, E. L., Briskin, M. J., Andrew, D. P., Kilshaw, P. J., Holzmann, B., Weissman, I. L., Hamann, A., and Butcher, E. C. (1993). Alpha 4 beta 7 integrin mediates lymphocyte binding to the mucosal vascular addressin MAdCAM-1. Cell *74*, 185-195.

Blair, J. M., Zheng, Y., and Dunstan, C. R. (2007). RANK ligand. Int J Biochem Cell Biol *39*, 1077-1081.

Bonizzi, G., Bebien, M., Otero, D. C., Johnson-Vroom, K. E., Cao, Y., Vu, D., Jegga, A. G., Aronow, B. J., Ghosh, G., Rickert, R. C., and Karin, M. (2004). Activation of IKKalpha target genes depends on recognition of specific kappaB binding sites by RelB:p52 dimers. EMBO J *23*, 4202-4210.

Bonizzi, G., and Karin, M. (2004). The two NF-kappaB activation pathways and their role in innate and adaptive immunity. Trends Immunol *25*, 280-288.

Boonstra, A., Asselin-Paturel, C., Gilliet, M., Crain, C., Trinchieri, G., Liu, Y. J., and O'Garra, A. (2003). Flexibility of mouse classical and plasmacytoid-derived dendritic cells in directing T helper type 1 and 2 cell development: dependency on antigen dose and differential toll-like receptor ligation. J Exp Med *197*, 101-109.

Bours, V., Franzoso, G., Azarenko, V., Park, S., Kanno, T., Brown, K., and Siebenlist, U. (1993). The oncoprotein Bcl-3 directly transactivates through kappa B motifs via association with DNA-binding p50B homodimers. Cell *72*, 729-739.

Bouskra, D., Brézillon, C., Bérard, M., Werts, C., Varona, R., Boneca, I. G., and Eberl, G. (2008). Lymphoid tissue genesis induced by commensals through NOD1 regulates intestinal homeostasis. Nature *456*, 507-510.

Bowman, E. P., Kuklin, N. A., Youngman, K. R., Lazarus, N. H., Kunkel, E. J., Pan, J., Greenberg, H. B., and Butcher, E. C. (2002). The intestinal chemokine thymus-expressed chemokine (CCL25) attracts IgA antibody-secreting cells. J Exp Med *195*, 269-275.

Brown, A. M., Linhoff, M. W., Stein, B., Wright, K. L., Baldwin, A. S., Basta, P. V., and Ting, J. P. (1994). Function of NF-kappa B/Rel binding sites in the major histocompatibility complex class II invariant chain promoter is dependent on cell-specific binding of different NF-kappa B/Rel subunits. Mol Cell Biol *14*, 2926-2935.

Browning, J. L., Allaire, N., Ngam-Ek, A., Notidis, E., Hunt, J., Perrin, S., and Fava, R. A. (2005). Lymphotoxin-beta receptor signaling is required for the homeostatic control of HEV differentiation and function. Immunity *23*, 539-550.

Browning, J. L., and French, L. E. (2002). Visualization of lymphotoxin-beta and lymphotoxin-beta receptor expression in mouse embryos. J Immunol *168*, 5079-5087.

Caamaño, J. H., Rizzo, C. A., Durham, S. K., Barton, D. S., Raventós-Suárez, C., Snapper, C. M., and Bravo, R. (1998). Nuclear factor (NF)-kappa B2 (p100/p52) is required for normal splenic microarchitecture and B cell-mediated immune responses. J Exp Med *187*, 185-196.

Carragher, D., Johal, R., Button, A., White, A., Eliopoulos, A., Jenkinson, E., Anderson, G., and Caamaño, J. (2004). A stroma-derived defect in NF-kappaB2-/- mice causes impaired lymph node development and lymphocyte recruitment. J Immunol *173*, 2271-2279.

Caux, C., Massacrier, C., Vanbervliet, B., Dubois, B., Van Kooten, C., Durand, I., and Banchereau, J. (1994). Activation of human dendritic cells through CD40 cross-linking. J Exp Med *180*, 1263-1272.

Cepek, K. L., Shaw, S. K., Parker, C. M., Russell, G. J., Morrow, J. S., Rimm, D. L., and Brenner, M. B. (1994). Adhesion between epithelial cells and T lymphocytes mediated by E-cadherin and the alpha E beta 7 integrin. Nature *372*, 190-193.

Chen, C., Mobley, J. L., Dwir, O., Shimron, F., Grabovsky, V., Lobb, R. R., Shimizu, Y., and Alon, R. (1999). High affinity very late antigen-4 subsets expressed on T cells are mandatory for spontaneous adhesion strengthening but not for rolling on VCAM-1 in shear flow. J Immunol *162*, 1084-1095.

Chieppa, M., Rescigno, M., Huang, A. Y., and Germain, R. N. (2006). Dynamic imaging of dendritic cell extension into the small bowel lumen in response to epithelial cell TLR engagement. J Exp Med *203*, 2841-2852.

Claudio, E., Brown, K., Park, S., Wang, H., and Siebenlist, U. (2002). BAFF-induced NEMO-independent processing of NF-kappa B2 in maturing B cells. Nature Immunology *3*, 958-965.

Coles, M. C., Veiga-Fernandes, H., Foster, K. E., Norton, T., Pagakis, S. N., Seddon, B., and Kioussis, D. (2006). Role of T and NK cells and IL7/IL7r interactions during neonatal maturation of lymph nodes. Proc Natl Acad Sci USA *103*, 13457-13462.

Coombes, J. L., Siddiqui, K. R., Arancibia-Cárcamo, C. V., Hall, J., Sun, C. M., Belkaid, Y., and Powrie, F. (2007). A functionally specialized population of mucosal CD103+ DCs induces Foxp3+ regulatory T cells via a TGF-beta and retinoic acid-dependent mechanism. J Exp Med *204*, 1757-1764.

Coope, H. J., Atkinson, P. G., Huhse, B., Belich, M., Janzen, J., Holman, M. J., Klaus, G. G., Johnston, L. H., and Ley, S. C. (2002). CD40 regulates the processing of NF-kappaB2 p100 to p52. EMBO J *21*, 5375-5385.

Crivellato, E., Vacca, A., and Ribatti, D. (2004). Setting the stage: an anatomist's view of the immune system. Trends Immunol *25*, 210-217.

Cuff, C. A., Sacca, R., and Ruddle, N. H. (1999). Differential induction of adhesion molecule and chemokine expression by LTalpha3 and LTalphabeta in inflammation elucidates potential mechanisms of mesenteric and peripheral lymph node development. J Immunol *162*, 5965-5972.

Cupedo, T., Vondenhoff, M. F., Heeregrave, E. J., De Weerd, A. E., Jansen, W., Jackson, D. G., Kraal, G., and Mebius, R. E. (2004). Presumptive lymph node organizers are differentially represented in developing mesenteric and peripheral nodes. J Immunol *173*, 2968-2975.

Cyster, J. G., Ngo, V. N., Ekland, E. H., Gunn, M. D., Sedgwick, J. D., and Ansel, K. M. (1999). Chemokines and B-cell homing to follicles. Curr Top Microbiol Immunol *246*, 87-92; discussion 93.

De Togni, P., Goellner, J., Ruddle, N. H., Streeter, P. R., Fick, A., Mariathasan, S., Smith, S. C., Carlson, R., Shornick, L. P., and Strauss-Schoenberger, J. (1994). Abnormal development of peripheral lymphoid organs in mice deficient in lymphotoxin. Science *264*, 703-707.

De Trez, C., Schneider, K., Potter, K., Droin, N., Fulton, J., Norris, P. S., Ha, S. W., Fu, Y. X., Murphy, T., Murphy, K. M., Pfeffer, K., Benedict, C. A., and Ware, C. F. (2008). The inhibitory HVEM-BTLA pathway counter regulates lymphotoxin receptor signaling to achieve homeostasis of dendritic cells. J Immunol *180*, 238-248.

De Trez, C., and Ware, C. F. (2008). The TNF receptor and Ig superfamily members form an integrated signaling circuit controlling dendritic cell homeostasis. Cytokine Growth Factor Rev *19*, 277-284.

Dejardin, E., Deregowski, V., Greimers, R., Cai, Z., Chouaib, S., Merville, M. P., and Bours, V. (1998). Regulation of major histocompatibility complex class I expression by NF-kappaB-related proteins in breast cancer cells. Oncogene *16*, 3299-3307.

Dejardin, E., Droin, N. M., Delhase, M., Haas, E., Cao, Y., Makris, C., Li, Z. W., Karin, M., Ware, C. F., and Green, D. R. (2002). The lymphotoxin-beta receptor induces different patterns of gene expression via two NF-kappaB pathways. Immunity *17*, 525-535.

del Rio, M. L., Bernhardt, G., Rodriguez-Barbosa, J. I., and Förster, R. (2010). Development and functional specialization of CD103+ dendritic cells. Immunol Rev *234*, 268-281.

del Rio, M. L., Rodriguez-Barbosa, J. I., Bölter, J., Ballmaier, M., Dittrich-Breiholz, O., Kracht, M., Jung, S., and Förster, R. (2008). CX3CR1+ c-kit+ bone marrow cells give rise to CD103+ and CD103- dendritic cells with distinct functional properties. J Immunol *181*, 6178-6188.

Dieleman, L. A., Ridwan, B. U., Tennyson, G. S., Beagley, K. W., Bucy, R. P., and Elson, C. O. (1994). Dextran sulfate sodium-induced colitis occurs in severe combined immunodeficient mice. Gastroenterology *107*, 1643-1652.

Dieu, M. C., Vanbervliet, B., Vicari, A., Bridon, J. M., Oldham, E., Aït-Yahia, S., Brière, F., Zlotnik, A., Lebecque, S., and Caux, C. (1998). Selective recruitment of immature and mature dendritic cells by distinct chemokines expressed in different anatomic sites. J Exp Med *188*, 373-386.

Do, R. K., and Chen-Kiang, S. (2002). Mechanism of BLyS action in B cell immunity. Cytokine Growth Factor Rev *13*, 19-25.

Dong, C. (2008). TH17 cells in development: an updated view of their molecular identity and genetic programming. Nat Rev Immunol *8*, 337-348.

Dougall, W. C., Glaccum, M., Charrier, K., Rohrbach, K., Brasel, K., De Smedt, T., Daro, E., Smith, J., Tometsko, M. E., Maliszewski, C. R., Armstrong, A., Shen, V., Bain, S., Cosman, D., Anderson, D., Morrissey, P. J., Peschon, J. J., and Schuh, J. (1999). RANK is essential for osteoclast and lymph node development. Genes Dev *13*, 2412-2424.

Eberl, G. (2005). Inducible lymphoid tissues in the adult gut: recapitulation of a fetal developmental pathway? Nat Rev Immunol *5*, 413-420.

Eberl, G. (2007). From induced to programmed lymphoid tissues: the long road to preempt pathogens. Trends Immunol *28*, 423-428.

Eberl, G., and Littman, D. R. (2004). Thymic origin of intestinal alphabeta T cells revealed by fate mapping of RORgammat+ cells. Science *305*, 248-251.

Eberl, G., Marmon, S., Sunshine, M. J., Rennert, P. D., Choi, Y., and Littman, D. R. (2004). An essential function for the nuclear receptor RORgamma(t) in the generation of fetal lymphoid tissue inducer cells. Nature Immunology *5*, 64-73.

Eberl, G., and Sawa, S. (2010). Opening the crypt: current facts and hypotheses on the function of cryptopatches. Trends Immunol *31*, 50-55.

Edelson, B. T., KC, W., Juang, R., Kohyama, M., Benoit, L. A., Klekotka, P. A., Moon, C., Albring, J. C., Ise, W., Michael, D. G., Bhattacharya, D., Stappenbeck, T. S., Holtzman, M. J., Sung, S. S., Murphy, T. L., Hildner, K., and Murphy, K. M. (2010). Peripheral CD103+ dendritic cells form a unified subset developmentally related to CD8alpha+ conventional dendritic cells. J Exp Med *207*, 823-836.

Edwards, A. D., Diebold, S. S., Slack, E. M., Tomizawa, H., Hemmi, H., Kaisho, T., Akira, S., and Reis e Sousa, C. (2003). Toll-like receptor expression in murine DC subsets: lack of TLR7 expression by CD8 alpha+ DC correlates with unresponsiveness to imidazoquinolines. Eur J Immunol *33*, 827-833.

Eliopoulos, A. G., Caamano, J. H., Flavell, J., Reynolds, G. M., Murray, P. G., Poyet, J. L., and Young, L. S. (2003). Epstein-Barr virus-encoded latent infection membrane protein 1 regulates the processing of p100 NF-kappaB2 to p52 via an IKKgamma/NEMO-independent signalling pathway. Oncogene *22*, 7557-7569.

Endres, R., Alimzhanov, M. B., Plitz, T., Fütterer, A., Kosco-Vilbois, M. H., Nedospasov, S. A., Rajewsky, K., and Pfeffer, K. (1999). Mature follicular dendritic cell networks depend on expression of lymphotoxin beta receptor by radioresistant stromal cells and of lymphotoxin beta and tumor necrosis factor by B cells. J Exp Med *189*, 159-168.

Fagarasan, S., Kinoshita, K., Muramatsu, M., Ikuta, K., and Honjo, T. (2001). In situ class switching and differentiation to IgA-producing cells in the gut lamina propria. Nature *413*, 639-643.

Fagarasan, S., Muramatsu, M., Suzuki, K., Nagaoka, H., Hiai, H., and Honjo, T. (2002). Critical roles of activation-induced cytidine deaminase in the homeostasis of gut flora. Science *298*, 1424-1427.

Fagarasan, S., Shinkura, R., Kamata, T., Nogaki, F., Ikuta, K., Tashiro, K., and Honjo, T. (2000). Alymphoplasia (aly)-type nuclear factor kappaB-inducing kinase (NIK) causes defects in secondary lymphoid tissue chemokine receptor signaling and homing of peritoneal cells to the gut-associated lymphatic tissue system. J Exp Med *191*, 1477-1486.

Farkas, S., Hornung, M., Sattler, C., Edtinger, K., Steinbauer, M., Anthuber, M., Schlitt, H. J., Herfarth, H., and Geissler, E. K. (2006). Blocking MAdCAM-1 in vivo reduces leukocyte extravasation and reverses chronic inflammation in experimental colitis. Int J Colorectal Dis *21*, 71-78.

Förster, R., Mattis, A. E., Kremmer, E., Wolf, E., Brem, G., and Lipp, M. (1996). A putative chemokine receptor, BLR1, directs B cell migration to defined lymphoid organs and specific anatomic compartments of the spleen. Cell *87*, 1037-1047.

Förster, R., Schubel, A., Breitfeld, D., Kremmer, E., Renner-Müller, I., Wolf, E., and Lipp, M. (1999). CCR7 coordinates the primary immune response by establishing functional microenvironments in secondary lymphoid organs. Cell *99*, 23-33.

Franzoso, G., Carlson, L., Poljak, L., Shores, E. W., Epstein, S., Leonardi, A., Grinberg, A., Tran, T., Scharton-Kersten, T., Anver, M., Love, P., Brown, K., and Siebenlist, U. (1998). Mice deficient in nuclear factor (NF)-kappa B/p52 present with defects in humoral responses, germinal center reactions, and splenic microarchitecture. J Exp Med *187*, 147-159.

Fu, Y. X., Huang, G., Matsumoto, M., Molina, H., and Chaplin, D. D. (1997). Independent signals regulate development of primary and secondary follicle structure in spleen and mesenteric lymph node. Proc Natl Acad Sci USA *94*, 5739-5743.

Fütterer, A., Mink, K., Luz, A., Kosco-Vilbois, M. H., and Pfeffer, K. (1998). The lymphotoxin beta receptor controls organogenesis and affinity maturation in peripheral lymphoid tissues. Immunity *9*, 59-70.

Geissmann, F., Manz, M. G., Jung, S., Sieweke, M. H., Merad, M., and Ley, K. (2010). Development of monocytes, macrophages, and dendritic cells. Science *327*, 656-661.

Ghosh, S., and Karin, M. (2002). Missing pieces in the NF-kappaB puzzle. Cell *109 Suppl*, S81-96.

Ghosh, S., May, M. J., and Kopp, E. B. (1998). NF-kappa B and Rel proteins: evolutionarily conserved mediators of immune responses. Annual Review of Immunology *16*, 225-260.

Gorfu, G., Rivera-Nieves, J., and Ley, K. (2009). Role of beta7 integrins in intestinal lymphocyte homing and retention. Curr Mol Med *9*, 836-850.

Gräbner, R., Lötzer, K., Döpping, S., Hildner, M., Radke, D., Beer, M., Spanbroek, R., Lippert, B., Reardon, C. A., Getz, G. S., Fu, Y. X., Hehlgans, T., Mebius, R. E., van der Wall, M., Kruspe, D., Englert, C., Lovas, A., Hu, D., Randolph, G. J., Weih, F., and Habenicht, A. J. (2009). Lymphotoxin beta receptor signaling promotes tertiary lymphoid organogenesis in the aorta adventitia of aged ApoE-/- mice. J Exp Med *206*, 233-248.

Grewal, I. S., and Flavell, R. A. (1998). CD40 and CD154 in cell-mediated immunity. Annual Review of Immunology *16*, 111-135.

Guo, F., Weih, D., Meier, E., and Weih, F. (2007). Constitutive alternative NF-kappaB signaling promotes marginal zone B-cell development but disrupts the marginal sinus and induces HEV-like structures in the spleen. Blood *110*, 2381-2389.

Hamada, H., Hiroi, T., Nishiyama, Y., Takahashi, H., Masunaga, Y., Hachimura, S., Kaminogawa, S., Takahashi-Iwanaga, H., Iwanaga, T., Kiyono, H., Yamamoto, H., and Ishikawa, H. (2002). Identification of multiple isolated lymphoid follicles on the antimesenteric wall of the mouse small intestine. J Immunol *168*, 57-64.

Hashi, H., Yoshida, H., Honda, K., Fraser, S., Kubo, H., Awane, M., Takabayashi, A., Nakano, H., Yamaoka, Y., and Nishikawa, S. (2001). Compartmentalization of Peyer's patch anlagen before lymphocyte entry. J Immunol *166*, 3702-3709.

Hashimoto, C., Hudson, K. L., and Anderson, K. V. (1988). The Toll gene of Drosophila, required for dorsal-ventral embryonic polarity, appears to encode a transmembrane protein. Cell *52*, 269-279.

He, L., Grammer, A. C., Wu, X., and Lipsky, P. E. (2004). TRAF3 forms heterotrimers with TRAF2 and modulates its ability to mediate NF-{kappa}B activation. The Journal of biological chemistry *279*, 55855-55865.

Heusch, M., Lin, L., Geleziunas, R., and Greene, W. C. (1999). The generation of nfkb2 p52: mechanism and efficiency. Oncogene *18*, 6201-6208.

Hieshima, K., Kawasaki, Y., Hanamoto, H., Nakayama, T., Nagakubo, D., Kanamaru, A., and Yoshie, O. (2004). CC chemokine ligands 25 and 28 play essential roles in intestinal extravasation of IgA antibody-secreting cells. J Immunol *173*, 3668-3675.

Honda, K., Nakano, H., Yoshida, H., Nishikawa, S., Rennert, P., Ikuta, K., Tamechika, M., Yamaguchi, K., Fukumoto, T., Chiba, T., and Nishikawa, S. I. (2001). Molecular basis for hematopoietic/mesenchymal interaction during initiation of Peyer's patch organogenesis. J Exp Med *193*, 621-630.

Hori, S., Nomura, T., and Sakaguchi, S. (2003). Control of regulatory T cell development by the transcription factor Foxp3. Science *299*, 1057-1061.

Hostager, B. S., and Bishop, G. A. (1999). Cutting edge: contrasting roles of TNF receptor-associated factor 2 (TRAF2) and TRAF3 in CD40-activated B lymphocyte differentiation. J Immunol *162*, 6307-6311.

Iezzi, G., Scheidegger, D., and Lanzavecchia, A. (2001). Migration and function of antigen-primed nonpolarized T lymphocytes in vivo. J Exp Med *193*, 987-993.

Ishikawa, H., Carrasco, D., Claudio, E., Ryseck, R. P., and Bravo, R. (1997). Gastric hyperplasia and increased proliferative responses of lymphocytes in mice lacking the COOH-terminal ankyrin domain of NF-kappaB2. J Exp Med *186*, 999-1014.

Ivanov, I. I., Diehl, G. E., and Littman, D. R. (2006). Lymphoid tissue inducer cells in intestinal immunity. Curr Top Microbiol Immunol *308*, 59-82.

Iwasaki, A., and Kelsall, B. L. (2001). Unique functions of CD11b+, CD8 alpha+, and double-negative Peyer's patch dendritic cells. J Immunol *166*, 4884-4890.

Iwasaki, A., and Medzhitov, R. (2010). Regulation of adaptive immunity by the innate immune system. Science *327*, 291-295.

Jaensson, E., Uronen-Hansson, H., Pabst, O., Eksteen, B., Tian, J., Coombes, J. L., Berg, P. L., Davidsson, T., Powrie, F., Johansson-Lindbom, B., and Agace, W. W. (2008). Small intestinal CD103+ dendritic cells display unique functional properties that are conserved between mice and humans. J Exp Med *205*, 2139-2149.

Johansson-Lindbom, B., Svensson, M., Pabst, O., Palmqvist, C., Marquez, G., Förster, R., and Agace, W. W. (2005). Functional specialization of gut CD103+ dendritic cells in the regulation of tissue-selective T cell homing. J Exp Med *202*, 1063-1073.

Josien, R., Li, H. L., Ingulli, E., Sarma, S., Wong, B. R., Vologodskaia, M., Steinman, R. M., and Choi, Y. (2000). TRANCE, a tumor necrosis factor family member, enhances the longevity and adjuvant properties of dendritic cells in vivo. J Exp Med *191*, 495-502.

Josien, R., Wong, B. R., Li, H. L., Steinman, R. M., and Choi, Y. (1999). TRANCE, a TNF family member, is differentially expressed on T cell subsets and induces cytokine production in dendritic cells. J Immunol *162*, 2562-2568.

Jung, S., Aliberti, J., Graemmel, P., Sunshine, M. J., Kreutzberg, G. W., Sher, A., and Littman, D. R. (2000). Analysis of fractalkine receptor CX(3)CR1 function by targeted deletion and green fluorescent protein reporter gene insertion. Mol Cell Biol *20*, 4106-4114.

Jungbeck, M., Stopfer, P., Bataille, F., Nedospasov, S. A., Männel, D. N., and Hehlgans, T. (2008). Blocking lymphotoxin beta receptor signalling exacerbates acute DSS-induced intestinal inflammation--opposite functions for surface lymphotoxin expressed by T and B lymphocytes. Mol Immunol *45*, 34-41.

Kabashima, K., Banks, T. A., Ansel, K. M., Lu, T. T., Ware, C. F., and Cyster, J. G. (2005). Intrinsic lymphotoxin-beta receptor requirement for homeostasis of lymphoid tissue dendritic cells. Immunity *22*, 439-450.

Kaipainen, A., Korhonen, J., Mustonen, T., van Hinsbergh, V. W., Fang, G. H., Dumont, D., Breitman, M., and Alitalo, K. (1995). Expression of the fms-like tyrosine

kinase 4 gene becomes restricted to lymphatic endothelium during development. Proc Natl Acad Sci USA *92*, 3566-3570.

Kaisho, T., Takeda, K., Tsujimura, T., Kawai, T., Nomura, F., Terada, N., and Akira, S. (2001a). IkappaB kinase alpha is essential for mature B cell development and function. J Exp Med *193*, 417-426.

Kaisho, T., Takeuchi, O., Kawai, T., Hoshino, K., and Akira, S. (2001b). Endotoxin-induced maturation of MyD88-deficient dendritic cells. J Immunol *166*, 5688-5694.

Kanamori, Y., Ishimaru, K., Nanno, M., Maki, K., Ikuta, K., Nariuchi, H., and Ishikawa, H. (1996). Identification of novel lymphoid tissues in murine intestinal mucosa where clusters of c-kit+ IL-7R+ Thy1+ lympho-hemopoietic progenitors develop. J Exp Med *184*, 1449-1459.

Kang, W., Kudsk, K. A., Sano, Y., Lan, J., Yang-Xin, F., Gomez, F. E., and Maeshima, Y. (2007). Effects of lymphotoxin beta receptor blockade on intestinal mucosal immunity. JPEN J Parenter Enteral Nutr *31*, 358-64; discussion 364-5.

Karkkainen, M. J., Haiko, P., Sainio, K., Partanen, J., Taipale, J., Petrova, T. V., Jeltsch, M., Jackson, D. G., Talikka, M., Rauvala, H., Betsholtz, C., and Alitalo, K. (2004). Vascular endothelial growth factor C is required for sprouting of the first lymphatic vessels from embryonic veins. Nature Immunology *5*, 74-80.

Karlsson, M. C., Guinamard, R., Bolland, S., Sankala, M., Steinman, R. M., and Ravetch, J. V. (2003). Macrophages control the retention and trafficking of B lymphocytes in the splenic marginal zone. J Exp Med *198*, 333-340.

Karrer, U., Althage, A., Odermatt, B., Hengartner, H., and Zinkernagel, R. M. (2000). Immunodeficiency of alymphoplasia mice (aly/aly) in vivo: structural defect of secondary lymphoid organs and functional B cell defect. Eur J Immunol *30*, 2799-2807.

Kim, D., Mebius, R. E., MacMicking, J. D., Jung, S., Cupedo, T., Castellanos, Y., Rho, J., Wong, B. R., Josien, R., Kim, N., Rennert, P. D., and Choi, Y. (2000). Regulation of peripheral lymph node genesis by the tumor necrosis factor family member TRANCE. J Exp Med *192*, 1467-1478.

Knoop, K. A., Kumar, N., Butler, B. R., Sakthivel, S. K., Taylor, R. T., Nochi, T., Akiba, H., Yagita, H., Kiyono, H., and Williams, I. R. (2009). RANKL is necessary and sufficient to initiate development of antigen-sampling M cells in the intestinal epithelium. J Immunol *183*, 5738-5747.

Kobayashi, T., Walsh, P. T., Walsh, M. C., Speirs, K. M., Chiffoleau, E., King, C. G., Hancock, W. W., Caamano, J. H., Hunter, C. A., Scott, P., Turka, L. A., and Choi, Y. (2003). TRAF6 is a critical factor for dendritic cell maturation and development. Immunity *19*, 353-363.

Koike, R., Nishimura, T., Yasumizu, R., Tanaka, H., Hataba, Y., Hataba, Y., Watanabe, T., Miyawaki, S., and Miyasaka, M. (1996). The splenic marginal zone is absent in alymphoplastic aly mutant mice. Eur J Immunol *26*, 669-675.

Kong, Y. Y., Yoshida, H., Sarosi, I., Tan, H. L., Timms, E., Capparelli, C., Morony, S., Oliveira-dos-Santos, A. J., Van, G., Itie, A., Khoo, W., Wakeham, A., Dunstan, C. R., Lacey, D. L., Mak, T. W., Boyle, W. J., and Penninger, J. M. (1999). OPGL is a key regulator of osteoclastogenesis, lymphocyte development and lymph-node organogenesis. Nature *397*, 315-323.

Koni, P. A., Sacca, R., Lawton, P., Browning, J. L., Ruddle, N. H., and Flavell, R. A. (1997). Distinct roles in lymphoid organogenesis for lymphotoxins alpha and beta revealed in lymphotoxin beta-deficient mice. Immunity *6*, 491-500.

Kraehenbuhl, J. P., and Neutra, M. R. (2000). Epithelial M cells: differentiation and function. Annu Rev Cell Dev Biol *16*, 301-332.

Kuai, J., Nickbarg, E., Wooters, J., Qiu, Y., Wang, J., and Lin, L. L. (2003). Endogenous association of TRAF2, TRAF3, cIAP1, and Smac with lymphotoxin beta receptor reveals a novel mechanism of apoptosis. The Journal of biological chemistry *278*, 14363-14369.

Kühn, R., Löhler, J., Rennick, D., Rajewsky, K., and Müller, W. (1993). Interleukin-10-deficient mice develop chronic enterocolitis. Cell *75*, 263-274.

Kuprash, D. V., Alimzhanov, M. B., Tumanov, A. V., Grivennikov, S. I., Shakhov, A. N., Drutskaya, L. N., Marino, M. W., Turetskaya, R. L., Anderson, A. O., Rajewsky, K., Pfeffer, K., and Nedospasov, S. A. (2002). Redundancy in tumor necrosis factor (TNF) and lymphotoxin (LT) signaling in vivo: mice with inactivation of the entire TNF/LT locus versus single-knockout mice. Mol Cell Biol *22*, 8626-8634.

Kurebayashi, S., Ueda, E., Sakaue, M., Patel, D. D., Medvedev, A., Zhang, F., and Jetten, A. M. (2000). Retinoid-related orphan receptor gamma (RORgamma) is essential for lymphoid organogenesis and controls apoptosis during thymopoiesis. Proc Natl Acad Sci USA *97*, 10132-10137.

Kweon, M. N., Yamamoto, M., Rennert, P. D., Park, E. J., Lee, A. Y., Chang, S. Y., Hiroi, T., Nanno, M., and Kiyono, H. (2005). Prenatal blockage of lymphotoxin beta receptor and TNF receptor p55 signaling cascade resulted in the acceleration of tissue genesis for isolated lymphoid follicles in the large intestine. J Immunol *174*, 4365-4372.

Lacey, D. L., Timms, E., Tan, H. L., Kelley, M. J., Dunstan, C. R., Burgess, T., Elliott, R., Colombero, A., Elliott, G., Scully, S., Hsu, H., Sullivan, J., Hawkins, N., Davy, E., Capparelli, C., Eli, A., Qian, Y. X., Kaufman, S., Sarosi, I., Shalhoub, V., Senaldi, G., Guo, J., Delaney, J., and Boyle, W. J. (1998). Osteoprotegerin ligand is a cytokine that regulates osteoclast differentiation and activation. Cell *93*, 165-176.

Laffont, S., Siddiqui, K. R., and Powrie, F. (2010). Intestinal inflammation abrogates the tolerogenic properties of MLN CD103(+) dendritic cells. Eur J Immunol *40*, 1877-1883.

Lanoix, J., Lacoste, J., Pepin, N., Rice, N., and Hiscott, J. (1994). Overproduction of NFKB2 (lyt-10) and c-Rel: a mechanism for HTLV-I Tax-mediated trans-activation via the NF-kappa B signalling pathway. Oncogene *9*, 841-852.

Leenen, P. J., Radosević, K., Voerman, J. S., Salomon, B., van Rooijen, N., Klatzmann, D., and van Ewijk, W. (1998). Heterogeneity of mouse spleen dendritic cells: in vivo phagocytic activity, expression of macrophage markers, and subpopulation turnover. J Immunol *160*, 2166-2173.

Lehmann, J., Huehn, J., de la Rosa, M., Maszyna, F., Kretschmer, U., Krenn, V., Brunner, M., Scheffold, A., and Hamann, A. (2002). Expression of the integrin alpha Ebeta 7 identifies unique subsets of CD25+ as well as CD25- regulatory T cells. Proc Natl Acad Sci USA *99*, 13031-13036.

Leithäuser, F., Trobonjaca, Z., Möller, P., and Reimann, J. (2001). Clustering of colonic lamina propria CD4(+) T cells to subepithelial dendritic cell aggregates precedes the development of colitis in a murine adoptive transfer model. Lab Invest *81*, 1339-1349.

Lemaitre, B., Nicolas, E., Michaut, L., Reichhart, J. M., and Hoffmann, J. A. (1996). The dorsoventral regulatory gene cassette spätzle/Toll/cactus controls the potent antifungal response in Drosophila adults. Cell *86*, 973-983.

Liao, F., Alderson, R., Su, J., Ullrich, S. J., Kreider, B. L., and Farber, J. M. (1997). STRL22 is a receptor for the CC chemokine MIP-3alpha. Biochem Biophys Res Commun *236*, 212-217.

Liao, G., Zhang, M., Harhaj, E. W., and Sun, S. C. (2004). Regulation of the NF-kappaB-inducing kinase by tumor necrosis factor receptor-associated factor 3-induced degradation. The Journal of biological chemistry *279*, 26243-26250.

Linterman, M. A., and Vinuesa, C. G. (2010). Signals that influence T follicular helper cell differentiation and function. Semin Immunopathol *32*, 183-196.

Liptay, S., Schmid, R. M., Nabel, E. G., and Nabel, G. J. (1994). Transcriptional regulation of NF-kappa B2: evidence for kappa B-mediated positive and negative autoregulation. Mol Cell Biol *14*, 7695-7703.

Liu, K., Victora, G. D., Schwickert, T. A., Guermonprez, P., Meredith, M. M., Yao, K., Chu, F. F., Randolph, G. J., Rudensky, A. Y., and Nussenzweig, M. (2009). In vivo analysis of dendritic cell development and homeostasis. Science *324*, 392-397.

Lo, J. C., Basak, S., James, E. S., Quiambo, R. S., Kinsella, M. C., Alegre, M. L., Weih, F., Franzoso, G., Hoffmann, A., and Fu, Y. X. (2006). Coordination between NF-kappaB family members p50 and p52 is essential for mediating LTbetaR signals in the development and organization of secondary lymphoid tissues. Blood *107*, 1048-1055.

Lorenz, R. G., Chaplin, D. D., McDonald, K. G., McDonough, J. S., and Newberry, R. D. (2003). Isolated lymphoid follicle formation is inducible and dependent upon lymphotoxin-sufficient B lymphocytes, lymphotoxin beta receptor, and TNF receptor I function. J Immunol *170*, 5475-5482.

Lorenz, R. G., and Newberry, R. D. (2004). Isolated lymphoid follicles can function as sites for induction of mucosal immune responses. Ann N Y Acad Sci *1029*, 44-57.

Lu, T. T., and Cyster, J. G. (2002). Integrin-mediated long-term B cell retention in the splenic marginal zone. Science *297*, 409-412.

Luftig, M., Yasui, T., Soni, V., Kang, M. S., Jacobson, N., Cahir-McFarland, E., Seed, B., and Kieff, E. (2004). Epstein-Barr virus latent infection membrane protein 1 TRAF-binding site induces NIK/IKK alpha-dependent noncanonical NF-kappaB activation. Proc Natl Acad Sci USA *101*, 141-146.

Lügering, A., and Kucharzik, T. (2006). Induction of intestinal lymphoid tissue: the role of cryptopatches. Ann N Y Acad Sci *1072*, 210-217.

Luther, S. A., Tang, H. L., Hyman, P. L., Farr, A. G., and Cyster, J. G. (2000). Coexpression of the chemokines ELC and SLC by T zone stromal cells and deletion of the ELC gene in the plt/plt mouse. Proc Natl Acad Sci USA *97*, 12694-12699.

Mackey, M. F., Gunn, J. R., Maliszewsky, C., Kikutani, H., Noelle, R. J., and Barth, R. J. (1998). Dendritic cells require maturation via CD40 to generate protective antitumor immunity. J Immunol *161*, 2094-2098.

MacLennan, I. C., Toellner, K. M., Cunningham, A. F., Serre, K., Sze, D. M., Zúñiga, E., Cook, M. C., and Vinuesa, C. G. (2003). Extrafollicular antibody responses. Immunol Rev *194*, 8-18.

Maldonado-López, R., and Moser, M. (2001). Dendritic cell subsets and the regulation of Th1/Th2 responses. Seminars in Immunology *13*, 275-282.

Masopust, D., Vezys, V., Marzo, A. L., and Lefrançois, L. (2001). Preferential localization of effector memory cells in nonlymphoid tissue. Science *291*, 2413-2417.

Matsumoto, M., Fu, Y. X., Molina, H., and Chaplin, D. D. (1997). Lymphotoxin-alpha-deficient and TNF receptor-I-deficient mice define developmental and functional characteristics of germinal centers. Immunol Rev *156*, 137-144.

Matsumoto, M., Mariathasan, S., Nahm, M. H., Baranyay, F., Peschon, J. J., and Chaplin, D. D. (1996). Role of lymphotoxin and the type I TNF receptor in the formation of germinal centers. Science *271*, 1289-1291.

Matsushima, A., Kaisho, T., Rennert, P. D., Nakano, H., Kurosawa, K., Uchida, D., Takeda, K., Akira, S., and Matsumoto, M. (2001). Essential role of nuclear factor (NF)-kappaB-inducing kinase and inhibitor of kappaB (IkappaB) kinase alpha in NF-kappaB activation through lymphotoxin beta receptor, but not through tumor necrosis factor receptor I. J Exp Med *193*, 631-636.

Mauri, D. N., Ebner, R., Montgomery, R. I., Kochel, K. D., Cheung, T. C., Yu, G. L., Ruben, S., Murphy, M., Eisenberg, R. J., Cohen, G. H., Spear, P. G., and Ware, C. F. (1998). LIGHT, a new member of the TNF superfamily, and lymphotoxin alpha are ligands for herpesvirus entry mediator. Immunity *8*, 21-30.

McDonald, K. G., McDonough, J. S., Dieckgraefe, B. K., and Newberry, R. D. (2010). Dendritic Cells Produce CXCL13 and Participate in the Development of Murine Small Intestine Lymphoid Tissues. Am J Pathol .

McDonald, K. G., McDonough, J. S., Wang, C., Kucharzik, T., Williams, I. R., and Newberry, R. D. (2007). CC chemokine receptor 6 expression by B lymphocytes is essential for the development of isolated lymphoid follicles. Am J Pathol *170*, 1229-1240.

Mebius, R. E. (2003). Organogenesis of lymphoid tissues. Nat Rev Immunol *3*, 292-303.

Mebius, R. E., and Kraal, G. (2005). Structure and function of the spleen. Nat Rev Immunol *5*, 606-616.

Mebius, R. E., Rennert, P., and Weissman, I. L. (1997). Developing lymph nodes collect CD4+CD3- LTbeta+ cells that can differentiate to APC, NK cells, and follicular cells but not T or B cells. Immunity *7*, 493-504.

Mebius, R. E., Schadee-Eestermans, I. L., and Weissman, I. L. (1998). MAdCAM-1 dependent colonization of developing lymph nodes involves a unique subset of CD4+CD3- hematolymphoid cells. Cell Adhes Commun *6*, 97-103.

Mebius, R. E., Streeter, P. R., Michie, S., Butcher, E. C., and Weissman, I. L. (1996). A developmental switch in lymphocyte homing receptor and endothelial vascular

addressin expression regulates lymphocyte homing and permits CD4+ CD3- cells to colonize lymph nodes. Proc Natl Acad Sci USA *93*, 11019-11024.

Medzhitov, R. (2001). Toll-like receptors and innate immunity. Nat Rev Immunol *1*, 135-145.

Medzhitov, R. (2010). Innate immunity: quo vadis? Nature Immunology *11*, 551-553.

Medzhitov, R., and Janeway, C. (2000). Innate immunity. N Engl J Med *343*, 338-344.

Medzhitov, R., Preston-Hurlburt, P., and Janeway, C. A. (1997). A human homologue of the Drosophila Toll protein signals activation of adaptive immunity. Nature *388*, 394-397.

Michelsen, K. S., Aicher, A., Mohaupt, M., Hartung, T., Dimmeler, S., Kirschning, C. J., and Schumann, R. R. (2001). The role of toll-like receptors (TLRs) in bacteria-induced maturation of murine dendritic cells (DCS). Peptidoglycan and lipoteichoic acid are inducers of DC maturation and require TLR2. The Journal of biological chemistry *276*, 25680-25686.

Miga, A. J., Masters, S. R., Durell, B. G., Gonzalez, M., Jenkins, M. K., Maliszewski, C., Kikutani, H., Wade, W. F., and Noelle, R. J. (2001). Dendritic cell longevity and T cell persistence is controlled by CD154-CD40 interactions. Eur J Immunol *31*, 959-965.

Miles, A., Liaskou, E., Eksteen, B., Lalor, P. F., and Adams, D. H. (2008). CCL25 and CCL28 promote alpha4 beta7-integrin-dependent adhesion of lymphocytes to MAdCAM-1 under shear flow. Am J Physiol Gastrointest Liver Physiol *294*, G1257-67.

Miyawaki, S., Nakamura, Y., Suzuka, H., Koba, M., Yasumizu, R., Ikehara, S., and Shibata, Y. (1994). A new mutation, aly, that induces a generalized lack of lymph nodes accompanied by immunodeficiency in mice. Eur J Immunol *24*, 429-434.

Moser, B., Schaerli, P., and Loetscher, P. (2002). CXCR5(+) T cells: follicular homing takes center stage in T-helper-cell responses. Trends Immunol *23*, 250-254.

Mottet, C., Uhlig, H. H., and Powrie, F. (2003). Cutting edge: cure of colitis by CD4+CD25+ regulatory T cells. J Immunol *170*, 3939-3943.

Mowat, A. M. (2003). Anatomical basis of tolerance and immunity to intestinal antigens. Nat Rev Immunol *3*, 331-341.

Müller, J. R., and Siebenlist, U. (2003). Lymphotoxin beta receptor induces sequential activation of distinct NF-kappa B factors via separate signaling pathways. The Journal of biological chemistry *278*, 12006-12012.

Naito, A., Azuma, S., Tanaka, S., Miyazaki, T., Takaki, S., Takatsu, K., Nakao, K., Nakamura, K., Katsuki, M., Yamamoto, T., and Inoue, J. (1999). Severe osteopetrosis, defective interleukin-1 signalling and lymph node organogenesis in TRAF6-deficient mice. Genes Cells *4*, 353-362.

Nakano, H., Mori, S., Yonekawa, H., Nariuchi, H., Matsuzawa, A., and Kakiuchi, T. (1998). A novel mutant gene involved in T-lymphocyte-specific homing into peripheral lymphoid organs on mouse chromosome 4. Blood *91*, 2886-2895.

Nascimbeni, R., Di Fabio, F., Di Betta, E., Mariani, P., Fisogni, S., and Villanacci, V. (2005). Morphology of colorectal lymphoid aggregates in cancer, diverticular and inflammatory bowel diseases. Mod Pathol *18*, 681-685.

Neumann, B., Luz, A., Pfeffer, K., and Holzmann, B. (1996). Defective Peyer's patch organogenesis in mice lacking the 55-kD receptor for tumor necrosis factor. J Exp Med *184*, 259-264.

Ngo, V. N., Cornall, R. J., and Cyster, J. G. (2001). Splenic T zone development is B cell dependent. J Exp Med *194*, 1649-1660.

Ngo, V. N., Korner, H., Gunn, M. D., Schmidt, K. N., Riminton, D. S., Cooper, M. D., Browning, J. L., Sedgwick, J. D., and Cyster, J. G. (1999). Lymphotoxin alpha/beta and tumor necrosis factor are required for stromal cell expression of homing chemokines in B and T cell areas of the spleen. J Exp Med *189*, 403-412.

Niess, J. H., Brand, S., Gu, X., Landsman, L., Jung, S., McCormick, B. A., Vyas, J. M., Boes, M., Ploegh, H. L., Fox, J. G., Littman, D. R., and Reinecker, H. C. (2005). CX3CR1-mediated dendritic cell access to the intestinal lumen and bacterial clearance. Science *307*, 254-258.

Norvell, A., and Monroe, J. G. (1996). Acquisition of surface IgD fails to protect from tolerance-induction. Both surface IgM- and surface IgD-mediated signals induce apoptosis of immature murine B lymphocytes. J Immunol *156*, 1328-1332.

Oetke, C., Kraal, G., and Crocker, P. R. (2006). The antigen recognized by MOMA-I is sialoadhesin. Immunol Lett *106*, 96-98.

Osborn, L., Hession, C., Tizard, R., Vassallo, C., Luhowskyj, S., Chi-Rosso, G., and Lobb, R. (1989). Direct expression cloning of vascular cell adhesion molecule 1, a cytokine-induced endothelial protein that binds to lymphocytes. Cell *59*, 1203-1211.

Ostanin, D. V., Bao, J., Koboziev, I., Gray, L., Robinson-Jackson, S. A., Kosloski-Davidson, M., Price, V. H., and Grisham, M. B. (2009). T cell transfer model of chronic colitis: concepts, considerations, and tricks of the trade. Am J Physiol Gastrointest Liver Physiol *296*, G135-46.

Ouaaz, F., Arron, J., Zheng, Y., Choi, Y., and Beg, A. A. (2002). Dendritic cell development and survival require distinct NF-kappaB subunits. Immunity *16*, 257-270.

Pabst, O., Bernhardt, G., and Förster, R. (2007). The impact of cell-bound antigen transport on mucosal tolerance induction. J Leukoc Biol *82*, 795-800.

Pabst, O., Herbrand, H., Worbs, T., Friedrichsen, M., Yan, S., Hoffmann, M. W., Körner, H., Bernhardt, G., Pabst, R., and Förster, R. (2005). Cryptopatches and isolated lymphoid follicles: dynamic lymphoid tissues dispensable for the generation of intraepithelial lymphocytes. Eur J Immunol *35*, 98-107.

Pasparakis, M., Alexopoulou, L., Grell, M., Pfizenmaier, K., Bluethmann, H., and Kollias, G. (1997). Peyer's patch organogenesis is intact yet formation of B lymphocyte follicles is defective in peripheral lymphoid organs of mice deficient for tumor necrosis factor and its 55-kDa receptor. Proc Natl Acad Sci USA *94*, 6319-6323.

Paxian, S., Merkle, H., Riemann, M., Wilda, M., Adler, G., Hameister, H., Liptay, S., Pfeffer, K., and Schmid, R. M. (2002). Abnormal organogenesis of Peyer's patches in

mice deficient for NF-kappaB1, NF-kappaB2, and Bcl-3. Gastroenterology *122*, 1853-1868.

Randall, T. D., Carragher, D. M., and Rangel-Moreno, J. (2008). Development of secondary lymphoid organs. Annual Review of Immunology *26*, 627-650.

Rayet, B., and Gélinas, C. (1999). Aberrant rel/nfkb genes and activity in human cancer. Oncogene *18*, 6938-6947.

Rennert, P. D., James, D., Mackay, F., Browning, J. L., and Hochman, P. S. (1998). Lymph node genesis is induced by signaling through the lymphotoxin beta receptor. Immunity *9*, 71-79.

Rescigno, M., Rotta, G., Valzasina, B., and Ricciardi-Castagnoli, P. (2001a). Dendritic cells shuttle microbes across gut epithelial monolayers. Immunobiology *204*, 572-581.

Rescigno, M., Urbano, M., Valzasina, B., Francolini, M., Rotta, G., Bonasio, R., Granucci, F., Kraehenbuhl, J. P., and Ricciardi-Castagnoli, P. (2001b). Dendritic cells express tight junction proteins and penetrate gut epithelial monolayers to sample bacteria. Nature Immunology *2*, 361-367.

Rocha, S., Martin, A. M., Meek, D. W., and Perkins, N. D. (2003). p53 represses cyclin D1 transcription through down regulation of Bcl-3 and inducing increased association of the p52 NF-kappaB subunit with histone deacetylase 1. Mol Cell Biol *23*, 4713-4727.

Rock, F. L., Hardiman, G., Timans, J. C., Kastelein, R. A., and Bazan, J. F. (1998). A family of human receptors structurally related to Drosophila Toll. Proc Natl Acad Sci USA *95*, 588-593.

Saito, H., Kanamori, Y., Takemori, T., Nariuchi, H., Kubota, E., Takahashi-Iwanaga, H., Iwanaga, T., and Ishikawa, H. (1998). Generation of intestinal T cells from progenitors residing in gut cryptopatches. Science *280*, 275-278.

Saito, N., Courtois, G., Chiba, A., Yamamoto, N., Nitta, T., Hironaka, N., Rowe, M., Yamamoto, N., and Yamaoka, S. (2003). Two carboxyl-terminal activation regions of Epstein-Barr virus latent membrane protein 1 activate NF-kappaB through distinct signaling pathways in fibroblast cell lines. The Journal of biological chemistry *278*, 46565-46575.

Sallusto, F., Schaerli, P., Loetscher, P., Schaniel, C., Lenig, D., Mackay, C. R., Qin, S., and Lanzavecchia, A. (1998). Rapid and coordinated switch in chemokine receptor expression during dendritic cell maturation. Eur J Immunol *28*, 2760-2769.

Schaerli, P., Loetscher, P., and Moser, B. (2001). Cutting edge: induction of follicular homing precedes effector Th cell development. J Immunol *167*, 6082-6086.

Schneider, G., Saur, D., Siveke, J. T., Fritsch, R., Greten, F. R., and Schmid, R. M. (2006). IKKalpha controls p52/RelB at the skp2 gene promoter to regulate G1- to S-phase progression. EMBO J *25*, 3801-3812.

Schneider, P., Mackay, F., Steiner, V., Hofmann, K., Bodmer, J. L., Holler, N., Ambrose, C., Lawton, P., Bixler, S., Acha-Orbea, H., Valmori, D., Romero, P., Werner-Favre, C., Zubler, R. H., Browning, J. L., and Tschopp, J. (1999). BAFF, a novel ligand of the tumor necrosis factor family, stimulates B cell growth. J Exp Med *189*, 1747-1756.

Schulz, O., Jaensson, E., Persson, E. K., Liu, X., Worbs, T., Agace, W. W., and Pabst, O. (2009). Intestinal CD103+, but not CX3CR1+, antigen sampling cells migrate in lymph and serve classical dendritic cell functions. J Exp Med *206*, 3101-3114.

Sellon, R. K., Tonkonogy, S., Schultz, M., Dieleman, L. A., Grenther, W., Balish, E., Rennick, D. M., and Sartor, R. B. (1998). Resident enteric bacteria are necessary for development of spontaneous colitis and immune system activation in interleukin-10-deficient mice. Infect Immun *66*, 5224-5231.

Senftleben, U., Cao, Y., Xiao, G., Greten, F. R., Krähn, G., Bonizzi, G., Chen, Y., Hu, Y., Fong, A., Sun, S. C., and Karin, M. (2001). Activation by IKKalpha of a second, evolutionary conserved, NF-kappa B signaling pathway. Science *293*, 1495-1499.

Shinkura, R., Kitada, K., Matsuda, F., Tashiro, K., Ikuta, K., Suzuki, M., Kogishi, K., Serikawa, T., and Honjo, T. (1999). Alymphoplasia is caused by a point mutation in the mouse gene encoding Nf-kappa b-inducing kinase. Nat Genet *22*, 74-77.

Shortman, K., and Liu, Y. J. (2002). Mouse and human dendritic cell subtypes. Nat Rev Immunol *2*, 151-161.

Siddiqui, K. R., and Powrie, F. (2008). CD103+ GALT DCs promote Foxp3+ regulatory T cells. Mucosal immunology *1 Suppl 1*, S34-8.

Silverman, N., and Maniatis, T. (2001). NF-kappaB signaling pathways in mammalian and insect innate immunity. Genes Dev *15*, 2321-2342.

Sitohy, B., Hammarström, S., Danielsson, A., and Hammarström, M. L. (2008). Basal lymphoid aggregates in ulcerative colitis colon: a site for regulatory T cell action. Clin Exp Immunol *151*, 326-333.

Spahn, T. W., Herbst, H., Rennert, P. D., Lügering, N., Maaser, C., Kraft, M., Fontana, A., Weiner, H. L., Domschke, W., and Kucharzik, T. (2002). Induction of colitis in mice deficient of Peyer's patches and mesenteric lymph nodes is associated with increased disease severity and formation of colonic lymphoid patches. Am J Pathol *161*, 2273-2282.

Speirs, K., Lieberman, L., Caamano, J., Hunter, C. A., and Scott, P. (2004). Cutting edge: NF-kappa B2 is a negative regulator of dendritic cell function. J Immunol *172*, 752-756.

Stopfer, P., Obermeier, F., Dunger, N., Falk, W., Farkas, S., Janotta, M., Möller, A., Männel, D. N., and Hehlgans, T. (2004). Blocking lymphotoxin-beta receptor activation diminishes inflammation via reduced mucosal addressin cell adhesion molecule-1 (MAdCAM-1) expression and leucocyte margination in chronic DSS-induced colitis. Clin Exp Immunol *136*, 21-29.

Sun, Z., Unutmaz, D., Zou, Y. R., Sunshine, M. J., Pierani, A., Brenner-Morton, S., Mebius, R. E., and Littman, D. R. (2000). Requirement for RORgamma in thymocyte survival and lymphoid organ development. Science *288*, 2369-2373.

Suto, H., Katakai, T., Sugai, M., Kinashi, T., and Shimizu, A. (2009). CXCL13 production by an established lymph node stromal cell line via lymphotoxin-beta receptor engagement involves the cooperation of multiple signaling pathways. Int Immunol *21*, 467-476.

Takada, Y., Hisamatsu, T., Kamada, N., Kitazume, M. T., Honda, H., Oshima, Y., Saito, R., Takayama, T., Kobayashi, T., Chinen, H., Mikami, Y., Kanai, T., Okamoto,

S., and Hibi, T. (2010). Monocyte chemoattractant protein-1 contributes to gut homeostasis and intestinal inflammation by composition of IL-10-producing regulatory macrophage subset. J Immunol *184*, 2671-2676.

Tanaka, Y., Imai, T., Baba, M., Ishikawa, I., Uehira, M., Nomiyama, H., and Yoshie, O. (1999). Selective expression of liver and activation-regulated chemokine (LARC) in intestinal epithelium in mice and humans. Eur J Immunol *29*, 633-642.

Taylor, R. T., Lügering, A., Newell, K. A., and Williams, I. R. (2004). Intestinal cryptopatch formation in mice requires lymphotoxin alpha and the lymphotoxin beta receptor. J Immunol *173*, 7183-7189.

Taylor, R. T., Patel, S. R., Lin, E., Butler, B. R., Lake, J. G., Newberry, R. D., and Williams, I. R. (2007). Lymphotoxin-independent expression of TNF-related activation-induced cytokine by stromal cells in cryptopatches, isolated lymphoid follicles, and Peyer's patches. J Immunol *178*, 5659-5667.

Teramoto, K., Miura, S., Tsuzuki, Y., Hokari, R., Watanabe, C., Inamura, T., Ogawa, T., Hosoe, N., Nagata, H., Ishii, H., and Hibi, T. (2005). Increased lymphocyte trafficking to colonic microvessels is dependent on MAdCAM-1 and C-C chemokine mLARC/CCL20 in DSS-induced mice colitis. Clin Exp Immunol *139*, 421-428.

Thompson, J. S., Bixler, S. A., Qian, F., Vora, K., Scott, M. L., Cachero, T. G., Hession, C., Schneider, P., Sizing, I. D., Mullen, C., Strauch, K., Zafari, M., Benjamin, C. D., Tschopp, J., Browning, J. L., and Ambrose, C. (2001). BAFF-R, a newly identified TNF receptor that specifically interacts with BAFF. Science *293*, 2108-2111.

Tumanov, A., Kuprash, D., Lagarkova, M., Grivennikov, S., Abe, K., Shakhov, A., Drutskaya, L., Stewart, C., Chervonsky, A., and Nedospasov, S. (2002). Distinct role of surface lymphotoxin expressed by B cells in the organization of secondary lymphoid tissues. Immunity *17*, 239-250.

Tumanov, A. V., Kuprash, D. V., Mach, J. A., Nedospasov, S. A., and Chervonsky, A. V. (2004). Lymphotoxin and TNF produced by B cells are dispensable for maintenance of the follicle-associated epithelium but are required for development of lymphoid follicles in the Peyer's patches. J Immunol *173*, 86-91.

Uss, E., Rowshani, A. T., Hooibrink, B., Lardy, N. M., van Lier, R. A., and ten Berge, I. J. (2006). CD103 is a marker for alloantigen-induced regulatory CD8+ T cells. J Immunol *177*, 2775-2783.

van de Pavert, S. A., Olivier, B. J., Goverse, G., Vondenhoff, M. F., Greuter, M., Beke, P., Kusser, K., Höpken, U. E., Lipp, M., Niederreither, K., Blomhoff, R., Sitnik, K., Agace, W. W., Randall, T. D., de Jonge, W. J., and Mebius, R. E. (2009). Chemokine CXCL13 is essential for lymph node initiation and is induced by retinoic acid and neuronal stimulation. Nature Immunology *10*, 1193-1199.

Veiga-Fernandes, H., Coles, M. C., Foster, K. E., Patel, A., Williams, A., Natarajan, D., Barlow, A., Pachnis, V., and Kioussis, D. (2007). Tyrosine kinase receptor RET is a key regulator of Peyer's patch organogenesis. Nature *446*, 547-551.

Velaga, S., Herbrand, H., Friedrichsen, M., Jiong, T., Dorsch, M., Hoffmann, M. W., Förster, R., and Pabst, O. (2009). Chemokine receptor CXCR5 supports solitary intestinal lymphoid tissue formation, B cell homing, and induction of intestinal IgA responses. J Immunol *182*, 2610-2619.

Vinuesa, C. G., Tangye, S. G., Moser, B., and Mackay, C. R. (2005). Follicular B helper T cells in antibody responses and autoimmunity. Nat Rev Immunol *5*, 853-865.

Vondenhoff, M. F., van de Pavert, S. A., Dillard, M. E., Greuter, M., Goverse, G., Oliver, G., and Mebius, R. E. (2009). Lymph sacs are not required for the initiation of lymph node formation. Development *136*, 29-34.

Wajant, H., Henkler, F., and Scheurich, P. (2001). The TNF-receptor-associated factor family: scaffold molecules for cytokine receptors, kinases and their regulators. Cell Signal *13*, 389-400.

Wang, C., McDonald, K. G., McDonough, J. S., and Newberry, R. D. (2006). Murine isolated lymphoid follicles contain follicular B lymphocytes with a mucosal phenotype. Am J Physiol Gastrointest Liver Physiol *291*, G595-604.

Wang, C., McDonough, J. S., McDonald, K. G., Huang, C., and Newberry, R. D. (2008). Alpha4beta7/MAdCAM-1 interactions play an essential role in transitioning cryptopatches into isolated lymphoid follicles and a nonessential role in cryptopatch formation. J Immunol *181*, 4052-4061.

Wang, Y. G., Kim, K. D., Wang, J., Yu, P., and Fu, Y. X. (2005). Stimulating lymphotoxin beta receptor on the dendritic cells is critical for their homeostasis and expansion. J Immunol *175*, 6997-7002.

Weatherill, A. R., Lee, J. Y., Zhao, L., Lemay, D. G., Youn, H. S., and Hwang, D. H. (2005). Saturated and polyunsaturated fatty acids reciprocally modulate dendritic cell functions mediated through TLR4. J Immunol *174*, 5390-5397.

Weih, D. S., Yilmaz, Z. B., and Weih, F. (2001). Essential role of RelB in germinal center and marginal zone formation and proper expression of homing chemokines. J Immunol *167*, 1909-1919.

Weih, F., and Caamaño, J. (2003). Regulation of secondary lymphoid organ development by the nuclear factor-kappaB signal transduction pathway. Immunol Rev *195*, 91-105.

Weih, F., Carrasco, D., Durham, S. K., Barton, D. S., Rizzo, C. A., Ryseck, R. P., Lira, S. A., and Bravo, R. (1995). Multiorgan inflammation and hematopoietic abnormalities in mice with a targeted disruption of RelB, a member of the NF-kappa B/Rel family. Cell *80*, 331-340.

Westerheide, S. D., Mayo, M. W., Anest, V., Hanson, J. L., and Baldwin, A. S. (2001). The putative oncoprotein Bcl-3 induces cyclin D1 to stimulate G(1) transition. Mol Cell Biol *21*, 8428-8436.

White, A., Carragher, D., Parnell, S., Msaki, A., Perkins, N., Lane, P., Jenkinson, E., Anderson, G., and Caamaño, J. H. (2007). Lymphotoxin a-dependent and -independent signals regulate stromal organizer cell homeostasis during lymph node organogenesis. Blood *110*, 1950-1959.

Wigle, J. T., and Oliver, G. (1999). Prox1 function is required for the development of the murine lymphatic system. Cell *98*, 769-778.

Williams, I. R. (2006). CCR6 and CCL20: partners in intestinal immunity and lymphorganogenesis. Ann N Y Acad Sci *1072*, 52-61.

Wing, K., Fehérvári, Z., and Sakaguchi, S. (2006). Emerging possibilities in the development and function of regulatory T cells. Int Immunol *18*, 991-1000.

Wirtz, S., Neufert, C., Weigmann, B., and Neurath, M. F. (2007). Chemically induced mouse models of intestinal inflammation. Nat Protoc *2*, 541-546.

Withers, D. R., Kim, M. Y., Bekiaris, V., Rossi, S. W., Jenkinson, W. E., Gaspal, F., McConnell, F., Caamano, J. H., Anderson, G., and Lane, P. J. (2007). The role of lymphoid tissue inducer cells in splenic white pulp development. Eur J Immunol *37*, 3240-3245.

Wong, B. R., Josien, R., and Choi, Y. (1999). TRANCE is a TNF family member that regulates dendritic cell and osteoclast function. J Leukoc Biol *65*, 715-724.

Wong, B. R., Josien, R., Lee, S. Y., Sauter, B., Li, H. L., Steinman, R. M., and Choi, Y. (1997). TRANCE (tumor necrosis factor [TNF]-related activation-induced cytokine), a new TNF family member predominantly expressed in T cells, is a dendritic cell-specific survival factor. J Exp Med *186*, 2075-2080.

Wu, L., D'Amico, A., Winkel, K. D., Suter, M., Lo, D., and Shortman, K. (1998). RelB is essential for the development of myeloid-related CD8alpha- dendritic cells but not of lymphoid-related CD8alpha+ dendritic cells. Immunity *9*, 839-847.

Wu, Q., Wang, Y., Wang, J., Hedgeman, E. O., Browning, J. L., and Fu, Y. X. (1999). The requirement of membrane lymphotoxin for the presence of dendritic cells in lymphoid tissues. J Exp Med *190*, 629-638.

Xiao, G., Harhaj, E. W., and Sun, S. C. (2001). NF-kappaB-inducing kinase regulates the processing of NF-kappaB2 p100. Mol Cell *7*, 401-409.

Xu, L. G., and Shu, H. B. (2002). TNFR-associated factor-3 is associated with BAFF-R and negatively regulates BAFF-R-mediated NF-kappa B activation and IL-10 production. J Immunol *169*, 6883-6889.

Xu, Y., Hunt, N. H., and Bao, S. (2007). The correlation between proinflammatory cytokines, MAdCAM-1 and cellular infiltration in the inflamed colon from TNF-alpha gene knockout mice. Immunol Cell Biol *85*, 633-639.

Yamada, T., Mitani, T., Yorita, K., Uchida, D., Matsushima, A., Iwamasa, K., Fujita, S., and Matsumoto, M. (2000). Abnormal immune function of hemopoietic cells from alymphoplasia (aly) mice, a natural strain with mutant NF-kappa B-inducing kinase. J Immunol *165*, 804-812.

Yamamoto, M., Rennert, P., McGhee, J. R., Kweon, M. N., Yamamoto, S., Dohi, T., Otake, S., Bluethmann, H., Fujihashi, K., and Kiyono, H. (2000). Alternate mucosal immune system: organized Peyer's patches are not required for IgA responses in the gastrointestinal tract. J Immunol *164*, 5184-5191.

Yeung, M. M., Melgar, S., Baranov, V., Oberg, A., Danielsson, A., Hammarström, S., and Hammarström, M. L. (2000). Characterisation of mucosal lymphoid aggregates in ulcerative colitis: immune cell phenotype and TcR-gammadelta expression. Gut *47*, 215-227.

Yilmaz, Z. B., Weih, D. S., Sivakumar, V., and Weih, F. (2003). RelB is required for Peyer's patch development: differential regulation of p52-RelB by lymphotoxin and TNF. EMBO J *22*, 121-130.

Yin, L., Wu, L., Wesche, H., Arthur, C. D., White, J. M., Goeddel, D. V., and Schreiber, R. D. (2001). Defective lymphotoxin-beta receptor-induced NF-kappaB transcriptional activity in NIK-deficient mice. Science *291*, 2162-2165.

Yoshida, H., Honda, K., Shinkura, R., Adachi, S., Nishikawa, S., Maki, K., Ikuta, K., and Nishikawa, S. I. (1999). IL-7 receptor alpha+ CD3(-) cells in the embryonic intestine induces the organizing center of Peyer's patches. Int Immunol *11*, 643-655.

Yoshida, H., Kawamoto, H., Santee, S. M., Hashi, H., Honda, K., Nishikawa, S., Ware, C. F., Katsura, Y., and Nishikawa, S. I. (2001). Expression of alpha(4)beta(7) integrin defines a distinct pathway of lymphoid progenitors committed to T cells, fetal intestinal lymphotoxin producer, NK, and dendritic cells. J Immunol *167*, 2511-2521.

Yoshida, H., Naito, A., Inoue, J., Satoh, M., Santee-Cooper, S. M., Ware, C. F., Togawa, A., Nishikawa, S., and Nishikawa, S. (2002). Different cytokines induce surface lymphotoxin-alphabeta on IL-7 receptor-alpha cells that differentially engender lymph nodes and Peyer's patches. Immunity *17*, 823-833.

Sabin, F. On the origin of the lymphatic system from the veins and the development of the lymph hearts and thoracic in the pig. Am. J. Anat. 1: 367–389 (1902).

9. Appendix

Figure 9.1 Expression of CCR6 and CCD9 on B and T lymphocytes

*Single cell suspensions from spleen, mLN and colon from WT and p100Δ mice where analysed for expression of CCR6 (**A**) and CCR9 (**B**) by flow cytometry. Populations were gated on B220+ B cells and CD3+ T cells and the percentage of cells positive for CCR6 (**A**) or CCR9 (**B**) are shown. Bar indicates median.*

A

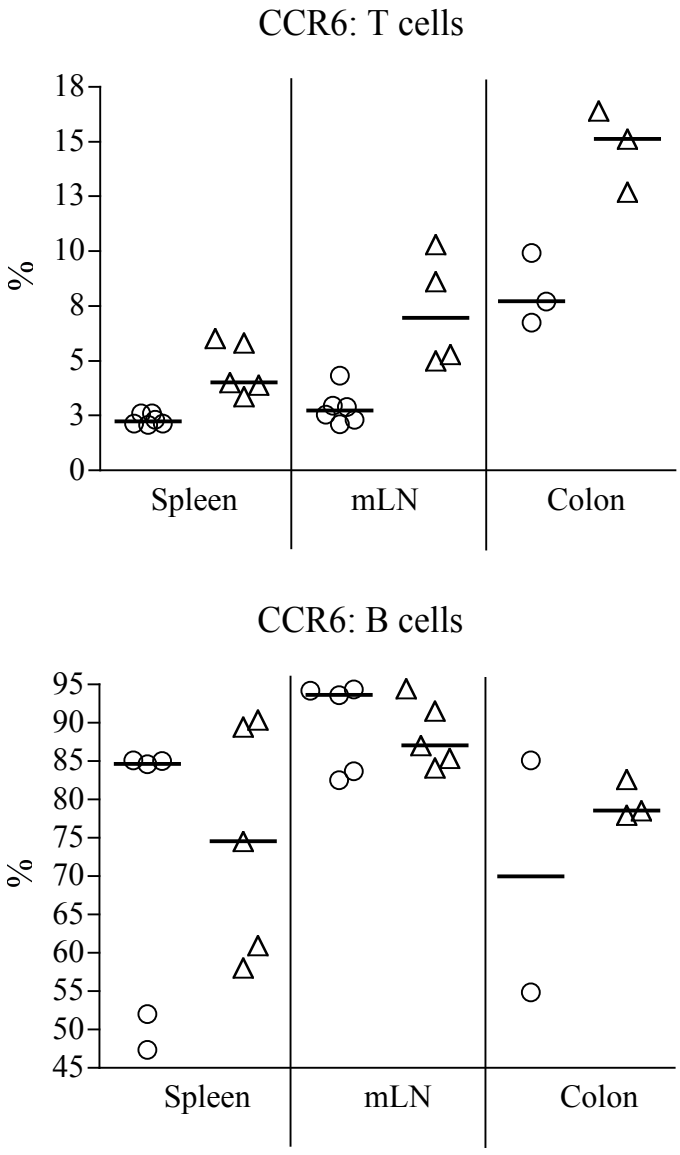
CCR6: T cells
18
15
13
10
8
5
3
0
%
Spleen
mLN
Colon
CCR6: B cells
95
90
85
80
75
70
65
60
55
50
45
%
Spleen
mLN
Colon

Figure 9.1

B

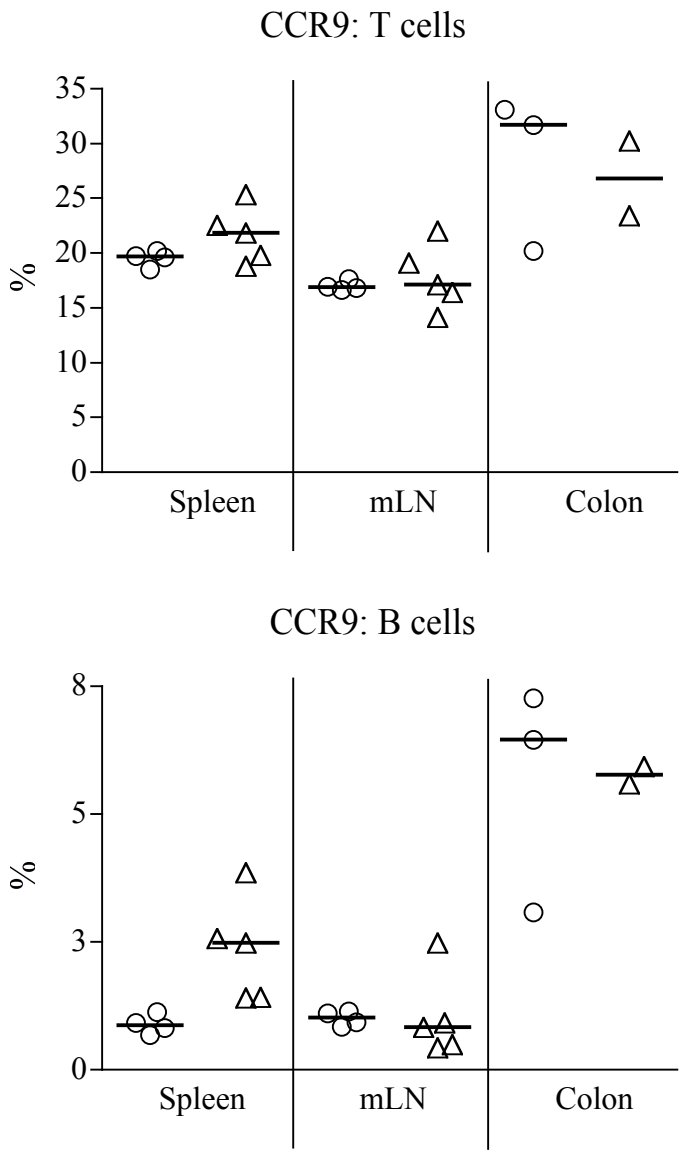
CCR9: T cells
35
30
25
20
15
10
5
0
%
Spleen
mLN
Colon
CCR9: B cells
8
5
3
0
%
Spleen
mLN
Colon

Figure 9.1

Figure 9.2 CD103 and CD11b expression on CD11c^{high} DCs

Single cell suspensions from spleen, mLN and colon from WT and p100Δ mice where analysed for CD103 and CD11b expression on CD11c^{high} DCs. Cells were gated on CD11c^{high} and the profile of CD103 and CD11b expression analysed. Representative FACs plots are shown.

*Cells were gated on CD11c^{high}CD103^{+} and CD11b expression analysed. Graph showing percentage of CD11c^{high}CD103^{+} DCs not expressing CD11b. Bar indicates median. n≥5, from two independent experiments. ns= not significant, * p≤0.01.*

Gated on CD11c^{high}

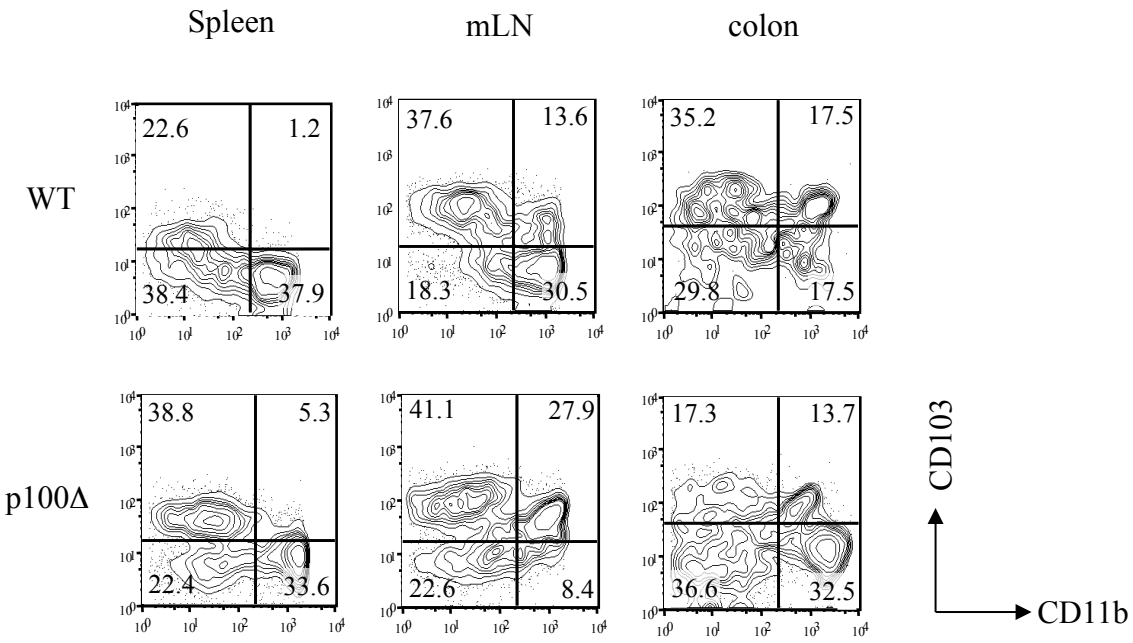

Gated on CD11c^{high}CD103^{+}

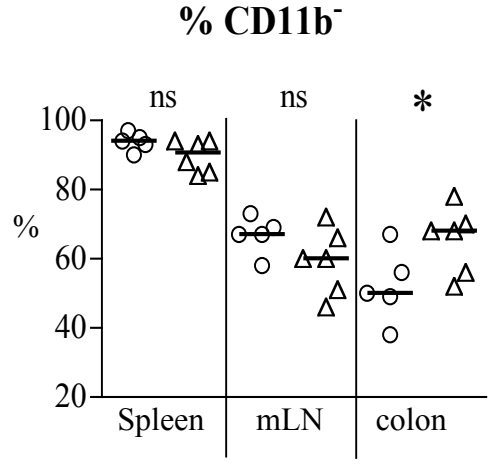

Figure 9.2

Figure 9.3 CD4/CD8 profile of CD11c^{high} DCs

Single cell suspensions from spleen, mLN and colon from WT and p100Δ mice where analysed for CD4 and CD8 expression on CD11c^{high} DCs. Cells were gated on B220^{-} CD3^{-}CD11c^{high} and the profile of CD4 and CD8 expression analysed. Representative FACs plots are shown.

Graph showing the percentage of CD4^{+}CD11c^{high} and CD8^{+}CD11c^{high} DCs. Cells were gated on B220^{-}CD3^{-}CD11c^{high}. Bar indicates median. n≥4. ns= not significant.

Gated on B220^{-}CD3^{-} CD11c^{high}

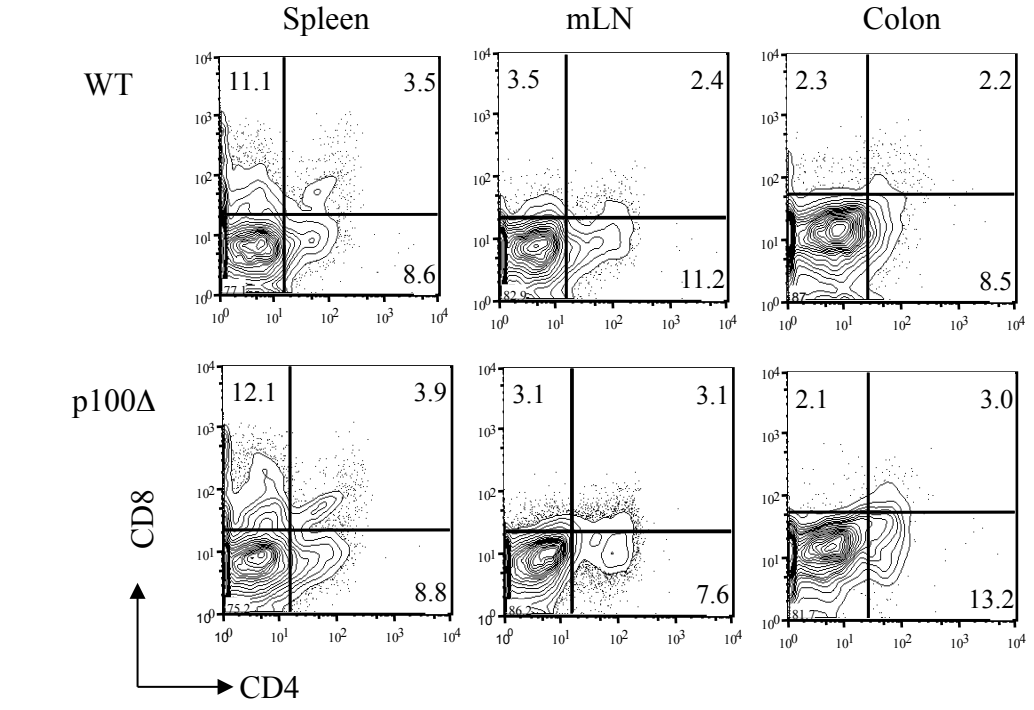

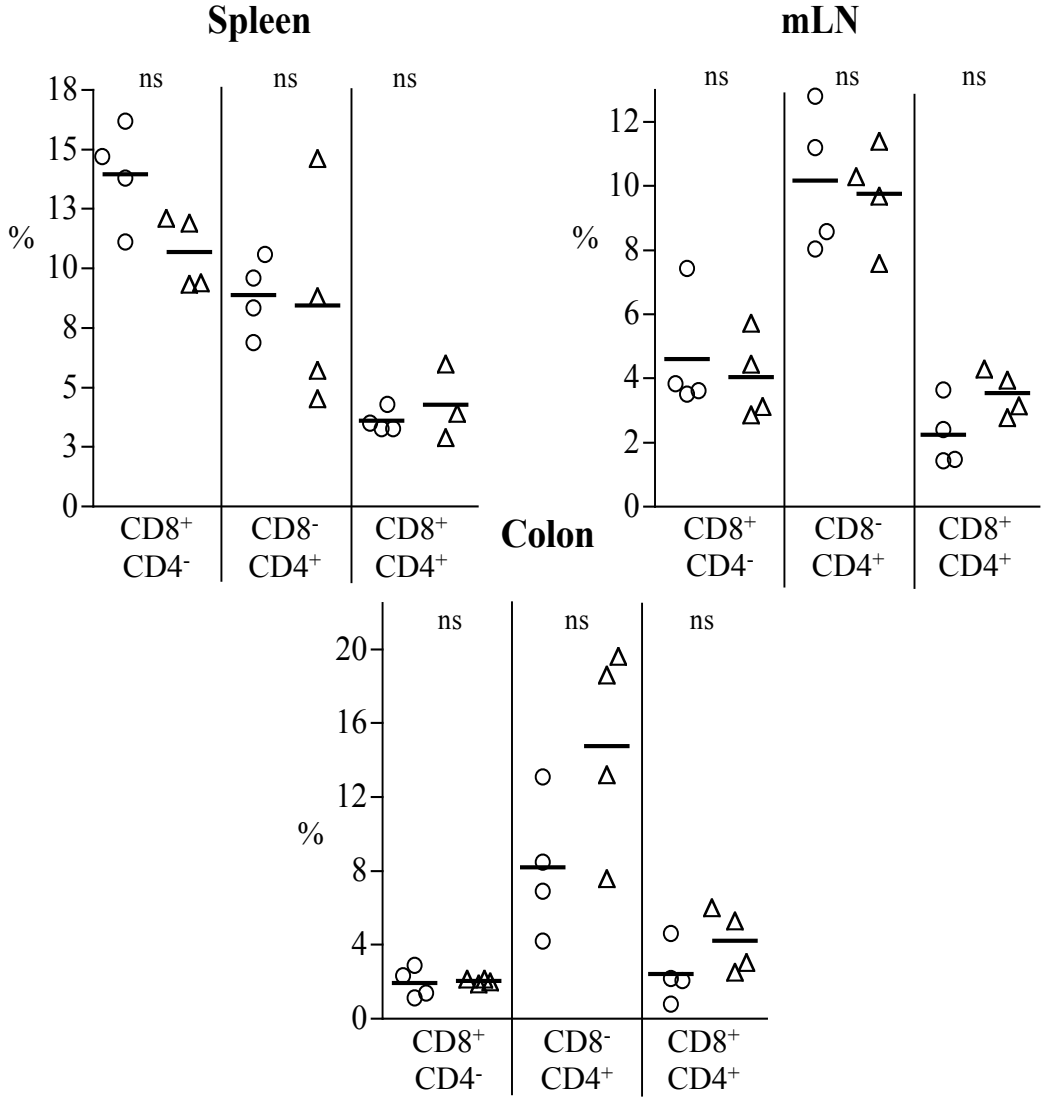

Figure 9.3

Figure 9.4 Foetal liver cell reconstitutions.

WT mice were lethally irradiated and reconstituted with either WT (CD45.1$^+$, n=4), p100Δ (CD45.2$^+$, n=3) or a mixture of WT:p100Δ (n=5) foetal liver cells (FLCs) and harvested three months post transfer. Isolated splenocytes were stained with anti-CD45.1, anti-CD45.2, anti-CD3 and anti-B220 anitobodies, and analysed by flow cytometry. Representative FACs plots show the relative populations of transferred cells in the host mice.

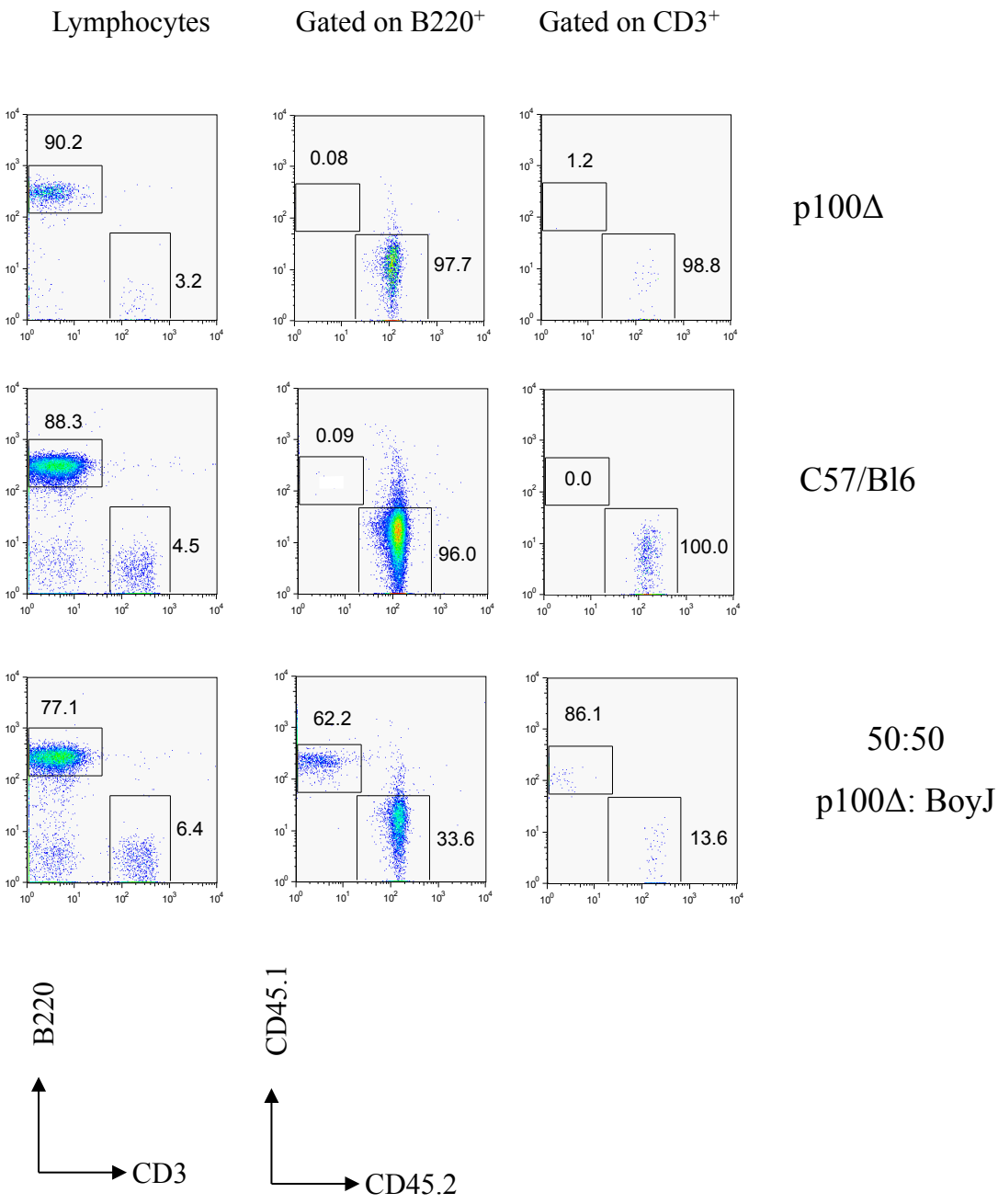
Lymphocytes
Gated on B220+
Gated on CD3+
90.2
3.2
0.08
97.7
1.2
98.8
p100Δ
88.3
4.5
0.09
96.0
0.0
100.0
C57/Bl6
77.1
6.4
62.2
33.6
86.1
13.6
50:50
p100Δ: BoyJ
B220
CD3
CD45.1
CD45.2

Figure 9.4